

A140485

A Submarine Electric Propulsion System
With Large Hub Propeller

By

Michael Scott Hamner

B.S.E.E., United States Naval Academy
(1977)

SUBMITTED TO THE DEPARTMENT OF OCEAN ENGINEERING
IN PARTIAL FULFILLMENT OF THE
DEGREES OF

OCEAN ENGINEER

AND

MASTER OF SCIENCE IN
ELECTRICAL ENGINEERING
AND COMPUTER SCIENCE

at the

MASSACHUSETTS INSTITUTE OF TECHNOLOGY

MAY, 1983

© Michael Scott Hamner, 1983

The author grants to M.I.T. permission to reproduce and to
distribute copies of this thesis document in whole or in part

Signature of Author Michael S. Hamner
Department of Ocean Engineering
May 6, 1983

Certified by James L. Kirtley Jr
James L. Kirtley
Thesis Supervisor
Associate Professor, Department of Electrical Engineering

Thesis Reader David V. Burke
David V. Burke
Professor, Department of Ocean Engineering

Accepted by A. Douglas Carmichael
A. Douglas Carmichael
Chairman, Ocean Engineering Department Committee

Accepted by _____
Arthur L. Smith
Chairman, Electrical Engineering Department Committee

N66314-70-A-0073

DISTRIBUTION STATEMENT A

Approved for public release
Distribution Unlimited

DTIC
ELECTE
APR 23 1984
B

A Submarine Electric Propulsion System

With Large Hub Propeller

By

Michael Scott Hamner

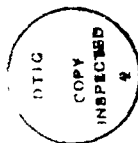
Submitted to the Department of Ocean Engineering on May 6, 1983 in partial fulfillment of the requirements for the degrees of Ocean Engineer and Master of Science in Electrical Engineering, and Computer Science.

ABSTRACT

Traditional submarine propulsion systems consist of a prime mover such as a steam turbine, a gear reduction unit, a shaft, thrust and journal bearings coupled to the propeller. This system severely volume limits the submarine as it requires precise alignment of equipment. It also requires a mechanically complex shaft sealing system. A novel scheme is proposed which utilizes a large hub propeller mounted forward of the control surfaces and powered by a seawater-cooled inverted induction motor mounted around the exterior of the hull. This system also promises to reduce propeller noise and increase low speed maneuverability. Computer analysis of the electric motor design is achieved.

Thesis Supervisor: James L. Kirtley

Title: Associate Professor of Electrical Engineering

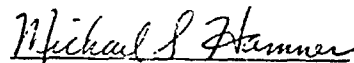


Accession For	
NTIS GRA&I	<input checked="checked" type="checkbox"/>
DTIC TAB	<input type="checkbox"/>
Unannounced	<input type="checkbox"/>
Justification	
PER CALL JC	
PER FORM 50	
Availability Codes	
Dist	Avail and/or Special
A-1	

ACKNOWLEDGMENTS

I would like to thank the following people: my thesis advisor, Dr. James L. Kirtley, for his patience, guidance and assistance in this design effort; David R. Hauger and Mario J. Santarelli, directors of the Simulation Laboratory for the Charles Stark Draper Laboratory, for their computer programming assistance; Mack D. O'Brien, Jr. and Sandra A. Seabrook, from CSDL, for their facilities support; Dr. Damon Cummings, also from CSDL, for his propeller design instruction; Mo Hwa Wang, in the Ocean Engineering Department, for his kindness in sharing his current research work with me; and especially my sister, Linda J. Cunningham, whose skill and long hours in preparing this manuscript made this work possible.

I hereby assign my copyright of this thesis to
The Charles Stark Draper Laboratory, Inc.,
Cambridge, Massachusetts


Michael S. Hamner

Permission is hereby granted by The Charles Stark Draper Laboratory, Inc. to the Massachusetts Institute of Technology to reproduce any or all of this thesis.

TABLE OF CONTENTS

	<u>Page</u>
TITLE PAGE	1
ABSTRACT	2
ACKNOWLEDGMENTS	3
TABLE OF CONTENTS	4
NOMENCLATURE	6
Main Program INDUC.FOR and Body of Text.	6
Subroutine CIRCT	19
Subroutine MAGNET	20
Subroutine SLOTS	20
Subroutine WDGFACT	22
Subroutine CMBNTN	23
Propeller Nomenclature	24
CHAPTER 1, INTRODUCTION	30
CHAPTER 2, BACKGROUND	39
CHAPTER 3, TEMPERATURE RISE CONSIDERATIONS	50
A. Conduction Mode	60
B. One-Dimensional Bulk Conduction	65
C. Two-Dimensional Bulk Conduction	69
D. The Model for the Stator Winding	71
E. Stator Iron in the Axial Direction	35
F. Stator Iron Core in the Axial Direction Through the Encapsulation.	87
G. Stator Iron Core in the Axial Direction Through the End Frame	93
H. Rotor Iron Core in the Axial Direction Through the End	94
I. Rotor Iron Core in the Radial Direction	95
J. The Model for the Rotor Squirrel Cage.	96
K. Rotor Iron Core in the Axial Direction	99
L. Preparing the Computer Thermal Analysis.	100
M. Summary of the Thermal Model and Areas for Further Work	119

Table of Contents (cont'd)

	<u>Page</u>
CHAPTER 4, THE ELECTRIC MOTOR DESIGN	121
A. Motor Type Selection	121
B. Configuration	127
C. Induction Motor Analysis Program	129
D. Motor Insulation System	135
E. Computer Program Results/Design Requirements	141
F. Motor Speed Control	176
G. Dynamic Braking	179
CHAPTER 5, PRELIMINARY PROPELLER DESIGN	181
A. Introduction	181
B. Propeller Design Computer Programs	183
C. Analysis of Results	204
D. Hub Effects	207
E. Propeller Design Summary	211
CHAPTER 6, CONCLUSIONS AND SUGGESTIONS FOR FURTHER WORK	215
A. Summary	215
B. Suggestions for further work	216
APPENDIX A, FOOTNOTES FROM DATA INPUT FILE INDUC.DAT .	218
APPENDIX B, FOOTNOTES FROM MAIN PROGRAM INDUC.FOR. . .	224
APPENDIX C, FOOTNOTES FROM SLOTS.FOR	237
APPENDIX D, FOOTNOTES FROM WDGFACT.FOR	238
APPENDIX E, FOOTNOTES FROM CIRCT.FOR	240
APPENDIX F, FOOTNOTES FROM MAGNET.FOR	245
APPENDIX G, USING THE PROGRAM CURVES	246
REFERENCES	248
COMPUTER LISTINGS	253

NOMENCLATURE

Many variables in the text are described within the paper. Where variable meanings are evident, they will not be listed here. Also, computer program variables (in capital letters) and variables found within the text (normal and subscripted letters) are put together here since these two types of variables are used interchangeably.

Main Program INDUC.FOR and Body of Text

A	cross-sectional area, in. ²
A _{cu}	area of copper in slot, in. ²
A _{slot}	area of slot, in. ²
AAMAT	REAL*8 [A] matrix
ADUM	dummy [A] matrix used in matrix inversion subroutine
AE	expanded area
AI	coordinates of points on rotor and stator material magnetization curves
AINV	inverse of the [A] matrix
AIRGAP	NAMLIST name
ALPHA	vector used in thermal analysis
ALPHAS	vector used in thermal analysis
AMAT	REAL*16 [A] matrix
ARTOTH	cross-sectional area of rotor teeth (used in magnetic calculations), in. ²
ARYOKE	cross-sectional area of rotor yoke (used in magnetic calculations), in. ²
ASTOTH	cross-sectional area of stator teeth (used in magnetic calculations), in. ²

ASTRND	cross-sectional area of stator strand, in. ²
ASYOKE	cross-sectional area of stator yoke (used in magnetic calculations), in. ²
ATAG	ampere-turns across airgap, ampere-turns
ATRT	ampere-turns across rotor tooth, ampere-turns
ATRY	ampere-turns across rotor yoke, ampere-turns
ATST	ampere-turns across stator tooth, ampere-turns
ATSY	ampere-turns across stator yoke, ampere-turns
ATTOT	total ampere-turn drop, ampere-turns
AW	see writeup
AWG	strand size of stator winding (American Wire Gage)
AXR	rotor slot leakage permeance ratio
AXS	stator slot leakage permeance ratio
AY	length of one end-turn, in.
AY	multiplier in slot and end-connection reactance calculations and in rotor resistance calculations
B	armature coil extension, in.
B1	length of hypothetical stator embedded winding, in.
B2 °	length of hypothetical endwinding
BG	average airgap flux density, kilolines/in. ²
BINV	inverse matrix of [B] used in thermal analysis
BK	flux density at which WPE and WCORE are specified, kilolines/in. ²
BLANK	storage location for storing a BCD blank
BMAT	[B] matrix used in thermal analysis
BR	spacing between end-ring and rotor laminations (Reference 1, p. 336, Fig. 199), in.
BRT	flux density in rotor tooth, kilolines/in. ²

BRY flux density in rotor yoke, kilolines/in.²
 BST flux density in stator tooth, kilolines/in.²
 BSY flux density in stator yoke, kilolines/in.²
 C vector of constants used in thermal analysis
 C0 coefficient of viscosity polynomial (see VSCSTY)
 C1 coefficient of viscosity polynomial (see VSCSTY)
 C2 coefficient of viscosity polynomial (see VSCSTY)
 C3 coefficient of viscosity polynomial (see VSCSTY)
 C4 coefficient of viscosity polynomial (see VSCSTY)
 CALPHA cosine (alpha) (Reference 1, p. 209, Fig. 135)
 CCR Carter coefficient (rotor)
 CCS Carter coefficient (stator)
 CIR common block name
 CIRCT subroutine name
 CLOSS array containing core-loss data
 CMBNTN subroutine name
 CSRATO space factor (= CSS*SS/SSAREA)
 CSS number of conductors per stator slot
 CURDEN current density in armature, A/in.²
 D rotor lamination inside diameter, in.
 D1R overall conductor depth in rotor slot, in.
 D1S overall conductor depth in stator slot, in.
 D2R rotor slot dimension, in.
 D2S stator slot dimension, in.
 D3R rotor slot dimension, in.
 D3S stator slot dimension, in.
 D4R rotor slot dimension (slot-opening depth), in.

D4S	stator slot dimension (slot-opening depth), in.
D5S	stator slot dimension, in.
D6R	rotor slot dimension, in.
D6S	stator slot dimension, in.
DALPHA	vector used in thermal analysis
DBRS	depth below rotor slot, in.
DBS	depth below stator slot, in.
DC	distance between center of endring and center of stator slot (Reference 1, p. 336, Fig. 199), in.
DEIGINV	inverse matrix used in thermal analysis
DEIGVEC	matrix used in thermal analysis
DELTAS	increment by which S is increased, percent
DER1	endring outside diameter, in.
DER2	endring inside diameter, in.
DIAMREF	reference diameter for scaling windage loss, in.
DIFF	smallest of all values of DIFF1 calculated, in.
DIFF1	difference between lamination thickness and lamination thickness specified on \$FELOSS data card, in.
DIS	stator lamination inside diameter, in.
DMAT	matrix used in thermal analysis
DNSTY	array containing density values for various rotor and stator winding material possibilities, lb/in. ³
DOR	rotor lamination outside diameter, in.
DS	stator lamination outside diameter, in.
DSR	rotor slot depth, in.
DSS	stator slot depth, in.
DUMMY	common block name
EFF	efficiency, percent
ENDTRN	axial length of end turn, in.
EXPON	matrix used in thermal analysis

f frequency of line voltage = F, Hz
 F = f
 Fl part of horizontal extension of armature winding
 (Reference 1, p. 209, Fig. 135), in.
 FCORE frequency at which WCORE is given, Hz
 FELOSS NAMELIST name
 FLDNME name of fluid in motor cavity (must be limited to
 six characters or less)
 FPOLE flux per pole, kilolines
 FTOTAL total flux, kilolines
 FTR mean thickness of rotor frame behind rotor lamination,
 in.
 FW windage loss at rotor speed (RPM), W
 FW1 windage loss at synchronous speed, W
 G airgap, in.
 GAMMA vector used in thermal analysis
 GAPREF reference gap for scaling windage loss, in.
 GE effective airgap, in.
 Gl part of horizontal extension of armature winding
 (Reference 1, p. 209, Fig. 135), in.
 HOMOG vector used in thermal analysis
 H12 equals H6
 H6 surface heat transfer coefficient, watts/°F-in.²
 HP shaft power, hp
 I subscript or index
 Il line current, A
 JA subscript or index
 IBAR rms current in one rotor bar, A
 ICNT1 counts number of iterations on R0 during no-load
 magnetic calculations

ICNT2	counts number of iterations on magnetizing current during no-load magnetic calculations
IMAG	magnetizing current, A
IMAG2	magnetizing current, A
INITL	common block name
J	subscript or index
JBAR	current density in rotor bar, A/in. ²
JRING	current density in endring, A/in. ²
J _{slot}	current density in the slot, in. ²
k	thermal conductivity, watts/°F-in.
KC	conductor thermal conductivities, watts/°F-in.
k _x	thermal conductivity in the x-direction, watts/°F-in.
k _y	thermal conductivity in the y-direction, watts/°F-in.
k _c	conductor thermal conductivity, watts/°F-in.
k _i	insulation thermal conductivity, watts/°F-in.
KDS	distribution factor for stat winding
KE	encapsulation thermal conductivity, watts/°F-in.
KEI	insulation thermal conductivity around slot conductor group, watts/°F-in.
KLX	lamination transverse thermal conductivity, watts/°F-in.
KLY	lamination axial thermal conductivity, watts/°F-in.
KODE	input to plotting routine PLOTXY
KPS	pitch factor for stator winding
KRING	correction factor for endring resistance (Reference 1, p. 334, Fig. 194)
KS	steel thermal conductivity, watts/°F-in.
KSS	slot leakage pitch factor (Reference 1, p. 185, Figure 7.3)
KSAT	saturation indicator
KT	index

L	stator core length, in.
LARM	total length of wire of armature winding, ft.
LAST	logical variable - LAST =.TRUE. - indicates last core-loss data card has been read
LB	length of rotor bar (including portion inserted in endring), in.
LEFS	length of stator end frame, in.
LREF	reference length for scaling windage loss, in.
LPROP	length of propeller hub, in.
LRYOKE	length of flux path through rotor yoke, in.
LS	length of one armature conductor (half of armature coil length), in.
LSYOKE	length of flux path through stator yoke, in.
LT	thickness of laminations at which core-loss data are given in material deck, in.
LTOTAL	overall axial armature length ($2 * \text{ENDTRN} + L$), in.
LTR	thickness of rotor laminations, in.
LTS	thickness of stator laminations, in.
MAG	common block name
MAGNET	subroutine name
n	propeller rpm
N	number of stator conductors in series per phase [$2 * (\text{number of stator turns in series per phase})$]
NB	number of rotor bars (equal to number of rotor slots)
NSYNCH	synchronous speed of motor, rpm
P	number of poles
PC	number of parallel circuits
PF	power factor
PFLUID	pressure of fluid in airgap, psi
PHAS	common block name
PHASE	if PHASE equals BCD BLANK, PF is lagging; if PHASE

equals *, PF is leading
 PHIR one-half of angle at which rotor slot sides diverge, deg
 PHIS one-half of angle at which rotor slot sides diverge, deg
 PIN power input to motor, W
 POUT output power available at motor shaft, W
 PP vector used in thermal analysis
 PPP vector used in thermal analysis
 PREF reference pressure of fluid in airgap used for scaling windage loss, psi
 Q heat input, watts/in.
 Q_o open water propeller torque, ft-lbs.
 QS number of stator slots
 R0 shunt resistance of equivalent circuit, ohms
 R0OLD value of R0 calculated during previous iteration pass, ohms
 R1 armature resistance, ohms
 R2 rotor resistance referred to stator winding, ohms
 R2BAR component of R2 attributable to rotor bars, ohms
 R2RIN component of R2 attributable to endrings, ohms
 R410 thermal resistance between stator core and gap, °F-in/watt
 R411 thermal resistance between stator endfram and overhang region, °F/watt
 R412 thermal resistance between stator core and backiron cooling water, °F-in/watt
 R810 thermal resistance between rotor core and gap, °F-in/watt
 R812 thermal resistance between rotor core and environment, °F-in/watt
 RATING NAMELIST name
 RATIO WSS4/WSS3 for trapezoidal stator slot; WSR4/WSR3 for trapezoidal rotor slot; DER2/DER1 for rotor-winding endring

RE1	thermal resistance between stator embedded winding and stator core, °F-in/watt
RE2	thermal resistance between stator endwinding and overhang region, °F-in/watt
RE3	thermal resistance between rotor bars and rotor core °F-in/watt
REQ1- REQ4	equivalent thermal resistance, °F/watt
RESET1	array made equivalent to common block INITL
RESET2	array made equivalent to first seven entries in common block CIR
RNAME	character variable equal to rotor name
ROTOR	NAMELIST name
RPM	rotor speed at slip S, rpm
RPMREF	reference RPM for scaling windage loss, rpm
RRSTVY	resistivity of rotor winding material at temperature TRW, μ in.-ohm
REAREA	rotor slot area, in. ²
RSLOTS	NAMELIST name
RSTVTY	array containing resistivity values for various rotor and stator winding materials at 27°C, μ in.-ohm
RSTYPE	rotor slot type
RTRWDG	NAMELIST name
RTWDTH	rotor tooth width (if constant), in.
RTWMAG	rotor tooth width used in magnetic calculations, in.
RWMAT	code for rotor winding material: 1 for aluminum; 2 for brass; 3 for copper
S	clearance between armature coils at end turns (Reference 1, p. 309, Table 26; and p. 209, Fig. 135), in.
SALPHA	sin(ALPHA) (Reference 1, p. 209, Figure 135)
SB	cross-sectional area of rotor bar, in. ²

SCAREA	slot area remaining after subtracting, from total slot area, slot opening and approximate areas occupied by slot liners, separators, wedges, etc., in. ²
SER	endring cross-sectional area, in. ²
SFR	rotor lamination stacking factor
SFS	stator lamination stacking factor
SKEW	skew of rotor slots measured along rotor circumference, in.
SLIP	array containing values of slip at which motor performance is calculated, percent
SLOPE	slope of core-loss-against-frequency curve (for constant flux density) on log-log graphs, measured at frequency FCORE and flux density BK
SLOTS	subroutine name
SMAT	dummy vector used in thermal analysis calculations
SMAX	maximum value of S for which motor performance is calculated, percent
*SNAME	character variable set equal to stator name
SOLD	previous value of S at which motor performance was calculated (used to calculate S at rated torque and to resume calculations at proper value of S following calculations at rated torque), percent
SPITCH	stator winding pitch expressed as a decimal fraction, per unit
SS	cross-sectional area of stator conductor, in. ²
SSAREA	total area of stator slot, in. ²
SSLOTS	NAMelist name
SSTYPE	stator slot type
STATOR	NAMelist name
STRNDS	number of strands per armature conductor
STRWDG	NAMelist name
STWDTH	stator tooth width (if constant), in.

STWMAG	stator tooth width used in magnetic calculations, in.
SUBVEC	vector used in thermal analysis
SWMAT	code for stator winding material: 1 for aluminum; 2 for brass; 3 for copper
T	propeller thrust, lbs.
T	shaft torque at slip S, in.-lb.
T1	stator winding temperature, °F
T4	stator core temperature, °F
T5	rotor bar temperature, °F
T8	rotor core temperature, °F
T1R	rotor slot pitch at airgap, in.
T1S	stator slot pitch at airgap, in.
TEN	thickness of the encapsulation, in.
TENGAP	thickness of metal liner in the gap, in.
TEFS	thickness of stator end fram, in.
T ₁₂	environment temperature, °F
TER	endring thickness, in.
TFLUID	temperature of fluid in motor cavity, °F
TITLE	array which contains name or description of design to be analyzed, used to print heading on output listing
TMPCF	array containing temperature coefficients of resistivity for various possible rotor and stator winding materials, per °F
TOLD	value of T at previous value of S, in.-lb.
TORQUE	array containing values of T corresponding to values of S stored in array SLIP, in.-lb.
TRATED	rated torque, in.-lb.
TREF	reference temperature for scaling windage loss, °F
TRW	temperature of rotor winding, °F
TSW	temperature of stator winding, °F

U spacing between stator conductors, in.
 UMAT [U] matrix
 V1 line-to-neutral voltage, rms volts
 V2 airgap voltage, rms volts
 V_o maximum line voltage, volts
 VMAT REAL*16 eigenvector matrix
 VVMAT REAL*8 eigenvector matrix
 VSCFLD viscosity of fluid in motor cavity, lbm/ft-sec
 VSCREF reference viscosity for scaling windage loss, lbm/ft-sec
 VSCSTY arithmetic statement function, $VSCSTY = C0 + C1 * T + C2 * T^{**2} + C3 * T^{**3} + C4 * T^{**4}$, where VSCSTY is fluid viscosity in lbm/ft-sec and T is fluid temperature in °F; C0 to C4 are program input
 W0 core loss, W
 W1 losses in armature winding, W
 W2 losses in armature winding, W
 WAREA array containing cross-sectional areas of standard wire gages, in.²
 WARM weight of armature (exclusive of insulation), lb.
 WBAR power loss in one rotor bar, W
 WCORE core loss for stator laminations at frequency FCORE and at flux density BK, W/lb
 WDGFACT subroutine name
 WEIGHT total electromagnetic weight, lb
 WFE core loss for stator laminations at frequency F and at flux density BK, W/lb
 WI REAL*16 imaginary eigenvalue vector
 WR REAL*16 real eigenvalue vector
 WL windage loss at reference conditions, W
 WNDAGE NAMELIST name

WRING	loss per endring, W
WROT	rotor iron weight, lb.
WRWNDG	weight of rotor winding, lb.
WSR	rotor slot width (if constant), in.
WSR1	width of rotor slot opening (for partially closed slot), in.
WSR2- WSR6	rotor slot dimension, in.
WSS	stator slot width (if constant), in.
WSS1	width of stator slot opening (for partially-closed slot), in.
WSS2- WSS6	stator slot dimension, in.
WSTAT	stator iron weight, lb.
WSTOTH	weight of stator teeth, lb.
WSYOKE	weight of stator yoke (back iron), lb.
WWI	REAL*8 imaginary eigenvalue vector
WWR	REAL*8 real eigenvalue vector
WX	individual stator conductor width, in. equals W_x
WY	individual stator conductor depth, in. equals W_y
X	state space vector used in thermal analysis
X0	magnetizing reactance, ohms
X0AG	magnetizing reactance of airgap only, ohms
X1	armature leakage reactance, ohms
X2	rotor leakage reactance referred to stator winding, ohms
XLGND	array containing legend printed to left of slip-torque plot

XP	peripheral airgap leakage reactance, ohms
XRE	rotor endturn leakage reactance, ohms
XRS	rotor slot leakage reactance, ohms
XRZ	rotor zigzag reactance, ohms
XSE	stator endturn leakage reactance, ohms
XSK	one-half of total skew reactance, ohms
XSS	stator slot leakage reactance, ohms
XSZ	stator zigzag reactance, ohms
XX	index used during no-load magnetic calculations: 1.0 if X0 is to be calculated; 0. if X0 was read in
XY	index used during no-load magnetic calculations: 1.0 if R0 is to be calculated; 0. if R0 was read in
XZ	multiplier for zigzag reactances
Z	axial coordinate along length of motor in REAL*16
ZZ	axial coordinate along length of motor in REAL*4 for plotting, in.
η_B	$\eta_o \eta_{rr}$
η_o	open water efficiency
η_{rr}	relative rotative efficiency
ρ	density, lbs/in. ³
ϕ_{max}	maximum flux, kilolines

Subroutine CIRCT

Definitions of those variables that are not listed are the same as in the main program.

A	real part of various complex variables
B	imaginary part of various complex variables
C	constant (C = 2.5)
D	determinant of coefficients of circuit equations

F1	complex input voltage to equivalent circuit (line-to-neutral input voltage to motor), rms
F2	complex voltage across shunt branch of equivalent circuit, rms
I2	current through Z2, A
IA	complex current through Z1, A
IB	complex current through Z2, A
IC	complex current through Z0, A
STAR	storage locations storing BCD character *
Z0	impedance of shunt branch of equivalent circuit, ohms
Z1	stator impedance, ohms
Z2	rotor impedance referred to stator, ohms

Subroutine MAGNET

Definitions of those variables that are not listed are the same as in the main program.

AT	ampere-turn drop across various sections of magnetic circuit, ampere-turns
NA	subscript
K	index
X	flux density at which AT is found by interpolation between points on magnetization curve, kilolines/in. ²
XX	slope of magnetization curve at flux density X
Y	used in interpolation procedure for AT

Subroutine SLOTS

Definitions of those variables that are not listed are the same as in the main program.

A	arithmetic function
A1	constant used in slot permeance ratio calculations

A2	constant used in slot permeance ratio calculations
AR	slot area needed for intermediate calculations for slot type 6 only, in. ²
AS	slot area needed for intermediate calculations for slot type 6 only, in. ²
AXX	slot leakage permeance ratio
CAREA	slot area remaining after subtracting slot opening, slot liners, separator, etc., in. ²
CAREA2	value of CAREA during a previous iteration pass (used with slot type 6 only)
COSPHI	cos (phi)
D	arithmetic function
D1X-D6X	slot dimension, in.
DIA	rotor outside diameter if SLTLOC=-1.0; stator inside diameter if SLTLOC=1.0, in.
DSX	slot dimension, in.
KX	equals 1.0 for rotor slots; equals slot leakage pitch factor for stator slots (Reference 1, p. 185, Fig. 7.3)
N	number of slots
PHIX	one-half of angle at which slot sides diverge (PHIX is negative for rotor slots, positive for stator slots), rad
SAREA	total slot area, in. ²
SINPHI	sin(phi)
SLOTS	subroutine name
SLTLOC	indicates slot location: 1.0 for stator slots; 1.0 for rotor slots
TANPHI	tan (phi)
W	slot dimension, in.
W1-W2	slot dimension, in.
WA	dummy variable used in arithmetic function definition
WB	arithmetic function

WSX slot dimension, in.

WSX1-
WSX6 slot dimension, in.

WSXA equals WSX for slot type 2; equals WSX2 for slot
types 4 and 6, in.

XSTYPE slot type

XTWDTH tooth width (for slot types 2, 4 and 6 only), in.

XTWMAG average tooth width used in magnetic calculations
in subroutine MAGNET, in.

Y1-Y2 slot dimension, in.

Subroutine WDGFACT

Definitions of those variables that are not listed are
the same as in the main program.

D constant: 1.0 for windings with phase belt less
than 60°; 2.0 for windings with phase belt greater
than 60°

DF distribution factor

FNQ real variable equal to IIQQ after fraction "slots
per pole per phase" has been reduced to lowest terms

I integer that is tested to see if it is a common divider
of fraction "slots per pole per phase"

IC number of parallel circuits (integer variable)

IDM multiple of IZY

IIQQ numerator of fraction "slots per pole per phase"

IPN number of phases (set equal to 3)

IPX number of poles (integer variable)

IQQ number of stator slots (integer variable)

IZY product of number of poles and number of phases

P number of poles (real variable)

PBA phase belt angle, deg

PC	number of parallel circuits (real variable)
PF	pitch factor
PN	number of phases (set equal to 3)
QN	number of stator slots per pole per phase
QS	number of stator slots (real variable)
WDGFCT	subroutine name
WDGPCH	stator winding pitch expressed as decimal fraction, per unit
YY	slots spanned per armature coil (number slots between coil sides plus 1)

Subroutine CMBNTN

Definitions of those variables that are not listed are the same as in the main program.

A	$3 * \text{FLOAT}(I) * P$, where $I=1,2,3,\dots, 1000$
CMBNTN	subroutine name
D	$\text{ABS}(QS-F)$
F	number of rotor bars
FF	rotor skew, expressed as fraction of rotor circumference, necessary to eliminate certain undesirable characteristics in torque-speed curve
I-Il	index
K	indicator (if $K=1$, the slot combination is found to be undesirable; the subroutine will then search for an alternate number of rotor slots)
L	F (L is an integer variable)
M	an indicator showing seriousness of an undesirable slot combination ($M=1$ is most serious; $M=3$ is least serious)
NB	number of rotor slots
P	number of poles
QS	number of stator slots
X	constant ($1.0E-15$)

Propeller Nomenclature

A_e/A_o	expanded area ratio
c	blade section chord length
CL	two-dimensional lift coefficient
CP	coefficient
CT	coefficient of thrust
DCP	differential coefficient of power
DCT	differential coefficient of thrust
D_p	propeller diameter = D
f	blade camber function
f_o	maximum blade section camber at a given radius
E	efficiency = η_o
G	circulation coefficients
h	depth, ft.
J	advance coefficient
K_Q	torque coefficient
K_T	thrust coefficient
n	propeller rotational speed, revolutions per unit time
N_b	number of blades
P_a	ambient pressure
P_v	vapor pressure
PI	propeller pitch = P
r	radial coordinate
r_H	hub radius
R_o	propeller radius
s	fraction of chord from leading edge
t	blade thickness function

UA^*- UA^*	axial and tangential velocities induced by helical tip vortices
$u_{an}(r)-$ $u_{tn}(r)$	axial and tangential induced velocities at blade trailing edge
V	total velocity
$V_A(r)$	axial component of inflow velocity = V_X
$V_R(r)$	radial component of inflow velocity
V_S	ship speed
$V_T(r)$	tangential component of inflow velocity
x	distance along chord for two-dimensional foils
x'	axial distance downstream of blade trailing edge along a given streamline
x_{ult}	distance downstream of blade trailing edge at which wake pitch stops changing
$x_m(r)$	rake, x-coordinate of midchord line, positive in direction of positive x
α	angle of attack
β	advance angle
β_i	hydrodynamic inflow angle
θ	angular coordinate in propeller fixed coordinates
$\theta_m(r)$	skew angle: angular coordinate of midchord line as measured from y-axis, positive clockwise when looking toward positive x-axis
τ	thickness ratio
ρ	mass density of fluid
$\sigma(r)$	section cavitation index
ϕ	nose-tail pitch angle of propeller blade section
ω	propeller rotational speed, radians per unit time

Main Program CURVES

AACDA	appendage area times drag coefficient, ft. ²
AAREA	aft body wetted surface area, ft. ²
AAWP	aft body waterplane area at each draft, ft. ²
AB	sail wetted surface area, ft. ²
ADISPI	aft body displacement for each draft, tons
AINERT	moment of inertia of aft body waterplane area at each draft, ft. ³
AKB	aft body vertical center of buoyancy, ft.
ALCB	aft body longitudinal center of buoyancy from nose of submarine, ft.
AREASM	sectional area times Simpson's multiplier, ft. ²
AREA	array containing underwater sectional area for each station, ft. ²
ARM	array containing moment arm for each station, ft.
AVOL	underwater volume of aft body for completely submerged submarine, ft. ³
AVOL1	underwater volume of aft body at each draft, ft. ³
AWP	array containing waterplane area at each draft, ft. ²
BM	metacentric radius for each draft, ft.
CAREA	array containing sectional areas at each station for each draft, ft. ²
CDB	sail drag coefficient
CF	array containing coefficient of friction at each speed chosen
CIRCUM	array containing circumferences of sectional hull at each station, ft.
CP	prismatic coefficient of submerged submarine

CR	form drag coefficient
CTBH	array containing bare hull coefficient of friction at each speed increment
CWS	wetted surface coefficient of submerged submarine
DELCF	ΔC_f , differential coefficient of friction accounting for surface roughness, imperfections, etc.
DISP	array containing displacement at each draft in question, tons
DRAFT	array containing drafts in feet, usually taken in one foot increments
EHP	array containing effective horsepower at each speed
FAREA	forebody wetted surface area
FAWP	forebody waterplane area at each draft, ft. ²
FDISP1	forebody displacement at each draft, tons
FINERT	moment of inertia of forebody waterplane area at each draft
FKB	forebody vertical center of buoyancy at each draft, ft.
FLCB	forebody longitudinal center of buoyancy, ft.
FM	multiplier used in computing LCB of forebody, ft. ²
FM	AREASM times station for each waterline
FDFA	a counter
FVOL	underwater volume of forebody for completely submerged submarine, ft. ³
FVOL1	underwater volume of forebody at each waterline, ft. ³
INERT	array containing moment of inertia at each station for each waterline
KB	array containing vertical centers of buoyancy for each draft, in.

LCB array containing longitudinal centers of buoyancy
for each draft, ft.

LENGTH overall length of the submarine, ft.

LPMB length of the parallel midbody, ft.

MOMENT sectional area times moment arm at each station
for each waterline

NU seawater kinematic viscosity at temperature being
used in computations, ft.²/sec.

OFFSET array containing offsets of hullform. Read in
as follows (in feet):

forebody OFFSET(1) STA 0
 OFFSET(2) STA 1/2
 OFFSET(13) STA 10
aftbody OFFSET(14) STA 10
 OFFSET(24) STA 0

PAREA parallel midbody wetted surface area, ft.²

PAWP parallel midbody waterplane area at each draft,
ft.²

PC assumed propulsive coefficient

PDISPl parallel midbody displacement at each draft, tons

PINERT moment of inertia of parallel midbody waterplane
area, ft.³

PKB parallel midbody vertical center of buoyancy at
each draft, ft.

PLCB parallel midbody longitudinal center of buoyancy
from nose of submarine, ft.

PVOL underwater volume of parallel midbody for com-
pletely submerged submarine, ft.³

PVOL1 underwater volume of parallel midbody at each
draft, ft.³

RN Reynold's number

SAB spacing between stations on aft body, ft.

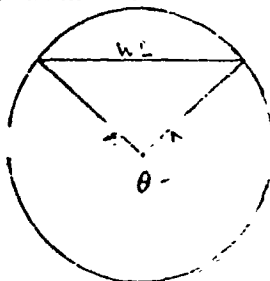
SFB spacing between stations on forebody, ft.

SHP array containing shaft horsepower at each speed

SIMPMT array containing Simpson's Multipliers as found
in DATA statement

STA individual stations on forebody and aft body as
shown in Figure 4.6

THETA array containing angle in degrees formed between
submarine metacenter and waterline for each
station as follows:



TOTLCB overall longitudinal center of buoyancy not
taking sail or appendages into account. From
nose, ft.

TVOL total underwater volume of completely submerged
submarine minus sail and appendages, ft.³

VK array containing speed in knots

VOL array containing underwater volume at each draft,
ft.³

WL length of sectional waterline, ft.

WSAREA overall wetted surface area of completely sub-
merged submarine, ft.²

Chapter One

INTRODUCTION

Submarine propulsion systems have generally been very similar to those found in surface vessels. The basic system usually consists of a prime mover such as a steam turbine, a geared reduction unit, a shaft and thrust and journal bearings coupled to a propeller. Alternately, especially in smaller submersibles, an internal electric motor can be substituted for the prime mover. Each of the elements that make up this system have been developed into highly reliable units. However, as with any system which is incorporated into a seagoing vessel, there are usually disadvantageous tradeoffs or weaknesses which limit system performance. The purpose of this thesis is to investigate the use of a large hub propeller powered by an externally mounted electric propulsion motor in an effort to improve these weaknesses.

It is often difficult to make major changes to a propulsion system because of the requirements to position the elements in some standard way. Precise alignment requirements of the turbines, gears, bearings, and shafting necessitates valuable volume allotments for internal arrangements within the submarine. Also, considerable structural weight must be added to support these equipments in their locations. This reason alone is the primary driving

force in eliminating the mechanical transmission system in favor of the easily arrangeable electric transmission system consisting of electric propulsion generators and motor. But again, these systems, depending on the particular study done, generally are heavier and less efficient than mechanical systems. A system such as is shown in Figure 1.1 would allow the primary propulsion machinery to be mounted exterior to the pressure hull and would offer sufficient arrangement flexibility. In addition, it may reduce the overall weight of the submarine.

In the area of shaft sealing systems, technology has been stretched to its limit in solving the problem of reducing the water flow rate into the submarine through the shaft hull penetration. As shaft diameters become larger with submarine propulsive power increases, conventional shaft sealing systems may present extensive maintenance problems. In any event, it would be a significant improvement in system complexity no matter what size submarine was being considered if the shaft and shaft sealing system were eliminated. Of course, the alternative being proposed here would introduce its own complexities. Would the tradeoffs be worth it?

Of significant concern to the submarine designer is the need to maintain an acoustic advantage over the enemy if a combat mission is being considered. Propeller noise generated by conventional propeller blades remains to be an

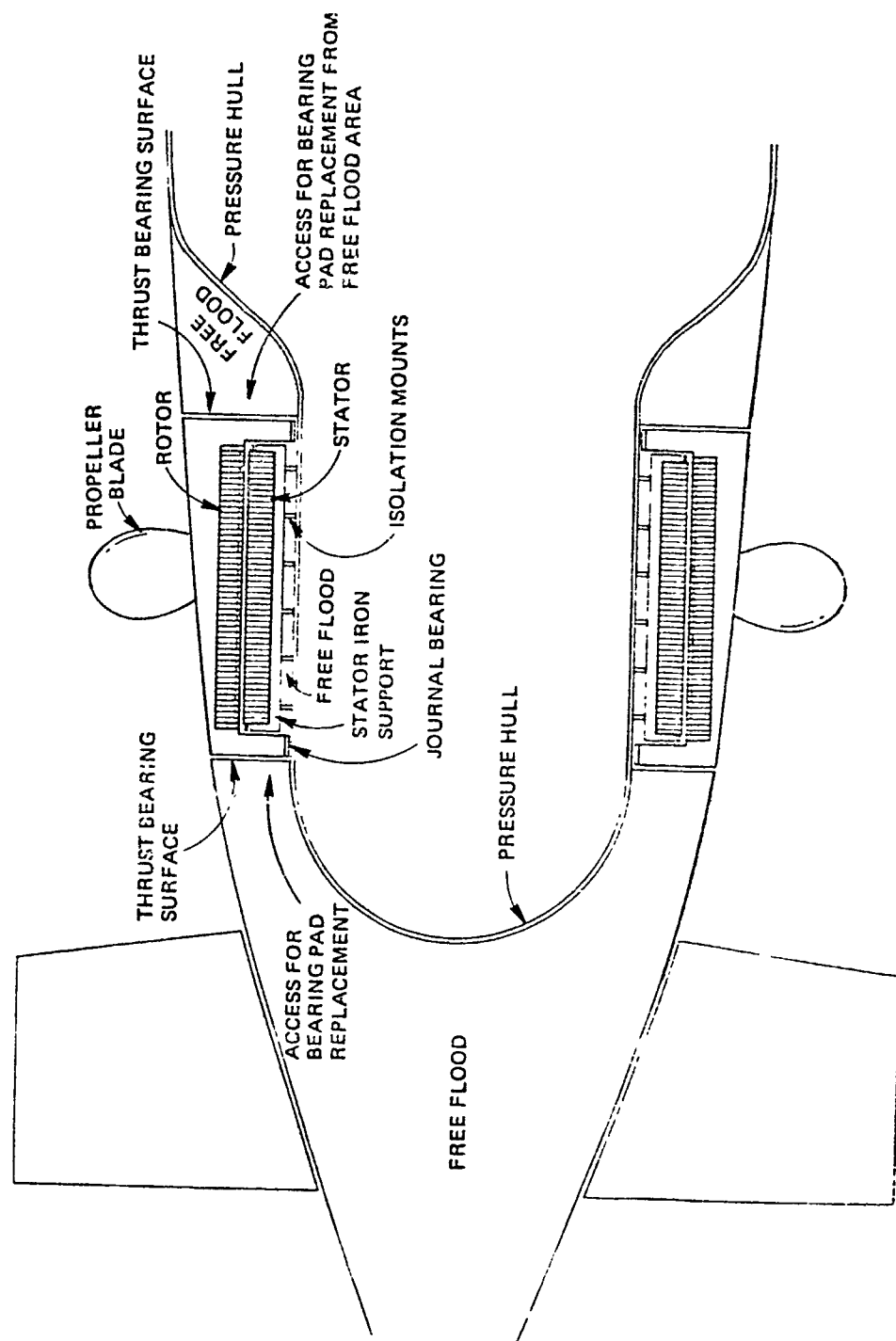


Figure 1.1

area of large concern despite efforts to reduce it. In its conventional location at the stern of the submarine, a screw propeller works in water that has been disturbed by the passage of the hull. In general, water particles that originally were motionless acquire velocities in the direction of ship motion. This forward moving water is called wake, and because of this the propeller does not advance in the water at the same speed as the submarine, V_k , but at some lower speed, V , called the speed of advance. The wake velocity at the propeller plane may be broken down into axial, tangential and radial components. These velocities are influenced by the stern appendages and asymmetries on the hull and usually vary radially and circumferentially. Figure 2 illustrates a typical flow velocity profile as seen at the propeller.

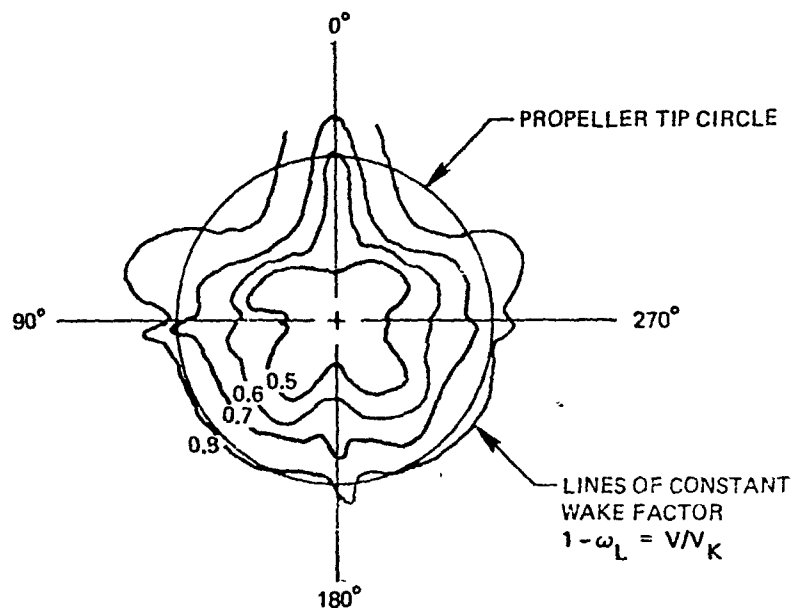


Figure 1.2

Thus, because of the submarine sail, rudder, and stern planes, nonuniform wake causes variations in the lift forces on the propeller blades. These in turn give rise to fluctuating thrust and torque on the propeller shaft. The end result is hull vibration, a primary source of noise generation. An even greater problem is set up when rudder or stern planes deflections are initiated. Hence, propeller noise significantly increases during submarine maneuvers. A large hub propeller mounted forward of the control surfaces would see an almost even flow velocity profile around its entire 360° periphery. Only the submarine sail, if one exists, would disturb the flow pattern. Boundary layer considerations and the velocity induced separation point would certainly continue to affect propeller performance; however, as is revealed later, propeller performance is improved. While the wake effect would remain (though reduced), noise generated due to inflow gradients would be significantly reduced.

Whereas ships have always required their rudders to be aft of the propellers for maneuverability reasons, submarines have not necessarily maintained this philosophy. After World War II, conventional fleet type submarines underwent the change from almost totally surfaced operations to totally submerged operations. In addition, the necessity

of having two propellers for highly maneuverable surface operations was removed when submarines began to totally operate at high speeds submerged. At high speeds, the control surfaces act much like the wings of an airplane in forcing submarine motion. The propeller backwash against the rudder is not needed when going fast enough. Consequently, since a single propeller with the control surfaces mounted forward of the propeller proved advantageous structurally, this concept was maintained despite its inherent noise problems. At low speeds, however, the lift forces on the control surfaces which are proportional to the square of the velocity are much smaller and maneuverability is significantly retarded. On a large combat submarine designed for high speed operations, this may not be a significant weakness. For smaller submersibles, however, especially those that are unmanned, tight turning characteristics at low speed may be of paramount importance. The large hub propeller concept then would permit greater flow velocity across the control surfaces mounted downstream and hence would improve overall maneuverability and controllability.

Propeller cavitation in addition to generating extremely large noise profiles creates large erosion problems on the blades themselves. With this erosion comes ever increasing blade noise, ultimately concluding in a very expensive

propeller changeout. Reduction of propeller cavitation can be achieved in one of two ways: increasing the water pressure by going deeper or reducing the blade tip velocity (or shaft RPM). The large hub propeller concept with a larger number of blades and a larger thrust area will allow much smaller propeller RPMs and improved cavitation performance.

With new designs in both manned and unmanned submarines ongoing, providing another form of propulsion may save weight and volume, improve propeller performance, reduce noise and cavitation, and improve maneuverability and controllability, but it is probably just as likely to present new challenges. This does not mean that one should abandon an idea. It is reasonable, however, to remain somewhat skeptical for any radical departure from tried and proven designs.

At this point, it is appropriate to list the good and bad factors as they appear to a designer about to embark on building such a system:

<u>Benefits</u>	<u>Challenges</u>
1. Eliminate shafting	1. Design induction motor
2. Eliminate shaft seals	2. Provide for thrust transmission
3. Increase arrangement flexibility	3. Provide for radial support

Benefits (cont.)

4. Eliminate reduction gears
5. Reduce propeller inflow variations caused by control surfaces ahead of propeller
6. Increase useful blade area
7. Reduce cavitation
8. Increase low speed controllability
9. Reduce propeller noise
10. Reduce maintenance
11. Natural sea water cooling
12. Possible improvement in propulsive coefficient

Challenges (cont.)

4. Provide electrical power
5. Determine blade shape
6. Design structures for loading
7. Seawater cooling
8. Encapsulation
9. Maintenance philosophy
10. Variable depth effects
11. Materials selection
12. Determining load curve
13. Side thrust problem?
14. If needed, develop shroud for protection and improved hydrodynamics performance

Undoubtedly the design of the induction motor offers the biggest challenge. As every aspect of the total system impacts on the electric motor in some way (and vice versa), a good understanding of the geometry, limitations, and function of the other aspects will have to certainly be understood. The first question to be asked is if the motor is even feasible in the first place. Can it provide the necessary power reliably without undue heating or breakdown? Is traditional thinking of always keeping equipments away from the corrosive and dangerous seawater environment sound? Or can the motor be properly protected via encapsulation or alternate insulation systems? The design of a propeller that will function

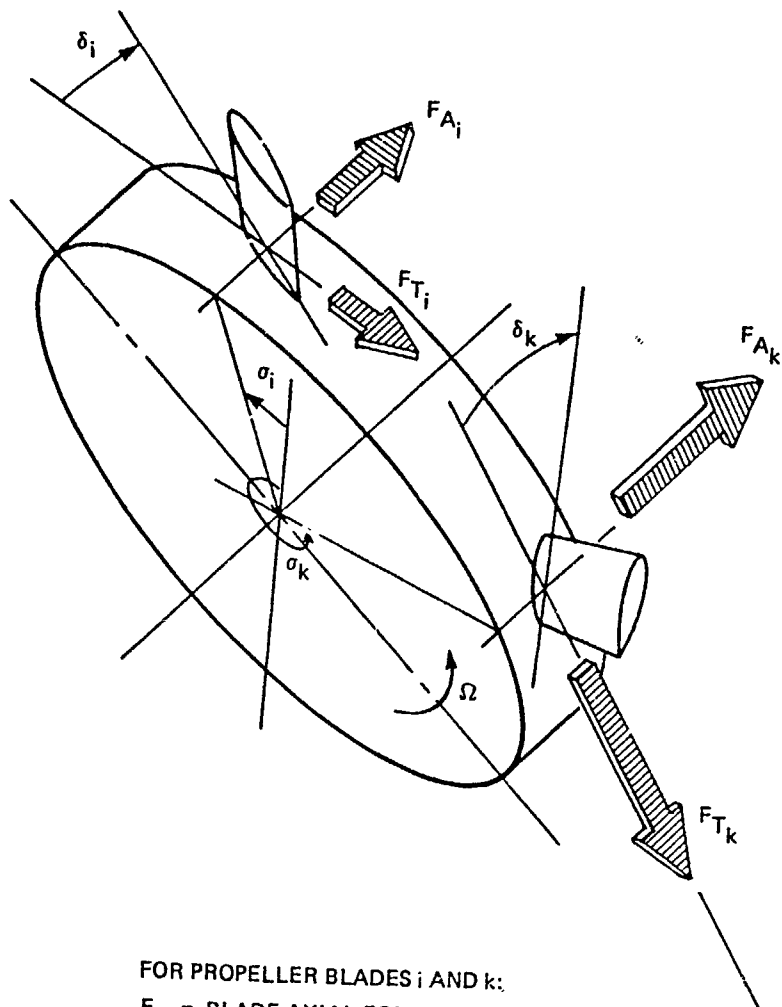
efficiently with the electric propulsion motor will also present some degree of challenge. Propeller design programs exist at M.I.T. but these have not been utilized for large hub ratios. At this point, there is some question as to just how the propeller is to be matched with the motor and under what constraints it is to be designed. These are areas that this thesis will address in assessing the externally-mounted electric propulsion system concept.

Chapter Two

BACKGROUND

Early in the 1960s a great deal of work was performed on two new submarine propulsion concepts based on a patent issued in 1963 to LCDR F. R. Haselton, U.S.N. Both systems utilized large hub propellers as the primary means of propulsion.

The tandem propeller submarine (TPS) illustrated in Reference 40 utilized a pair of large hub to diameter ratio propellers, one located near the bow and the other near the stern of the vehicle. Of particular significance in addition to the position of the propellers and the way in which these were mounted was the fact that the pitch of the blades could be varied collectively as well as cyclically and that the propellers rotated in opposite directions in order to produce any desired combination of forces and moments. As applied to this system, the blades of each propeller were collectively variable (all blades assume the same angle) or they were cyclically variable (each blade assumed an incremental angle as a function of its instantaneous position around the propeller periphery with respect to horizontal and vertical axes). Thus, the forces illustrated in Figure 2.1³⁹ were used for both propulsion and maneuvering of the buoyant vehicle by programmed control of the pitch angle, δ , as a function of the rotation angle, σ . Note how the magnitudes of F_{A_k} and F_{T_k} are increased over F_{A_i} and F_{T_i} due to a large blade angle of attack ($\delta_k > \delta_i$).



FOR PROPELLER BLADES i AND k :
 F_A = BLADE AXIAL FORCE (THRUST)
 F_T = BLADE TRANSVERSE FORCE (DRAG)
 δ = BLADE PITCH ANGLE
 σ = BLADE ANGULAR POSITION ON HUB

Figure 2.1

Six degrees of motion could then be realized without the use of any control surfaces. That is, the rudder, fair-water planes, and stern planes on conventional submarines could be removed as they were not required for control. This permitted significant appendage resistance reductions with a consequent increase in maximum speed given the same amount of shaft horsepower.

The Tandem Propeller Submarine research program, under the guidance of the Office of Naval Research, culminated in four years of research studies by the following organizations:

- 1) Electric Boat Division of General Dynamics in association with the General Electric Co. and the Elliott Co. on propulsion machinery;
- 2) David Taylor Naval Ship Research and Development Center (DTNSRDC) on captive model tests;
- 3) Honeywell on manual controllability;
- 4) Netherlands Ship Model Basin(NSMB) on propeller design and fabrication of the basic model;
- 5) Cornell Aeronautical Laboratory on hydrodynamics and stability and control.

Much of the work done by these groups is proprietary in nature. Nevertheless, the literature does contain a great deal of information and lessons learned from the research performed.^{30,31,39,40}

In October, 1961, a feasibility study was initiated by the NSMB on propellers with large hub to diameter ratio and cyclic pitch control. The purpose of this research

was to investigate the efficiency of such a device, the excitation of transverse forces by the propeller due to cyclic pitch changes and finally the power required for generating a certain transverse force. From the experimental results the following conclusions could be drawn:

- a. the maximum propulsion efficiency is of the same order as obtained with more conventional propeller types with small hubs;
- b. the transverse forces do not decrease with increasing velocity;
- c. the direction of the transverse forces changes by an appreciable amount when the velocity is increased.

With the promising results of this study, the NSMB started in October, 1962 with the design and manufacture of a 13-1/2 foot submarine model with two (forward and aft) large hub to diameter ratio propellers with programmed blade control. References 30 and 40 contain further illustrations and descriptions of this model. A listing of the model's pertinent physical characteristics is as follows:

Length:	13.45 feet
Center of buoyancy:	5.95 feet
Maximum hull diameter:	1.97 feet
Length/diameter ratio:	6.83
Propeller tip diameter:	1.61 feet
Displacement:	1500 lbs.
Blade characteristics--	
Number/propeller:	12
Chord:	.885 inches
Length:	1.77 inches
Description	16% thickness, symmetrical
Collective pitch angle	
operating point:	
(nominal)	30 degrees
Collective pitch angle range:	+ 10 degrees
Cyclic pitch angle range:	+ 25 degrees
Propeller speed:	200 RPM

Hydrodynamic tests were then conducted both at NSMB and at DTNSRDC. Some of the significant conclusions are listed below:

- 1) The forward rotor was a turbulent flow promotor.
- 2) It would be very difficult to determine ad hoc the optimum shroud shapes that provide maximum efficiencies as a function of the design variables (hub to diameter ratio, propeller loading, etc.).
- 3) Any generation of side forces due to maneuvering under cyclic pitch operation resulted in a decrease in thrust and an increase in propeller torque.
- 4) Though the propellers were identical in configuration, their relative locations produced performance deviations. For example, the magnitude of the total transverse force generated by the forward propeller of the submarine is, if compared with the aft propeller, much smaller. Also, the aft propeller, due to the wake effect, produces larger thrust values for high values of the advance ratio.
- 5) The maximum propulsion efficiency of the forward or aft propeller would be in the region of 50-55% at a value of 1.3 advance ratio. These maximum efficiencies are lower than that which could be achieved on a single aft-mounted propeller.
- 6) The magnitude of the transverse forces is for low values of advance ratio, equal to approximately 10% of the thrust and increases by an appreciable amount if the

velocity is increased.

7) The presence of a shroud does not have a large effect on the magnitude of the side forces.

8) The submarine without rudder, stern planes and fairwater planes was dynamically unstable in straight and level flight.

9) Turning moments utilizing cyclic pitch control at high speeds were considerably less than those achievable with conventional control surfaces.

Most of these hydrodynamic conclusions lead one to believe that the TPS would be an extremely complex system to design, build and test on a full scale. From a mechanical viewpoint, the hydraulic system for variable and cyclic pitch control would not be a trivial matter. Furthermore, maintenance may be extremely frequent.

Simplifying TPS to a single aft, large hub propeller mounted forward of the rudder and stern planes would certainly present advantages. At about the same time that TPS was being evaluated by the U. S. Navy, General Dynamics Corporation's Electric Boat Division was evaluating another concept -- NEPPS (Novel Electric Power Propulsion System).³⁷ This system is illustrated in Figure 2.2.

NEPPS consisted of a pair of free flooding AC motors, the rotors of which rotate around the stators. Segments of the envelope of the hull formed the outer housings of the rotors and rotated with them. Propeller blades were

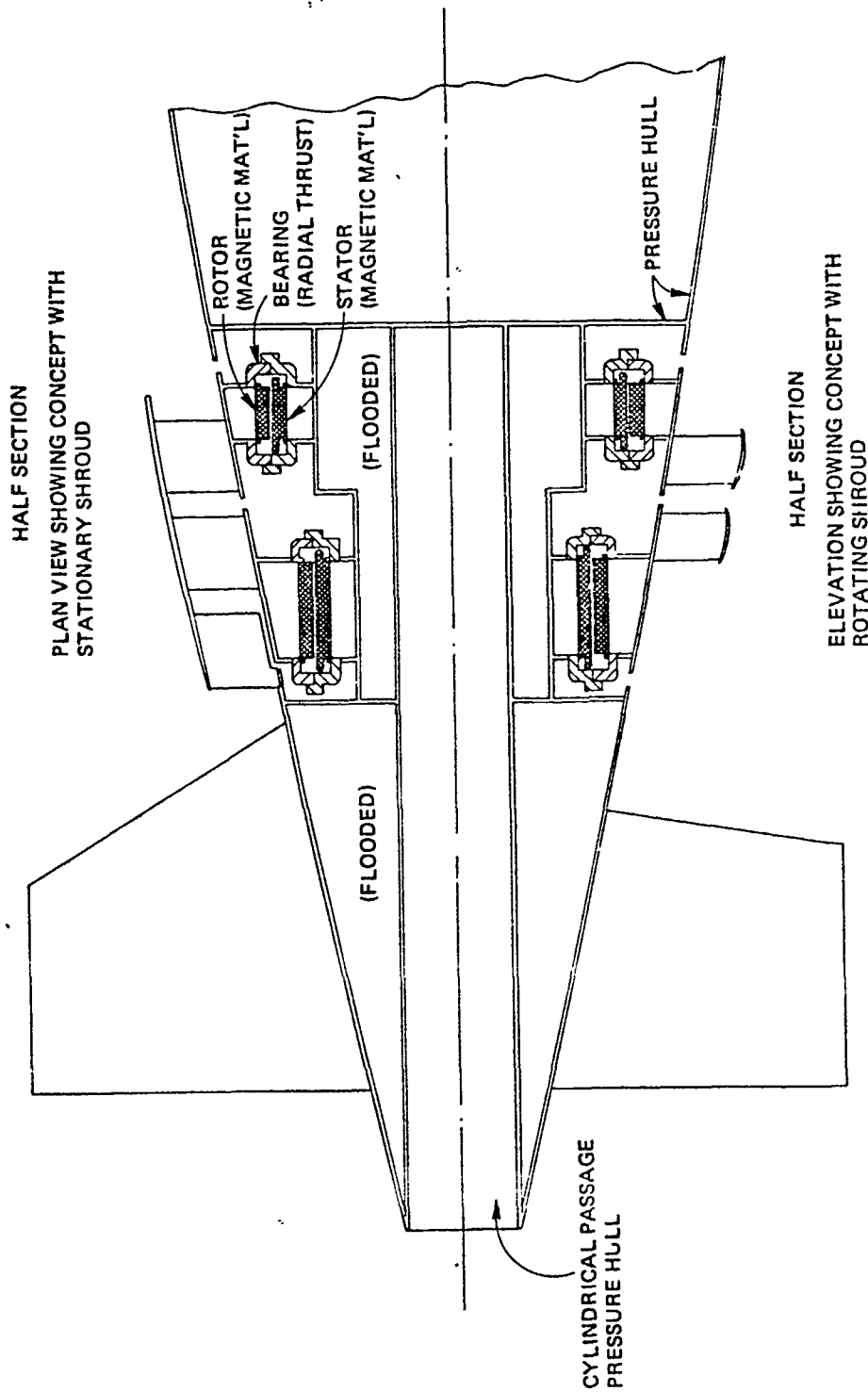


Figure 2.2

mounted on the rotating segments of the hull and comprised a pair of counter-rotating propellers. Noteworthy, however, is the fact that these propellers were not variable or cyclic pitch. That is, they had fixed pitch. To support their hydrodynamic work, General Dynamics constructed a 1/28 scale model, the stern of which is illustrated in Reference 42. Other particulars on the model include:

Length:	10.71 feet	
Diameter:	14.75 in.	
Length/diameter ratio:	8.71	
<u>Propeller Geometry</u>	<u>Fwd</u>	<u>Aft</u>
Tip diameter (ft):	1.004	0.882
Hub diameter (ft):	.829	0.695
Number of blades:	9	7
Root cord (ft):	0.074	0.0948
Tip chord:	0.033	0.042
Thickness ratio (t/c):	0.1	0.1
Blade form:	NACA 65 Series	

Electrical and mechanical research work done on NEPPS is proprietary in nature and not available in the literature. Hydrodynamic results, however, led to the following conclusions:

- 1) Comparison of model cavitation data indicated that the cavitation performance of the NEPPS propeller was better than that of the conventional propeller. The superior

propulsor cavitation performance indicated that the NEPPS prototype would have a better overall acoustic quality than a conventional propeller-driven submarine.

2) Tests made at zero advance speed both for forward and reverse propulsor rotation indicated very good reverse thrust characteristics, the reverse thrust being 78% of the forward thrust.

3) The propulsive coefficient, based on the power at the blades of the model, was 0.90. This efficiency was 3% less than predicted; however, this reduction resulted in a change in speed of less than half a knot.

4) The NEPPS prototype submarine would attain a speed of approximately 24 knots, which was approximately 1.3 knots less than was predicted.

These conclusions are obviously noteworthy since they characterize the large hub propeller as a better overall performer than the conventional propeller. Of course, in areas such as ease of construction, ease of repair and transverse force generation, questions remain unanswered.

With the introduction of these two concepts from the past, one obviously wonders why no submarine to date, large or small, has ever utilized the large hub propeller concept. Certainly TPS suffered from undue complexity. Its advantages of maneuvering without control surfaces and elimination of the need for a shaft and shaft seal just could not outweigh the projected weight increase (both in the

motor and structural support) and the very large reduction in ship turning moment above six knots compared to the conventional rudder reaction forces. A motor efficiency of 78% also was estimated by the Electric Boat Division of General Dynamics. This cannot compare to conventional gear trains which have efficiencies well above 90%.

The exact reason for NEPPS' demise is not clear. Without a doubt, it appears as a more viable concept than TPS. Fixed pitch propeller blades eliminate hydraulic complexities, and counter-rotating propellers reduce, but do not eliminate, side thrust problems. One can speculate however, upon studying Figure 2.2, that structural impacts on the submarine were large, but more importantly, the motor designed suffered. It is well known that the power density of any electrical machine can be described analytically as follows⁴:

$$D^2 L = a_2 \left(\frac{P}{n} \right)^{0.65}$$

where, D = airgap diameter
L = rotor active length
P = power output
n = rotational speed (rpm)
a₂ = an empirical constant

While the motors have very large diameters, they are very limited in length. In fact, the length parameter if one motor was used could probably be doubled. The two-motor concept illustrated would only be able then to generate

one-half as much power as one motor. Also noteworthy in Figure 2.2 is the extremely small bearing surfaces and the lack of any forced cooling water flow to keep these surfaces clear of seawater particles. The pressure hull could not have the sharp corners illustrated at structural junctions and still maintain its original operating depth characteristics. Finally, it seems unlikely that the cylindrical pressure hull could extend all the way to the stern and still maintain proper control surface linkage mechanisms.

With this background, Figure 1.1 is presented as an option that may make the large hub propeller competitive in future design scenarios for manned and unmanned submersibles. The large hub propeller by itself has indeed proven itself to be competitive. The intent there is to investigate more precisely the limitations in the induction motor design and its incorporation with a single large hub propeller.

Chapter Three

TEMPERATURE RISE CONSIDERATIONS

Development of a steady state heat transfer model was given heavy emphasis since any induction motor employed in a propulsive mode as proposed here would operate at high power densities. As an example,¹⁷ consider a propulsion motor development for a submarine approximately 300 feet in length and 30 feet in diameter. Frictional drag calculations utilizing a maximum speed constraint of 30 knots would require a typical output power of 30,000 shaft horsepower. Making additional assumptions that:

1. Maximum magnetic flux density = $B_m = 100 \frac{\text{kilolines}}{\text{sq. in.}}$
2. Maximum RPM = 60 RPM = $2 \times (\text{NSYNCH})/60$
radians/sec = ω

it becomes possible for the geometry considered in this thesis to calculate power:

$$\begin{aligned} P &= \text{traction surface area} \times \text{moment arm} \times \text{average} \\ &\quad \text{traction stress} \times \omega \\ &= 2\pi \left(\frac{DS}{2} \right) L \times \left(\frac{DS}{2} \right) \times \langle T_\theta \rangle \times \omega \end{aligned} \quad (3.1)$$

where DS = stator diameter (in.)

L = stator length (in.)

P = output power (watts)

It can be shown that the average traction stress is approximately one-half the maximum magnetic flux density, B_m , times the maximum surface current density, K_s . To express the maximum surface current density in terms of the maximum current density in each individual conductor in a stator slot, consider the following:

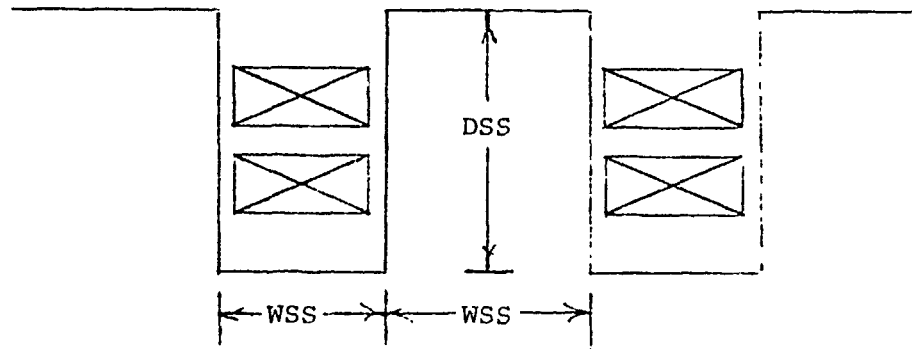


Figure 3.1

Define the ratio of the slot width to the slot pitch to be λ_p which in this case is:

$$\lambda_p = \frac{WSS}{WSS + WSS} = \frac{1}{2} \quad (3.2)$$

Also define the ratio of the slot copper area to the overall slot area to be λ_s . Thus:

$$\lambda_s = \frac{A_{cu}}{A_{slot}} \approx 0.5 \quad (3.3)$$

If the slot current density is represented as J_{slot} then it follows that:

$$K_s = \lambda_s \lambda_p (DSS) J_{\text{slot}} \quad (3.4)$$

Substituting and solving (3.1) for J_{slot} :

$$J_{\text{slot}} = \frac{4P}{\pi (DS)^2 L B_m \lambda_s \lambda_p (DSS) \omega} \quad (3.5)$$

Some typical values that may be seen for an electric propulsion motor on a large U. S. Navy submarine are:

$$DS = 180 \text{ in.}$$

$$L = 100 \text{ in.}$$

$$B_m = 100 \text{ kilolines/in.}^2$$

$$DSS = 2.5 \text{ in.}$$

$$P = 22 \times 10^6 \text{ watts}$$

$$\omega = 2 \text{ rad/sec}$$

Inserting these values into (5), a current density as seen in the copper of approximately 2200 amps/in.² can be obtained. The literature contains guides for the designer in the preliminary planning stages for what this maximum current density can be. Still and Siskind⁵ quote 1700 amps/in.² for low speed machines and 3500 amps/in.² for high speed machines. The induction motor proposed here will be ultra slow but still will be completely unique in that it will be water-cooled.

Thus, while the above current density calculation is somewhat crude, it does raise some question as to whether the motor can eliminate the heat it is generating without coil destruction. The purpose then of this chapter will be to develop a computer analysis that will allow calculation of the motor hot spot temperatures for various operating conditions. The most important operating point will be at locked rotor where maximum currents are generated.

In order to obtain the expected hot spots in the induction motor, it is necessary to construct a thermal model. From this model the equations necessary for the computer subroutine RESIST.FOR are obtained. With RESIST.FOR, coupled to the main program, INDUC.FOR, it becomes possible to check if a given design as input in INDUC.DAT meets the standard requirements on temperature rises in electrical machinery.

The model put forth by Perez^{13,14} will be used primarily along with Reference 16 to elaborate the thermal model. The first step is the choice of an idealized machine geometry (Figures 3.2, 3.3) and the division of the machine into basic thermal elements or nodes (Figure 3.4). Then at each node an equation expressing the conservation of energy at each node can be written. Assuming steady state conditions:

$$L_i = Q_i + C_i + R_i, \quad i = 1, \dots, N \quad (3.6)$$

where,

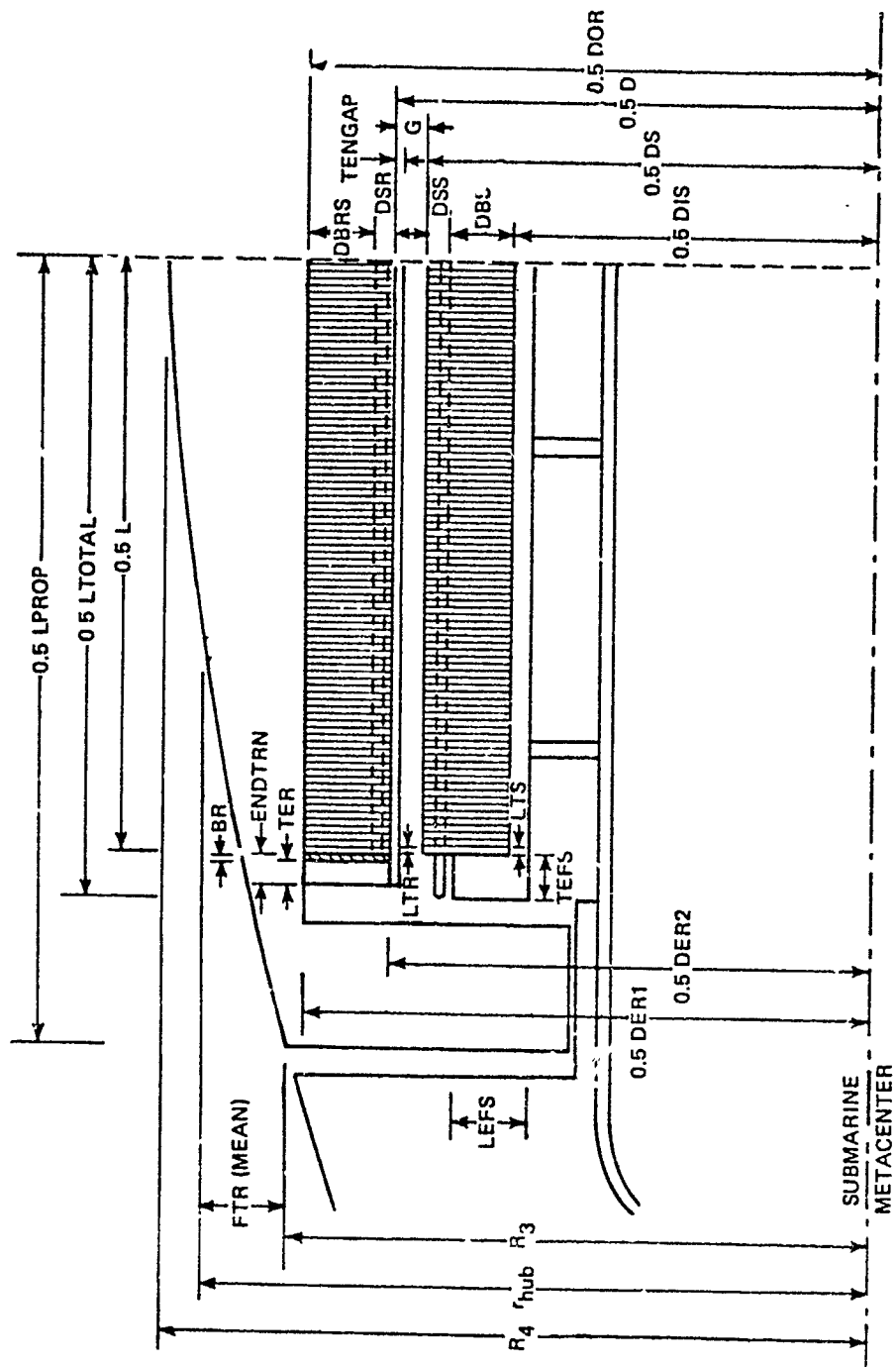


Figure 3.2 (a.)

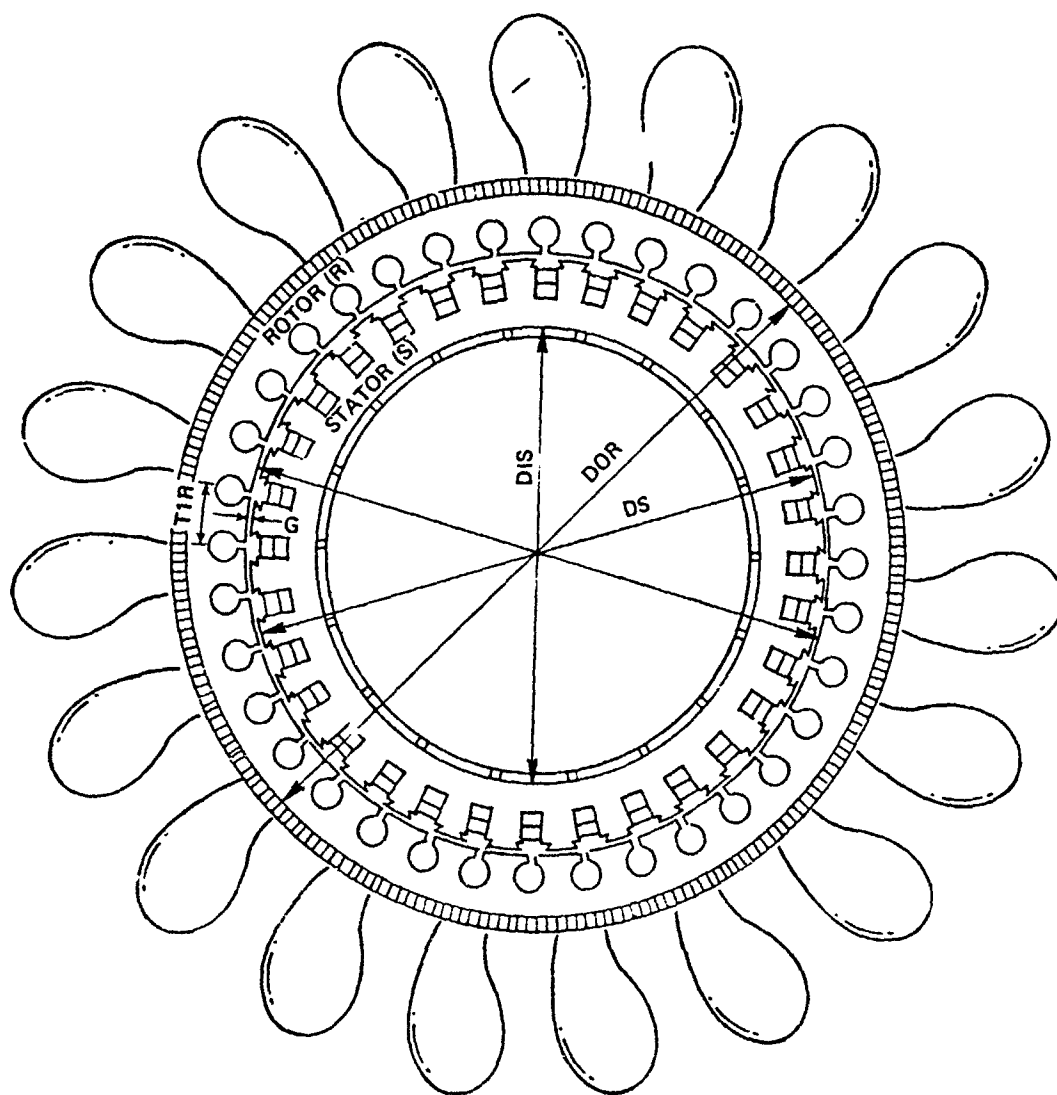


Figure 3.2 (b.)

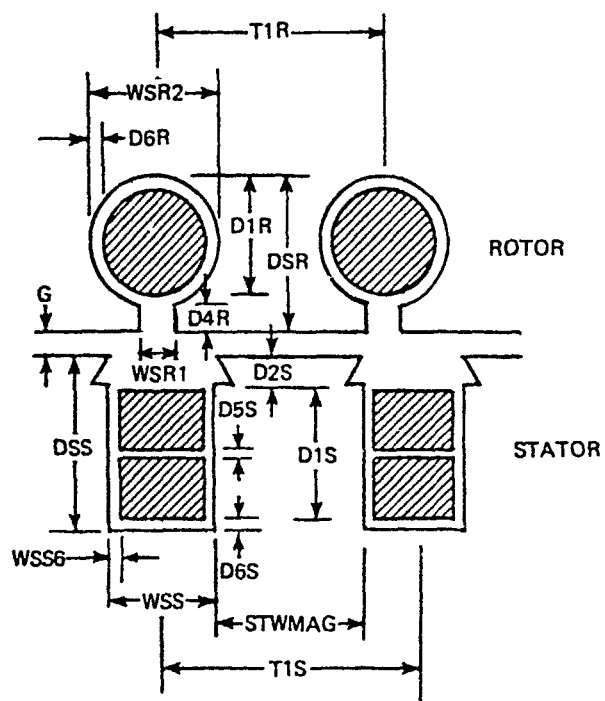
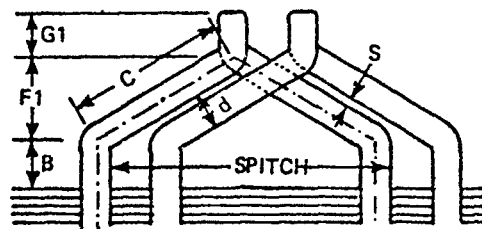


Figure 3.3

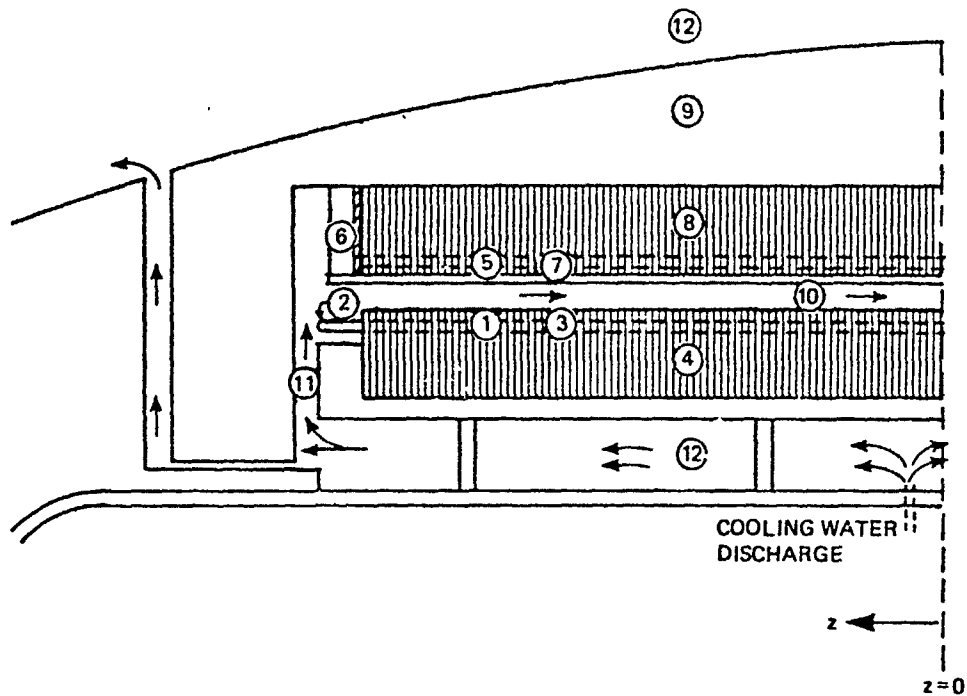


Figure 3.4

N = number of elements

L_i = rate of heat produced at element i

Q_i = rate of heat flow from element i by conduction

C_i = rate of heat flow from element i by convection

R_i = rate of heat flow from element i by radiation

A heat exchange map (Figure 3.5) is set up illustrating the heat flux paths between the basic elements into which the machine is divided. In this initial thermal model, many assumptions will be made in order to simplify matters. Ideally, when further refinements are necessary, or after a final configuration is obtained, more detailed analysis procedures can be used such as finite difference techniques. In any case, where assumptions are made they will be conservative so as to make the node temperature higher than what it would be in reality. In this way the designer establishes an upper bound on the temperatures. If he can make this upper bound within design specifications, then actual temperatures will be well within the safe range. If this upper bound is much too high then he knows that he cannot drive the motor as hard or he must provide greater cooling.

The model presented here does not attempt to be valid for all types of rotating machines. Rather for the idealized induction motor presented in Figure 3.2, the following features have been assumed:

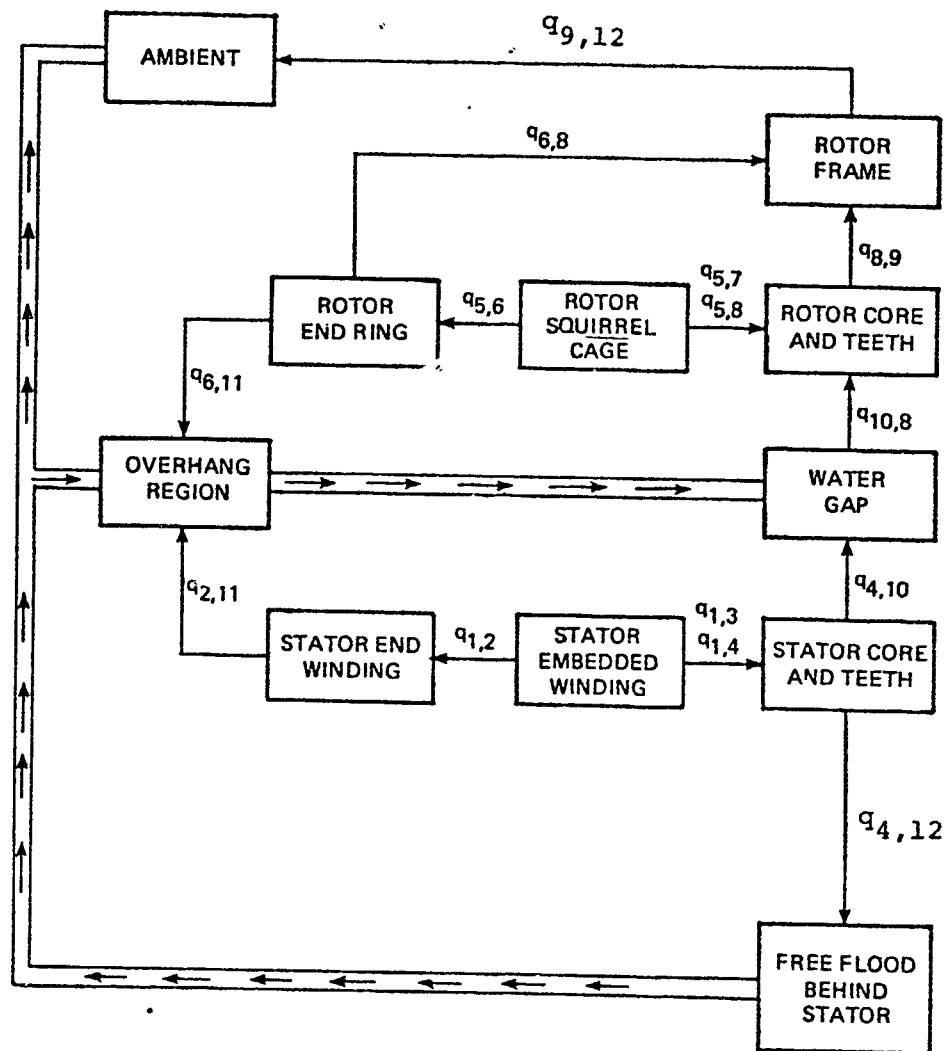


Figure 3.5

- a) Wound stator and solid rotor;
- b) Axially symmetric cooling system (same temperature distribution at both ends of the machine);
- c) The contribution of radiation to the total cooling of the machine will be assumed small (much less than 5%) and, thus, will be ignored. To include it later in the model, see Reference 13.

Additional assumptions will be presented, as appropriate, in the model development to follow.

A. Conduction Mode

Fourier's law for the steady flow in one dimension of heat by conduction can be expressed in differential form by

$$\left(\frac{Q}{A}\right)_{i,j} = -k_{i,j} \left(\frac{dT}{dy}\right), \quad \begin{matrix} i = 1, \dots, 14 \\ j = 1, \dots, 14 \end{matrix} \quad (3.7)$$

or for isotropic materials where the gradient of T is linear,

$$\left(\frac{Q}{A}\right)_{i,j} = -k_{i,j} \left[\frac{T_i - T_j}{y_i - y_j} \right] \quad (3.8)$$

where,

+Q = heat flow into element (watts)

A = cross sectional area (in.²)

k = thermal conductivity of the medium (watt/in.°F)

T = temperature (°F)

y = a distance (in.)

The heat transfer process may be compared by analogy with the flow of electricity in an electrical resistance. The flow of heat, Q , as a result of a temperature difference, $T_i - T_j$, is analogous to the flow of electric current, I , as a result of an electrical potential difference, $E_i - E_j$. From Ohm's law for electricity,

$$R_{\text{elect}} = \frac{E_i - E_j}{I} \quad (3.9)$$

and by analogy a heat transfer resistance may be defined as

$$R_{\text{thermal}} = \frac{T_i - T_j}{Q} \quad (3.10)$$

It can then be shown¹⁶ for the following cases:

$$\text{Infinite flat plate: } R = \frac{l}{kA} \quad (3.11)$$

$$\text{Infinite cylinder: } R = \frac{\ln(r_2/r_1)}{2k} \quad (3.12)$$

$$\text{Surface to fluid: } R = \frac{1}{Ah} \quad (3.13)$$

where,

l, A = length and cross sectional area of the element, respectively

r_2, r_1 = outer and inner radius, respectively

h = surface heat transfer coefficient (watt/in² °F)

k = thermal conductivity (watt/in. °F)

If heat flow takes place in more than one direction, Laplace's equation in the form

$$\nabla^2 T = 0 \quad (3.14)$$

must be solved with appropriate boundary conditions for the particular case. A network of thermal resistances will then be found that will approximately reproduce the heat flow through the element. In the development to follow, assumptions and simplifications will be made that reduce all heat fluxes to unidimensional flows thereby allowing appropriate thermal resistances to be computed.

The heat inputs to the different elements of the system are known from the outset. That is, heat will be generated in the stator winding, stator core, rotor bars, and rotor core and nowhere else. These heat inputs will be obtained in the main program INDUC.FOR and will be known for any prescribed operating condition. From these heat input sites, heat will flow according to the heat exchange map shown in Figure 3.5. Heat generated in the journal bearings and thrust bearing will not be considered here but should be added after design of the bearings has been formulated. It is also assumed that no conservative adjustments will need to be made since any heat generated in the bearings will be almost entirely removed through convective cooling water flow. Every element whose temperature has to be calculated will be represented in the equivalent circuit by one node, so that the node temperature coincides with the mean temperature of the element. The only temperature known at the outset is the ambient temperature. Thus, once the resistive network is known, heat fluxes and node temperatures are computed analytically.

From Figure 3.5 it becomes possible to convert the thermal model to an equivalent network with element nodes and thermal resistances, Figure 3.6. However, closer scrutiny of the problem at hand will reveal a discrepancy in the modeling process that was assumed for Figure 3.6. Several of the node temperatures are not constant values but vary with z along the axial length of the machine. For example, since the thermal conductivity of the stack of laminations in the transverse direction is roughly 30 times higher than in the axial direction, the temperature of every single lamination will be assumed uniform. Thus, $T_3 = T_4$ for each lamination and likewise for nodes 7 and 8, $T_7 = T_8$. In the axial direction, however, the temperature from lamination to lamination is changing. Thus, T_4 is a function of z , being a maximum at the very center of the machine ($z = 0$). Similarly, T_1 , T_3 , T_5 , T_7 and T_8 are also assumed functions of z . Heat flow will be assumed purely radial through the rotor frame; hence concerns over T_9 being a function of z need not be addressed. The goal of this chapter then is to greatly simplify Figure 3.6 and to introduce node temperatures that are a function of z . The ultimate result can be seen in Figure 3.22. The development to follow illustrates how this simplification was obtained and the inherent assumptions that were made.

It must be emphasized that in order to develop a thermal resistive network that represents heat transfer between constant temperature nodes, these temperatures must be the mean

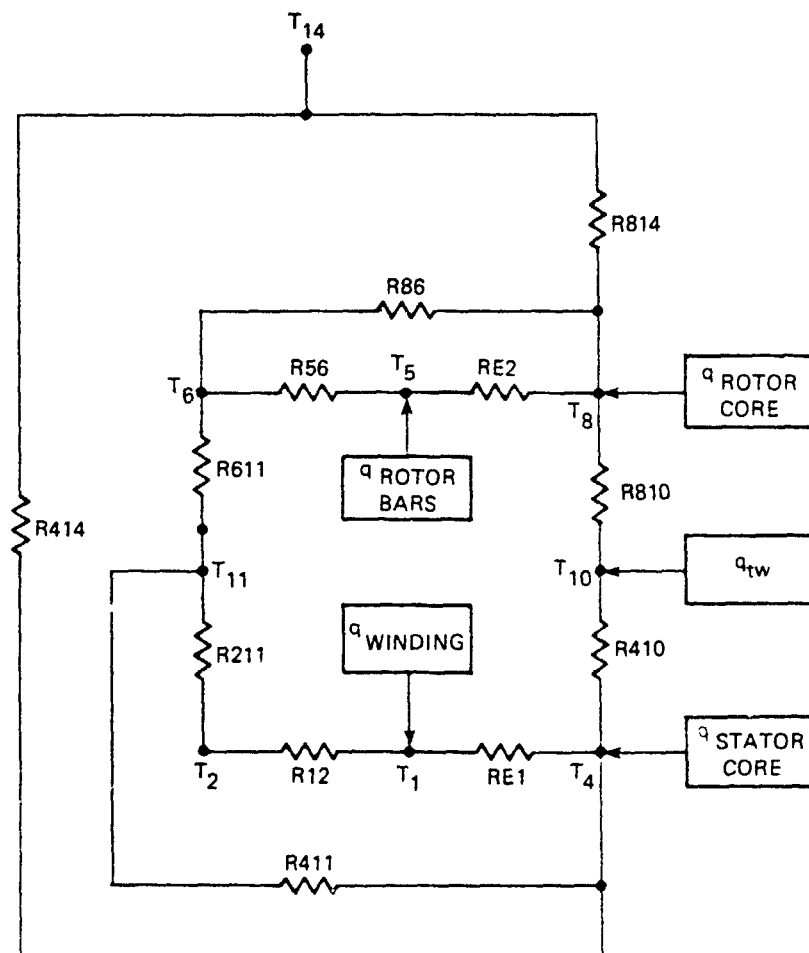


Figure 3.6

temperatures of the corresponding element. From one-dimensional and two-dimensional models of the conduction process, it becomes possible to take this mean temperature and obtain the entire temperature distribution along the element as a function of z .

B. One-dimensional bulk conduction

Consider the following model for one-dimensional heat conduction:

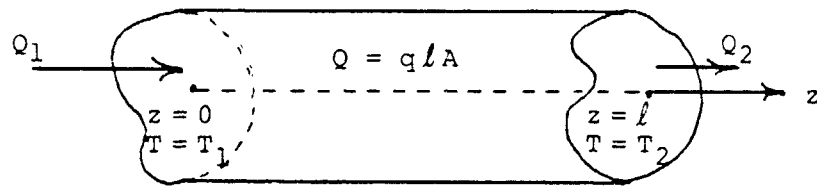


Figure 3.7 One-dimensional heat conduction.

Here the temperatures at any perpendicular cross section are assumed to be uniform and the lateral surface is perfectly isolated thermally. From

$$-k \frac{d^2 T}{dz^2} = q, \quad (3.15)$$

Perez¹³ shows that:

$$T(x) = \frac{Qz(l-z)}{2k l A} + \frac{(T_2 - T_1)z}{l} + T_1, \quad (3.16)$$

$$Q_1 = -\frac{Q}{2} + \frac{kA(T_1 - T_2)}{l} , \quad (3.17)$$

$$Q_2 = \frac{Q}{2} + \frac{kA(T_1 - T_2)}{l} , \quad (3.18)$$

$$T_{\max} = \frac{Ql}{8kA} + \frac{kA(T_2 - T_1)^2}{2Ql} + \frac{T_2 + T_1}{2} , \quad (3.19)$$

$$T_{\text{av}} = \frac{T_1 + T_2}{2} + \frac{Ql}{12kA} . \quad (3.20)$$

The network in Figure 3.8 is an attempt to model thermally the element in Figure 3.7. The resistances R_1 , R_2 and R_3 will be determined in order to match the following conditions for any T_1 , T_2 and Q :

$$T_{\text{av}} = T_1 - R_1 Q_1 + R_3 Q = \frac{T_1 + T_2}{2} + \frac{Ql}{12kA} , \quad (3.21)$$

$$T_{\text{av}} = T_2 + R_2 Q_2 + R_3 Q = \frac{T_1 + T_2}{2} + \frac{Ql}{12kA} . \quad (3.22)$$

The coefficients of T_1 , T_2 and Q at both sides of these expressions have to be identical. This is satisfied for the following values of the resistances:

$$R_2 = R_1 = \frac{l}{2kA} , \quad (3.23)$$

$$R_3 = \frac{-l}{6kA} . \quad (3.24)$$

If a reference resistance, R_0 , is defined as

$$R_0 = \frac{l}{kA} , \quad (3.25)$$

the resistances can be written as:

$$R_2 = R_1 = \frac{R_O}{2} \quad , \quad (3.26)$$

$$R_3 = \frac{-R_O}{6} \quad . \quad (3.27)$$

In Figure 3.8, note that Q is heat being generated in the differential element and Q_1 and Q_2 are heat fluxes passing through the element. The center node is imaginary and represents the point where the three heat fluxes join.

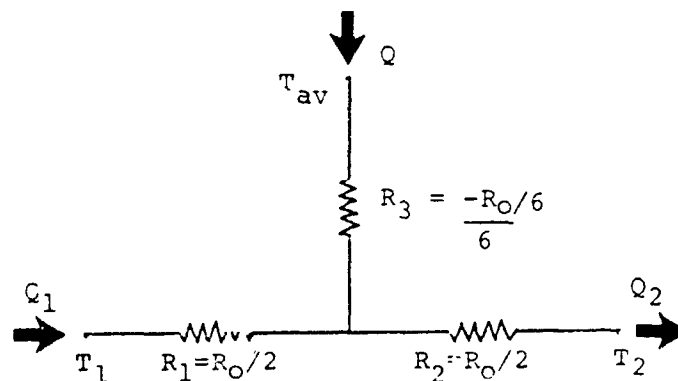


Figure 3.8 Equivalent network for one-dimensional heat conduction

In the case where there are no I^2R losses or hysteresis or eddy current losses within the differential element, then $Q = 0$ and Figure 3.8 reduces to:

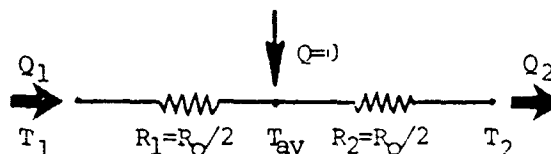


Figure 3.9

This is a case that represents simple one-dimensional heat transfer between two nodes, for example, nodes 4 and 11. Thus between two nodes where no internal heat is generated, the equivalent thermal resistance is $R_1 + R_2$ or R_0 . From T_{av} in Figure 3.9, the temperature T_{max} can be obtained from Eq. (3.19).

Figure 3.10 shows the important particular case of the network in Figure 3.8 for situations in which $T_1 = T_2 = T_0$:

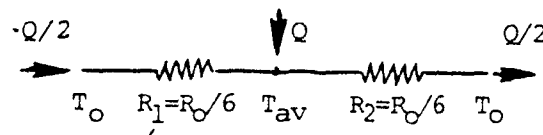


Figure 3.10

In this case,

$$R_1 = R_2 = \frac{R_0}{2} + 2\left(\frac{-R_0}{6}\right) = \frac{R_0}{6} \quad (3.28)$$

Thus, Figure 3.10 presents the situation where no externally imposed heat transfer passes through the element; rather, only internally imposed heat is generated which travels out to equal temperature regions. This case will not be used by itself in the upcoming analysis. It will, however, be combined with Figure 3.8 to obtain a general two-dimensional thermal model.

C. Two-dimensional bulk conduction

Consider the following model for two-dimensional heat conduction:

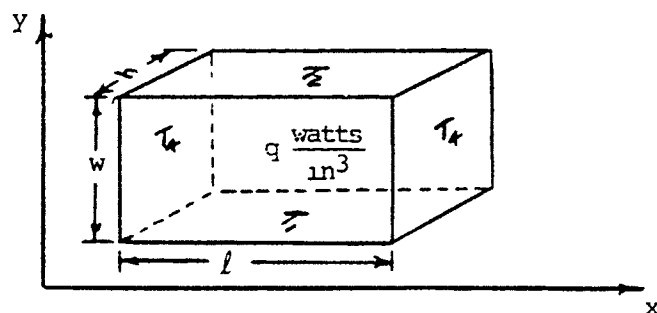


Figure 3.11 Two dimensional heat conduction.

In this case, heat flow takes place only in the x and y directions. There is also internal heat generation that is assumed to be uniformly distributed, the rate being $+q$ watts/in³ when the heat is considered to enter the model. For the case where there is net heat conduction due to external sources only in the y direction ($T_3 = T_4 = T_0$ and $T_1 \neq T_2$), an equivalent thermal network is obtained and is shown in Figure 3.12.

In this approximate model, the heat flows in the two main directions are assumed to be completely independent and the mean temperature of the element along both directions is the same. Also in this model:

$$R_{ox} = \frac{l}{k_x w h} \quad (3.29)$$

$$R_{oy} = \frac{w}{k_y l h} \quad (3.30)$$

$$Q = qwh \quad (3.31)$$

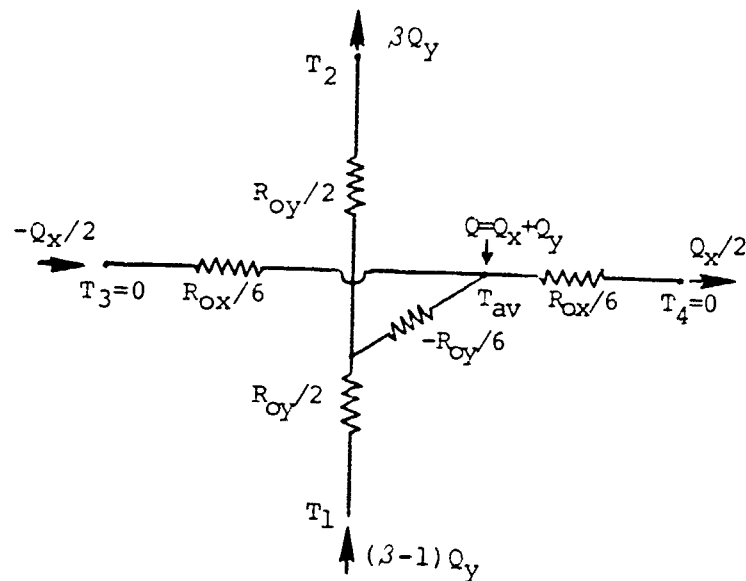


Figure 3.12 Equivalent network for two-dimensional heat conduction

Again from this model, Perez has shown that:

$$Q = Q_x + Q_y \quad (3.32)$$

$$T_{av_x} = T_{av_y} = T_0 + \frac{Q_x l}{12k_x h w} = \frac{T_1 + T_2}{2} + \frac{Q_y w}{12k_y h l} \quad (3.33)$$

$$Q_x = \frac{k_x w^2 Q + (6T_1 + 6T_2 - 12T_0) h l w k_x k_y}{l^2 k_y + w^2 k_x} \quad (3.34)$$

$$Q_y = \frac{k_y l^2 Q - (6T_1 + 6T_2 - 12T_0) h l w k_x k_y}{2k_y + w^2 k_x} \quad (3.35)$$

$$T_{max_x} = T_{av_x} + \frac{1}{2} (T_{av_x} - T_0) \quad (3.36)$$

$$T_{max_y} = \frac{Q_y w}{8k_y l h} + \frac{k_y l h}{2w Q_y} (T_2 - T_1)^2 + \frac{T_2 - T_1}{2} \quad (3.37)$$

The assumption of setting $T_{av_x} = T_{av_y}$ yields $T_{max_x} = T_{max_y}$ in general. The element hot spot temperature, to be on the conservative side, will be taken as the maximum of T_{max_x} and T_{max_y} .

D. The model for the stator winding

It has already been stated that the temperature of the embedded stator winding varies axially in the z direction being a maximum at the center of the machine ($z = 0$). Also, because it is assumed that each lamination is a uniform temperature throughout, then the same temperature exists at both sides of the slot ($T_3 = T_4$). This fact allows one to

model the transverse heat flow in one stator slot as the two-dimensional heat flow case illustrated in Figure 3.12. The purpose of this section is two-fold:

- 1) By first assuming that there is no heat flow in the axial direction, a model will be developed which presents the parameters per unit of axial length;
- 2) With a per unit length transverse thermal resistance computed, axial temperature variation will then be introduced.

Since each slot carries an identical winding distribution to all other slots, and because there exists a geometric repetition of conductor and insulator in the slot, an equivalent medium with respect to the thermal conductivities can be developed for the entire winding.

In the development to follow, several assumptions have been adopted:

- a) All the wires have the same insulation;
- b) The thickness t of every insulation is uniform around every wire.
- c) No air gaps are present.
- d) The thickness of the peripheral insulation is uniform for every direction.
- e) There is no heat flow through the wedge.

- f) Heat flow in the x direction will be represented by a thermal conductivity, k_x , and heat flow in the y direction will be represented by a thermal conductivity, k_y .

Initially, general variable terms will be used to develop the model. Later, variables to be used in the computer program will be substituted.

In a general case, an equivalent slot cross section is shown below:

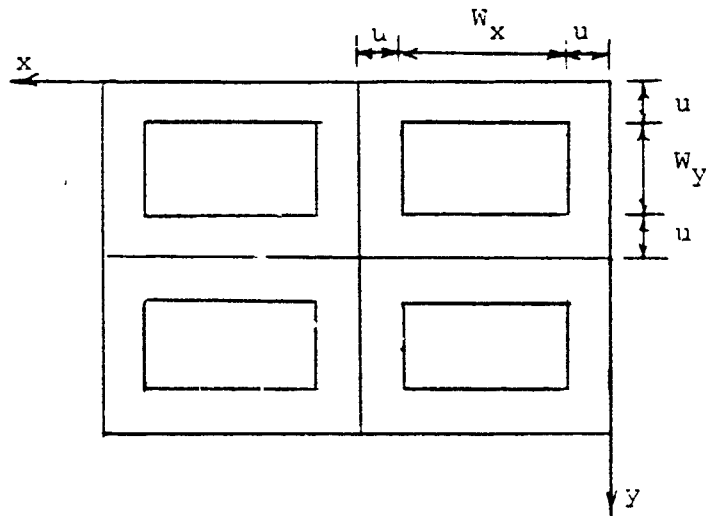


Figure 3.13

Now it is assumed that for heat flow in the vertical (y) direction, the horizontal (xz) planes are isothermals. Likewise for heat flow in the horizontal (x) direction, the vertical planes (yz) are considered isothermals. This allows

the thermal resistances of one generalized element for heat flow in the two main directions to be calculated in a straightforward manner:

$$R_x = \frac{2u}{(k_1)(w_y + 2u)(1)} + \frac{w_x}{(k_1)(2u)(1) + (k_c)(w_y)(1)} \quad (3.38)$$

$$R_y = \frac{2u}{(k_1)(w_x + 2u)(1)} + \frac{w_y}{(k_1)(2u)(1) + (k_c)(w_x)(1)} \quad (3.39)$$

where unit depth in the z-direction has been assumed. These resistances can be written in another way by introducing a fictitious homogeneous medium represented by equivalent thermal conductivities, k_x and k_y , as follows:

$$R_x = \frac{w_x + 2u}{(k_x)(w_y + 2u)(1)} \quad (3.40)$$

$$R_y = \frac{w_y + 2u}{(k_y)(w_x + 2u)(1)} \quad (3.41)$$

It then easily follows that k_x and k_y can be written in terms of k_1 and k_c by simultaneous solution of the above equations. If the further simplification of k_c being considered infinite is made, then it follows:

$$k_x = k_1 \left(1 + \frac{w_x}{2u} \right) \quad (3.42)$$

$$k_y = k_1 \left(1 + \frac{w_y}{2u} \right) \quad (3.43)$$

These two general expressions for thermal conductivity in terms of specific insulation thermal conductivity and slot geometry will be used later in the computation for the transverse winding resistance.

In order to develop a thermal model for the entire stator winding, a fictitious piece of winding has been devised which summarizes the whole stator:

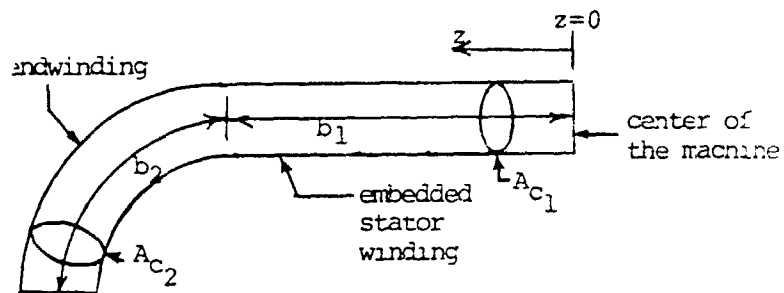


Figure 3.14

Each turn of a bunch of wires can be divided into four parts. Because of symmetry about the machine axial center point, only two of these parts need to be considered as shown in Figure 3.14. Since there are QS total slots making up the stator winding, then there are $2XQS$ elements making up the embedded part of the winding and $2XQS$ elements making up the endwinding. For the electric propulsion motor, it will

be assumed that A_{C1} equals A_{C2} and these quantities are equivalent to:

$$A_c = 2(QS)(CSS)(SS) \quad (3.44)$$

The lengths of the elements in terms of computer variables also follows:

$$b_1 = L/2 \quad (3.45)$$

$$b_2 = 0.5(LS - L) \quad (3.46)$$

Let q_1 and q_2 equal $2XQS$ times the total internal heat input per unit length to the parts 1 or 2 of the bunch of wires corresponding to one slot. Hence,

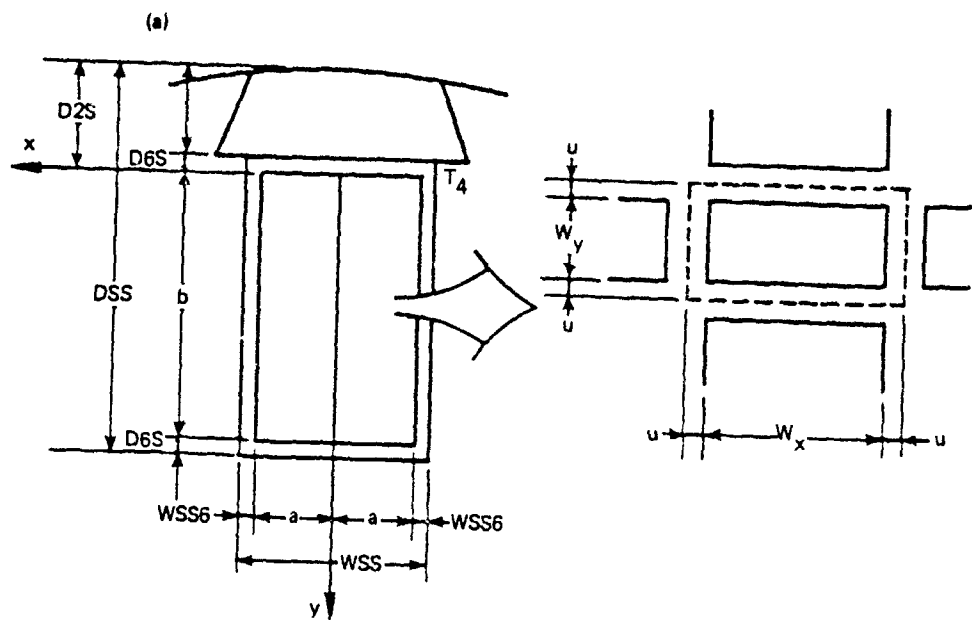
$$\begin{aligned} q_1 = q_2 &= \frac{1}{b_1 + b_2} \text{ (copper losses in whole winding)} \quad (3.47) \\ &= \frac{wl}{b_1 + b_2} \\ &= q_{\text{winding}} \end{aligned}$$

An overall thermal resistance, R , per unit of axial length, between the winding (represented as usual by the spot with the mean temperature T_{lav}) and the lamination at temperature T_4 is:

$$R_{\text{overall}} = \frac{T_{lav} - T_4}{Q} = \frac{1}{2(QS)} R_{\text{for the bunch in one slot}} = REL \quad (3.48)$$

It should be noticed that the quantities Q , T_4 , T_{lav} and T_{max} can change along the axial direction (different transverse sections). However, the overall resistance parameter, REl , defined above is invariant along the axial direction as long as the geometrical dimensions of the slot do not change. In the electrical analogy, this means that if, for example, each lamination and each differential element of winding is represented as a voltage node, then the resistance between nodes would be the same. An electrical resistor's resistance to a first approximation is not a function of the voltage across it or the current flowing through it.

Figure 3.15 shows the cross section to be modeled. For the embedded part of the winding there is no thermal resistance between the exterior surface of the external layer of insulation and the environment (the laminations). Also, there is no heat flow across the x (because of the wedge) and y (because of the azimuthal symmetry) axis. Therefore, the configuration can be studied with a two-dimensional conduction model with uniformly-distributed internal heat input and no external heat input. Figure 3.15(b) gives the approximate equivalent network for the transverse heat flow. The values for the resistances are the following (the first expression being in terms of Figure 3.15, the second term being in terms of computer program variables):



(b.)

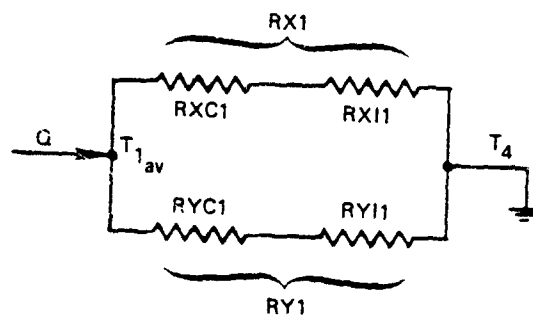


Figure 3.15

$$RXC1 = \frac{1}{2(QS)} \times \frac{a}{(6b)(KX)} = \frac{1}{2(QS)} \times \frac{0.5[WSS-2(WSS6)]}{6(D1S)(KX)} \quad (3.49)$$

$$RYC1 = \frac{1}{2(QS)} \times \frac{b}{(6a)(KY)} = \frac{1}{2(QS)} \times \frac{D1S}{3[WSS-2(WSS6)]KY} \quad (3.50)$$

$$RXI1 = \frac{1}{2(QS)} \times \frac{1}{2} \times \frac{WSS6}{(b)(KEI)} = \frac{1}{2(QS)} \times \frac{WSS6}{(D1S)(KEI)} \quad (3.51)$$

$$RYI1 = \frac{1}{2(QS)} \times \frac{D6S}{(2a)(KEI)} = \frac{1}{2(QS)} \times \frac{D6S}{[WSS-2(WSS6)]KEI} \quad (3.52)$$

$$RX1 = RXC1 + RXI1 \quad (3.53)$$

$$RY1 = RYC1 + RYI1 \quad (3.54)$$

where:

$$KX = KI \left(1 + \frac{WX}{2u} \right) \quad (3.55)$$

$$KY = KI \left(1 + \frac{WY}{2u} \right) \quad (3.56)$$

At first these equations may not be obvious. However, the network in Figure 3.15(b) can be developed directly from the more general case of Figure 3.10. This can be seen from the series of illustrations shown in Figure 3.16. The bunch of conductors can be considered to be one-half of the configuration shown in Figure 3.16(a). Its equivalent circuit can be obtained from Figure 3.12 by setting $T_1 = T_2$ and $T_3 = T_4$, and has been represented by Figure 3.16(b). It can be further simplified into Figure 3.16(c) which is equivalent, as far as T_{av} is concerned, to the circuit in Figure 3.16(d),

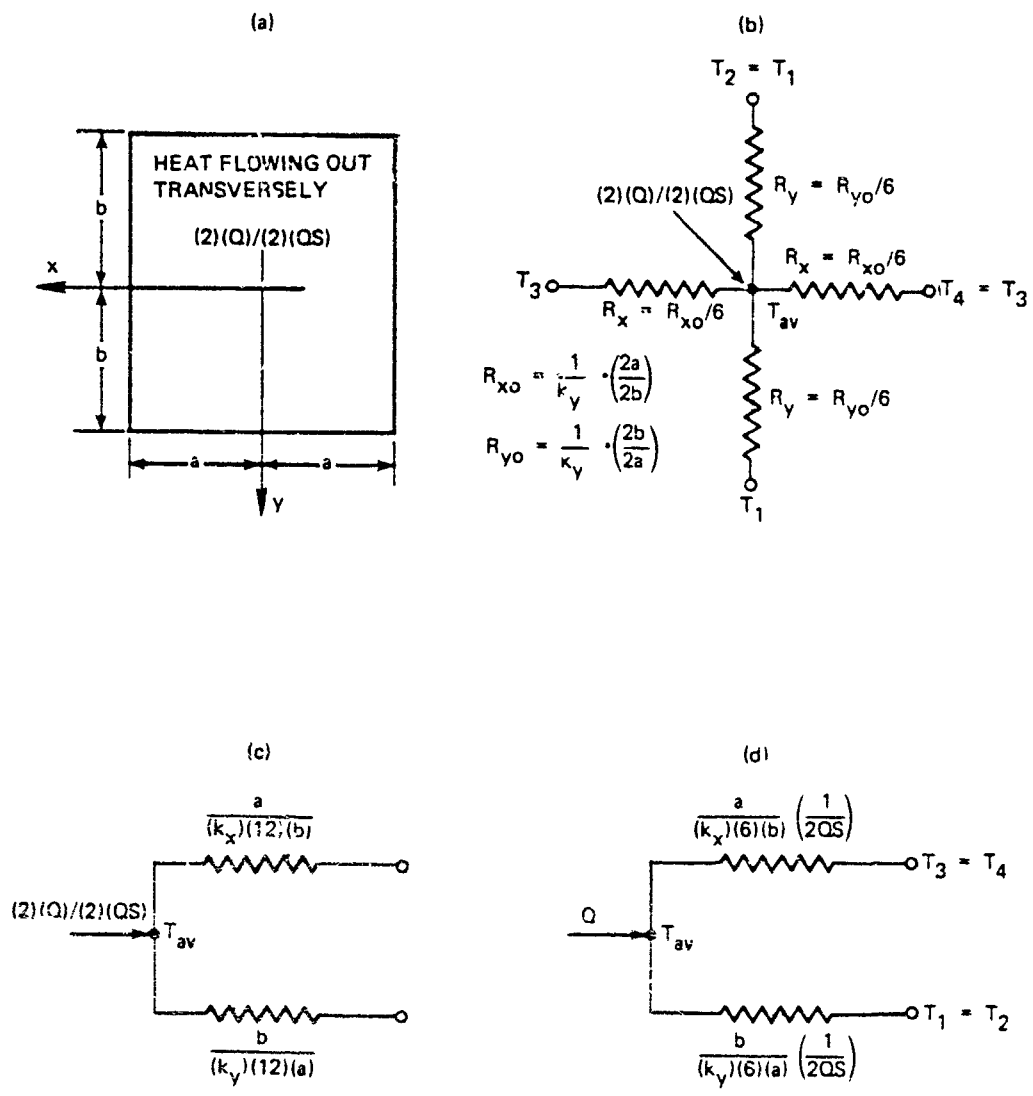


Figure 3.16

giving the values of $RXC1$ and $RYC1$. The resistances $RXI1$ and $RYI1$ are just the thermal resistances offered by the external layer of insulation in the directions x and y :

$$RXI1 = \left[\frac{WSS6}{(b)(KEI)} \right] // \left[\frac{WSS6}{(b)(KEI)} \right] \quad (3.57)$$

$$RYI1 = \frac{D6S}{(2a)(KEI)} \quad (3.58)$$

which again must be divided by $2XQS$.

To obtain the mean and maximum temperatures of the cross section, Eq. (3.33), (3.36) and (3.37) could be used directly. For this particular case, however, where there is no externally-imposed heat flow, the expressions obtained by Soderberg⁵³ are applicable and will be used here since they provide better accuracy:

$$T_{lav} = T_4 + \frac{(Q)(RX1)(RY1)}{RX1 + RY1} \left[1 - \frac{(RXC1)(RYC1)}{5(RX1)(RY1)} \right] \quad (3.59)$$

$$T_{lmax} = T_4 + \frac{(Q)(RXI1 + 1.5RXC1)(RYI1 + 1.5RYC1)}{RX1 + RY1} \left[1 - \frac{3(RXC1)(RYC1)}{(RX1)(RY1)} \right] \quad (3.60)$$

It thus follows that

$$RE1 = \frac{T_{lav} - T_4}{Q} = \frac{(RX1 + RY1)}{(RX1)(RY1)} \left[1 - \frac{(RXC1)(RYC1)}{5(RX1)(RY1)} \right] \quad (3.61)$$

This important thermal resistance is computed in the subroutine RESIST.FOR.

At this point, it becomes necessary to model the transverse conduction phenomenon at the end part of the winding, that is, the part of the stator winding exposed to seawater. Previously, an expression for the overall transverse thermal resistance, $RE1$, was obtained for the embedded stator winding. Furthermore, it was argued that this value of $RE1$ is constant along the active length of machine. In a similar manner to that presented previously, an overall transverse thermal resistance can be obtained for the endwindings. So as to differentiate these two resistances, the embedded winding transverse resistance will be called $RE1$ and the endwinding transverse resistance will be called $RE2$.

If it is assumed that the surface temperature of the winding is uniform around its periphery, then it is possible to set up the model as shown in Figure 3.12 where the primary difference from the previous development is that there are no wedges. Hence, heat will flow in all transverse directions. Now it can be shown that again

$$RE2 = \frac{(RX2)(RY2)}{(RX2) + (RY2)} \left[1 - \frac{(RXC2)(RYC2)}{5(RX2)(RY2)} \right] \quad (3.62)$$

where:

$$RXC2 = RXC1 \quad (3.63)$$

$$RYC2 = \frac{RYC1}{4} \quad (3.64)$$

$$RX2 = RX1 \quad (3.65)$$

$$RY2 = 0.25RYC1 + RY1 - RYC1 = RY1 - 0.75RYC1 \quad (3.66)$$

With this value of $RE2$, it becomes possible to obtain a complete model for the stator windings.

Up to this point, only transverse heat fluxes have been assumed in the winding. Heat flow in the axial direction has been assumed to be zero in order to obtain a per unit length analysis of the transverse thermal model. Figure 3.17 presents a model for the winding in the axial direction. The results of the previous development for the transverse heat flow can be incorporated into this model by considering the point $Z = 0$ to be the middle of the embedded winding within the machine and $Z = L/2$ to be the end of the embedding winding. Thus, at $Z = 0$, the stator winding will logically experience $T_{\max 1}$ and the middle of the endwinding will see the greatest cooling.

Now a heat balance in steady state conditions allows the differential equation:

$$q_{\text{winding}} - \frac{T_1(Z) - T_4(Z)}{RE1} + kA_{CS} \frac{d^2 T_1(Z)}{dz^2} = 0 \quad (3.67)$$

to be written to describe the temperature as a function of Z along the conductor. The term q_{winding} is positive for heat flow into the winding (a heat sink) and has units of watts per inch.

The temperatures $T_1 (Z = 0)$ and $T_4 (Z = 0)$ are mean temperatures, $T_{\text{av max}}$, in the cross sections. These are not

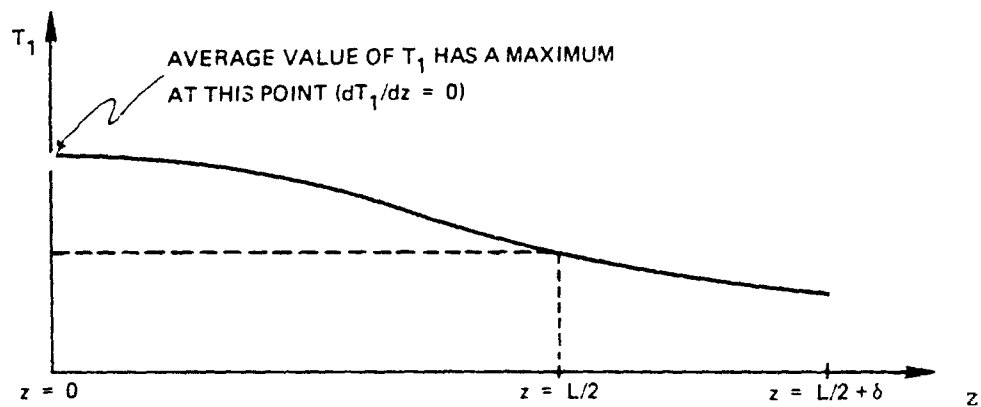
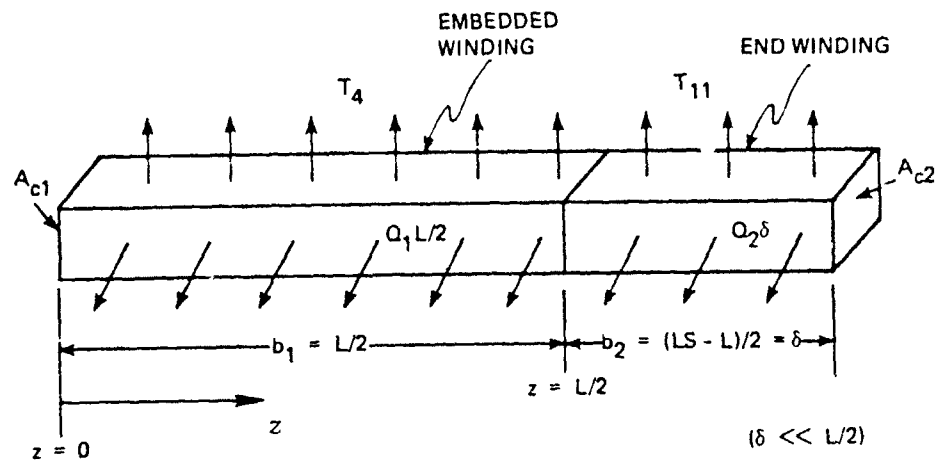


Figure 3.]7

the absolute maximum temperatures experienced over a parabolic temperature distribution for the cross section of each slot. Rather, Eq. (3.60) must be utilized with Q obtained for the corresponding cross section. Thus, to find the absolute maximum stator winding temperature, first find the value of Q :

$$Q = \frac{T_1(z=0) - T_4(z=0)}{REl} \quad (3.68)$$

then,

$$T_{1\max} = T_1(z=0) + \frac{Q(R_{x1} + 1.5R_{xc})(R_{y1} + 1.5R_{yc})}{R_x + R_y} \times \left[1 - \frac{3R_{xc}R_{yc}}{8R_xR_y} \right] \quad (3.69)$$

E. Stator iron in the axial direction

In his thermal model, Perez makes an assumption that greatly simplifies the mathematical complexity of the analysis. Specifically, he assumes the iron core temperature is not a function of the axial distance along the machine. Thus, T_4 is constant throughout the entire core. At first it may seem that this is a gross oversimplification; however, a few observations must be made here to clarify this matter.

For a machine with a small number of poles, as in Perez's case, the back iron dimensions will have to be relatively large in order to accommodate the large fluxes to be seen. For this reason, the core temperature will have a tendency to be less than smaller cross sectional areas of stator core. Hence, the maximum temperature difference between the center of the core and the end of the core will not be as great as that in the windings. Also, the heat

generated due to iron losses will be relatively less than that generated by the windings.

For a machine with a large number of poles, as is the case for the submarine electric propulsion motor, the back iron dimensions will be on the order of the slot dimensions. While the flux density will be of the same order as the machine with a small number of poles, the actual flux will be less. Thus, the iron losses will be nearly the same in the two cases since the flux densities are nearly the same. The heat generated in the windings will be treated differently though. When the back iron dimension is small, the iron will have a greater tendency to heat up to the temperature of the windings and thus assume a larger temperature difference between the center and the end of the core. The bottom line, then, is that the iron core cannot be treated as a constant temperature axially and still maintain some degree of reality in the model.

Again assuming steady state conditions, a heat balance in the stator core yields an equation similar to that for the windings:

$$q_{\text{stator core}} + \frac{T_1(z) - T_4(z)}{R_{E1}} - \frac{T_4(z) - T_{10}(z)}{R_{410}} - \frac{T_4(z) - T_{12}}{R_{412}} + kA_{\text{cores}} \frac{d^2 T_4(z)}{dz^2} = 0 \quad (3.70)$$

The thermal resistances R_{410} and R_{412} will be estimated later.

F. Stator iron core in the radial direction through the encapsulation

The heat that is generated in the core will not transfer to the windings since the latter are assumed to be at a higher temperature. Thus, the heat input to the core will be a combination of the heat generated due to axially uniform core losses and the transverse heat flow from the windings. The heat that leaves a unit length element of the stator iron will travel axially to neighboring space elements or travel radially out of the stator teeth or the back iron. Both of these surfaces will be covered by an encapsulation material that hinders heat transfer through a thermal resistance, R .

In a worst case scenario, the motor being considered here would have to operate without any cooling water flowing axially. For example, if, due to an underwater explosion or mechanical breakdown, the cooling water flow was cut off, the motor should still be able to function without overheating at some reduced speed. Maximum heat rise in the windings will occur with zero axial cooling water flow. This case then will provide the basis for the thermal model of both the gap between the rotor and stator and the gap between the stator and the submarine hull.

In order to find the resistance of the back iron, it will be assumed that the water between the back iron and the hull will have enough motion imparted due to motor revolutions to maintain a constant ambient temperature, T_{12} , throughout. However, rather than assume a convective heat transfer process,

a purely conductive case will be used for conservative simplicity. Also, any of the heat transfer surface that is impeded by structural frames holding the stator in place or together will be neglected. Figure 3.18 illustrates the case that is being considered.

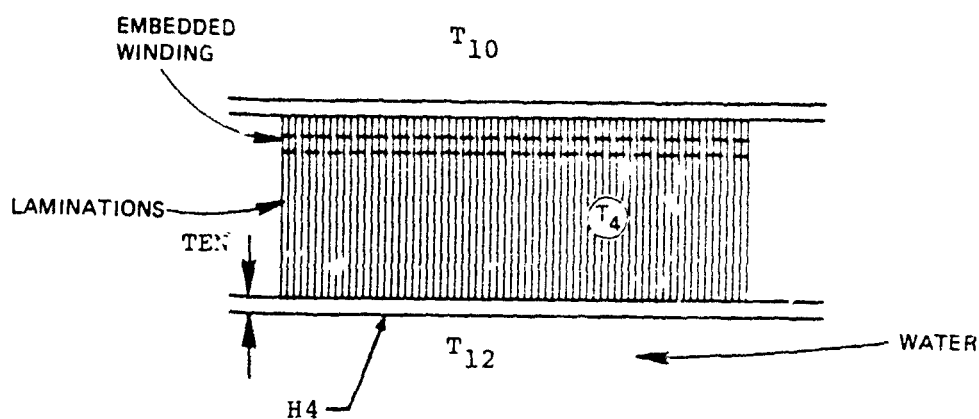


Figure 3.18

Though the iron core temperature varies axially, the resistance presented to transverse heat transfer will be constant. It will be made up of components due to the encapsulation material and the surface to fluid film. From Figure 3.8 it follows that Q equals zero and Figure 3.9 accurately models the case presented here. It then becomes possible to find R_{412} from Eqs. (3.13) and (3.25) :-

$$R_{412} = \frac{1}{\pi(DIS)} \left[\frac{TEN}{KE} + \frac{1}{H4} \right] \quad (3.71)$$

The heat transfer from the stator iron core to the water gap is a little more complex an issue. The method modeled by Perez will be utilized to obtain the thermal resistance of the gap. The following assumptions are made:

- 1) The slots have no appreciable effect on the rotor-stator heat transfer characteristics, i.e. there is zero heat flux across the wedge.
- 2) Surface roughness is considered small.
- 3) Velocity of the water flow axially is zero.
- 4) The gap is modeled as an outer smooth-rotating cylinder and also as a smooth-stationary coaxial cylinder.
- 5) The gap is much smaller than the machine radius.
- 6) The stator teeth are at the same temperature as the stator core.

Thus, the gap can be modeled as follows:

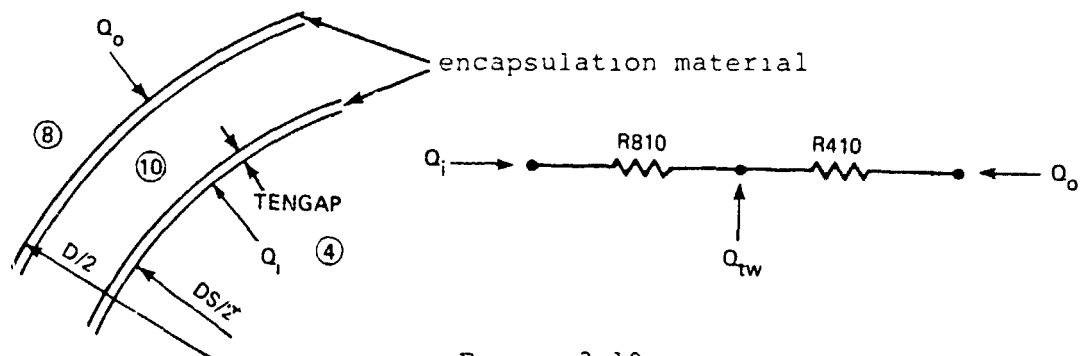


Figure 3.19

where Q_0 and Q_1 are the total heat transferred from the rotor and stator surfaces, respectively. Also, Q_{tw} represents the total windage losses for both the rotor and stator. It follows that:

$$R_{410} = \frac{1}{4 \pi (U) (DS/2)} + \frac{TENGAP}{\pi (KS) (DS)} \quad (3.72)$$

$$R_{810} = \frac{1}{4 \pi (U) (D/2)} + \frac{TENGAP}{\pi (KS) (D)} \quad (3.73)$$

$$U = \frac{KE (N_{NU})}{G - 2(TENGAP)} \quad (3.74)$$

$$N_{TA} = \frac{\rho \omega R [G - 2(TENGAP)]}{\mu} \left[\frac{G - 2(TENGAP)}{R} \right]^{0.5} \quad (3.75)$$

$$\ln C_f = \frac{1.18 [R + 2(TENGAP)] C_f^{-0.5}}{R + [G - 2(TENGAP)]/2} =$$

$$2 \times \ln \left\{ \frac{2.83 \mu [R + G - 2(TENGAP)]}{\rho \omega [G - 2(TENGAP)] R^2} \right\} - 17.16 \quad (3.76)$$

$$N_{NU} = 0.44 C_f \left[\frac{R}{G - 2(TENGAP)} \right]^{0.5} N_{TA} N_{PR}^{1/3} \quad (3.77)$$

$$R = DS/2 \quad (3.78)$$

where U is the overall stator-rotor heat transfer coefficient, N_{NU} is the Nusselt number, N_{TA} is the Taylor number, C_f is the frictional drag coefficient, and N_{PR} is the Prandtl number.

An initial estimate of the windage loss in the gap can be obtained from the following expression:

$$P_{gap} = C_f \pi R^4 L \rho \omega^3 \quad (3.79)$$

Also, the drag on the outer part of the rotor frame can be obtained by neglecting the part of the length, L_{PROP} , that is taken up by the propeller blades and considering the rotor as a cylinder rotating in a fluid as shown below:

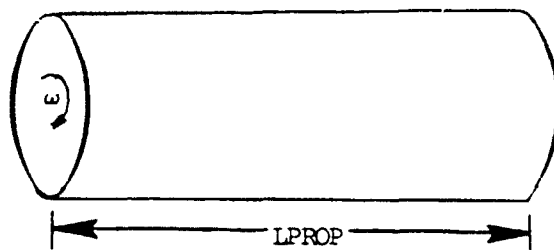


Figure 3.20

This drag will be neglected since it will be relatively small when compared to other windage losses. Furthermore, the propeller blades themselves create a drag force that also becomes part of the windage loss. This force will be a function of the propeller's efficiency, η_o , in converting the electromechanical power delivered to it to propulsive thrust. The propeller in open water, with a uniform inflow velocity, at a speed of advance V_A , has an open water efficiency given by:

$$\eta_o = \frac{T(V_A)}{2\pi n Q_o} \quad (3.50)$$

where Q_o is the torque measured in open water when the propeller is delivering thrust T at n revolutions per minute. When the propeller is coupled to the submarine hull, viscous effects cause the flow to be more turbulent resulting in a larger torque, Q_o , being necessary to turn the propeller. A relative rotative efficiency can be defined to be

$$\eta_{rr} = \frac{\eta_B}{\eta_o} = \frac{Q_o}{Q} \approx 1.05 \quad (3.81)$$

Furthermore, with a propeller diameter, D_p , the following definitions can be made:

$$\text{Advance ratio} = J = \frac{V_A}{nD_p} \quad (3.82)$$

$$\text{Thrust coefficient} = K_T = \frac{T}{\rho n^2 D_p^4} \quad (3.83)$$

$$\text{Torque coefficient} = K_Q = \frac{Q}{\rho n^2 D_p^5} \quad (3.84)$$

$$\text{Propeller efficiency} = \eta_{rr} \eta_o = \eta_{rr} \frac{JK_T}{2\pi K_Q} \quad (3.85)$$

where K_T , K_Q and η_o are functions of J . From these definitions and after the propeller design has yielded the above plots as a function of J , the propeller induced windage loss to the motor, becomes

$$P_{\text{prop}} = EHP (1 - \eta_{rr} \eta_o) = EHP \left[1 - \eta_{rr} \frac{JK_T}{2\pi K_Q} \right] \quad (3.86)$$

Clearly, this loss will be a function of J , that is, how fast the submarine is moving through the water and the rate at which the propeller is revolving. Finally, neglecting other windage effects that originate in the bearings and overhang region, the total windage loss to be used in the computer program becomes,

$$FWl \approx P_{gap} + P_{prop} \quad (3.87)$$

It must be emphasized that windage losses will not be considered in this thesis as heat inputs to the motor elements. While viscous effects will heat up the water in the gap and around the propeller hub, these temperature rises will be considered extremely small and thus neglected. However, the windage losses do require more electromechanical torque to be generated and, hence, more current will need to flow in the machine windings. This in turn will generate more I^2R losses. Also, because the motor is being driven harder, the core losses will be greater. In any motor design, therefore, the windage losses are important from a thermal point of view.

G. Stator iron in the axial direction through the end frame

For the case where T_{11} is identical on each end of the machine and where there is a common element (in this case, water) at both ends, Figure 3.9 is applicable. From Eqs. (3.11), (3.13) and (3.21), it follows that:

$$\begin{aligned}
R_{411} &\approx \frac{1}{2} \left[\frac{TEFS}{2\pi (0.5DS) (LEFS) (KS)} + \frac{TEN}{2\pi (0.5DS) (LEFS) (KE)} \right. \\
&\quad \left. + \frac{1}{2\pi (0.5DS) (LEFS) (H12)} \right] \\
&\approx \frac{1}{2\pi (DS) (LEFS)} \left[\frac{TEFS}{KS} + \frac{TEN}{KE} + \frac{1}{H12} \right] \quad (3.88)
\end{aligned}$$

The 1/2 factor indicates there are two endframes and twice the area of one endframe. The first term in the braces represents the resistance in going from the end stator iron lamination through the stator endframe; the second term represents the resistance through the encapsulation material; and the last term represents the surface to fluid resistance.

Another approach to this heat flux would be to totally neglect it since the backiron dimension is much smaller than the core length. Thus, R_{411} would be very large compared to R_{412} and could be neglected.

H. Rotor iron core in the axial direction through the end

In order to simplify the model, the last rotor lamination at $Z = L/2$ will be assumed to be separated from the endring by an insulated spacer which inhibits corrosion in the event seawater penetrates the protective can. This spacer of thickness, BR , will have thermal conductivity KIN and area, A_i . Thus,

$$R_{86} = \frac{BR}{2\pi (DER1 - DER2) (D) (KIN)}$$

and there will exist a linear temperature gradient between node 5 and node 8 over thickness BR .

I. Rotor iron core in the radial direction

Node 9 is not necessary to the thermal model since all the heat from node 8 passes directly through it and arrives at node 12, the outside environment. In a manner similar to the calculation for R412, it follows:

$$R_{812} = \frac{1}{\pi [DOR + 2(FTR)]} \left(\frac{FTR}{K_9} + \frac{1}{H_9} \right) \quad (3.89)$$

The surface heat transfer coefficient, H_9 , can be estimated using a flat plate convective law, Eq. (8.67a) of Reference 16, namely:

$$H_9 \approx 0.29 \left[\frac{T_8 - T_{12}}{L_{PROP}} \right]^{0.25} \quad (3.90)$$

Of course, T_8 and T_{12} are not known initially. Hence, initial estimates have to be inserted and then H_9 solved iteratively in the subroutine RESIST.FOR.

J. The model for the rotor squirrel cage

An analysis very similar to that presented for the stator winding can be used here with a few notable differences:

- 1) The slots will be round.
- 2) There is no need to account for inter-winding insulation, KI , since the slot is completely full of conductors except for the slot lining insulation, KEI .
- 3) The endwinding now has become an endring.

Again, it can be argued that an overall resistance parameter, RE3, defined by

$$R_{\text{overall}} = \frac{T_5 - T_8}{Q} = \frac{1}{2(NB)} R_{\text{for one bar}} = \text{RE3} \quad (3.91)$$

RE3 is invariant along the axial direction as long as the geometrical dimensions of the slot do not change. The transverse heat transfer out of the slot will occur as shown below:

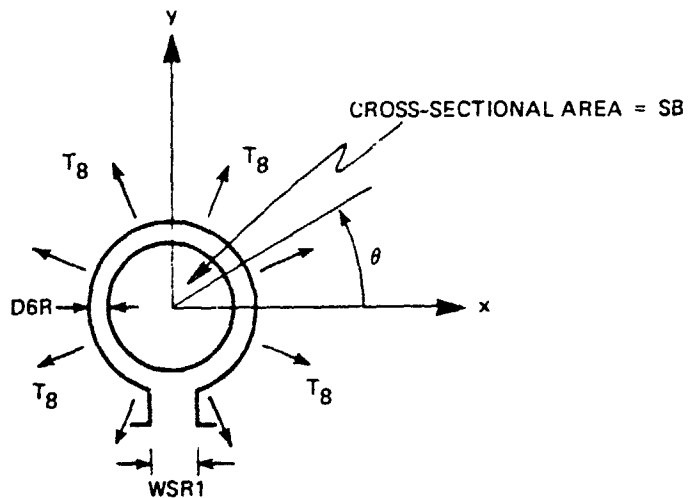


Figure 3.21

Again assuming each rotor lamination is at a uniform temperature throughout, then heat transfer out of the slot will be independent of θ . In other words, the thermal resistance will be the same for all values of θ , except for the area near WSR1 ($\theta = 270^\circ$) where no outward heat flux will be assumed.

To model the round bar, imagine it replaced by a rectangular conductor of identical cross sectional area, and an insulation of uniform thickness and of the same cross sectional area as the actual insulation. An example is shown below:

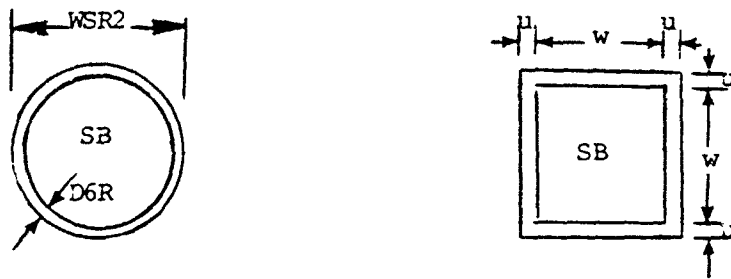


Figure 3.22

It follows that:

$$SB = \frac{\pi}{4} [WSR2 - 2(D6R)]^2 = w^2 \quad (3.92)$$

$$\frac{\pi (WSR2)^2}{4} - SB = 4uw + 4u^2 \quad (3.93)$$

$$u = -\frac{w}{2} + \frac{\pi^{0.5}}{4} (WSR2) \quad (3.94)$$

$$u = \frac{\pi^{0.5}}{2} (D6R) \quad (3.95)$$

$$w = (SB)^{0.5} = \frac{\pi^{0.5}}{2} [WSR2 - 2(D6R)] \quad (3.96)$$

Then Eqs. (3.49) to (3.56) are valid with appropriate dimensions substituted. Thus:

$$RXC3 = \frac{1}{2(NB)} \times \frac{0.5w}{(6w)KX} = \frac{1}{24(NB)KX} \quad (3.97)$$

$$RYC3 = \frac{1}{2(NB)} \times \frac{w}{6(0.5w)KY} = \frac{1}{6(NB)KY} \quad (3.98)$$

$$RXI3 = \frac{1}{2(NB)} \times \frac{u}{2w(KI)} = \frac{u}{4(NB)(w)KEI} \quad (3.99)$$

$$RYI3 = RXI3 \quad (3.100)$$

$$RX3 = RXC3 + RXI3 \quad (3.101)$$

$$RY3 = RYC3 + RYI3 \quad (3.102)$$

$$KX = KY = KI \left(1 + \frac{w}{2u}\right) \quad (3.103)$$

Eq.(3.61) can then be used to find the overall thermal resistance of the rotor bars, $RE3$. From the overall thermal resistance, a heat balance in the rotor bars is possible:

$$q_{\text{rotor bars}} - \frac{T_5(z) - T_8(z)}{RE3} + kA_{CR} \frac{d^2 T_5(z)}{dz^2} = 0 \quad (3.104)$$

The rotor endrings are undoubtedly complex to model accurately. For simplicity, it will be assumed that the heat flux travels outward into the uniform temperature T_{11} . The endring will be assumed to be a uniform temperature throughout.

equal to the temperature at the end of the rotor bar. This assumption is valid as long as the circular distance between rotor bars is small compared to the length of the bar. Again, a pure conduction process will be assumed for the heat flow through an encapsulation material into the overhang region. Also, since the resistance of the endring is less than five percent of the total rotor resistance, the heat generated due to losses in the endring will be assumed negligible. Therefore, Figure 3.8 simplifies to a case similar to Figure 3.9 and it follows that:

$$R_{611} \approx \frac{1}{2\pi D} \left[\frac{T_{EN}}{(0.5)(DER1-DE2)(KE)} + \frac{T_{EN}}{(TER)(KE)} + \frac{1}{[(0.5)(DER1-DE2) + TER]H6} \right] \quad (3.105)$$

The endring will then be at a uniform temperature, T_5 ($Z = L/2$), the water will be at a uniform temperature, T_{11} , and the encapsulation material will incur a linear thermal gradient over its thickness, T_{EN} .

K. Rotor iron core in the axial direction

In a manner similar to the case presented for axial heat flux in the stator, it can be argued that the rotor core temperature will also vary with Z . From a heat balance, it follows that:

$$q_{\text{rotor core}} - \frac{T_8(Z) - T_{12}}{R_{812}} + \frac{T_5(Z) - T_8(Z)}{R_{E3}} - \frac{T_8(Z) - T_{10}(Z)}{R_{810}} + kA_{\text{coreR}} \frac{d^2 T_8(Z)}{dz^2} = 0 \quad (2.106)$$

L. Preparing the computer thermal analysis

A very crude, but necessary, approximation is that the water temperature behind the stator core is at ambient temperature. A properly designed motor with cooling provided by rotor motion and forced flow would have this as a goal in order to keep temperature rises to a minimum.

In the model, because radial dimensions are much smaller than axial dimensions, T_{11} will be assumed equal to T_{12} . If water with heat capacity C_p flows at a rate M lbm/sec, then the water in the gap will undergo a temperature rise ΔT . This temperature rise would be a maximum if all the losses generated in the motor were input to the gap. This of course will never be the case but it does allow a simple and conservative calculation for T_{10} to be made. It follows that

$$T_{10} \approx T_{11} + .5 (\Delta T) \quad (3.107)$$

$$\Delta T = \frac{(q_{\text{winding}} + q_{\text{rotor bars}} + q_{\text{stator core}} + q_{\text{rotor core}})}{(C_p)(M)} \quad (3.108)$$

Ideally T_{10} should be introduced as a state variable in the model to follow since it varies with z . However this variance is small and for simplicity the above equation is assumed.

It becomes possible to rewrite Eqs. (3.67), (3.70), (3.104) and (3.106) as follows:

$$\frac{d^2 T_1(z)}{dz^2} = \frac{1}{(KC)A_{C1}} \left[\frac{T_1(z)}{RE1} - \frac{T_4(z)}{RE1} \right] - \frac{1}{(KC)A_{C1}} q_{\text{winding}} \quad (3.109)$$

$$\frac{d^2 T_4(z)}{dz^2} = \frac{1}{(KLY)A_{\text{core}_S}} \left[\frac{T_4(z)}{REQ1} - \frac{T_1(z)}{RE1} \right] - \frac{1}{(KLY)A_{\text{core}_S}} \left[q_{\text{stator}}^{\text{core}} + \frac{T_{12}}{R_{412}} + \frac{T_{10}}{R_{410}} \right] \quad (3.110)$$

$$\frac{d^2 T_5(z)}{dz^2} = \frac{1}{(KC)A_{CR}} \left[\frac{T_5(z)}{REQ3} - \frac{T_8(z)}{REQ4} \right] - \frac{1}{(KC)A_{CR}} q_{\text{rotor}}^{\text{bars}} \quad (3.111)$$

$$\frac{d^2 T_8(z)}{dz^2} = \frac{1}{(KLY)A_{\text{core}_P}} \left[\frac{T_8(z)}{REQ3} - \frac{T_5(z)}{REQ4} \right] - \frac{1}{(KLY)A_{\text{core}_P}} \left[q_{\text{rotor}}^{\text{core}} + \frac{T_{12}}{R_{812}} + \frac{T_{10}}{R_{410}} \right] \quad (3.112)$$

where, $\frac{1}{REQ1} = \left[\frac{1}{RE1} + \frac{1}{R_{410}} + \frac{1}{R_{412}} \right] \quad (3.113)$

$$\frac{1}{REQ2} = \left[\frac{1}{RE1} + \frac{1}{2(R_{410})} \right] \quad (3.114)$$

$$\frac{1}{REQ3} = \left[\frac{1}{RE3} + \frac{1}{R_{810}} + \frac{1}{R_{812}} \right] \quad (3.115)$$

$$\frac{1}{REQ4} = \left[\frac{1}{RE3} + \frac{1}{2(R_{810})} \right] \quad (3.116)$$

$$A_{CR} = \text{rotor conductor area} = (SB)(NB) \quad (3.117)$$

$$A_{\text{core}_S} = \text{stator iron cross sectional area} = \frac{\pi(DIS + DS)(DBS)}{2} + (DS)(STWMAG)(OS) \quad (3.118)$$

$$A_{\text{core}_P} = \text{rotor iron cross sectional area} = \frac{\pi(DOR + D)(DBRS + DOR)}{2} - (RSAREA)(NB) \quad (3.119)$$

These four differential equations have four unknowns: $T_1(z)$, $T_4(z)$, $T_5(z)$ and $T_8(z)$. All of the resistances are calculated from the geometry and structure of the design in the subroutine RESIST; the core losses and I^2R losses are known from the program INDUC.FOR and again are a function of the design; and the temperature T_{12} is the known ambient temperature.

For use in the program, Eqs. (109) to (112) must be broken down into eight first order differential equations and put into state space form:

$$\underline{\dot{x}} = [A]\underline{x} + [B]\underline{u} \quad (3.1.10)$$

The \underline{x} vector corresponds to

$$\underline{x} = \begin{bmatrix} x_1 \\ x_2 \\ x_3 \\ x_4 \\ x_5 \\ x_6 \\ x_7 \\ x_8 \end{bmatrix} = \begin{bmatrix} dT_1(z)/dz \\ T_1(z) \\ dT_4(z)/dz \\ T_4(z) \\ dT_5(z)/dz \\ T_5(z) \\ dT_8(z)/dz \\ T_8(z) \end{bmatrix} \quad (3.121)$$

The \underline{u} vector corresponds to

$$\underline{u} = \begin{bmatrix} q_{\text{winding}} \\ q_{\text{stator core}} \\ q_{\text{rotor bars}} \\ q_{\text{rotor core}} \\ T_{12} \end{bmatrix} \quad (3.122)$$

The [A] matrix corresponds to

$$[A] = \begin{bmatrix} 0 & a_{12} & 0 & a_{14} & 0 & 0 & 0 & 0 \\ 1 & 0 & 0 & 0 & 0 & 0 & 0 & 0 \\ 0 & a_{32} & 0 & a_{34} & 0 & a_{36} & 0 & 0 \\ 0 & 0 & 1 & 0 & 0 & 0 & 0 & 0 \\ 0 & 0 & 0 & 0 & 0 & a_{56} & 0 & a_{58} \\ 0 & 0 & 0 & 0 & 1 & 0 & 0 & 0 \\ 0 & a_{72} & 0 & 0 & 0 & a_{76} & 0 & a_{78} \\ 0 & 0 & 0 & 0 & 0 & 0 & 1 & 0 \end{bmatrix} \quad (3.123)$$

where the non-zero and non-unity a_{ij} terms are easily obtained from Eqs. (3.109) to (3.112). The [B] matrix corresponds to

$$[B] = \begin{bmatrix} b_{11} & 0 & 0 & 0 & 0 \\ 0 & 0 & 0 & 0 & 0 \\ 0 & b_{32} & 0 & 0 & b_{35} \\ 0 & 0 & 0 & 0 & 0 \\ 0 & 0 & b_{53} & 0 & 0 \\ 0 & 0 & 0 & 0 & 0 \\ 0 & 0 & 0 & b_{74} & b_{75} \\ 0 & 0 & 0 & 0 & 0 \end{bmatrix} \quad (3.124)$$

where, again, the non-zero b_{ij} terms are easily obtained from Eqs. (3.109) to (3.112).

The boundary conditions to this problem add some degree of difficulty to the solution of this system. From Figure 3.17, it can immediately be deduced that since the average temperatures are maximum at the center of the machine ($Z = 0$), then the slopes of the temperature distributions must also be zero at $Z = 0$. Therefore, $x_1 = x_3 = x_5 = x_7 = 0$ at $Z = 0$. However, nothing is known at this point on the values of x_2 , x_4 , x_6 and x_8 when $Z = 0$ and when $Z = L/2$. The boundary conditions at $Z = L/2$ can be written as:

$$x_1(Z) \bigg|_{Z=L/2} = \frac{dT_1(Z)}{dZ} \bigg|_{Z=L/2} = - \frac{T_1(Z=L/2) - T_{11}}{(RE2)(KEI)(TIN)} \quad (3.125)$$

$$x_3(Z) \bigg|_{Z=L/2} = \frac{dT_4(Z)}{dZ} \bigg|_{Z=L/2} = - \frac{T_4(Z=L/2) - T_{11}}{(R411)(KEND)(A_e)} \quad (3.126)$$

$$x_5(Z) \bigg|_{Z=L/2} = \frac{dT_5(Z)}{dZ} \bigg|_{Z=L/2} = - \frac{T_5(Z=L/2) - T_{11}}{(R611)(KE)(A_r)} \quad (3.127)$$

$$x_7(Z) \bigg|_{Z=L/2} = \frac{dT_8(Z)}{dZ} \bigg|_{Z=L/2} = - \frac{T_8(Z=L/2) - T_5(Z=L/2)}{(R85)(KIN)(A_i)} \quad (3.128)$$

where, TIN = thickness of insulation around endwinding

$KEND$ is the thermal conductivity of the steel endframe and encapsulation combined. Found in a manner similar to Eq. (3.167).

$$A_e = (2)(\pi)(DIS)(LEFS)$$

$$A_r = (2)(\pi)(D)[(.5)(DER1 - DER2) + TEFS]$$

$$KIN \approx .003$$

$$A_i = (2)(\pi)(D)[(.5)(DER1 - DER2)] - 2(NB)(SB)$$

Eqs. (3.125) to (3.128) are obtained from Eqs. (3.7) and (3.10). Note that for the heat going from one temperature node to another temperature node at $Z = L/2$, the heat must travel through a thin material with a distinctive thermal conductivity. In Eq. (3.125), this thin material is the encapsulation material which increases the winding perimeter by an estimated 50%. Any surface heat transfer coefficient has been neglected. In Eq. (3.126), the thin material consists of a combination of the steel end frame and encapsulation. In Eq. (3.127), the rotor endring is considered as the end of the rotor embedded bars and has an encapsulation material covering it. In Eq. (3.128), the last rotor lamination is assumed to be separated from the endring by a corrosion preventative layer of thickness BR , thermal conductivity KIN , thermal resistance $R86$ and area A_1 .

It has already been argued that, because the machine is much longer than it is deep, only a relatively small amount of heat is transferred out of its ends. The resistances then in (3.125) to (3.128) essentially become infinite and the temperature gradients go to zero at $Z = L/2$. It is not mandatory, however, that this assumption be made; the data is available to make the calculations. The resistances presented earlier for $RE2$, $R411$ and $R611$ can, at best, be called crude estimates since the heat transfer in the end regions is extremely difficult to model accurately.

For an initial conservative analysis, the end conditions at $Z = 0$ and $Z = L/2$ can be considered adiabatic so that no heat is transferred out the ends. If this is the case, then

the states in Eqs. (3.125) to (3.128) are set equal to zero at $z = 0$ and $z = L/2$. The thermal model then becomes a simple case of transverse heat flow only. Axial heat transfer does not occur since the thermal gradients in the z -direction have been forced to be zero by the end conditions. Equation (3.120) does not have to be solved since the states are not functions of z . A thermal model of the transverse heat flow can then be simply represented as is shown in Figure 3.23.

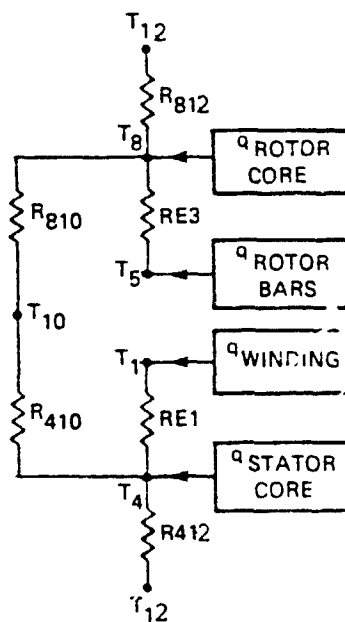


Figure 3.23

where again:

T_1 = stator winding average temperature

T_4 = stator core average temperature

T_5 = rotor bar average temperature
 T_8 = rotor core average temperature
 T_{10} = water gap temperature
 T_{12} = ambient water temperature
 q = per unit length heat input (watts/in.)
 $RE1$ = stator winding to stator core equivalent thermal resistance ($^{\circ}F\text{-in/watt}$)
 $RE3$ = rotor bar to rotor core equivalent thermal resistance ($^{\circ}F\text{-in/watt}$)
 $R812$, $R810$, $R410$ and $R412$ are equivalent between node thermal resistances. ($^{\circ}F\text{-in/watt}$)

Perhaps the easiest was to obtain the node temperatures as a function of the q 's and T_{12} is to go back to Eqs. (3.109) to (3.112) and set the second derivative term to zero. This is permitted because of the zero axial heat transfer assumption. Another alternative is to use node voltage analysis in writing four simultaneous equations at nodes 1, 4, 5 and 8. The latter approach will be used herein since it eliminates the need for the use of equivalent resistance terms represented in Eqs. (3.113) to (3.117). Solving for the four unknowns:

$$T_1 = A + \frac{B + C + D}{E} \quad (3.129)$$

where

$$A = q_{\text{winding}} (RE1)$$

$$B = (R410)(R812)(q_{\text{winding}} + q_{\text{stator core}})$$

$$C = T_{12}(R_{410})$$

$$D = T_{10}(R_{412})$$

$$E = R_{410} + R_{412}$$

It is obvious that T_1 is independent of T_5 and RE3 directly. T_1 , however, is indirectly a function of T_5 and RE3 since these quantities influence T_8 . Also, it is easily seen that $T_1 = T_{12}$ as it should when the q 's are zero. Furthermore, it follows that:

$$T_4 = T_1 - q_{\text{winding}} \quad (\text{RE1}) \quad (3.130)$$

$$T_8 = \frac{(R_{812})(R_{810})(q_{\text{rotor core}} + q_{\text{rotor bars}}) + T_{12}(R_{810}) + T_{10}(R_{812})}{R_{810} + R_{812}} \quad (3.131)$$

$$T_5 = T_8 + q_{\text{rotor bars}} \quad (\text{RE2}) \quad (3.132)$$

It must be emphasized that T_1 and T_4 are average temperatures in the electrical conductor. To find their maximum values, Eq. (3.60) must be utilized.

If a good estimate of the machine geometry and structure are known, then a more refined analysis becomes possible for the case where the end conditions in Eqs. (3.125) to (3.128) are nonzero. When heat flows out of the ends, the temperatures become a function of Z and Eq. (3.120) defines this variance.

The solution to Eq. (3.120) involves finding the eigenvalues and eigenvectors of the $[A]$ matrix. Rewriting Eq. (3.120) in canonical form:

$$\dot{\underline{h}} = [A]\underline{h} + [V]^{-1}[B]\underline{u} \quad (3.133)$$

where,

$$[A] = \begin{bmatrix} \lambda_1 & 0 & 0 & 0 & 0 & 0 & 0 & 0 \\ 0 & \lambda_2 & 0 & 0 & 0 & 0 & 0 & 0 \\ 0 & 0 & \lambda_3 & 0 & 0 & 0 & 0 & 0 \\ 0 & 0 & 0 & \lambda_4 & 0 & 0 & 0 & 0 \\ 0 & 0 & 0 & 0 & \lambda_5 & 0 & 0 & 0 \\ 0 & 0 & 0 & 0 & 0 & \lambda_6 & 0 & 0 \\ 0 & 0 & 0 & 0 & 0 & 0 & \lambda_7 & 0 \\ 0 & 0 & 0 & 0 & 0 & 0 & 0 & \lambda_8 \end{bmatrix} \quad (3.134)$$

$$[V] = [\underline{v}_1, \underline{v}_2, \dots, \underline{v}_8] \quad (3.135)$$

$$\underline{x} = [V]\underline{h} \quad (3.136)$$

In this case, $[A]$ is an 8 X 8 diagonal matrix made up of the system eigenvalues, λ_i , and $[V]$ is an 8 X 8 transformation matrix consisting of the eight system eigenvectors. To find the unforced or homogeneous response, the right term of (3.133) is set equal to zero and

$$\dot{\underline{h}} = [A]\underline{h} \quad (3.137)$$

Solving for \underline{h} and inserting this solution back into Eq. (3.136):

$$\underline{x}_h(z) = [V] \begin{bmatrix} e^{\lambda_1 z} & 0 & 0 & 0 & 0 & 0 & 0 & 0 \\ 0 & e^{\lambda_2 z} & 0 & 0 & 0 & 0 & 0 & 0 \\ 0 & 0 & e^{\lambda_3 z} & 0 & 0 & 0 & 0 & 0 \\ 0 & 0 & 0 & e^{\lambda_4 z} & 0 & 0 & 0 & 0 \\ 0 & 0 & 0 & 0 & e^{\lambda_5 z} & 0 & 0 & 0 \\ 0 & 0 & 0 & 0 & 0 & e^{\lambda_6 z} & 0 & 0 \\ 0 & 0 & 0 & 0 & 0 & 0 & e^{\lambda_7 z} & 0 \\ 0 & 0 & 0 & 0 & 0 & 0 & 0 & e^{\lambda_8 z} \end{bmatrix} \begin{bmatrix} C_1 \\ C_2 \\ C_3 \\ C_4 \\ C_5 \\ C_6 \\ C_7 \\ C_8 \end{bmatrix} \quad (3.138)$$

where the vector \underline{C} is a function of system boundary conditions. It should be noted that the eigenvectors only determine the direction in the state space that each state variable tends. The magnitude of the eigenvector is arbitrary but properly compensated for when the coefficients, C_1 , are found from the boundary conditions. Eq. (3.138) can then be written as:

$$\underline{x}_h(z) = \underline{v}_1 C_1 e^{\lambda_1 z} + \underline{v}_2 C_2 e^{\lambda_2 z} + \dots + \underline{v}_8 C_8 e^{\lambda_8 z} \quad (3.139)$$

The forced response (particular solution) will be a convolution integral of the form:

$$\underline{h}_p = \int_0^z e^{[A](z-\tau)} [V]^{-1} [B] \underline{u} d\tau \quad (3.140)$$

Since the term $[V]^{-1} [B] \underline{u}$ is constant throughout z , it can be brought out of the integral so that

$$\underline{h}_p = [V]^{-1} [B] \underline{u} \int_0^Z e^{[A](Z-\tau)} d\tau \quad (3.141)$$

$$= [P] \underline{\gamma}$$

where,

$$[P] = [A]^{-1} \left\{ e^{[A]Z} - [I] \right\} \quad (3.142)$$

and

$$\underline{\gamma} = [V]^{-1} [B] \underline{u} \quad (3.143)$$

Finally combining Eqs. (3.138) and (3.141):

$$\underline{X}(Z) = \underline{X}_h(Z) + \underline{X}_p(Z) = [V] [e^{\lambda_1 Z}] \underline{C} + [V] [P] \underline{\gamma} \quad (3.144)$$

To obtain the eigenvalues and eigenvectors of this system, a software package from M.I.T.'s Joint Computer Facility called EISPAC will be used. In the main program INDUC.FOR, it will be called in the subroutine DEIGEN. Once the eigenvalues and eigenvectors are computed, supplementary matrix algebra subroutines from MATRIX.FOR allow the vector $[V] [P] \underline{\gamma} = \underline{\alpha}(Z)$ to be computed. Since $[P]$ is a function of Z , this new vector, $\underline{\alpha}(Z)$, will also be a function of Z . Rewriting Eq. (3.144):

$$\underline{X}(Z) = [V] [e^{\lambda_1 Z}] \underline{C} + \underline{\alpha}(Z) \quad (3.145)$$

All the vectors and matrices in Eq. (3.145) are known except for \underline{C} . To find \underline{C} , the boundary conditions consisting of:

$$x_1(z) \bigg|_{z=0} = \frac{dT_1(z)}{dz} \bigg|_{z=0} = 0 \quad (3.146)$$

$$x_3(z) \bigg|_{z=0} = \frac{dT_4(z)}{dz} \bigg|_{z=0} = 0 \quad (3.147)$$

$$x_4(z) \bigg|_{z=0} = \frac{dT_5(z)}{dz} \bigg|_{z=0} = 0 \quad (3.148)$$

$$x_7(z) \bigg|_{z=0} = \frac{dT_8(z)}{dz} \bigg|_{z=0} = 0 \quad (3.149)$$

and Eqs. (3.125) to (3.128) are applied to Eq. (3.145). Thus, with eight boundary conditions on the temperature derivatives at the endpoints of the machine, it becomes possible to find the eight constants in the vector \underline{C} .

From Eq. (3.146) through (3.149), the following four equations are obtained:

$$0 = \sum_{i=1}^8 v_{i1} C_i \quad (3.150)$$

$$0 = \sum_{i=1}^8 v_{i2} C_i \quad (3.151)$$

$$0 = \sum_{i=1}^8 v_{i3} C_i \quad (3.152)$$

$$0 = \sum_{i=1}^8 v_{i4} C_i \quad (3.153)$$

where v_{ij} is the j^{th} element of the i^{th} eigenvector. Note that these four equations come from analysis of X_1 , X_3 , X_5 and X_7 . The other four states, X_2 , X_4 , X_6 and X_8 , have not been considered at all.

At $Z = L/2$, the following four equations can be written:

$$\left. \frac{dT_1(Z)}{dZ} \right|_{Z=L/2} = \frac{T_{11}}{(RE2)(KE)(TIN)} - \frac{T_1(Z=L/2)}{(RE2)(KE)(TIN)} = \left[\sum_{i=1}^8 v_{i1} C_i e^{\lambda_i L/2} \right] + \alpha_1(Z=L/2) \quad (3.154)$$

$$\begin{aligned} \left. \frac{dT_4(Z)}{dZ} \right|_{Z=L/2} &= \frac{T_{11}}{(R411)(KEND)(A_e)} - \frac{T_4(Z=L/2)}{(R411)(KEND)(A_e)} \\ &= \left[\sum_{i=1}^8 v_{i3} C_i e^{\lambda_i L/2} \right] + \alpha_3(Z=L/2) \end{aligned} \quad (3.155)$$

$$\begin{aligned} \left. \frac{dT_5(Z)}{dZ} \right|_{Z=L/2} &= \frac{T_{11}}{(R611)(KE)(A_r)} - \frac{T_5(Z=L/2)}{(R611)(KE)(A_r)} \\ &= \left[\sum_{i=1}^3 v_{i5} C_i e^{\lambda_i L/2} \right] + \alpha_5(Z=L/2) \end{aligned} \quad (3.156)$$

$$\left. \frac{dT_8(Z)}{dZ} \right|_{Z=L/2} = \frac{T_8(Z=L/2)}{(R86)(KIN)(A_1)} - \frac{T_5(Z=L/2)}{(R86)(KIN)(A_1)}$$

$$= \left[\sum_{i=1}^8 v_{i7} C_i e^{iL/2} \right] + \alpha_7(Z=L/2) \quad (3.157)$$

These four equations can then be solved for $T_1(Z = L/2)$, $T_4(Z = L/2)$, $T_5(Z = L/2)$ and $T_8(Z = L/2)$. From Eq. (3.145), it is also possible to find these four quantities by using states X_2 , X_4 , X_6 and X_8 as follows:

$$T_1(Z=L/2) = \left[\sum_{i=1}^8 v_{i2} C_i e^{\lambda_1 L/2} \right] + \alpha_2(Z=L/2) \quad (3.158)$$

$$T_4(Z=L/2) = \left[\sum_{i=1}^8 v_{i4} C_i e^{\lambda_1 L/2} \right] + \alpha_4(Z=L/2) \quad (3.159)$$

$$T_5(Z=L/2) = \left[\sum_{i=1}^8 v_{i6} C_i e^{\lambda_1 L/2} \right] + \alpha_6(Z=L/2) \quad (3.160)$$

$$T_8(Z=L/2) = \left[\sum_{i=1}^8 v_{i8} C_i e^{\lambda_1 L/2} \right] + \alpha_8(Z=L/2) \quad (3.161)$$

Equating these four equations with the four obtained from Eqs. (3.154) to (3.157), the following expressions result:

$$0 = \sum_{i=1}^8 [v_{i2} + v_{i1}(RE2)(KE)(TIN)] C_i e^{\lambda_1 L/2}$$

$$+ [\alpha_2 + (RE2)(KE)(TIN) \alpha_1 - T_{11}] \quad (3.162)$$

$$0 = \sum_{i=1}^8 [v_{14} + v_{13} (R411) (KEND) (A_e)] C_i e^{\lambda_i L/2} + [\alpha_4 + (R411) (KEND) (A_e) \alpha_3 - T_{11}] \quad (3.163)$$

$$0 = \sum_{i=1}^8 [v_{16} + v_{15} (R611) (KE) (A_r)] C_i e^{\lambda_i L/2} + [\alpha_6 + (R611) (KE) (A_r) \alpha_5 - T_{11}] \quad (3.164)$$

$$0 = \sum_{i=1}^8 [v_{18} + v_{17} (R86) (KIN) (A_1) + v_{15} (R611) (KE) (A_r)] C_i e^{\lambda_i L/2} + [\alpha_8 + (R86) (KIN) (A_1) \alpha_7 + (R611) (KE) (A_r) \alpha_5 - T_{11}] \quad (3.165)$$

Eqs. (3.150) to (3.153) and (3.162) to (3.165) form a system of eight equations and eight unknowns (the constants in the \underline{C} vector). The constants of \underline{C} can be factored out of the equations and, with appropriate manipulation of terms, the vector \underline{C} can be obtained from Cramer's Rule as is shown in Eq. (3.166) on the following page.

Once the \underline{C} vector has been obtained, it becomes possible to obtain $\underline{X}(Z)$ for different values of Z by setting up a DO loop around Eq. (3.144). In the program, the interval between $Z = 0$ and $Z = L/2$ is broken up into 100 equal segments and the four node temperatures and four node temperature derivatives are computed for each segment. These values are stored in appropriate arrays for output and plotting purposes.

$$\begin{bmatrix} C_1 \\ C_2 \\ C_3 \\ C_4 \\ C_5 \\ C_6 \\ C_7 \\ C_8 \end{bmatrix} = \begin{bmatrix} V_{11} & V_{21} & V_{31} & V_{41} & V_{51} & V_{61} & V_{71} & V_{81} \\ V_{13} & V_{23} & V_{33} & V_{43} & V_{53} & V_{63} & V_{73} & V_{83} \\ V_{15} & V_{25} & V_{35} & V_{45} & V_{55} & V_{65} & V_{75} & V_{85} \\ V_{17} & V_{27} & V_{37} & V_{47} & V_{57} & V_{67} & V_{77} & V_{87} \\ f_1 & f_2 & f_3 & f_4 & f_5 & f_6 & f_7 & f_8 \\ g_1 & g_2 & g_3 & g_4 & g_5 & g_6 & g_7 & g_8 \\ h_1 & h_2 & h_3 & h_4 & h_5 & h_6 & h_7 & h_8 \\ k_1 & k_2 & k_3 & k_4 & k_5 & k_6 & k_7 & k_8 \end{bmatrix} \begin{bmatrix} 0 \\ 0 \\ 0 \\ 0 \\ m \\ n \\ p \\ r \end{bmatrix}$$

(3.166)

$$f_i = [V_{i2} + V_{i1} (RE2) (KE) (TIN)] e^{\lambda_i L/2}$$

$$g_i = [V_{i4} + V_{i3} (R11) (KEND)] (\Lambda_e) e^{\lambda_i L/2}$$

$$h_i = [V_{i6} + V_{i5} (R611) (KE) (\Lambda_r)] e^{\lambda_i L/2}$$

$$k_i = [V_{i3} + V_{i7} (R86) (KIN) (\Lambda_1) + V_{i5} (R611) (KE) (\Lambda_r)] e^{\lambda_i L/2}$$

$$m = -[\alpha_2 + (RE2) (KE) (\Lambda_w) \alpha_1 - T_{11}]$$

$$n = -[\alpha_4 + (R411) (KIND) (\Lambda_c) \alpha_3 - T_{11}]$$

$$p = -[\alpha_6 + (R611) (KE) (\Lambda_r) \alpha_5 - T_{11}]$$

$$r = -[\alpha_8 + (R86) (KIN) (\Lambda_1) \alpha_7 + (R611) (KE) (\Lambda_r) \alpha_5 - T_{11}]$$

Table 3.1 presents the values used in the program for the various material thermal conductivities. These are obtained from References 3, 13, 16 and 61.

<u>Material</u>	<u>Thermal Conductivity, k (watts/°F-in)</u>
Copper	5.426 = KC(3)
Aluminum	2.881 = KC(1)
Brass	1.563 = KC(2)
Sheet steel laminations	
- in the plane of the laminations, k_x	.710 = KLX
- normal to the plane of the laminations, k_y (cold rolled, 0.014 in. thick, flush enameled, 140 psi clamping pressure) ^x	.022 = KLY
Steel (1% mild)	.610 = KS
Water (100°F, .95 psia)	.00889 = KW
Micanite	.0025 = KI
Press board (varnished)	.0028
Cotton insulation (untreated)	.0011
Cotton insulation (impregnated or varnished)	0.006
Encapsulation	0.003 = KE = KIN

Table 3.1

One noteworthy value is that used for KLY. While Roberts⁶¹ quotes a figure of .022 for a lamination clamping pressure of 140 psi, it really is difficult to state with accuracy the value that will be seen on the electric propulsion motor. For the later case, clamping pressures on the order of the expected

seawater pressure will be used. These obviously will be much larger than 140 psi. In addition, a between lamination adhesive will be used to improve rigidity. Thus, the figure for KLY used in the computer program has been estimated from the formula

$$KLY = \frac{(L_{iron} + L_i)(k_{iron}k_i)}{L_{iron}k_i + L_ik_{iron}} \quad (3.167)$$

This formula is obtained by considering the core as a solid mass made up of laminations with thickness L_{iron} and lamination insulation thickness, L_i . Computing the overall core thermal resistance as a function of the individual lamination and insulation resistances allows the above expression to be obtained.

If,

$$\begin{aligned} L_{iron} &= .014 \text{ in.} \\ L_i &= .0005 \text{ in.} \\ k_{iron} &= .710 \\ k_i &= .003 \end{aligned}$$

then $KLY = 0.077 \text{ watts/}^\circ\text{F-in.}$ This is the value to be used in the computer program.

M. Summary of the thermal model and areas for further work

The expected thermal behavior of any electric machine is an extremely complex subject to tackle. From the work done in this chapter, it is obvious that a large number of simplifying assumptions have to be made in order to reduce this complexity. But, of course, this risks introducing large inaccuracies into the model. The only way to be safe is to ensure that these inaccuracies cause the temperatures calculated to be higher than actual expected values. In this way, the designer is not led to construct a motor only to have it overheat because of actual temperatures being higher than calculated.

Undoubtedly, the assumption of purely conductive heat transfer is extremely conservative. Water flow through the gap, around the overhang region, and behind the stator iron will introduce convective cooling that will substantially bring down calculated temperatures. On the other hand, modeling this process will be extremely difficult and will require experimental work in the laboratory. Also, the cooling process is, to a large extent, a function of the geometry involved which, at this point in the design, can only be labelled as crude. Fortunately, adding convective cooling will not greatly affect the model presented in this chapter. The resistances R_{410} , R_{810} , $RE2$, R_{611} and R_{811} would change since a different surface heat transfer coefficient, h , is involved. Also, T_{10} and T_{11} could be introduced as state

variables along with the stator back iron water (previously assumed to be at ambient temperature). The additions to the computer program would not be extensive and could be achieved with minimal rewrite of existing program code.

In any event, for any model developed, a test with a known motor design would be imperative. Water cooled encapsulated motors exist for which this would be possible (Reference 44).

The area presented with the least confidence in this chapter centers around the water gap resistances R_{410} and R_{810} . The method used was originally developed for high speed air-cooled motors. Thus, some skepticism about the accuracy of these two resistances should exist.

Also, the area of the rotor endring thermal behavior requires further scrutiny.

To conclude, this thermal model presents a stepping stone upon which initial estimates of machine hot spot temperatures can be obtained. Further refinement of the model using air-cooled motors could be achieved in the laboratory since much of the development presented here is independent of fluid flow.

Chapter Four

THE ELECTRIC MOTOR DESIGN

A. Motor Type Selection

The motor being proposed in this thesis must meet a number of design requirements. As this is an inverted design, the inner part of the motor, the stator, is stationary, supported by a foundation that provides vibration isolation. The stator is also totally submerged in seawater, thus providing constant water gap clearances between the rotor and stator. If the stator is mounted directly to the pressure hull two undesirable characteristics arise:

- 1) Magnetostrictive vibrations are directly transferred to the hull which increases acoustic noise propagation into the environment.

- 2) The stator lamination stack will be subjected to hull flexure in addition to outside seawater pressure. This, in effect, guarantees adjacent lamination movement and places a much greater stress on the outer corrosion protective layer. It also means that, since the rotor receives seawater pressure from all directions, the water gap distance, G , will be a function of depth.

The outer portion of the motor, the rotor, rotates and a large diameter hub is attached around it. To this large diameter hub are mounted detachable propeller blades. These blades extend radially outward around the circumference of the hub.

For any design subjected to seawater, sound engineering requires a "keep it simple" design philosophy. The many advantages that this system offers can only be realized if it is reliable and maintainable. For this reason, intricate mechanisms or an improperly supported structure will not be used. The rotor will be the only moving part outside the hull. All surfaces subject to corrosion or fouling are either coated with a protective polymer material or are encased in highly corrosion-resistant metals such as chromium or nickel-based steel alloys. In this way the motor can operate dependably between overhaul cycles. During these times, cleaning of material surfaces can be accomplished.

Prior to discussion of the actual motor configuration, two intriguing systems will be briefly presented. These two ideas are presented mainly because they allow the large hub propeller concept to be realized without the need for protection of the stator windings from seawater. However, they both possess characteristics that make them poor performers.

Figure 4.1 illustrates a concept that was posed by engineers at General Electric in the early 1960s. While the type of motor has not been specified, it consists of a stator lamination stack attached to the inside of the pressure hull. The stator consists of pole pieces which can be detached for maintenance purposes. The rotor is subjected to seawater and freely rotates about the hull.

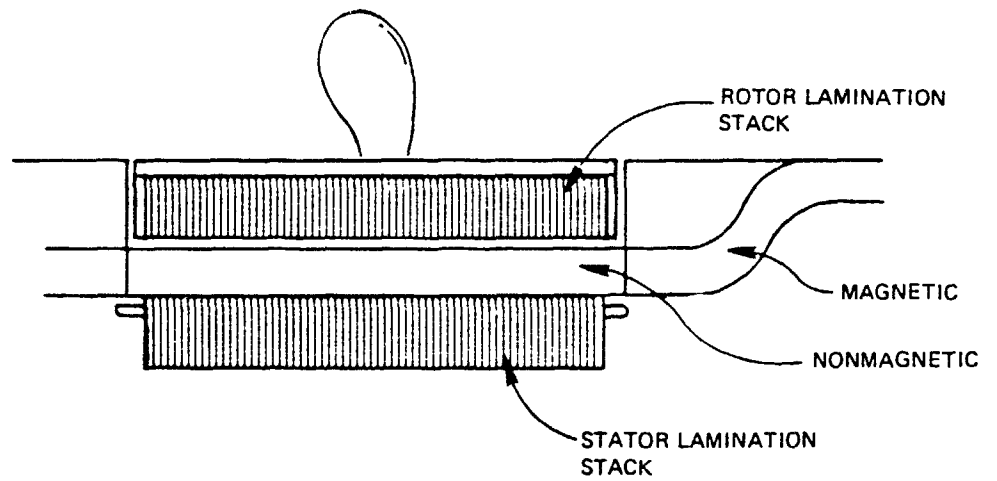


Figure 4.1

The sliding support for the rotor in the form of journal bearings is not shown on the sketch. Thrust bearing surfaces are easily constructed at either end of the rotor. The gap between the rotor and stator consists of a nonmagnetic material such as stainless steel or titanium. If this gap material is titanium, then the entire hull is titanium since changes in Young's Modulus of Elasticity cannot be tolerated on seawater pressure vessels. However, it is possible to avoid constructing the entire hull structure out of expensive stainless steel by using a less costly, high yield steel for the remainder of the pressure hull. Welding incompatibilities, however, at the interface of these magnetic and nonmagnetic materials must be addressed. On small submarines, fiber composite materials are also receiving a great deal of emphasis in submarine design today. These materials would be ideal for the nonmagnetic gap requirement.

Whereas this design does allow maintenance and repair of the stator windings from within the submarine, it does have limitations that preclude its use on deep-diving submarines. The primary detrimental factor is the large air gap created by the thick pressure hull. High leakage reactances imply very low efficiencies. The design presented later in this chapter proposes a gap dimension on the order of 0.200 to 0.300 inches on a 16.5-foot diameter motor. Gap clearances on the order of a hull thickness of approximately one inch are not tolerable. Also, as was mentioned earlier, magnetostrictive noise would originate at the stator-hull

structure interface. Thus, this motor would be large, heavy and noisy.

A second idea which places the stator inside the pressure hull centers on a dual materials pressure hull within the airgap. Figure 4.2 illustrates this concept.

With the alternating materials in the airgap, the leakage flux would be substantially reduced. The leakage flux, however, would still be higher than on a conventional motor due to the extremely large air gap distance. The choice of the materials for the pressure hull in the vicinity of the air gap has not been fully explored. However, problems in welding, corrosion, fatigue due to cyclic loading and hydrogen embrittlement certainly have to be studied in greater detail. At this point, the disadvantages of a large air gap in these two ideas outweigh the advantages of an internally-mounted stator.

To date, submersible motors used in deep-submergence applications have been mainly limited to squirrel-cage induction a-c motors and to compound-wound, shunt-wound and series-wound d-c motors. Reference 44 contains a large listing of existing submersible a-c and d-c motors, their respective size, rating and manufacturer. None of these is larger than 50 HP. The decision to employ an a-c squirrel cage induction motor to this design was relatively easy though for other cases in deep-submergence vehicles, the choice between a-c and d-c is not as clearly defined. Of paramount importance is the need

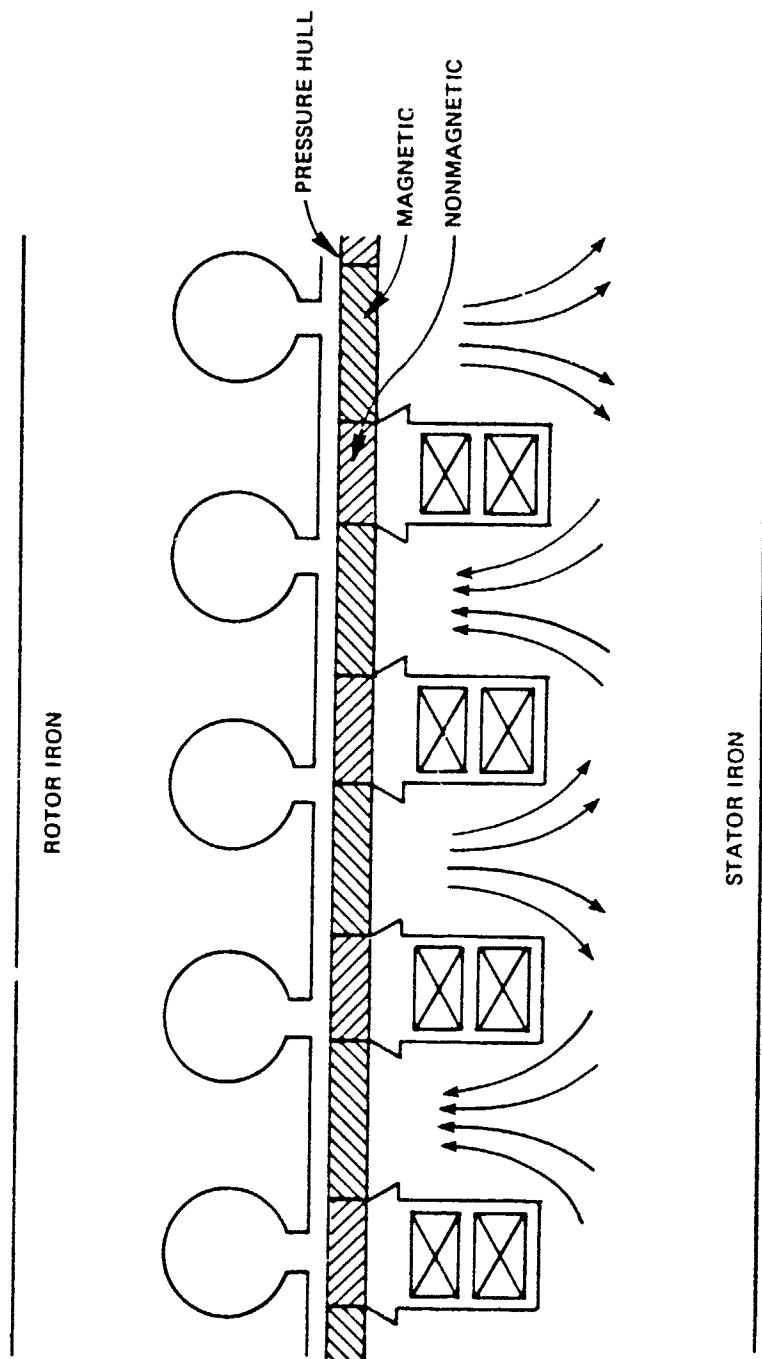


Figure 4.2

to maintain simplicity in the design. There is already enough technical risk presented in the many aspects of this proposal. The designer should not introduce more risk if it can be avoided. A d-c motor design will be more complex and expensive, requiring an oil-filled motor cavity to protect the commutator-brush electrical interface. Because natural seawater cooling cannot be used, the oil-filled motor would run much hotter. This high temperature operation of the motor will cause degradation of the fluid lubricity and of the electrical insulation and result in a less reliable motor. Also, the oil-filled motor design will require oil seals to prevent seawater contamination. This has the potential to be a designer's nightmare on such a large motor. For these reasons, the d-c motor has no application in this design.

B. Configuration

The possibilities for motor-mounting outside the pressure hull are numerous. Figure 4.3 illustrates some of the possibilities. Obviously, with some ingenuity, other options are possible. In any case, the final motor configuration will be determined by the chosen journal and thrust bearings with the correct geometry that maximizes power output according to Eq. (3.1).

The design presented in Chapter 1 remains simple both structurally and electrically. Though no detail is presented in this analysis, the bearings will be water-lubricated, sliding contact type bearings. Water cooling of the stator

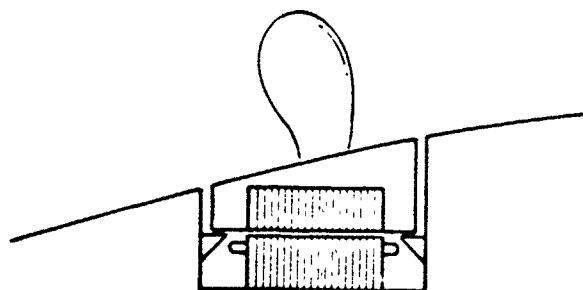
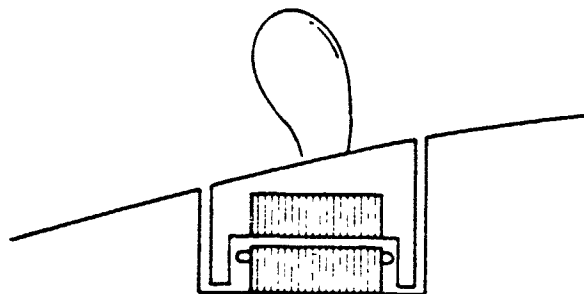
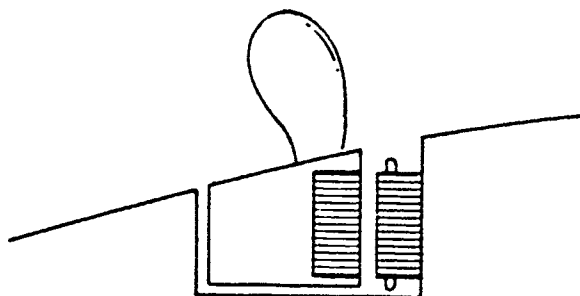
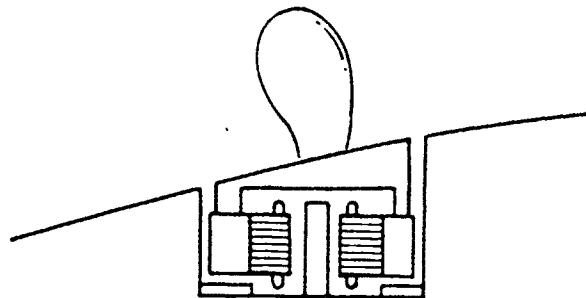


Figure 4.3

and rotor will allow higher conductor current densities.

C. Induction Motor Analysis Program

In order to effectively analyze alternative designs and arrive at a workable conclusion, a FORTRAN program is presented in Appendix H. Using Reference 11 as a foundation, the program assumes an inverted, three-phase induction motor configuration, that is, rotor outside stator. It encompasses calculations of torque-speed characteristics, electrical characteristics, magnetic flux densities, weight, temperature rise and various other parameters. Though there are a large number of modifications and additions, Reference 11 should be consulted prior to use as it provides a great deal of user information.

The program analyzes only a three-phase induction motor with a squirrel cage rotor winding and is limited to steady-state, balanced conditions. The armature is assumed to have a two-layer, Y-connected winding and may be either copper, aluminum, or brass. The rotor stack is assumed to be the same axial length as the stator stack. Double squirrel-cage windings are not permitted, although the program could be modified to account for them. Materials for the rotor winding may be either copper, aluminum or brass. A cross section of a typical induction motor assumed for this analysis is shown in Figure 3.3. This is not the only slot configuration permitted, however, as rotor and stator slots may be open or partially closed, rectangular, trapezoidal, round or trapezoidal with a round bottom. These are illustrated in detail in Reference 11. Thermal analysis as presented in Chapter 3

is included in the program to permit calculation of hot spot temperatures. This extremely complex analysis is, at this point, far from being fully developed; however, due to conservative assumptions, upper limits on the temperatures can be established.

The effects of windage on motor performance may be either omitted or included in the analysis. If they are to be included, the windage loss for a similar motor must be known. The program will then scale this known windage loss with respect to all pertinent parameters in order to approximate the windage loss of the motor under analysis. The scaling is unnecessary if windage loss at synchronous speed can be supplied to the program directly. In this case, the submarine electric propulsion motor windage loss due to the propeller drag and due to water gap friction are input with the variable FWL. Losses in the bearings are neglected in this design effort. However, for future designs, they must be considered.

Included in each of the main program and subroutine listing are footnotes which describe in further detail specific equations, input requirements, software procedures, etc. Appendices A through G are the annotations to these footnotes.

The use of this computer program requires that the complete electromagnetic design be known or assumed. The design information is then transferred into a datafile for use with the program. A typical input file is shown in Figure 4.3. It consists of one data set containing, in the order required, two materials data lists, windage data, and one

M-19 SILICON STEEL MANUFACTURED BY US STEEL
 104.2,25.8,1.27,32.2,1.43,38.1,1.62,45.2,
 1.82,51.6,2.08,58.0,2.43,64.5,2.89,70.9,
 3.64,77.4,4.79,83.8,7.07,90.3,11.92,96.1,
 20.76,103.2,64.07,104.2,71.25

SFELOSS

WCURF=13.5,
 FLURF=500.,
 SLURF=1.53,
 PK=64.5,
 LI=0.014

SEND

SFELOSS

LAST=.TRUE.

SEND

M-19 SILICON STEEL MANUFACTURED BY US STEEL
 104.2,25.8,1.27,32.2,1.43,38.1,1.62,45.2,
 1.82,51.6,2.08,58.0,2.43,64.5,2.89,70.9,
 3.64,77.4,4.79,83.8,7.07,90.3,11.92,96.1,
 20.76,103.2,64.07,104.2,71.25

SFELOSS

WCURF=13.5,
 FLURF=500.,
 SLURF=1.53,
 PK=64.5,
 LI=0.014

SEND

SFELOSS

LAST=.TRUE.

SEND

SWUDGE

SEND

***** SUPERFINE ELECTRIC PROPULSION MOTOR *****

SPATING

NSYMCH=50.,
 F=30.,
 V1=2309.,

Figure 4.3

```
FWI=0.0
FRATED=2.1405tb
SEND
```

```
SSAION
```

```
DIS=182.85,
I=102.,
LIS=.014,
SFS=.9655,
LHFS=1.5,
TrFS=1.
```

```
SEND
```

```
SSSLOTS
```

```
US=180.,
SSTYPE=1,
DZS=.78,
DSS=.132,
WSSb=.066,
DSS=2.5,
DSS=0.066,
WSS=1.60
```

```
SEND
```

```
SSTRWDG
```

```
CSS=2.,
PC=1.,
H=1.0,
SWAL=3,
SPICH=.6667,
S=.14,
ASTRND=1.4416,
SIRNCS=1.,
TSW=150.,
WX=.2074,
WY=.1241,
U=.004
```

```
SEND
```

```
SKUTOK
```

```
SKEX=1.0,
```

Figure 4.3(cont'd)

LTR=0.014,
D=191.5,
DUR=198.,
SPR=.9655,
LPRUP=115.,
FTR=4.

SEND

\$RSLOTS

KSTYPL=5,
DIR=1.60,
DOR=0.020,
DAP=0.025,
WSH1=0.4

SEND

\$RTRWDG

NB=200.,
TER=2.5,
RWMA1=1,
RR=0.5,
DER1=198.0,
DER2=191.5,
TRW=150.0

SEND

\$AIRGAP

G=0.200,
PLULU=75.0

SEND

\$ENCAP

TEN=.15
TENGAP=.005

SEND

Figure 4.3(cont'd)

motor design data list. A material list consists of from 5 to 15 lines. The first line is the material identification line. The next four lines are the saturation curve data lines. They contain the coordinate values of as many as 14 arbitrary data points located on the magnetization curve of the material. Following this are as many as 10 core-loss data groups -- one for each lamination thickness at which core-loss calculations are anticipated. More detail on the input requirements and use of the NAMELIST arguments can be obtained from Appendix A and Reference 11.

The computer program consists of a main program called INDUC and ten subroutines called CIRCT, MAGNET, SLOTS, WDGFACT, CMBNTN, MATRIX, VERSA, DEIGEN, FRIC and RESISTANCES. For a description of the purpose and use of each of these subroutines, the user is directed to the comments at the beginning of each listing at the end of this thesis. MATRIX is not a subroutine in and of itself but rather a file containing the matrix algebra subroutines DMATVMUL, MATINV, DVECADD, RITEMAT and RITEVEC. DEIGEN is a library file that is not included in the listings. It is called once in the main program and is used to compute the eigenvalues and eigenvectors of a given matrix. Again, one should note that specific sections of the listings have been footnoted and annotations appear in the appendices.

The program is written in the FORTRAN 77 programming language for use on a DEC Vax 11/780 digital computer. Care should be exercised in switching to another computer system,

especially those that do not initialize variables to zero unless told to do so in the program. Most of the real variables appear as REAL*16. This added precision becomes necessary in the heat transfer analysis when matrix operations require algebraic operations between very large and very small numbers.

D. Motor Insulation System

The submarine electric propulsion motor is seawater-flooded, requires no brushes, and is made impervious to seawater damage by a special insulation system. Protection of the motor from accidental seawater grounding or seawater corrosion is perhaps the most critical aspect of the design.

The seawater-flooded design, incorporating seawater-lubricated bearings, usually can be identified as one, or a combination of the following:^{12,44,45}

- 1) Epoxy-encapsulated design
- 2) Canned stator design
- 3) Wet winding design.

The epoxy-encapsulated design is generally arrived at by completely encapsulating the wound stator within a solid envelope. The success of the epoxy encapsulation system depends upon the elimination of voids and air inclusions within the envelope. In addition, the bulk modulus and thermal expansion of the epoxy compounds must closely match the encased stator assembly to ensure the integrity of the epoxy envelope.

A second approach to a seawater-flooded a-c motor is the canned stator design. The approach in the canned design is to place a thin sheet of corrosion-resistant metal with the proper magnetic properties (generally Inconel or Hastalloy C metal) into the bore of a wound stator such that it is expanded to a cylindrical shape conforming to the stator bore. The seam is welded, and the edges of the liner are welded to the inner diameters of the end rings of the stator housing. Within the water gap the liner can be made very thin since it will receive total structural support from the stator teeth and slot wedges. A second outer metallic surface (stator exterior housing), enclosing the wound stator assembly, is then welded to the outer diameter of the support end rings, forming a completely enclosed metallic envelope around the stator assembly. This enclosed cavity is then evacuated and filled with either a solid setting epoxy, a fluid or a slurry mixture to pressure/temperature compensate the cavity.

A third approach is the wet form-wound winding. The winding which has been protected by a seawater-impervious coating is exposed directly to the seawater. For the form-wound coil winding, a technique developed by the David Taylor Naval Ship Research and Development Center can be used.⁴⁴ This technique involves the use of a laminated stator epoxy-bonded by coating each individual lamination with a B stage epoxy adhesive dissolved in a solvent. After allowing the epoxy to partially cure, the laminations are stacked and clamped to a pressure expected

in the seawater, and the entire assembly is allowed to cure. The stator assembly is then cleaned of extruded bonding material, and a fluidized-bed epoxy corrosion-protection treatment is applied to a thickness of approximately .020 inches.⁵¹ The form-wound coil is formed by using standard varnished rectangular magnet wire. In the case of the design proposed here, all the wires making up one coil group (one-half of the stator slot) will be in parallel so that the wire-to-wire voltage will essentially be zero. Also, the short coil span demands extremely flexible coil throws. Hence, it is sufficient to skip wind a 1 mil layer of untreated glass tape around each wire to provide the necessary insulation. Thus, the value of u as discussed in Chapter 3 will be approximately .004 inches if an allowance of .001 inch is made for the polyester film around the copper wire. Flaherty¹² also discusses procedures for annealing the copper of the coil at 1100°F to obtain the proper amount of flexibility.

Alternate layers of silicon rubber paste and semicured rubber tape are then applied to each coil. Heat is finally applied to cure the paste and the rubber tape. This treatment creates a seawater-impervious coating for the coil. The motor proposed here is designed at 4 KV line-to-line. The general rule of thumb used in preliminary design for the insulation is:

$$D6S = WSS6 = \frac{V_{L-L}}{\sqrt{3} \times (50v/mil)} \quad (4.1)$$

Alternately, Reference 1, p. 205 provides good guidance on insulation thickness. This corresponds to $u = .046$ in. for 4KV applications. When this is combined to the stator core epoxy coating of thickness .020 inch, an overall thickness, TIN , between the coil and iron becomes .066 inches. The insulation between coils will have to be large enough to withstand twice the line voltage. Hence,

$$DSS = 2(.066) = .132$$

The coil sides then are placed in molds which serve to control the slot section of the coil when final curing of the insulation takes place. The cured coils are then placed in the slots of the bonded stator, and the wet-winding motor is assembled. The detailed procedure has been reported for motors tested at 6000 psi (depth equivalent to 13,000 ft) and at 13,200 psi (depth equivalent to 30,000 ft).^{12,46,51}

Table 4.1 compares the merits of the canned stator, wetwinding bonded stator and encapsulated stator approaches. Of the seawater designs, be they encapsulated, canned, or open wet winding, a limited interchange of water between the motor interior and the external sea is desired. That is advisable, first, from the viewpoint of excluding abrasive contaminants from the interior of the motor so as to maintain reasonable bearing life, and, secondly, to increase the probability of maintaining clear and open passages for the water circulation needed for bearing lubrication and heat transfer.

TABLE 4.1

COMPARISON OF CANNED, BONDED AND ENCAPSULATED STATOR APPROACHES

Type of Seawater Protection	Comments
Fluid Compensated, Canned Stator	<p>Recommended for all depths. Designs have passed 10,000 psi static pressure tests.</p> <p>Pressure cycling effects on cans not yet defined.</p> <p>Electrical insulation material/oil compatibility to be determined.</p> <p>Recommended for either fluid-compensated or seawater-flooded motor designs.</p> <p>Metallic can adds to motor structural weight.</p>
Open Winding, Bonded Stator	<p>Recommended for all depths.</p> <p>Recommended for both fluid compensated and seawater-flooded motor designs.</p> <p>Winding space factor within the slot is diminished.</p>
Epoxy Encapsulated Stator	<p>Questionable for pressures greater than 2000 psi.</p> <p>Difficult to ensure elimination of voids.</p> <p>Epoxy materials have characteristically poor heat transfer properties.</p> <p>Difficult to bring electrical terminal leads through wall of epoxy envelope.</p> <p>Individual coil repair impossible.</p>

For the application as a driver for a directly coupled large hub propeller, the wet winding bonded stator approach is most favorable. It is the simplest and provides the largest amount of a heat transfer from the windings. It also appears to be the easiest to repair and/or isolate damaged sections. Consider the following winding arrangement:

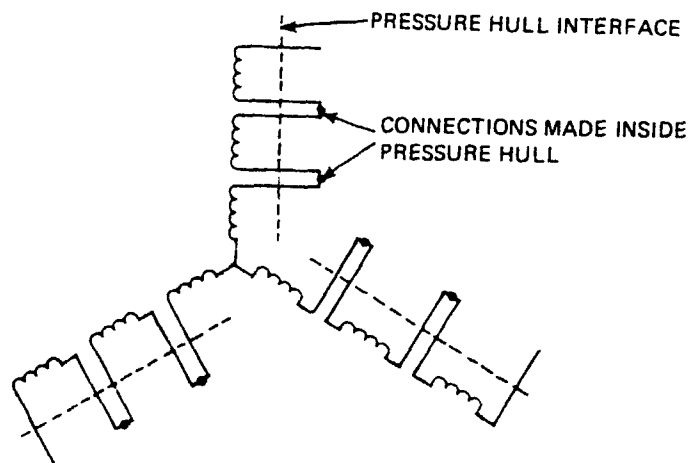


Figure 4.5

offer the best corrosion protection and heat transfer characteristics. Also, the inner liner is made very thin within the water gap and is supported by the rotor teeth. Again, just as with the stator, the rotor core laminations will be epoxy-bonded with a stacking pressure exceeding design depth. Also, burrs in the stacked laminations must all face in the same direction and epoxy coating thickness should exceed this lamination nonlinearity. Corrosion protection of the rotor slots by coating the inner diameter of the rotor slots with epoxy may or may not be done depending on the designer's efforts in ensuring that seawater does not penetrate the rotor can. For this design, no rotor slot protection is assumed ($D6R = 0$).

E. Computer Program Results/Design Requirements

The motor design in this thesis is to be for a large nuclear- or diesel-powered submarine. While it can be argued that this design's applicability would be greater for smaller submersibles, a 32-foot diameter hull is assumed so that comparisons to conventional propulsion systems can be made. A smaller submersible would not have the same construction or maintenance difficulties as would the 16.5-foot diameter motor proposed here. This is obvious since structural loading on individual motor parts would be significantly less. From the standpoint of the computer program, however, it is a very simple matter to scale up or scale down dimensions in the NAMELIST arguments of INDUC.DAT.

Sizing of the motor must come from a knowledge of the

actual submarine size and speed requirements. These requirements can be obtained from the computer program, CURVES. Assume the following submarine configuration:

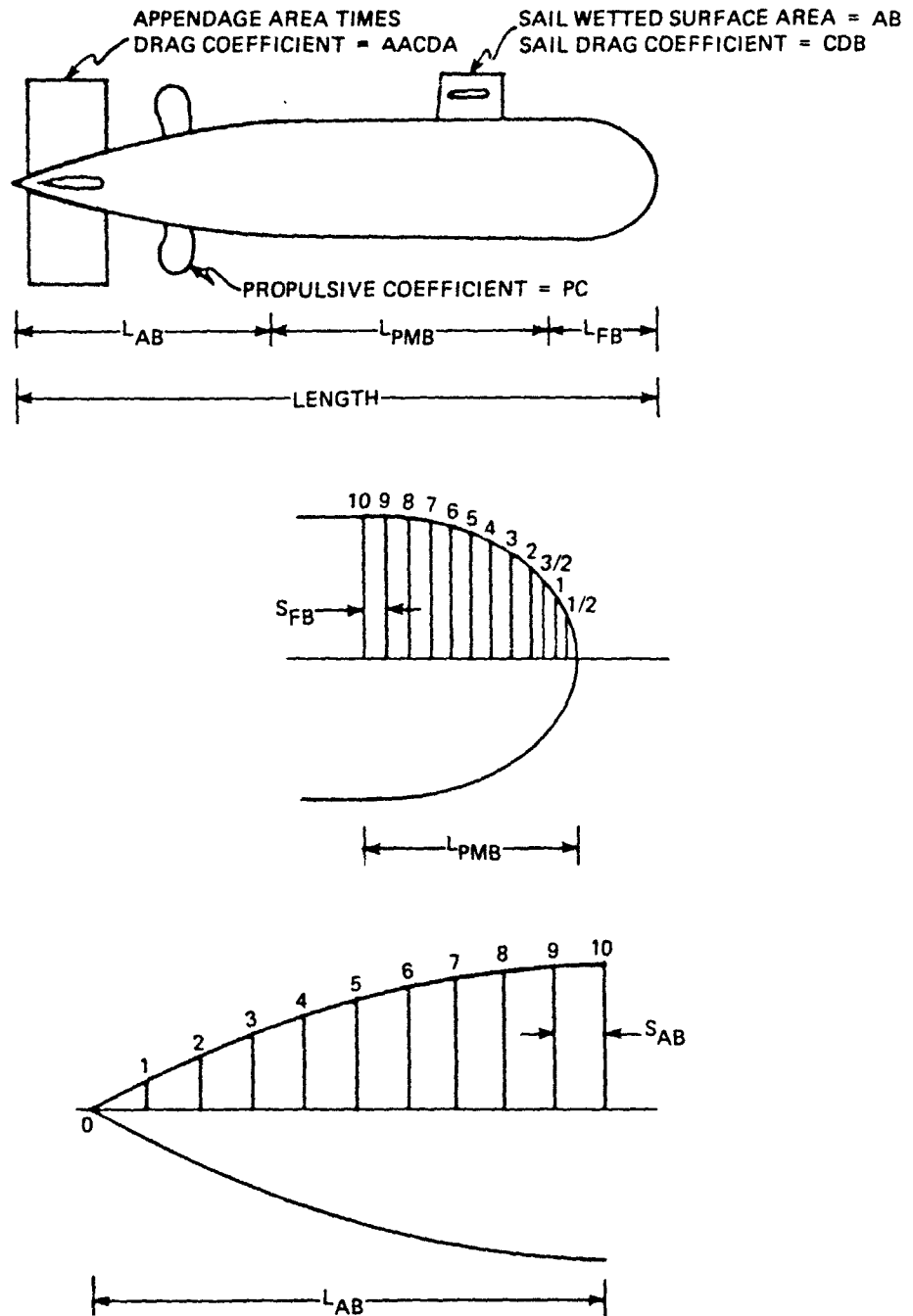


Figure 4.6

A selection of offsets for a 32-foot diameter hull is shown below in Table 4.2.

TABLE 4.2

STA	OFFSET (ft)
0	0.0000
1/2	5.0496
1	7.2304
3/2	8.8872
2	10.2400
3	12.2992
4	13.7984
5	14.8288
6	15.5136
7	15.8784
8	16.0000
9	15.8912
10	15.6096
-	-
10	15.6096
9	15.1024
8	14.4416
7	13.5872
6	12.5408
5	11.2544
4	9.7152
3	7.8592
2	5.4944
1	3.0544
0	0.0000

Also assume:

$$\begin{aligned}
 L_{PMB} &= 0.0 \text{ ft.} \\
 S_{FB} &= 11.74 \text{ ft.} \\
 S_{AB} &= 11.74 \text{ ft.}
 \end{aligned}$$

LENGTH = 234.88 ft.
 AB = 1000 ft.²
 CDB = .009
 AACDA = 10.0 ft.²
 PC = 0.80

These offsets and estimated appendage area and drag figures are derived for a mathematically-defined body of revolution²² of fineness ratio L/D = 7.34, belonging to TMB Series 58. Hull diameter is chosen to be 32 feet and a propulsive coefficient of 0.80 is assumed.

This data is set up into a datafile in the order shown above and read by the main program. Based upon frictional drag and form drag computations, the results are shown in Figures 4.8 and 4.9. The distinction between effective horsepower (EHP) and shaft horsepower (SHP) is:

$$SHP = \frac{EHP}{PC}$$

If it is desired that the submarine travel at a maximum speed of approximately 32 knots, then an estimated 17,364 horsepower must be delivered to the water to overcome drag (Figure 4.7) while an estimated 21,706 horsepower must be developed in the motor (Figure 4.8). Of course, the input power to the motor will be even higher than this by a factor equivalent to the inverse of the motor efficiency at peak power. This value of shaft horsepower becomes the basis for computing the rated torque of the motor:

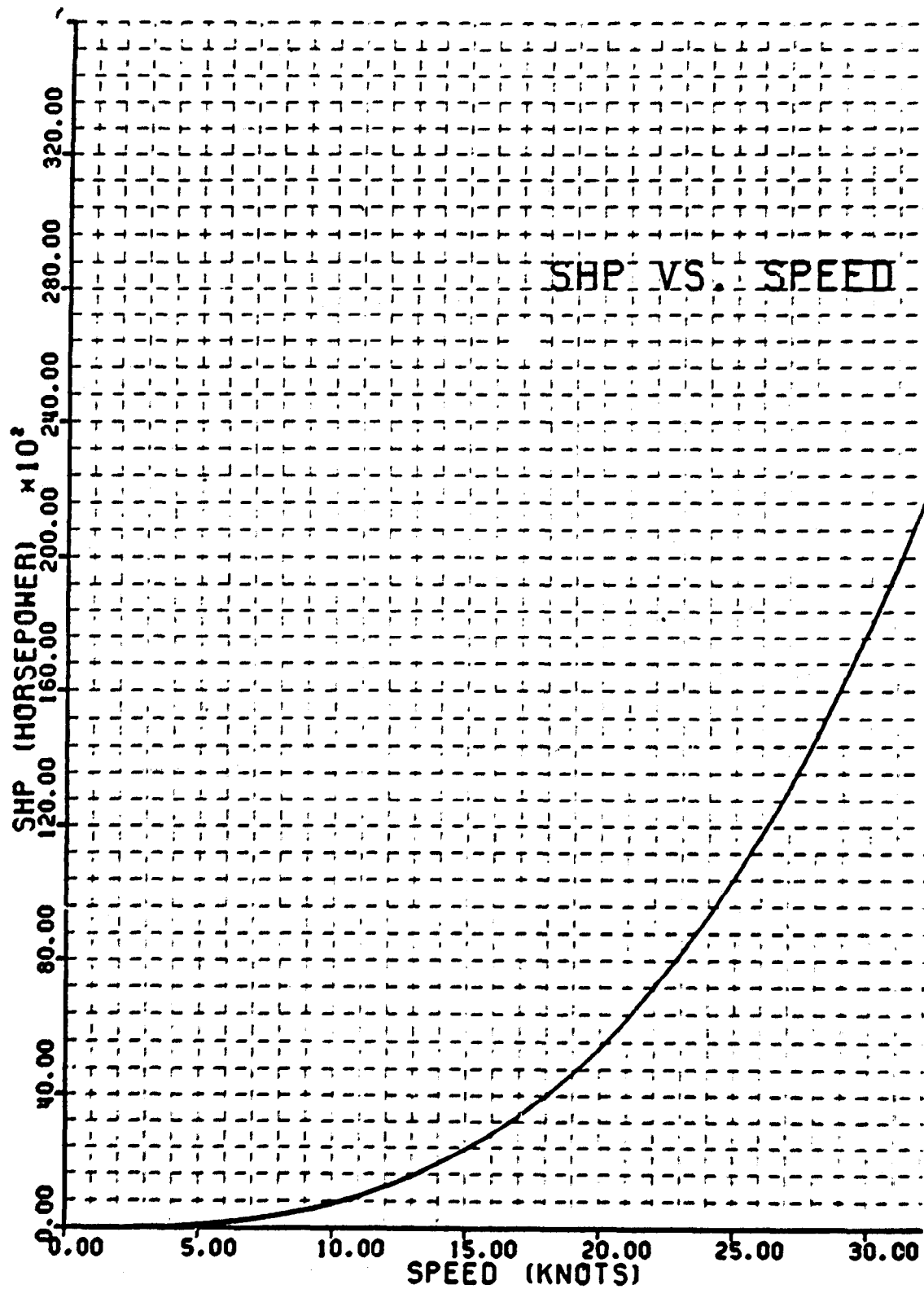
*****THE FOLLOWING DATA IS USED IN DETERMINING THE SPEED-POWER CURVE*****

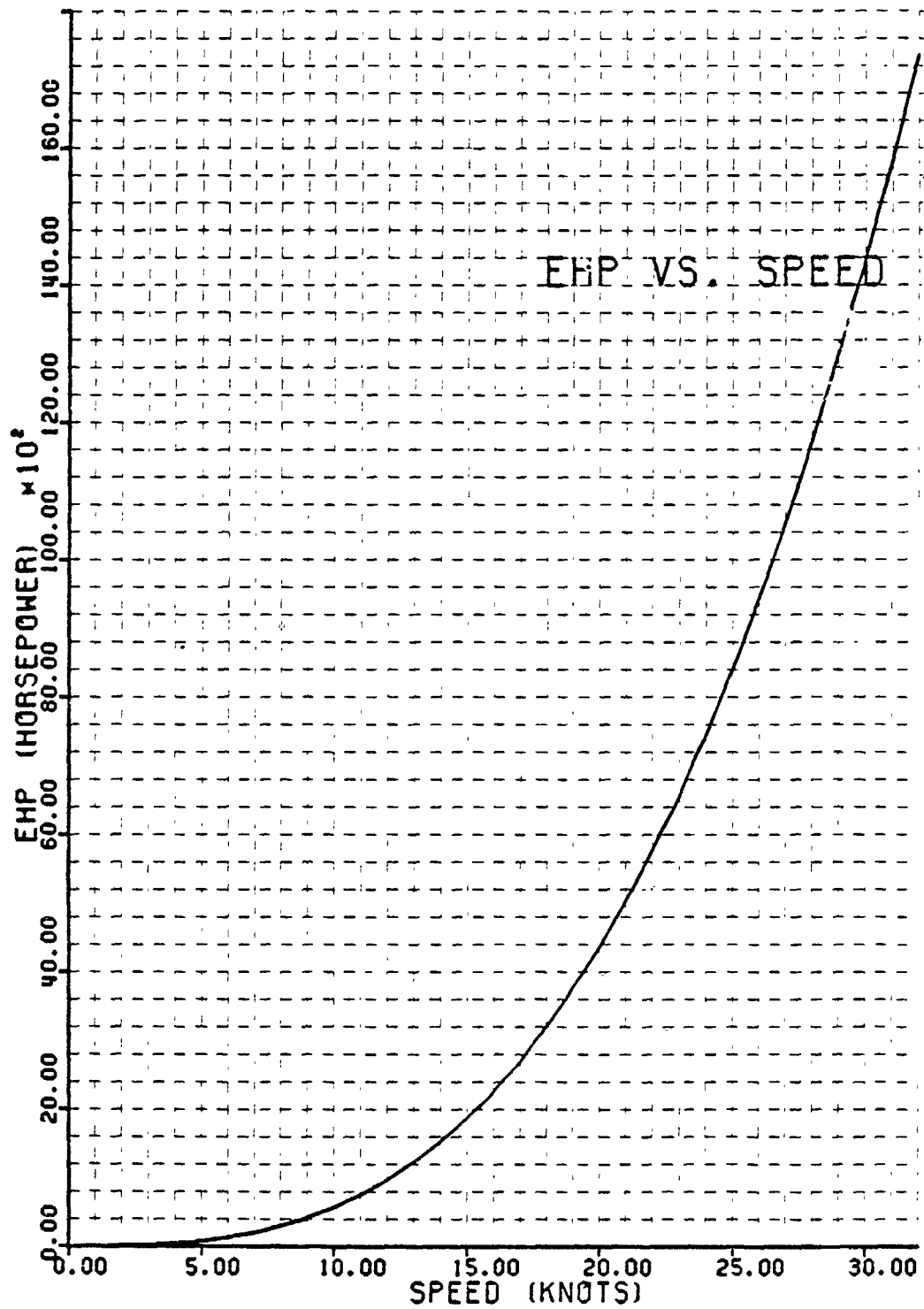
SPEED	CF	CFR	HP	SH
1.000	0.002478	0.003463	0.632	0.853
2.000	0.002227	0.003194	5.137	6.421
3.000	0.002098	0.003055	16.778	20.972
4.000	0.002013	0.002964	38.897	48.622
5.000	0.001951	0.002897	74.720	93.400
6.000	0.001902	0.002844	127.423	159.279
7.000	0.001867	0.002801	200.149	250.180
8.000	0.001828	0.002765	296.009	370.012
9.000	0.001800	0.002734	418.093	522.617
10.000	0.001774	0.002707	569.469	711.837
11.000	0.001752	0.002683	753.189	941.486
12.000	0.001732	0.002661	972.286	1215.357
13.000	0.001714	0.002642	1229.782	1537.228
14.000	0.001697	0.002624	1528.686	1910.858
15.000	0.001682	0.002608	1871.995	2339.993
16.000	0.001668	0.002593	2262.094	2828.368
17.000	0.001655	0.002579	2703.761	3379.701
18.000	0.001643	0.002566	3198.165	3997.706
19.000	0.001631	0.002553	3748.863	4686.079
20.000	0.001621	0.002542	4358.808	5448.509
21.000	0.001611	0.002531	5030.943	6288.679
22.000	0.001601	0.002521	5768.207	7210.259
23.000	0.001592	0.002511	6573.531	8216.913
24.000	0.001584	0.002502	7449.630	9312.295
25.000	0.001576	0.002493	8400.040	10500.058
26.000	0.001568	0.002485	9427.069	11783.837
27.000	0.001560	0.002477	10533.810	13167.271
28.000	0.001553	0.002469	11723.186	14653.964

Figure 4.7

29.000	0.001546	0.002462	12998.083	16247.606
30.000	0.001540	0.002455	14361.397	17951.746
31.000	0.001534	0.002446	15816.017	19770.020
32.000	0.001528	0.002442	17364.822	21706.027

Figure 4.7 (cont'd)





The windings are connected outside the stator core and this connection scheme is used advantageously in this wet winding motor. In Figure 4.5, each pole winding in each phase (only three coil groups per phase are illustrated here) has been isolated from the others by bringing each lead out separately. These leads are passed through hull penetrations where they are connected within the submarine pressure hull. In this way, each coil can be connected to appropriate meters to measure voltage, current and resistance. In a manned submersible, electricians could take appropriate isolation procedures to remove any problematic coil and reconnect the windings for resumed motor operations. In an unmanned submersible, computer-based monitoring and switching is possible. This winding scheme does have the drawback of marginally increasing the stator winding resistance. However, though the real input power must be increased somewhat, the amount of reactive power required will not change. Consequently, though the motor operates with less efficiency, it does so at a more favorable power factor.

For the rotor, similar insulation system arguments can be made as were done for the stator. Because the squirrel-cage rotor is one complete solid structural unit with no separated endwinding, it is logical to assume a canned approach. Because any damage that the rotor sustains can only be compensated for by entire rotor removal and replacement, a maintenance philosophy need not be established. The canned rotor would

$$T_{RATED} = \frac{(SHP) \left(33,000 \frac{\text{ft-lbs}}{\text{min-hp}} \right)}{(2\pi \times 60) \frac{\text{rad}}{\text{min}}} = 1.90 \times 10^6 \text{ ft-lbs.} \quad (4.2)$$

This value computed for T_{RATED} will be slightly less than ideal since the rated speed is assumed here to be 60 RPM when actually it will be slightly less due to slip.

A winding pattern consisting of 180 slots, 3 phases, 60 poles, 6 slots per pole pair and a pitch of $2/3$ was chosen for the design as shown in Figure 4.9:

a	b'	c	a'	b	c'	a
c'	a	b'	c	a'	b	c'

Figure 4.9

Also, the motor is located approximately between stations 3 and 4 on Figure 4.6.

Figure 4.10 lists the stator and rotor lamination magnetization data extracted from Reference 9. Note that the maximum flux density of 104.2 kilolines/in.² is also the desirable level of flux density in the stator and rotor iron. Above this value saturation increases rapidly. This design uses equal lamination thicknesses for both the stator and the rotor though it is conceivable that the rotor could have much thicker laminations and still have tolerable losses. This important factor results because of the very low slip

STATUR MATERIAL--- M-19 SILICON STEEL MANUFACTURED BY US STEEL

(KILOLINES/SQ-IN)	H		(A-TURN/IN)		FLUX DNSTY	SLOPE
	LAN THK	FREQ	FLUX DNSTY	SLOPE		
25.60	0.014	500.0	64.5	1.53		
32.20						
38.70						
45.20						
51.60						
58.00						
64.50						
70.90						
77.40						
83.80						
90.30						
96.70						
103.20						
104.20						
CURE-LOSS DATA						
CURE-LOSS						
13.5						

ROTUR MATERIAL--- M-19 SILICON STEEL MANUFACTURED BY US STEEL

(KILOLINES/SQ-IN)	H		(A-TURN/IN)		FLUX DNSTY	SLOPE
	LAN THK	FREQ	FLUX DNSTY	SLOPE		
25.60	0.014	500.0	64.5	1.53		
32.20						
38.70						
45.20						
51.60						
58.00						
64.50						

Figure 4.10

70.90	3.64
71.40	4.79
83.80	7.67
90.30	11.92
96.70	20.76
103.20	64.07
104.20	71.25

Figure 4.10(cont'd)

frequency seen on the rotor. It is well known that hysteresis loss is directly proportional to frequency whereas eddy current losses in the iron are directly proportional to the square of the frequency. From a structural point of view, it is desirable to make the rotor laminations thick since they will support the propeller hub and ultimately must absorb propeller thrust fluctuations. A strong inflexible rotor core is compatible with this design. Only one lamination thickness is used in the program though the program can handle as many as ten different thicknesses. Thus, it appears likely that motor efficiency could be improved a small amount if different thicknesses are tried.

Figures 4.11 and 4.12 are listings of the chosen stator data. During the course of this design effort, the goal was to achieve a workable concept. This was achieved by maximizing power output, efficiency and power factors. However, this is by no means the optimum concept. Small changes in much of the data presented can have significant impact on the design. Thus, though the results presented later appear quite satisfactory already, they can be improved by slightly varying the data presented in Figures 4.11 and 4.12. However, knowing exactly how to vary this data is not a trivial matter since there are such a large number of variables most of which are related nonlinearly. Computer-aided mathematical optimization is reserved for future research. The literature is extensive on recent techniques that have been applied

***** SUBMARINE ELECTRIC PROPULSION MOTOR *****

RATING

SYNCHRONOUS SPEED 60. RPM
 FREQUENCY 30. HZ
 POLES 60.
 L-W VOLTAGE 2309.0 VOLT
 RATED TORQUE 2140500.0 FT-LBS

STATOR

INSIDE DIAMETER 182.850
 OUTSIDE DIAMETER 191.100
 DEPTH BELOW SLOT 1.625
 LENGTH 102.000
 LAMINATION THICKNESS 0.0140
 STACKING FACTOR 0.9655
 STATOR IRON WEIGHT 46370.085

STATOR SLOTS

SLOT TYPE	1	NO. OF SLOTS	180.
SLOT WIDTH	1.000	SLOT DEPTH	2.500
WSS1	0.000	D1S	2.154
WSS2	0.000	D2S	0.280
WSS3	0.000	D3S	0.000
WSS4	1.600	D4S	0.000
WSS5	1.600	D5S	0.132
WSS6	0.066	D6S	0.066
USABLE AREA	2.968	TOTAL AREA	4.000
SPACE FACTOR	0.721		

Figure 4.11

STATOR WINDING	
MATERIAL	3
CONDUCTORS PER SLOT	2.
PARALLEL CIRCUITS	1.
PITCH	0.667
AXIAL EXTENSION BEYOND CORE	1.000
CONDUCTOR CROSS-SECTION	0.144E+01
STRAND CROSS-SECTION	0.144E+01
CONDUCTOR LENGTH	114.015
CLANCE MIN END-TURNS	0.140
TEMPERATURE (C)	150.
AXIAL END-TURN LENGTH	5.311
OVERALL ARMATURE LENGTH	112.623
PITCH FACTOR	0.866
DISTRIBUTION FACTOR	0.866
ARMATURE CONDUCTOR WEIGHT	18993.861
TOTAL ARMATURE WIRE LENGTH	3420.442 FEET
STRANDS/CONDUCTOR	1.

Figure 4.12

successfully and are certain to work for this induction motor design.

Perhaps one of the most significant results of using such a large number of poles in the design is the dimensions of the stator and rotor back iron. They roughly are on the order of or slightly smaller than the slot depth. Thus, in a profile view, the rotor and stator lamination heights are relatively small (approximately 4 or 5 inches) compared to the diameter of the hull. In order to aid in the reduction of the overall weight of the motor, the depth below the slot should be kept small.

Figure 4.13 is a listing of the rotor data. As is the case for the stator, the rotor data presented here is similarly chosen to meet the geometry requirements while maximizing power output, efficiency and power factor.

Figure 4.14 is a listing of water gap, reactance and weight data. A water gap equal to $G = 0.200$ inches is assumed. This is probably the most critical variable in the entire input file as it affects so many performance aspects of the machine. It is difficult to say at this point in the design exactly what this value will be. It largely depends on the journal bearing design. The effective airgap is computed by the use of Carter coefficients (see Appendix B). The magnetizing reactance and leakage reactance derivations are presented in Appendix B. The total motor electromagnetic weight will be used in Chapter 6 in comparison to conventional designs.

ROTOR	
OUTSIDE DIAMETER	198.000
INSIDE DIAMETER	191.500
LAMINATION THICKNESS	0.0140
STACKING FACTOR	0.9655
SLOT SKEW	1.000
DEPTH BELOW SLOT	1.625
ROTOR IRON WEIGHT	42807.575

ROTOR SLOTS		
SLOT TYPE	5	NO. OF SLOTS 206.
SLOT DIAMETER	0.000	SLOT DEPTH
WSK1	0.400	D1K
WSK2	1.600	D2R
WSK3	0.000	D3R
WSK4	0.000	D4R
WSK5	0.000	D6K
WSK6	0.000	
USABLE AREA	2.011	TOTAL AREA
		2.021

ROTOR WINDING	
MATERIAL	1
BAR LENGTH	108.005
BAR CROSS-SECTION	2.011
END-RING OUTSIDE DIA	198.000
END-RING INSIDE DIA	191.500
END-RING THICKNESS	2.500
STACK-TO-END-RING CLRNCE	0.500
WINDING TEMPERATURE (C)	150.
WEIGHT	5129.049
COMPONENT OF R2 DUE TO BARS	0.0103
COMPONENT OF R2 DUE TO END-RINGS	0.0002

Figure 4.13

AIRGAP		
ACTUAL AIRGAP		0.2000
EFFECTIVE AIRGAP		0.2976
MAGNETIZING REACTANCE (AIR GAP ONLY)		0.847
LEAKAGE REACTANCES (UHML)		
	STATOR	ROTOR
SLUT	0.073	0.050
END-CONNECTION	0.002	0.002
SKREW	0.003	0.003
ZIG-ZAG	0.067	0.075
PERIPHERAL	0.002	
WEIGHT		
TOTAL (ELECTROMAGNETIC)		112729.644

Figure 4.14

Figure 4.15 is a listing of magnetization data at no-load. From the B-H curve data in Figure 4.10, a maximum flux density of 104 kilolines/in.² is established. In the stator teeth, stator yoke, rotor teeth and rotor yoke, a value just under this flux density is achieved by appropriate manipulation of machine geometry. If the maximum flux density of 104 kilolines/in.² is exceeded during the design process, the computer will respond with an error message. Also, these values must remain at this level during speed changes of the motor. If the frequency is decreased to decrease speed of the motor, the magnitude of air gap flux is reduced due to increased magnetizing reactance, and thus, the developed torque is reduced. It is the job of the solid state motor controller to maintain this flux density despite changes in external variables. Since the motor at no-load operates at very close to synchronous speed, the rotor resistances, R_2/s , is extremely high. For this reason, the rotor branch in the equivalent circuit is essentially removed.

Figure 4.16 presents windage data. The message "INSUFFICIENT DATA TO SCALE WINDAGE LOSS" results because data from a previous or similar design is not used here. If a small or scaled version of the submarine electric propulsion motor was built for test purposes, the windage data obtained from that analysis could be scaled by the computer program to windage data on a full-scale version. Because the motor as yet has no prototype, however, windage data is assumed

MACHINE SATURATED, TOOTH AMPERE-TURNS NOT CALCULATED

STATOR MATERIAL - M-19 SILICON STEEL MANUFACTURED BY US STEEL
 B MAX = 104.
 CORE LOSS AT 64.5 KL/SQ-IN = 0.2 W/LB
 ROTOR MATERIAL -- M-19 SILICON STEEL MANUFACTURED BY US STEEL
 B MAX = 104.

MAGNETIZATION CHARACTERISTICS (NO-LOAD, RATED VOLTAGE)

TOTAL USEFUL FLUX	3029004.17 KILOLINES
USEFUL FLUX/POLE	32157.93

FLUX DENSITIES	
AIRGAP	49.46 KL/SQ-IN
STATOR TOOTH	100.15
STATOR YUKE	100.47
ROTOR TOOTH	105.67
ROTOR YUKE	103.01

AMPERE-TURNS PER POLE	
AIRGAP	4607.32
STATOR TOOTH	94.33
STATOR YUKE	192.88
ROTOR TOOTH	0.00
ROTOR YUKE	318.74

TOTAL	5213.26
-------	---------

Figure 4.15

MAGNETIZING CURRENT
AIRGAP VOLTAGE
N.L. CURRENT DENSITY
CORE LOSS

2580.91 AMPERES
1927.43
1790.33
61374. WATT

Figure 4.15(cont'd)

WINDAGE INSUFFICIENT DATA TO SCALE WINDAGE LOSS

DESIGN
CONDITION

REFERENCE
CONDITION

WINDAGE LOSS, W 0.

EQUIVALENT CIRCUIT PARAMETERS

R1 =	0.010	X1 =	0.148
R2 =	0.011	X2 =	0.131
R0 =	181.591	X0 =	0.748

Figure 4.16

according to Eq. (87) in Chapter 3. The values of the equivalent circuit parameters are used in the network shown in Appendix E to obtain torque-speed characteristics.

Figure 4.17 provides relevant data for the motor as a function of slip. The motor performance at TRATED computed in Eq. (4.2) is set apart by spaces from the remainder of the data. Synchronous speed of the motor is set at 60 RPM with an operating frequency of 30 Hz. Current density in the stator winding conductors is not exceedingly high as values between 1700 amps/in.² for slow speed machines and 3500 amps/in.² for high speed machines are set as design limits for air-cooled machines. This machine, while being extremely slow speed, will utilize seawater cooling with its inherent 50-to-1 improvement in cooling efficiency compared to air. Motor efficiency is highly dependent on windage losses which at this point in the design are somewhat vague. However, from initial estimates of the windage loss, the computed efficiency shown in Figure 4.17 looks promising. More discussion on system efficiency appears in Chapter 6. The power factor looks somewhat low. Improvement in this area certainly would reduce the weight of the motor and speed control equipment, lower the voltage and current density required and improve voltage regulation. A big improvement in power factor is achievable if the water gap clearance is reduced. Current density in the rotor bars at rated torque are within design limits, and with cooling water flow, should present no problem. Because of the need for a large number of rotor bars to reduce

WINDMILL PERFORMANCE AT 2309.00 VOLTS, 30.0 HZ

THROU (P1-I _{INS}) (P ₁ P ₂ P ₃ P ₄)	RPM	P-OUT (HP)	(KWAFF)	I (AMP)	I/A (AMPS/SQ IN)	EFF (PERCENT)	PF (*=LEADING)	P-IN (KWAIT)
1160891.16	1.00	59.40	13134.65	3250.08	2254.49	95.47	0.46	10259.73
1974217.06	2.00	58.80	22111.23	4478.27	3106.46	94.43	0.56	17461.52
2140500.00	2.31	58.61	23897.77	4442.67	3106.46	93.91	0.57	18975.47
2383161.52	3.00	58.20	26419.27	5565.54	3860.67	92.67	0.55	21258.28
2502045.36	4.00	57.00	27451.01	6362.54	4427.40	90.78	0.51	22549.83
2459816.90	5.00	57.00	26706.58	6968.85	4834.11	88.85	0.46	22413.42
2343054.23	6.00	56.40	25171.10	7387.79	5124.72	86.94	0.42	21590.10
2199212.56	7.00	55.80	23374.49	7690.85	5334.97	85.05	0.38	20494.79
2051665.05	8.00	55.20	21571.84	7914.30	5489.94	83.19	0.35	19337.01
1910957.94	9.00	54.60	19873.96	8082.35	5606.51	81.36	0.33	18214.65
1781146.31	10.00	54.00	18320.88	8211.25	5695.93	79.57	0.30	17168.83
1661431.09	11.00	53.40	16919.47	8311.97	5765.79	77.82	0.28	16212.78
1557312.96	12.00	52.80	15602.12	8391.98	5821.29	76.10	0.26	15346.63
1461917.32	13.00	52.20	14535.64	8455.51	5866.06	74.42	0.25	14564.74
1376148.83	14.00	51.60	13525.48	8509.26	5902.65	72.77	0.24	13859.31
1298674.30	15.00	51.00	12617.64	8552.97	5932.93	71.16	0.22	13222.16
1224101.43	16.00	50.40	11799.37	8589.45	5958.27	69.58	0.21	12645.45
1165906.64	17.00	49.80	11053.46	8620.32	5979.69	68.03	0.20	12122.10
1104488.80	18.00	49.20	10388.12	8646.64	5997.94	66.52	0.19	11645.78
1056152.33	19.00	48.60	9776.95	8689.26	6013.64	65.03	0.19	11210.97
1008296.08	20.00	48.00	9218.71	8688.86	6027.23	63.56	0.18	10812.86
964401.54	21.00	47.40	8707.17	8705.94	6039.09	62.15	0.17	10447.29
924020.36	22.00	46.80	8256.98	8720.94	6049.48	60.75	0.17	10110.64
886756.12	23.00	46.20	7803.54	8745.17	6058.66	59.38	0.16	9799.75
852303.27	24.00	45.60	7402.86	8745.90	6066.06	58.04	0.16	9511.94
820340.51	25.00	45.00	7031.49	8756.36	6074.06	56.72	0.15	9244.79
790673.97	26.00	44.40	6686.42	8765.73	6080.56	55.42	0.15	8996.25

Figure 4.17

762331.79	21.00	43.60	6305.03	4746.40	8774.15	6086.40	54.15	0.14	8764.48
737069.40	28.00	43.20	6065.03	4522.69	8781.76	6091.67	52.91	0.14	8547.90
712663.65	74.00	42.60	5784.40	4313.42	8786.65	6096.45	51.69	0.14	8345.10
690199.53	30.00	42.00	5521.36	4117.28	8794.91	6100.80	50.49	0.13	8154.84
668847.33	31.00	41.40	5274.34	3933.07	8800.62	6104.76	49.31	0.13	7976.01
648780.36	37.00	40.80	5041.95	3759.78	8805.85	6108.38	48.16	0.13	7807.63
627662.98	33.00	40.20	4822.95	3596.47	8810.64	6111.71	47.02	0.13	7646.83
617060.75	34.00	39.60	4616.23	3442.33	8815.05	6114.77	45.90	0.12	7498.84
595109.19	35.00	39.00	4420.81	3296.60	8819.12	6117.59	44.81	0.12	7356.94
574112.43	36.00	38.40	4235.79	3158.63	8822.87	6120.20	43.73	0.12	7222.51
563542.19	37.00	37.60	4060.36	3027.83	8826.35	6122.61	42.68	0.12	7094.99
544536.66	38.00	37.20	3893.86	2903.65	8829.59	6124.85	41.64	0.11	6973.87
535840.71	39.00	36.60	3735.58	2785.62	8832.59	6126.94	40.61	0.11	6858.67
526033.26	40.00	36.00	3584.94	2673.29	8835.39	6128.88	39.61	0.11	6746.98
510378.61	41.00	35.40	3441.41	2566.26	8838.01	6130.69	38.62	0.11	6644.42
498825.00	42.00	34.80	3304.51	2464.17	8840.46	6132.39	37.65	0.11	6544.64
487204.35	43.00	34.20	3173.79	2366.69	8842.75	6133.98	36.70	0.11	6449.33
476381.84	44.00	33.60	3048.64	2273.52	8844.90	6135.47	35.76	0.10	6358.19
465106.36	45.00	33.00	2929.30	2184.38	8846.92	6136.88	34.83	0.10	6270.96
450106.36	46.00	32.40	2814.83	2099.02	8848.82	6138.20	33.92	0.10	6187.39
440547.29	47.00	31.80	2705.10	2017.20	8850.61	6139.44	33.03	0.10	6107.27
437473.65	48.00	31.20	2593.84	1938.70	8852.31	6140.61	32.15	0.10	6030.37
42712.66	49.00	30.60	2498.76	1863.34	8853.90	6141.72	31.28	0.10	5956.52
420293.27	50.00	30.00	2401.68	1790.93	8855.42	6142.77	30.43	0.10	5885.54
412196.61	51.00	29.40	2308.38	1721.30	8856.85	6143.76	29.59	0.09	5817.26
404402.67	52.00	28.80	2218.44	1654.29	8858.21	6144.70	28.76	0.09	5751.54
396847.14	53.00	28.20	2131.90	1589.76	8859.50	6145.60	27.95	0.09	5688.23
389663.31	54.00	27.60	2048.52	1527.58	8860.72	6146.45	27.15	0.09	5627.21
382660.95	55.00	27.00	1968.10	1467.62	8861.88	6147.26	26.36	0.09	5568.34
375954.63	56.00	26.40	1890.51	1409.76	8862.99	6148.03	25.58	0.04	5511.54
369453.84	57.00	25.80	1815.60	1353.89	8864.05	6148.76	24.81	0.0	5456.67
363177.90	58.00	25.20	1743.23	1299.93	8865.06	6149.46	24.06	0.09	5403.66
357100.30	59.00	24.60	1673.27	1247.76	8866.02	6150.12	23.31	0.09	5352.40
351227.63	60.00	24.00	1605.61	1197.30	8866.94	6150.76	22.58	0.09	5302.82
345443.54	61.00	23.40	1540.14	1148.48	8867.82	6151.37	21.86	0.09	5254.83
340039.88	62.00	22.80	1476.74	1101.21	8868.66	6151.96	21.14	0.08	5208.35
334707.65	63.00	22.20	1415.34	1055.47	8869.46	6152.51	20.44	0.08	5163.32

Figure 4.17(cont'd)

329539.56	64.00	21.60	1355.82	1011.03	8870.24	6153.05	19.75	0.08	5119.67
329527.99	65.00	21.00	1298.11	908.00	8870.98	6153.50	19.07	0.08	5077.34
319005.97	66.00	20.40	1242.13	976.26	8871.69	6154.06	18.39	0.08	5036.27
314946.93	67.00	19.80	1187.80	885.74	8872.37	6154.53	17.73	0.06	4996.40
310304.08	68.00	19.20	1135.05	846.41	8873.02	6154.96	17.07	0.08	4957.68
305913.37	69.00	18.60	1083.81	808.20	8873.65	6155.42	16.43	0.06	4920.07
301587.49	70.00	18.00	1031.01	771.06	8874.26	6155.84	15.79	0.08	4883.51
297381.84	71.00	17.40	985.81	734.97	8874.84	6156.25	15.16	0.08	4847.97
293291.48	72.00	16.80	938.53	699.86	8875.41	6156.64	14.54	0.08	4813.40
289311.76	73.00	16.20	892.73	665.71	8875.95	6157.01	13.93	0.06	4779.76
285438.26	74.00	15.60	848.16	632.47	8876.47	6157.37	13.32	0.08	4747.01
281666.74	75.00	15.00	804.76	600.11	8876.98	6157.72	12.73	0.08	4715.13
277993.40	76.00	14.40	762.50	568.59	8877.46	6158.06	12.14	0.08	4684.07
274414.31	77.00	13.80	721.32	537.89	8877.93	6158.39	11.56	0.08	4653.81
270925.95	78.00	13.20	681.19	507.96	8878.39	6158.70	10.98	0.08	4624.32
267524.92	79.00	12.60	642.06	478.78	8878.83	6159.01	10.42	0.07	4595.56
264207.99	80.00	12.00	603.90	450.33	8879.25	6159.30	9.86	0.07	4567.51
260972.10	81.00	11.40	566.88	422.57	8879.66	6159.59	9.31	0.07	4540.14
257814.30	82.00	10.80	530.36	395.49	8880.06	6159.86	8.76	0.07	4513.43
254731.63	83.00	10.20	494.91	369.05	8880.45	6160.13	8.22	0.07	4487.36
251722.01	84.00	9.60	460.29	343.24	8880.82	6160.39	7.69	0.07	4461.90
248782.32	85.00	9.00	426.48	318.03	8881.18	6160.64	7.17	0.07	4437.03
245910.34	86.00	8.40	393.46	293.40	8881.53	6160.88	6.65	0.07	4412.74
243103.77	87.00	7.80	361.18	269.33	8881.87	6161.12	6.14	0.07	4388.99
240300.30	88.00	7.20	329.64	245.81	8882.20	6161.35	5.63	0.07	4365.78
237616.11	89.00	6.60	298.60	222.81	8882.52	6161.57	5.13	0.07	4343.09
235054.90	90.00	6.00	268.03	200.32	8882.83	6161.79	4.64	0.07	4320.89
232488.85	91.00	5.40	239.13	178.32	8883.14	6162.00	4.15	0.07	4299.18
229978.10	92.00	4.80	210.27	156.80	8883.43	6162.20	3.67	0.07	4277.93
227570.90	93.00	4.20	182.02	135.73	8883.72	6162.40	3.19	0.07	4257.14
225115.55	94.00	3.60	154.36	115.11	8883.99	6162.59	2.72	0.07	4236.78
222760.43	95.00	3.00	127.29	94.92	8884.26	6162.78	2.25	0.07	4216.85
220453.99	96.00	2.40	100.78	75.15	8884.53	6162.96	1.79	0.07	4197.33
218194.73	97.00	1.80	74.81	55.79	8884.78	6163.14	1.34	0.07	4178.20
215981.22	98.00	1.20	49.37	36.81	8885.03	6163.31	0.89	0.07	4159.47
213812.10	99.00	0.60	24.44	18.22	8885.28	6163.48	0.44	0.07	4141.11
212226.31	100.00	0.00	0.00	0.00	8885.51	6163.65	0.00	0.07	4123.11

Figure 4.17(cont'd)

CURRENT DENSITY AT RAISED TORQUE IN ROTOR BAR = 2354.49
IN END RING = 5036.89
IN ARMATURE = 3106.46

zig zag and rotor leakage reactance, current density in the endrings is about twice that in the rotor bars. Water cooling on the endrings, however, should provide the necessary cooling requirement.

Figure 4.18 provides loss data as a function of torque. Figure 4.19 presents the torque speed curve. It is well known that to a first approximation, the effective horsepower needed to drive a submarine through the water is directly proportional to its surface area and directly proportional to the cube of its velocity. Thus, in Figure 4.9 it is critical as to what maximum velocity the designer chooses to operate. Adding just one additional knot requirement on to the maximum speed requirement means adding a significant power requirement to the motor. At this point, the design voltage of 4 KV is relatively low for such a large machine compared to previous motor designs. Increasing the power requirement means increasing the voltage which, in turn, means adding more slot insulation thereby increasing slot current density. The motor then runs hotter and less efficiently. Thus, one conclusion to be made here is that for low to medium speed operations, the submarine electric propulsion motor will operate with no problems or major detriments. One can observe that the torque speed curve has a very steep slope around $S = 0$. This is a desirable characteristic for high efficiencies.

Figure 4.20 presents the thermal data as developed in the heat transfer model in Chapter 3. Until proven by experiment, these values should be approached with some degree of skepticism.

TOP-UP (FT-LBS)	PRI LOSS (KWATT)	SEC LOSS (KWATT)	IRUN LOSS (KWATT)	FW (KWATT)
116091.16	308.09	98.93	58.20	0.00
1974217.06	584.93	336.50	51.75	0.00
2140500.00	684.00	421.38	49.53	0.00
2383181.52	903.44	609.30	44.69	0.00
2502045.36	1188.15	852.93	38.54	0.00
2459816.90	1416.47	1048.16	33.70	0.00
2343054.23	1591.89	1198.09	30.03	0.00
2199212.36	1725.19	1311.96	27.29	0.00
2051669.09	1826.38	1398.79	25.22	0.00
1910957.94	1905.28	1465.72	23.64	0.00
1781196.31	1966.54	1517.99	22.42	0.00
1663431.09	2015.08	1559.39	21.46	0.00
1557312.96	2054.06	1592.62	20.70	0.00
1461517.32	2085.77	1619.65	20.09	0.00
1376136.83	2111.87	1641.90	19.59	0.00
12 9874.30	2133.60	1660.41	19.18	0.00
1229101.43	2151.86	1675.96	18.84	0.00
1165906.63	2167.36	1689.15	18.55	0.00
1108488.80	2180.61	1700.43	18.30	0.00
1056152.33	2192.04	1710.16	18.10	0.00
1008296.08	2201.96	1718.60	17.92	0.00
964401.34	2210.63	1725.97	17.76	0.00
924020.36	2218.25	1732.45	17.63	0.00
886766.12	2224.98	1738.17	17.51	0.00
852303.27	2230.97	1743.26	17.40	0.00
820340.51	2236.31	1747.79	17.31	0.00
790623.97	2241.09	1751.86	17.23	0.00
762931.79	2245.40	1755.52	17.15	0.00
737069.40	2249.30	1758.82	17.09	0.00
712865.65	2252.83	1761.82	17.03	0.00
690169.53	2256.04	1764.55	16.98	0.00

Figure 4.18

668047.33	2258.97	1767.03	16.93	0.00
648780.38	2261.66	1769.31	16.88	0.00
629862.98	2264.12	1771.40	16.84	0.00
612000.75	2266.38	1773.32	16.81	0.00
595109.19	2268.48	1775.09	16.77	0.00
579112.43	2270.41	1776.73	16.74	0.00
563442.19	2272.20	1778.25	16.72	0.00
549536.86	2273.87	1779.86	16.69	0.00
535840.71	2275.41	1780.97	16.67	0.00
522803.26	2276.86	1782.19	16.64	0.00
510378.61	2278.21	1783.33	16.62	0.00
498525.00	2279.47	1784.40	16.60	0.00
487204.35	2280.65	1785.40	16.59	0.00
476381.84	2281.76	1786.34	16.57	0.00
465025.58	2282.80	1787.22	16.55	0.00
456105.36	2283.78	1788.05	16.54	0.00
446597.29	2284.71	1788.83	16.53	0.00
437473.65	2285.58	1789.57	16.51	0.00
423712.66	2286.41	1790.27	16.50	0.00
420293.27	2287.19	1790.93	16.49	0.00
412196.01	2287.93	1791.55	16.48	0.00
404402.87	2288.63	1792.15	16.47	0.00
396897.14	2289.30	1792.71	16.46	0.00
389663.31	2289.93	1793.24	16.45	0.00
382686.95	2290.53	1793.75	16.45	0.00
375954.63	2291.10	1794.24	16.44	0.00
369453.84	2291.65	1794.70	16.43	0.00
363172.90	2292.17	1795.14	16.42	0.00
357100.90	2292.67	1795.56	16.42	0.00
351271.63	2293.14	1795.96	16.41	0.00
345543.54	2293.60	1796.34	16.41	0.00
340039.68	2294.03	1796.71	16.40	0.00
334707.65	2294.45	1797.06	16.39	0.00
329539.56	2294.85	1797.40	16.39	0.00
324527.99	2295.23	1797.72	16.38	0.00
319665.97	2295.60	1798.03	16.38	0.00
314946.93	2295.95	1798.33	16.38	0.00

Figure 4.18(cont'd)

310364.66	2296.29	1798.01	16.37	0.00
305913.37	2296.02	1798.89	16.37	0.00
301587.49	2296.93	1799.15	16.36	0.00
297381.84	2297.24	1799.40	16.36	0.00
293291.48	2297.51	1799.65	16.36	0.00
289311.76	2297.61	1799.89	16.35	0.00
285435.26	2298.08	1800.11	16.35	0.00
281666.79	2298.34	1800.33	16.35	0.00
277993.40	2298.59	1800.55	16.34	0.00
274414.31	2298.64	1800.75	16.34	0.00
270925.95	2299.07	1800.95	16.34	0.00
267524.92	2299.30	1801.14	16.34	0.00
264207.99	2299.52	1801.32	16.33	0.00
260972.10	2299.73	1801.50	16.33	0.00
257614.30	2299.94	1801.68	16.33	0.00
254731.63	2300.14	1801.84	16.33	0.00
251722.01	2300.33	1802.01	16.32	0.00
248782.32	2300.52	1802.16	16.32	0.00
245910.34	2300.70	1802.32	16.32	0.00
243103.77	2300.88	1802.47	16.32	0.00
240360.39	2301.05	1802.61	16.32	0.00
237678.11	2301.21	1802.75	16.31	0.00
235054.90	2301.37	1802.88	16.31	0.00
232488.85	2301.53	1803.02	16.31	0.00
229976.10	2301.68	1803.14	16.31	0.00
227520.90	2301.83	1803.27	16.31	0.00
225115.55	2301.98	1803.39	16.31	0.00
222760.43	2302.12	1803.51	16.31	0.00
220453.99	2302.25	1803.62	16.30	0.00
218194.73	2302.38	1803.73	16.30	0.00
215981.22	2302.51	1803.84	16.30	0.00
213812.10	2302.64	1803.95	16.30	0.00
212226.31	2302.76	1804.05	16.30	0.00

Figure 4.18(con'td)

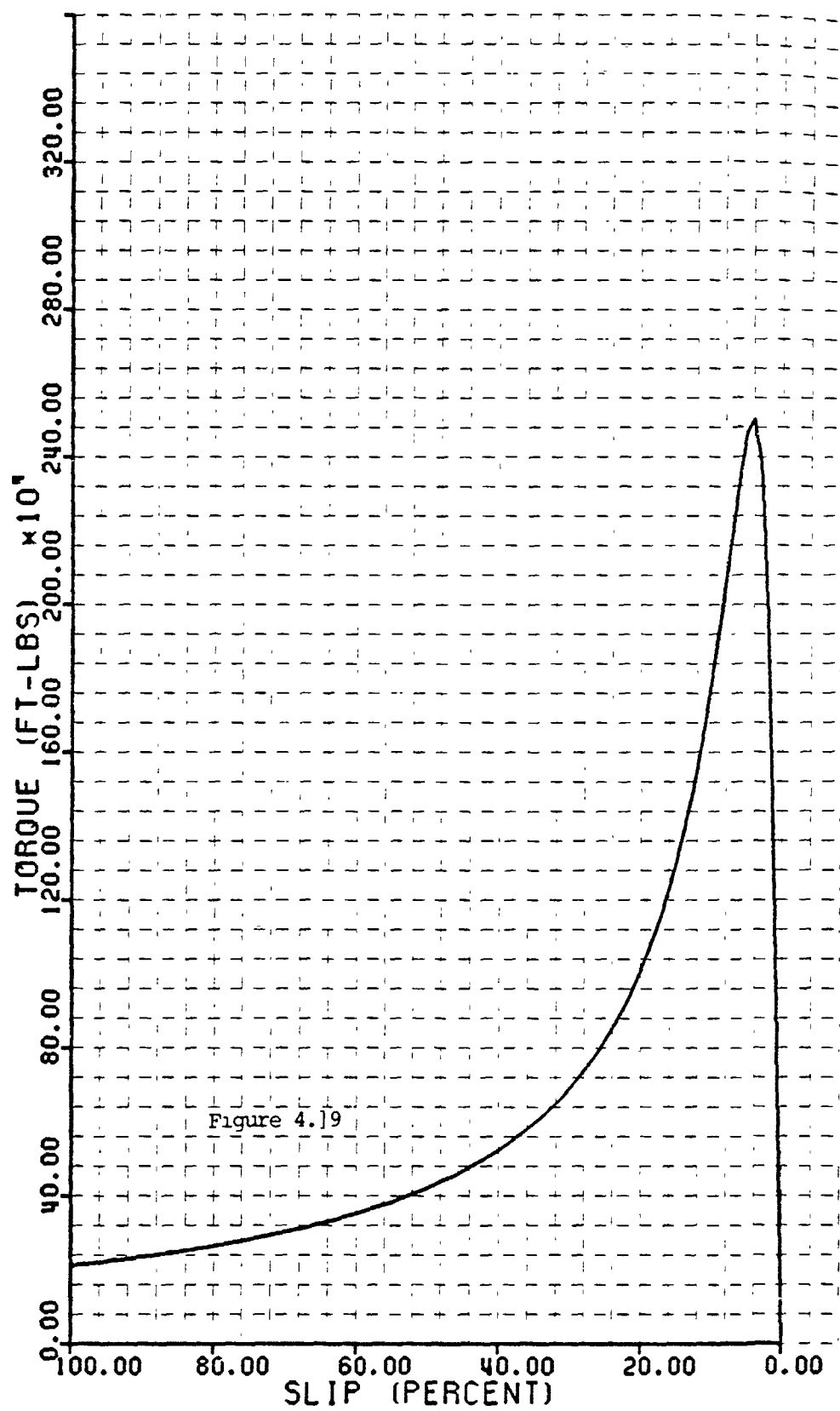


Figure 4.19

RE1	=	0.02132
RE2	=	0.00828
RE3	=	0.00620
R412	=	0.09830
R410	=	0.00038
R810	=	0.00038
R411	=	0.03226
R86	=	0.02131
R611	=	0.03060
R812	=	0.01741
REU1	=	0.00161
REU2	=	0.00304
REU3	=	0.00128
REU4	=	0.00225

NUSSULT NUMBER = 137.089,7

Figure 4.20

TAYLOR NUMBER = 5281.43779

OMEGA = 6.28320

OVERALL RESISTANCE COEF = 2.16456

COEFFICIENT OF FRICTION = 0.00138

They do, however, allow a picture to be obtained of the heat transfer process and the relative orders of magnitudes involved. When these resistances, coupled with the losses at rated output, are inserted into the lumped parameter model of Figure 3.23, the following average temperatures are obtained:

$$T_1 = 211.7 \text{ deg. F}$$

$$T_4 = 84.7 \text{ deg. F}$$

$$T_5 = 109.2 \text{ deg. F}$$

$$T_8 = 83.6 \text{ deg. F}$$

These values have assumed a water velocity of 1.689 ft/sec in a 0.2 inch gap. Ambient temperature is taken as a conservative value of 82 degrees F. Not included here are:

- 1) heat transfer out of the ends;
- 2) convection;
- 3) radiation.

Though it is not shown here, heat transfer out the ends is accounted for in the axial variation model presented in this chapter. Convection is accounted for by reductions in thermal resistances that are a function of cooling water flow. This would significantly reduce the temperatures obtained above. Radiation effects would not be significant, though when added to the model, the temperatures would be reduced further.

Based upon the current densities obtained in the motor analysis program, it appears logical to assume that ade-

quate cooling can be achieved. Of critical importance is the value used in the program for the encapsulation thickness. It significantly impacts on the resistances. Also, the thickness WSS6 has a large impact on the stator winding resistances RE1 and RE2. Noteworthy is the fact that it is possible to obtain computer printouts under logical unit 17 of all matrix operations performed in the thermal analysis including the eigenvalues and eigenvectors. These, however, are not shown here.

F. Motor Speed Control

Without having the elegance of today's modern solid-state motor control techniques, the feasibility of a submarine induction motor drive would certainly be remote. A quick review of the motor characteristics (Figures 4.17 and 4.19) reveal that extremely low starting torque and very high starting current exist for this motor whose configuration is similar to a NEMA Class A^{48,49} machine. This is a design choice in order to have a high maximum torque and high full load efficiency. It will always be the intention to operate the motor in the steady state on the extremely steep sloped section of the torque-speed curve. This occurs for nominal slip values between zero and four percent. During transient conditions, such as starting, braking or speed changing, solid state motor control will be employed. Other NEMA class options to

improve starting characteristics are possible. However, they suffer from the need to operate for a given torque at a higher value of slip and, consequently, are less efficient.

It is generally well known that there are only two ways to change the synchronous speed of an induction motor. The equation governing this relationship is:

$$\text{RPM} = \frac{120f}{p} \quad (4.3)$$

Changing the number of poles by the methods of consequent poles or pole-amplitude modulation will not be considered here since it generally is reserved for applications where two speed motors are needed. A variable speed or multi-speed motor is needed as a propeller drive. Controlling speed by changing the input frequency to the motor requires sophisticated and expensive solid state power conditioning equipment.

From Faraday's Law, it is easy to show that:

$$\phi_{\max} \propto \frac{V_o}{f} \quad (4.4)$$

Thus, as frequency is changed to alter motor speed, it is necessary to maintain the flux at approximately the same optimum maximum level near, but below saturation. In the computer program, this means that in order to maintain the flux density in the stator iron and the rotor iron at a value around 110 kilolines per square inch, the voltage applied must

be reduced when reducing the frequency. This is an ideal situation for the designer since lowering the frequency decreases the tendency towards high voltage breakdown of the winding insulation.

Figure 4.25 illustrates the principle of motor control for a hypothetical propeller load at a given submarine speed.

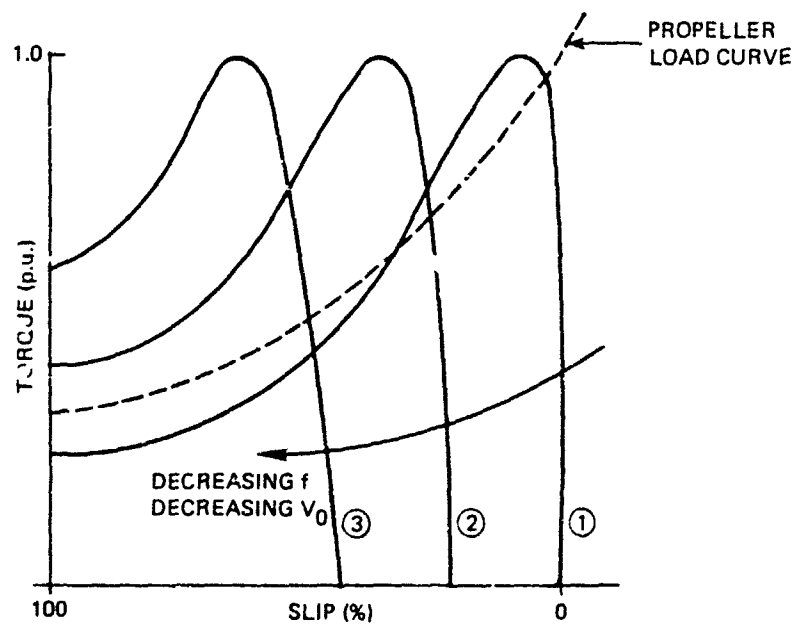


Figure 4.25

For case (1), the starting torque is not large enough to overcome propeller drag when initially turning over. However, case (2) permits starting and case (3) provides even better starting torque with lower starting current.

It is not the intention to fully develop the motor controller in this thesis. This undoubtedly would require a great deal of research and design effort. But, essentially, the technology is available to construct this piece of equipment which will be reliable and maintainable. The literature contains numerous articles on successful designs.^{44,48,49,52}

Undoubtedly of greater importance at this stage is the impact that the speed controller will have on the overall submarine design, namely in size and weight. This area will be discussed in greater detail in Chapter 6.

G. Dynamic Braking

Controlled dynamic braking of the submarine electric propulsion motor during maneuvering or crash-back operations can be achieved by either of two following methods.⁴⁴

If a variable frequency source such as an inverter-controller is available, a voltage can be applied at a frequency lower than the synchronous motor speed to achieve braking. This in turn, requires accurate sensing of the motor speed. The frequency is continuously adjusted to stay lower than synchronous speed by an amount corresponding to normal motor slip. The voltage is also varied to control the generated braking current and torque. In this mode, the motor is made to function as an induction generator and the energy removed is dissipated in

braking resistors within the submarine.

The second method of braking is to apply a controlled d-c voltage to one phase of the three-phase induction motor. The kinetic energy of the submarine in this case is absorbed by the rotor cage bars. With a good water cooling arrangement, this heat could be easily removed.

Chapter 5

PRELIMINARY PROPELLER DESIGN

A. Introduction

In the design of this submarine electric propulsion system, the electric motor is the driving factor around which all other subsystems focus. Unless the motor performs well, there is no point in proceeding further in the design. For this reason the propeller design and analysis comes after the initial motor concept is formulated. It is possible, however, to work in the reverse order; that is, design the propeller first based upon known submarine geometry and powering requirements. This propeller is optimized for efficiency at a particular advance coefficient, J . From this value of efficiency and advance coefficient, motor torque speed characteristics are obtained, and the motor designed around these factors. This second approach, however, restricts the electrical designer to a much greater extent and possibly forces him to select a slot/pole configuration that reduces motor efficiency somewhat. Obtaining a motor efficiency that is comparable to that achievable for a motor that is designed first is possible but only if a complete motor design and optimization computer program is on hand. These exist for conventional induction motors and would have to be revised for the configuration in this thesis. Based upon the extremely flexible computer methods for propeller design and analysis at M.I.T. and the Charles Stark Draper

Laboratory, proceeding first with the motor design appears the most logical. The propeller design proceeds after this with an ultimate goal of achieving the highest efficiency for the "matched" power unit.

The propeller design is based upon the requirements of satisfying the given constraints:

- 1) The maximum propeller diameter must be slightly less than the maximum submarine hull diameter of 32 feet so as to not impinge on submarine operations alongside a berth. A more stringent requirement of maintaining all propeller blades underwater while surfaced could be made. This restriction, however, will not be made here as it is assumed that the submersible is designed for totally submerged operations.
- 2) Efficiency is to be optimized for a maximum submarine speed of 30 knots at 58.8 RPM.
- 3) Based upon preliminary studies by Wilson and Bourgeois¹⁷, the number of propeller blades is set at 19.
- 4) Hub diameter is fixed by the motor size and location on the hull.
- 5) No cavitation is to be observed at design operation.
- 6) Steady flow is assumed though final propeller design should consider unsteady effects.
- 7) Propeller blades will be fixed pitch.
- 8) The maximum stress at each blade section is less than a maximum allowable value.

These requirements will be met while maximizing propeller efficiency at design speed.

Because no Troost or manufacturer's K_T , K_Q and J curves exist for this size and type of propeller, lifting line and lifting surface calculations are used for the design. These methods have become widely accepted as the most accurate way to determine the pitch and camber distribution required to generate a prescribed loading over the blades.

B. Propeller Design Computer Programs

Two computer programs are used to implement the design procedure for the large hub propeller. These are available in the Ocean Engineering Department at M.I.T.

The MIT-LLL-2 program developed by Kerwin²⁹, for a given number of blades, blade geometry, rpm, thrust and speed computes the hydrodynamic pitch angle and optimum circulation distribution by using Lerb's criterion.⁵⁷ The intent here is not to redevelop the theory that forms the foundation for their use but rather to illustrate the development of the data needed for the input file. There is a large array of literature on this subject for which reference 29 provides an excellent bibliography. After the program is run, analysis is performed.

Figure 5.1 illustrates the blade geometry notation for a conventional propeller developed by Kerwin.²⁹ This notation is also applicable to the large hub propeller. The blade is formed starting with a midchord line, which is a space curve defined parametrically by the radial distribution of skew,

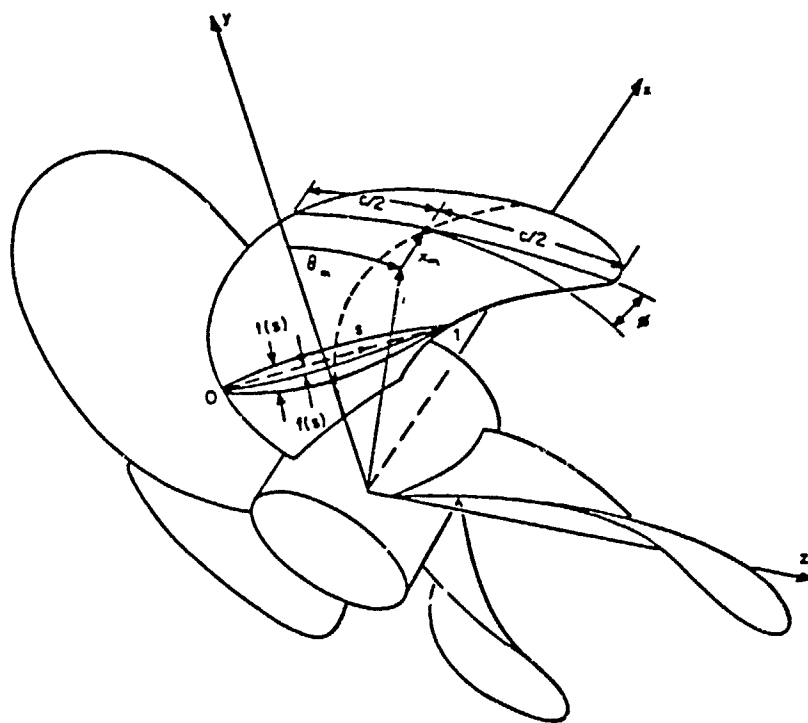


Figure 5.1

$\theta_m(r)$ and rake, $X_m(r)$. By advancing a distance $\pm c(r)/2$ along a helix of pitch angle, $\phi'(r)$, passing through the mid-chord line, one obtains the blade leading and trailing edge, respectively. The blade mean surface may then be defined in terms of a camber distribution, $f(r,s)$, where s is a nondimensional curvilinear coordinate along the nose-tail helix which is zero at the leading edge and one at the trailing edge. The camber, f , is measured in the plane of a cylinder of radius r at right angles to the nose-tail helix. Finally, thickness, $t(r,s)$ is added symmetrically with respect to the mean line at each radius, again in a cylinder of radius r , and at right angles to f . The maximum values of f and t at a given radius are $f_0(r)$ and $t_0(r)$, and upon nondimensionalization with respect to the chord, $c(r)$, are defined as the section camber and thickness ratios.

Figure 5.2 illustrates the geometry chosen to represent the blade between the hub and tip. It is divided into eight equal radial intervals, with half stations at each end. It is not critical that the blade shape be chosen close to optimum at the very outset. It will be changed during the course of the iterative optimization procedure performed in the second program, PBD10. For simplicity, an elliptical blade geometry is chosen (Figure 5.3)²².

The portion of the area equal to $0.45 \frac{\pi M}{4}$ is masked by the hub from $\frac{Y}{M} = -0.3$ to -0.5 and has a local blade-section chord length, c , equal to $2X$.

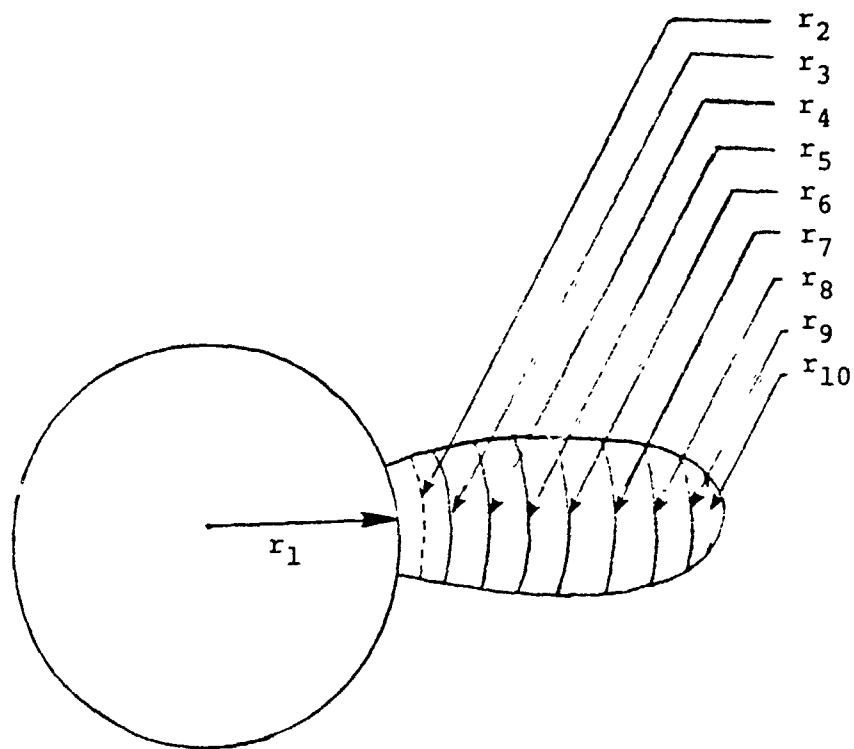


Figure 5.2

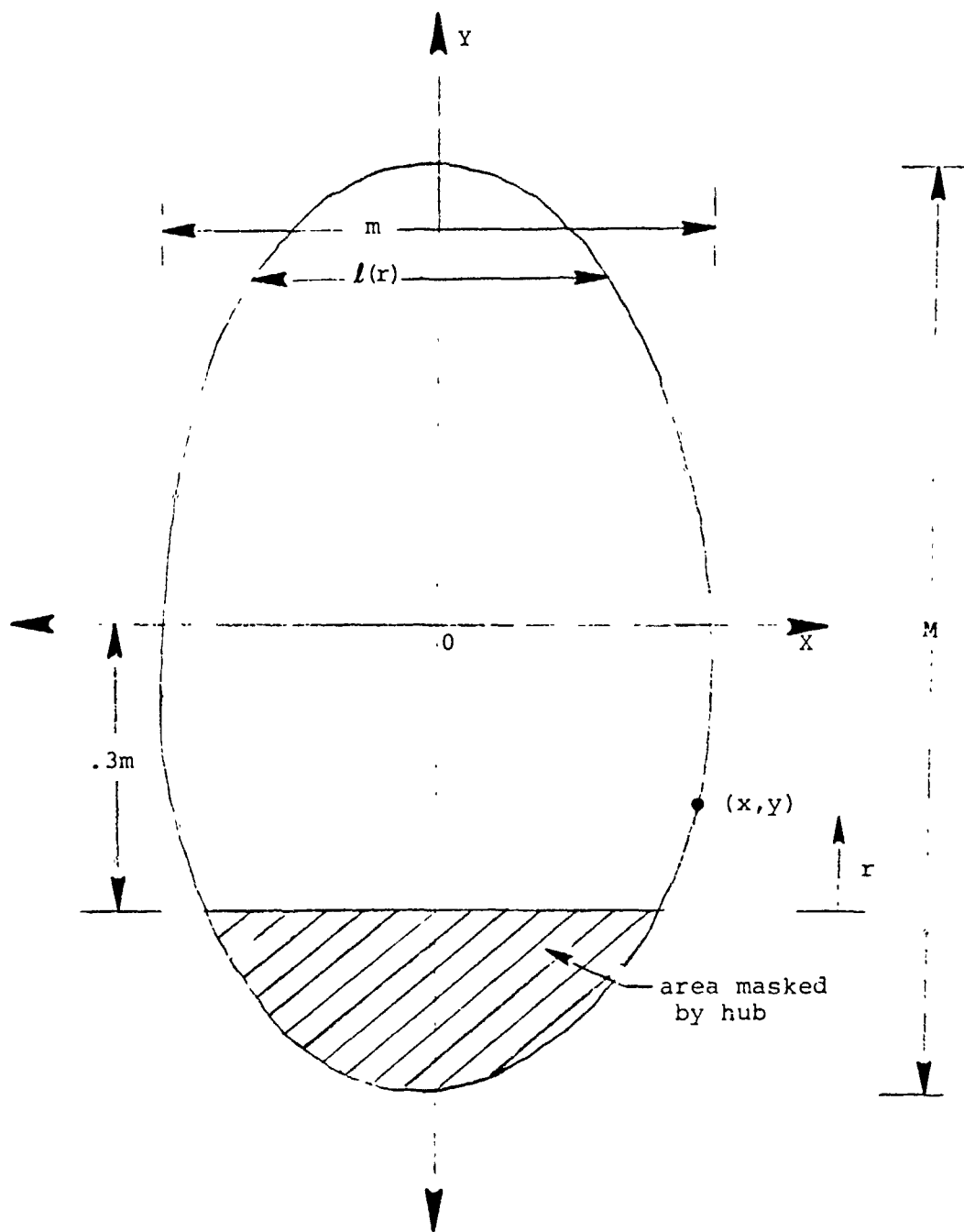


Figure 5.3

The chord ratio, $l(r)/D_p$, for this simple blade geometry is as follows:²²

$$\frac{c(r)}{D_p} = \frac{1.8675(A_e/A_o)}{N_b(1 - r_1/R_o)} \sqrt{1 - 4\left(\frac{0.8(r - r_1)}{(R_o - r_1)} - 0.3\right)^2} \quad (5.1)$$

The number of blades, N_b , is set equal to nineteen and an expanded area ratio of 0.6 is assumed. The radius of hub, r_1 , and the radius of the blade tip, R_o , is determined from the geometry of the submarine stern section and the chosen motor. The forward end of the motor is chosen to be 80% of the submarine length from the nose. This places it exactly at station 4 on Figure 4.6 and extending back another 102 inches from this point. Since the distance between stations is 11.74 feet, the rear end of the motor is 41 inches forward of station 3. With this motor placement and knowledge of the offsets at station 3 and station 4 the hub radius, r_1 , is calculated to be 9.04 feet or 108.5 inches. R_o is then chosen based upon a submarine outer hull radius of 16 feet (192 inches), to be 185 inches. The hub ratio, r_1/R_o , becomes 0.59. Using these numbers, Eq. (5.1) simplifies to

$$\frac{c(r)}{D_p} = .00149 \sqrt{9143.2 - 4(r - 137.2)^2} \quad (5.2)$$

and chord ratio data is obtained as follows in Table 5.1.

TABLE 5.1

Radial Coordinate	r	$\frac{r}{R_0}$	$\frac{c(r)}{D_p}$	$\frac{c(r)}{R_0}$	$\frac{VA(r)}{VS}$
r_1	108.5	.5865	.1139	.2278	0.665
r_2	113.3	.6123	.1234	.2468	0.670
r_3	118.5	.6405	.1311	.2622	0.765
r_4	127.6	.6897	.1396	.2792	0.835
r_5	137.2	.7416	.1425	.2850	0.880
r_6	146.7	.7930	.1396	.2792	0.928
r_7	156.3	.8449	.1306	.2612	0.965
r_8	165.9	.8967	.1140	.2280	0.980
r_9	175.4	.9481	.0857	.1714	0.990
r_{10}	180.2	.9740	.0623	.1246	0.995
R_0	185.0	1.0000	0.0000	0.0000	1.000

The data in the fifth column, $\frac{c(r)}{R_0}$, is the input to the lifting line program and $\frac{c(r)}{D_p}$ will be output. Also needed for input to the program is the axial inflow velocity ratio, $VA(r)/VS$, as a function of radial distance along the blade. These quantities are obtained from Reference 25 and also are shown in Table 5.1.

It is important to note here that the selection of the chord ratios in Table 5.1 is not, at this point, optimum from a cavitation and stress point of view. Eq. (5.1) is only a means of establishing an estimate of the expected values. The selection of $c(r)$ as well as $f(r)$ and $t(r)$ must be accomplished in an iterative procedure which satisfies the constraints of cavitation and strength.

The major limitation of the MIT-LLL-2 program in a design scenario is that the section chord ratios from Table 5.1 are required as inputs into the program for the calculation of viscous drag. Also, since it performs no strength or cavitation calculations, it does not need $f(r)$ and $t(r)$ as input. A more favorable approach is to input an arbitrary set of chord lengths into a modified MIT-LLL2 and then iterate on these values by successively running through the program until "optimum" chord, camber and thickness ratios are obtained. These would then be inputs to the final propeller blade design program PBD-10, which generates the ultimate blade surface. This propeller would be optimized for efficiency and would meet strength and cavitation constraints.

Though it will not be done here, this is precisely what Kroeger and Cummings³² have done. They do not constrain the design problem to a given RPM as is done here. Thus, their program could be easily modified to work at one given RPM. Alternatively, if the propeller is to be designed first, their program could be used from the outset. Currently, this program can be obtained from Dr. Damon Cummings at the Charles Stark Draper Laboratory in Cambridge, Massachusetts.

The necessary propeller thrust is computed from:

$$T = \frac{2\pi n Q \eta_o}{V_S} \quad (5.3)$$

Setting n equal to 58.8 rpm, Q equal to TRAILD in Chapter 4, V_S to 30 knots and assuming an efficiency of .75, one

obtains the necessary thrust to be 195,042 pounds. Finally, after a drag coefficient typically seen on propellers of 0.007 is assumed, the complete input data set is complete. Values of $\tan \beta_i$ at each of the various radii can also be input if desired. This is not done for this sequence, however, since Lerb's criterion is assumed.⁵⁷

The results of MIT-LLL-2 are illustrated for a submarine centerline depth of 16 feet in Figure 5.3 and for a submarine depth of 600 feet in Figure 5.4. The output variables are described in the nomenclature at the beginning of this report. The only result of changing depth is to change the radial values of σ which, in the program, are computed as follows:

$$\sigma(r) = \frac{P_a + \rho g h - \rho g r - P_v}{\frac{1}{2} \rho V^2} \quad (5.4)$$

The values presented here for σ are unrealistically high since they assume a vapor pressure, P_v , of zero which for seawater at 59°F, ideally should be 2.50 psia. This need not be of concern when cavitation is being considered at large depths since $\rho g h \gg P_v$.

The output data obtained from MIT-LLL-2 forms the foundation for the preparation of the PBD-10 input file. Specifically, the pitch-to-diameter ratio, PI/D ; axial-induced velocity at the trailing edge ratio, UA^*/VS ; and the tangential-induced velocity at the trailing edge ratio, UT^*/VS , are inputs at each radial position. The circulation coefficients, G , are

*** MIT-LLL-2 ***
 PROPELLER LIFTING LINE CALCULATION USING LER-S 11-POINT INDUCTION FACTOR METHOD

***** LARGE HUB PROPELLER CALCULATIONS *****

DIAMETER-IN	370.00	SHIP SPEED-KNOTS	30.00	CT	0.102
HUB DIAM-IN	217.04	THRUST IN POUNDS	185042.0	CP	0.121
NO OF BLADES	19	PROP HORSEPOWER	21272.1	EFFY	0.742
REVS PER MIN	58.80	SHAFT DEPTH-Feet	16.000	KT	0.113
FLD DENSITY	1.9910	VOL MN. VEL (1-W)	0.908	KO*10	0.357
PROJ AREA/AO	0.497	EXPANDED AREA/AO	0.600	J(VOL)	1.523

CORRECT THRUST OBTAINED AFTER 4 TRIALS
 ASSUMED TAN B1(R) MULTIPLIED BY 0.94332

R/RD	VA/VS	TAN B	TAN B1	G	CL+C/D	SIGMA	DCT	DCP	G	CNEFFS
0.5866	0.665	0.6051	0.7670	0.0000	0.629	-0.009	0.013	0.003240	0.013	0.003240
0.6124	0.670	0.6399	0.7374	0.0035	0.0167	0.270	0.254	0.001287	0.254	0.001287
0.6383	0.765	0.6397	0.7561	0.0039	0.0173	0.493	0.318	0.000615	0.321	0.000615
0.6899	0.835	0.6460	0.7307	0.0037	0.0153	0.409	0.335	0.000141	0.361	0.000141
0.7416	0.880	0.6333	0.6979	0.0033	0.0128	0.350	0.317	0.000069	0.363	0.000069
0.7933	0.928	0.6244	0.6700	0.0027	0.0096	0.301	0.277	0.000050	0.340	0.000050
0.8450	0.965	0.6096	0.6414	0.0021	0.0073	0.263	0.234	0.000002	0.309	0.000002
0.8966	0.980	0.5834	0.6092	0.0018	0.0057	0.233	0.204	0.000021	0.281	0.000021
0.9483	0.990	0.5572	0.5789	0.0013	0.0041	0.209	0.165	0.000013	0.231	0.000013
0.9742	0.995	0.5452	0.5650	0.0010	0.0030	0.197	0.125	0.000010	0.177	0.000010
1.0000	1.000	0.5337	0.5517	0.0000	0.0000	0.187	0.000	0.000006	0.000	0.000006

EFFECT OF EXPANDED AREA RATIO
 VISCOUS DRAG COEFF-CD-O C0700

R/RD	UA*/VS	UT*/VS	CL	C/D	PI/D	AE/AO	CT	CP	EFFY	CT/CTI
0.5866	0.1036	-0.0970	0.0000	0.114	1.414	0.0	0.109	0.106	0.909	1.0000
0.6124	0.1104	-0.0892	0.1351	0.123	1.419	0.4	0.104	0.116	0.793	0.9586
0.6383	0.0861	-0.0702	0.1317	0.131	1.516	0.5	0.103	0.118	0.767	0.9483
0.6899	0.0699	-0.0544	0.1097	0.140	1.584	0.6	0.102	0.121	0.742	0.9379
0.7416	0.0534	-0.0435	0.0881	0.142	1.626	0.7	0.101	0.124	0.719	0.9278
0.7933	0.0464	-0.0320	0.0691	0.140	1.670	0.8	0.100	0.128	0.696	0.9172
0.8450	0.0356	-0.0232	0.0558	0.131	1.703	0.9	0.099	0.129	0.674	0.9069
0.8966	0.0315	-0.0194	0.0501	0.114	1.716	1.0	0.094	0.131	0.653	0.8966
0.9483	0.0288	-0.0168	0.0484	0.086	1.725	1.1	0.097	0.134	0.633	0.8862
0.9742	0.0274	-0.0155	0.0481	0.062	1.729	1.2	0.095	0.136	0.614	0.8759
1.0000	0.0259	-0.0143	0.0000	0.000	1.733	1.3	0.094	0.139	0.595	0.8655

Figure 5.3

*** MIT-LLL-2 ***
 PROPELLER LIFTING LINE CALCULATION USING LERBS 11-POINT INDUCTION FACTOR METHOD

***** LARGE HUB PROPELLER CALCULATIONS *****

DIAMETER-IN	370.00	SHIP SPEED-KNOTS	30.00	CT	0.102
HUB DIAM-IN	217.04	THRUST IN POUNDS	195042.0	CP	0.121
NO OF BLADES	19	PROP HORSEPOWER	21272.1	EFFY	0.742
REVS PER MIN	58.80	SHAFT DEPTH-Feet	600.000	KT	0.113
FLD DENSITY	1.9910	VOL. MN. VEL (1-W)	0.808	KQ*10	0.357
PROJ AREA/AD	0.497	EXPANDED AREA/AD	0.800	J(VOL)	1.523

CORRECT THRUST OBTAINED AFTER 4 TRIALS
 ASSUMED TAN BI(R) MULTIPLIED BY 0.94332

R/R0	VA/V5	TAN B	TAN BI	G	CL+C/D	SIGMA	DCT	DCP	G COEFFS
0.5866	0.665	0.6051	0.7670	0.0000	0.0000	9.807	0.009	0.013	0.003240
0.6124	0.670	0.5839	0.7374	0.0035	0.0167	9.041	0.270	0.254	0.001287
0.6383	0.765	0.6397	0.7561	0.0039	0.0173	7.844	0.318	0.321	0.000615
0.6899	0.835	0.6160	0.7307	0.0037	0.0153	6.632	0.335	0.361	0.000141
0.7416	0.880	0.6333	0.6978	0.0033	0.0128	5.783	0.317	0.363	0.000069
0.7933	0.928	0.6244	0.6700	0.0027	0.0096	5.078	0.277	0.340	0.000050
0.8450	0.965	0.6096	0.6414	0.0021	0.0073	4.525	0.234	0.309	0.000002
0.8966	0.980	0.5834	0.6092	0.0018	0.0057	4.105	0.204	0.281	0.000021
0.9483	0.990	0.5572	0.5789	0.0013	0.0041	3.748	0.165	0.231	0.000013
0.9742	0.995	0.5452	0.5650	0.0010	0.0030	3.588	0.125	0.177	0.000010
1.0000	1.000	0.5337	0.5517	0.0000	0.0000	3.433	0.000	0.000	0.000006

EFFECT OF EXPANDED AREA RATIO
 VISCIOUS DRAG COEFF-CD=0.00700

R/R0	UA*/V5	UT*/V5	CL	C/D	PI/U	AE/AD	CT	CP	EFFY	CT/CTI
0.5866	0.1036	-0.0970	0.0000	0.114	1.414	0.0	0.109	0.106	0.909	1.0000
0.6124	0.1104	-0.0892	0.1351	0.123	1.419	0.4	0.104	0.116	0.793	0.9586
0.6383	0.0861	-0.0702	0.1317	0.131	1.516	0.5	0.103	0.118	0.767	0.9483
0.6899	0.0699	-0.0544	0.1097	0.140	1.584	0.6	0.102	0.121	0.742	0.9379
0.7416	0.0594	-0.0435	0.0881	0.142	1.626	0.7	0.101	0.124	0.719	0.9276
0.7933	0.0464	-0.0320	0.0691	0.140	1.670	0.8	0.100	0.126	0.696	0.9172
0.8450	0.0358	-0.0232	0.0558	0.131	1.703	0.9	0.099	0.129	0.674	0.9069
0.8966	0.0315	-0.0194	0.0501	0.114	1.716	1.0	0.098	0.131	0.653	0.8966
0.9483	0.0288	-0.0168	0.0484	0.086	1.725	1.1	0.097	0.134	0.633	0.8862
0.9742	0.0274	-0.0155	0.0481	0.062	1.729	1.2	0.095	0.136	0.614	0.8759
1.0000	0.0259	-0.0143	0.0000	0.000	1.733	1.3	0.094	0.139	0.595	0.8655

Figure 5.4

also inputs. The section camber ratio, $f(r)/c(r)$, are input based on a NACA 66 (TMB Modified nose and tail) with the NACA $a = 0.8$ meanline. Thickness ratios, $t(r)/c(r)$, are arbitrarily chosen to be as shown in Table 5.2.

$\frac{r}{R_0}$	$\frac{t(r)}{c(r)}$
0.5865	0.0434
0.6123	0.0396
0.6405	0.0358
0.6897	0.0294
0.7416	0.0240
0.7930	0.0191
0.8449	0.0146
0.8967	0.0105
0.9481	0.0067
0.9740	0.0048
1.0000	0.0029

TABLE 5.2

The skew and rake for each blade is set equal to zero for simplicity. In addition, the inflow velocity is assumed to only vary axially with radial and tangential components set equal to zero. The results of the PBD-10 program are shown for 19 blades in Figure 5.5. Again, output variables are described in the nomenclature at the beginning of this report. Plotted output of the blade camber appears in Figure

```

----- MIT-PBD-10 -----
PROPELLER BLADE DESIGN FOR PRESCRIBED LOAD DISTRIBUTION
RELEASE DATE 02/11/82  COMPUTATION DATE 4/16/83  12*14*02.00
LARGE HUB PROPELLER DESIGN WITH 19 BLADES, 0.59 HUB RATIO, 0 WAKE 0 SKEW

-----RUN CONTROL OPTIONS-----

INPUT DATA:
NX=11  NUMBER OF INPUT RADII
NCI=2  0 GENERATE A=.8, 1-GENERATE B=.8, 2 OFFSETS GIVEN

BLADE LATTICE:
NBLADE=19  NUMBER OF BLADES
NKEY=8  CHORDWISE ELEMENTS ON KEY BLADE
NKEY=9  SPANWISE ELEMENTS ON KEY BLADE
NMOTHER=5  CHORDWISE ELEMENTS ON OTHER BLADES
NMOTHER=5  SPANWISE ELEMENTS ON OTHER BLADES
MCTRP=8  NUMBER OF CONTROL POINT PANELS OVER SPAN
MC(M) 1 2 3 4 5 6 7 8

CIRCULATION AND THICKNESS:
NGCOEF=4  NUMBER OF TERMS IN SPANWISE CIRCULATION SERIES
MLTYPE=0  0-A=8 CHORDWISE LOADING, 1-B=.8 LOADING
MTTHICK=0  0 MOD 66, 1-ELLIPTICAL, 2-ELLIPTIC/PARABOLIC

GRAPHICS OUTPUT:
NPLOT=1  0 NO PLOT OUTPUT, 1 PLOT OUTPUT FILE GENERATED
NPLOH=1  1 PLOT HUB, 0 OMIT
NPLOB=1  NUMBER OF BLADES TO BE PLOTTED
NPLOW=0  NUMBER OF WAKES TO BE PLOTTED

COMPUTATION OPTIONS:
NVEL=1  1 CALCULATE INDUCED VELOCITIES, 0 USE OLD VALUES
NWIMAX=10  NUMBER OF WAKE ALIGNMENT ITERATIONS
NITER=10  NUMBER OF MEAN LINE SHAPE ITERATIONS

-----ADVANCE COEFFICIENT AND SLIPSTREAM DEFORMATION-----
ADVCO=1.523  ADVANCE COEFFICIENT, U, BASED ON SHIP SPEED
RULT=0.830  ULTIMATE TIP VORTEX RADIUS
RHULT=0.610  ULTIMATE HUB VORTEX RADIUS
DCO=30.00  SLIPSTREAM CONTRACTION ANGLE-DEGREES
XULT=0.50  AXIAL EXTENT OF TRANSITION WAKE
XFINAL=0.57  AXIAL EXTENT OF WAKE VELOCITY GROWTH
DTPROP=15.0  PROP ROTATION INCREMENT FOR WAKE CONVECTION

-----COEFFICIENTS OF RADIAL DISTRIBUTION OF CIRCULATION-----
1 0 003240
2 0 001280
3 0 000620
4 0 000140

```

Figure 5.5

----- MIT-PBD-10 -----
 PROPELLER BLADE DESIGN FOR PRESCRIBED LOAD DISTRIBUTION
 RELEASE DATE 03/11/82 COMPUTATION DATE 4/16/83 12-14-02.00
 LARGE HUB PROPELLER DESIGN WITH 19 BLADES, 0.59 HUB RATIO, 0 RAKE 0 SKEW

-----BLADE GEOMETRY-----									
R/RO	P/D	XS/D	SKEW	C/D	FO/C	TO/A			
0.5865	1.2785	0.0000	0.000	0.1140	0.0253	0.0434			
0.6123	1.4273	0.0000	0.000	0.1230	0.0219	0.0396			
0.6405	1.5954	0.0000	0.000	0.1310	0.0186	0.0358			
0.6897	1.6377	0.0000	0.000	0.1400	0.0123	0.0294			
0.7416	1.6403	0.0000	0.000	0.1420	0.0076	0.0240			
0.7930	1.6834	0.0000	0.000	0.1400	0.0054	0.0191			
0.8449	1.6809	0.0000	0.000	0.1310	0.0045	0.0148			
0.8967	1.6457	0.0000	0.000	0.1140	0.0041	0.0105			
0.9481	1.6055	0.0000	0.000	0.0860	0.0054	0.0067			
0.9740	1.6007	0.0000	0.000	0.0620	0.0065	0.0048			
1.0000	1.6213	0.0000	0.000	0.0010	0.0081	0.0029			
-----INFLOW VELOCITIES-----									
R/RO	UX/VS	VR/VS	VI/VS	TRANS WAKE INDUCED VELOCITIES					
				UAINW	UTWNW	UAUW	UTUW		
0.5865	0.663	0.000	0.000	0.045	-0.092	0.086	-0.074		
0.6123	0.670	0.000	0.000	0.082	-0.131	0.098	-0.076		
0.6405	0.765	0.000	0.000	0.101	-0.150	0.116	-0.085		
0.6897	0.835	0.000	0.000	0.097	-0.143	0.145	-0.103		
0.7416	0.880	0.000	0.000	0.075	-0.110	0.150	-0.106		
0.7930	0.928	0.000	0.000	0.070	-0.089	0.100	-0.056		
0.8449	0.965	0.000	0.000	0.106	-0.102	-0.015	-0.026		
0.8967	0.980	0.000	0.000	0.142	-0.124	-0.123	0.110		
0.9481	0.990	0.000	0.000	0.125	-0.113	-0.131	0.112		
0.9740	0.995	0.000	0.000	0.079	-0.083	-0.069	0.058		
1.0000	1.000	0.000	0.000	-0.000	-0.029	0.054	-0.045		
-----MEAN LINE OFFSETS (F/C)*10**4 AT INPUT RADII-----									
XC	0.59	0.61	0.64	0.69	0.74	0.79	0.84	0.90	0.97
1.0	2.9	2.2	1.9	1.5	1.1	0.8	0.7	0.9	1.2
2.5	5.2	4.2	3.8	2.8	1.9	1.4	1.3	1.5	1.7
5.0	8.0	6.7	5.7	4.2	2.3	2.0	1.7	2.0	1.9
10.0	12.4	10.6	9.1	6.4	4.0	2.8	2.2	2.6	2.9
20.0	19.2	16.8	14.6	9.9	5.9	4.0	3.2	3.9	4.4
30.0	23.4	20.6	17.8	11.8	7.0	4.8	3.8	4.7	5.1
40.0	25.2	22.0	18.9	12.5	7.5	5.2	4.2	5.1	5.3
50.0	25.3	21.9	18.6	12.3	7.6	5.4	4.4	5.1	5.5
60.0	22.9	19.7	16.7	11.0	7.0	5.0	4.2	5.1	5.6
70.0	18.3	15.0	13.5	8.7	5.7	4.3	3.6	4.3	5.0
80.0	13.5	11.8	10.1	6.5	4.4	3.4	3.1	3.8	4.1
90.0	5.8	5.5	4.8	2.8	1.9	1.5	1.5	1.9	2.1
95.0	2.6	2.6	2.3	1.3	0.9	0.7	0.8	1.0	1.1
97.5	1.3	1.3	1.2	0.6	0.4	0.4	0.4	0.5	0.5
99.0	0.4	0.5	0.4	0.2	0.1	0.1	0.2	0.3	0.3

Figure 5.5 (cont'd)

MIT-PBD-10
 PROPELLER BLADE DESIGN FOR PRESCRIBED LOAD DISTRIBUTION
 RELEASE DATE 03/11/82 COMPUTATION DATE 4/16/83 12:14:02.00
 LARGE HUB PROPELLER DESIGN WITH 19 BLADES, 0.59 HUB RATIO, 0 RAKE 0 SKEW
 COMPUTATION DATE OF INDUCED VELOCITY FILE 4/16/83 12:14:02.00
 FILE IDENTIFICATION. LARGE HUB PROPELLER DESIGN WITH 19 BLADES, 0.59 HUB RATIO, 0 RAKE 0 SKEW

---CONTROL POINT---			---SPANWISE---			---CHORDWISE---			---VORTEX WAKE---			---THICKNESS---			---TOTAL---		
X	R	THETA	VX	VP	VT	VX	VR	VT	VX	VR	VT	VX	VR	VT	VX	VR	VT
-0.048	0.915	-5.2	-0.018	0.000	0.014	0.001	-0.002	-0.001	0.025	-0.031	-0.016	0.097	-0.007	0.104	0.105	-0.040	0.102
-0.037	0.915	-4.0	-0.008	-0.000	0.007	0.001	-0.002	-0.001	0.026	-0.032	-0.016	0.110	-0.004	0.124	0.131	-0.039	0.113
-0.020	0.915	-2.1	-0.001	-0.001	0.002	0.003	-0.001	-0.002	0.027	-0.033	-0.017	0.120	-0.009	0.140	0.149	-0.044	0.123
-0.001	0.915	0.0	0.001	-0.000	-0.001	0.006	-0.000	-0.004	0.030	-0.035	-0.018	0.124	-0.007	0.146	0.161	-0.043	0.123
0.019	0.915	2.2	0.005	-0.000	-0.005	0.007	-0.000	-0.004	0.035	-0.036	-0.021	0.104	-0.009	0.109	0.151	-0.045	0.080
0.036	0.915	4.0	0.018	0.000	-0.014	0.003	0.001	-0.002	0.043	-0.036	-0.025	0.060	-0.036	0.031	0.24	-0.072	-0.010
0.048	0.915	5.2	0.018	0.000	-0.016	-0.004	0.001	-0.002	0.052	-0.036	-0.030	-0.019	-0.105	-0.102	0.049	-0.140	-0.146
-0.030	0.963	-3.3	-0.024	0.000	0.014	-0.003	-0.001	0.001	0.019	-0.031	-0.012	0.077	-0.051	0.097	0.069	-0.084	0.101
-0.023	0.963	-2.5	-0.007	-0.000	0.005	-0.003	-0.001	0.001	0.019	-0.032	-0.012	0.096	-0.052	0.130	0.108	-0.084	0.124
-0.013	0.963	-1.3	0.000	-0.000	0.001	0.001	-0.001	-0.001	0.020	-0.032	-0.012	0.120	-0.028	0.140	0.130	-0.081	0.137
-0.001	0.963	0.0	0.001	-0.000	-0.001	0.008	-0.000	-0.004	0.022	-0.032	-0.013	0.111	-0.007	0.162	0.143	-0.040	0.133
0.012	0.963	1.4	0.004	-0.000	-0.003	0.009	0.000	-0.005	0.030	-0.033	-0.017	0.095	0.009	0.119	0.130	-0.024	0.094
0.022	0.963	2.5	0.021	-0.000	-0.014	-0.004	0.000	0.002	0.052	-0.033	-0.029	0.053	-0.016	0.041	0.122	-0.019	0.001
0.029	0.963	3.3	0.024	-0.000	-0.016	-0.012	0.001	0.006	0.068	-0.033	-0.037	-0.015	-0.128	-0.075	0.066	-0.161	-0.122

Figure 5.5 (cont'd)

MIT-PBD-10
 PROPELLER BLADE DESIGN FOR PRESCRIBED LOAD DISTRIBUTION
 RELEASE DATE 03/11/82 COMPUTATION DATE 4/16/83 12:14:02.00
 LARGE HUB PROPELLER DESIGN WITH 19 BLADES, 0.59 HUB RATIO, 0 RAKE 0 SKEW

----- INDUCED VELOCITIES RESOLVED INTO BLADE COMPONENTS -----

X	R	THETA	XC	VO/VS	VN/VO	VC/VO	VM/VO
-0.071	0.623	-8.4	3.81	1.465	-0.000	1.246	-0.065
-0.056	0.623	-6.3	14.64	1.465	-0.000	1.223	-0.063
-0.033	0.623	-3.3	30.87	1.465	-0.000	1.201	-0.022
-0.004	0.623	0.3	50.00	1.465	0.000	1.194	0.034
0.026	0.623	3.7	69.13	1.465	0.000	1.161	0.062
0.052	0.623	6.6	85.36	1.465	0.000	1.069	0.080
0.070	0.623	8.5	96.19	1.465	0.000	0.846	0.087
-0.078	0.672	-8.5	3.81	1.610	-0.000	1.183	0.019
-0.061	0.671	-6.4	14.64	1.610	-0.000	1.193	0.014
-0.035	0.671	-3.3	30.87	1.610	-0.000	1.191	0.036
-0.003	0.671	0.2	50.00	1.610	-0.000	1.187	0.000
0.030	0.671	3.7	69.13	1.610	0.000	1.152	-0.000
0.058	0.671	6.6	85.36	1.610	-0.000	1.057	0.011
0.077	0.672	8.5	96.19	1.610	0.000	0.859	-0.007
-0.077	0.720	-8.4	3.81	1.717	0.000	1.147	0.013
-0.060	0.720	-6.4	14.64	1.716	0.000	1.160	0.011
-0.034	0.720	-3.4	30.87	1.716	0.000	1.163	0.001
-0.002	0.720	0.1	50.00	1.716	-0.000	1.160	-0.010
0.030	0.720	3.6	69.13	1.716	-0.000	1.128	-0.020
0.058	0.720	6.5	85.36	1.716	-0.000	1.046	-0.031
0.076	0.720	8.4	96.19	1.717	-0.000	0.886	-0.043
-0.074	0.769	-8.0	3.81	1.827	-0.000	1.121	0.009
-0.057	0.769	-6.1	14.64	1.826	-0.000	1.132	0.004
-0.032	0.769	-3.2	30.87	1.826	-0.000	1.137	-0.006
-0.001	0.769	0.1	50.00	1.826	0.000	1.136	-0.016
0.029	0.769	3.4	69.13	1.826	0.000	1.107	-0.028
0.056	0.769	6.2	85.36	1.826	0.000	1.038	-0.039
0.073	0.769	8.0	96.19	1.827	-0.000	0.907	-0.058
-0.069	0.818	-7.4	3.81	1.935	0.000	1.097	-0.002
-0.053	0.817	-5.6	14.64	1.934	0.000	1.108	-0.005
-0.029	0.817	-3.0	30.87	1.934	0.000	1.115	-0.013
-0.001	0.817	0.0	50.00	1.934	-0.000	1.115	-0.019
0.027	0.817	3.1	69.13	1.934	-0.000	1.090	-0.026
0.052	0.817	5.7	85.36	1.934	-0.000	1.031	-0.039
0.068	0.818	7.4	96.19	1.935	-0.000	0.924	-0.065
-0.060	0.866	-6.5	3.81	2.034	-0.000	1.079	-0.011
-0.046	0.866	-4.9	14.64	2.034	-0.000	1.090	-0.012
-0.025	0.866	-2.7	30.87	2.034	-0.000	1.097	-0.017
-0.001	0.866	0.0	50.00	2.034	-0.000	1.099	-0.020
0.024	0.866	2.7	69.13	2.034	0.000	1.077	-0.024
0.045	0.866	5.0	85.36	2.034	0.000	1.026	-0.037
0.060	0.866	6.5	96.19	2.034	0.000	0.938	-0.066

Figure 5.5 (cont'd)

----- MIT-PBD-10 -----
 PROPELLER BLADE DESIGN FOR PRESCRIBED LOAD DISTRIBUTION
 RELEASE DATE 03/11/82 COMPUTATION DATE 4/18/83 12:14:02.00
 LARGE HUB PROPELLER DESIGN WITH 19 BLADES, 0.59 HUB RATIO, 0 RAKE 0 SKEW

----- INDUCED VELOCITIES RESOLVED INTO BLADE COMPONENTS -----

X	R	THETA	%C	VO/VS	VN/VO	VC/VO	VN/VO
-0.048	0.915	-5.2	3.81	2.128	0.000	1.065	-0.019
-0.037	0.915	-4.0	14.64	2.128	0.000	1.076	-0.018
-0.020	0.915	-2.1	30.87	2.128	0.000	1.084	-0.021
-0.001	0.915	0.0	50.00	2.128	-0.000	1.087	-0.020
0.019	0.915	2.2	69.13	2.128	0.000	1.067	-0.021
0.036	0.915	4.0	85.36	2.128	0.000	1.024	-0.034
0.048	0.915	5.2	96.19	2.128	0.000	0.951	-0.066

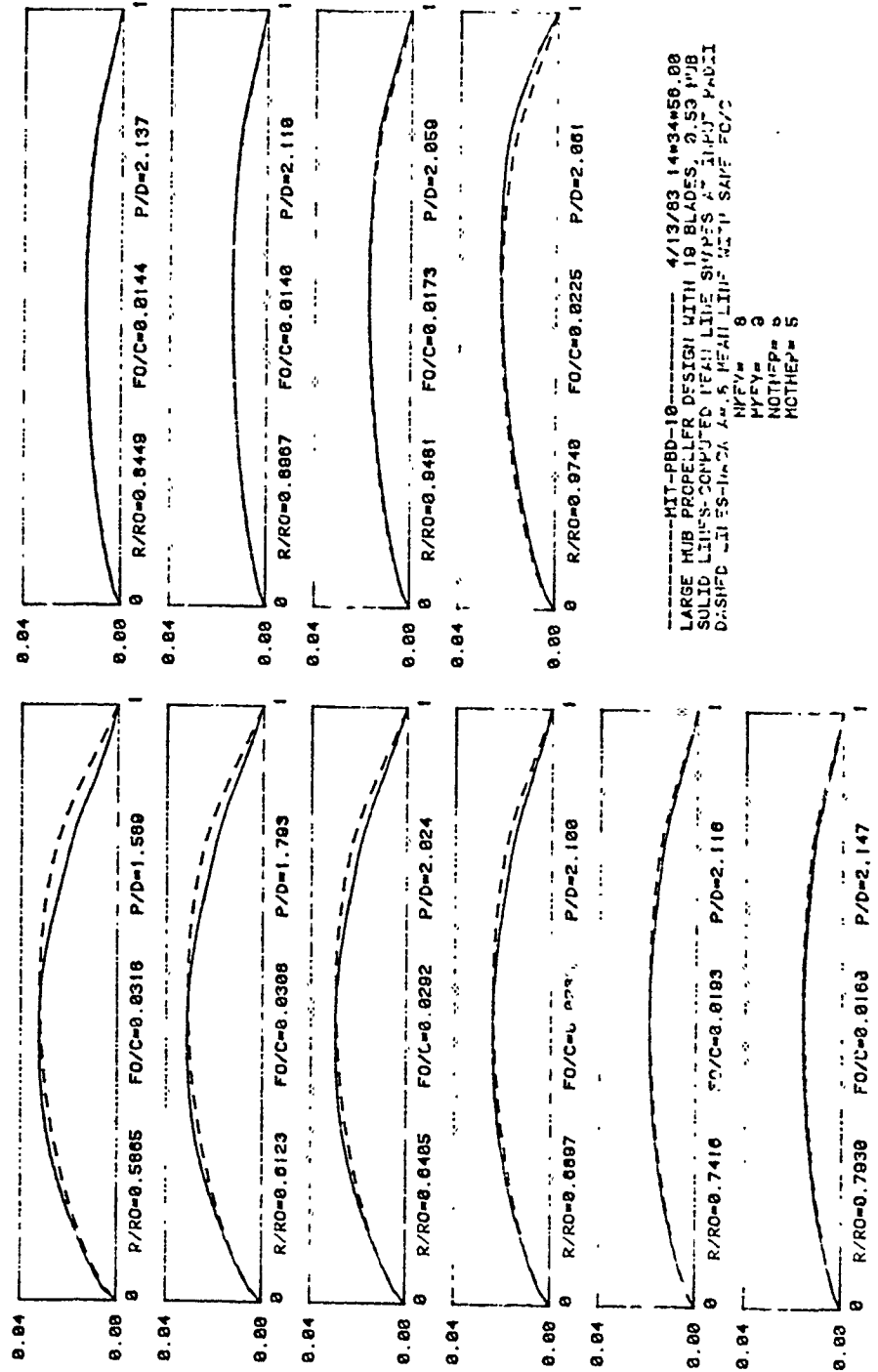
-0.030	0.963	-3.3	3.81	2.221	0.000	1.054	-0.044
-0.023	0.963	-5	14.64	2.221	0.000	1.071	-0.043
-0.013	0.963	-1.3	30.87	2.222	0.000	1.082	-0.030
-0.001	0.963	0.0	50.00	2.222	-0.000	1.083	-0.018
0.012	0.963	1.4	69.13	2.222	-0.000	1.066	-0.008
0.022	0.963	2.5	85.36	2.221	-0.000	1.026	-0.017
0.029	0.963	3.3	96.19	2.221	-0.000	0.966	-0.066

----- MIT-PBD-10 -----
 PROPELLER BLADE DESIGN FOR PRESCRIBED LOAD DISTRIBUTION
 RELEASE DATE 03/11/82 COMPUTATION DATE 4/16/83 12:14:02.00
 LARGE HUB PROPELLER DESIGN WITH 19 BLADES, 0.59 HUB RATIO, 0 RAKE 0 SKEW

-----CALCULATION OF THRUST AND TORQUE COEFFICIENTS-----

CD	KT	KQ	E/(1-W)
0.0000	0.108	0.0258	1.020
0.0060	0.103	0.0295	0.844
0.0065	0.102	0.0298	0.831
0.0070	0.102	0.0301	0.819
0.0075	0.101	0.0304	0.807
0.0080	0.101	0.0308	0.795
0.0085	0.100	0.0311	0.783
0.0090	0.100	0.0314	0.771
0.0095	0.099	0.0317	0.760
0.0100	0.099	0.0320	0.749

Figure 5.5 (cont'd)



HIT-RBD-10 4/13/83 14:34:50.00
 LARGE HUB PROPELLER DESIGN WITH 16 BLADES, 0.53 HUB
 SOLID LINE-S-COMPUTED HEAD LINE SHIP'S AT 1100' HAD 11
 DASHED LINE IS HEAD LINE WITH SAME FC/C
 NFEV= 8
 NTHF= 8
 NCTHEP= 5

Figure 5.6

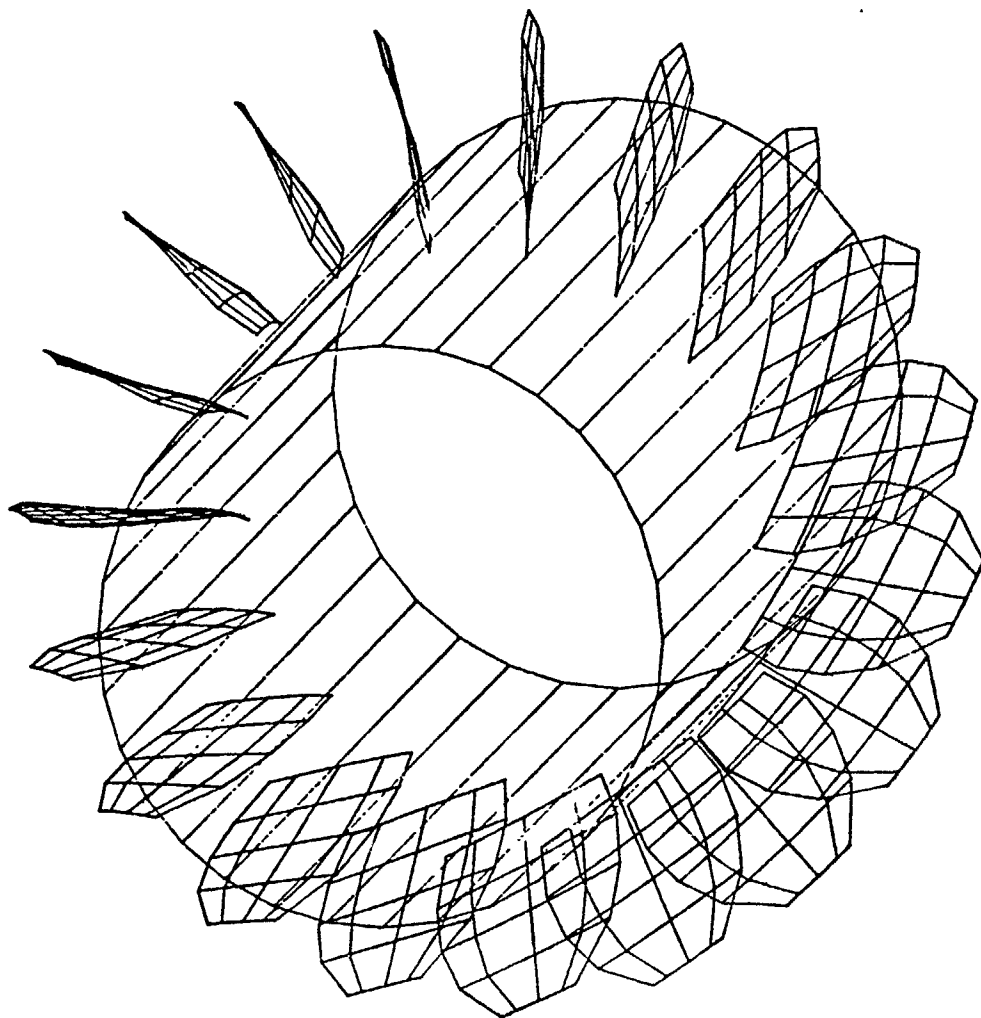


Figure 5.7

5.6 and a three-dimensional display of propeller hub and blades appears in Figure 5.7.

C. Analysis of Results

As input to the programs, the blades have maximum dimensions as shown in Figure 5.8, with maximum thickness of 1.83 inches at the propeller root and maximum camber of 1.07 inches also at the propeller root.

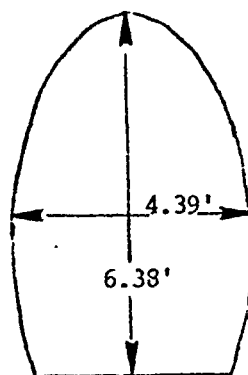


Figure 5.8

Assuming the blades are manufactured from manganese bronze which has a density of 0.30 lbs/in³ and the blade side view is triangular, blade weight can be estimated

$$W = \frac{0.30}{2} (t_{\text{root}}) \left(\frac{A_e}{A_o} \right) \left(\frac{\pi D^2}{4} \right) \quad (5.5)$$

to be 17,700 lbs. If the value of A_e/A_o is reduced from 0.6 to 0.4 to achieve greater thrust loading on the blades

then the propeller blade weight drops to 11,800 lbs. If the hub for the moment is assumed to be a 1.5-inches thick steel plate with a hub length of 115 inches, its weight would be approximately 15 to 20 tons. Combined propeller/hub weight is then observed to range between 21 and 28 tcns.

Cavitation inception can be analyzed by use of "bucket" curves shown in Figure 5.9. These curves are plotted for a given camber ratio, in this case .02, and various blade thickness ratios. Thus, a whole family of plots is needed for various camber ratios as well. The complete set of bucket curves is obtained in Reference 58. Entering arguments taken from the data provided by MIT-LLL-2 and PBD10 are TO/D, SIGMA and FO/C. FO/C determines which set of bucket curves to use, TO/D is equivalent to τ on the curve and $-C_{p_{min}}$ is set equal to SIGMA.

Use of these curves for a centerline depth of 16 feet indicates the blade will experience midchord bubble cavitation at the outer blade radii. This is due to the extremely small value of SIGMA while surfaced and to the small camber ratios computed in the PBD10 program. Increasing depth to 50 feet eliminates cavitation at all radii. It is also evident that there are too many propeller blades creating extremely low angles of β_i and extremely low sectional lift coefficients. An increase then in the blade loading up to a certain point by reducing the number of blades will serve to increase the pitch, increase β_i , increase CL and, most importantly, increase the efficiency.

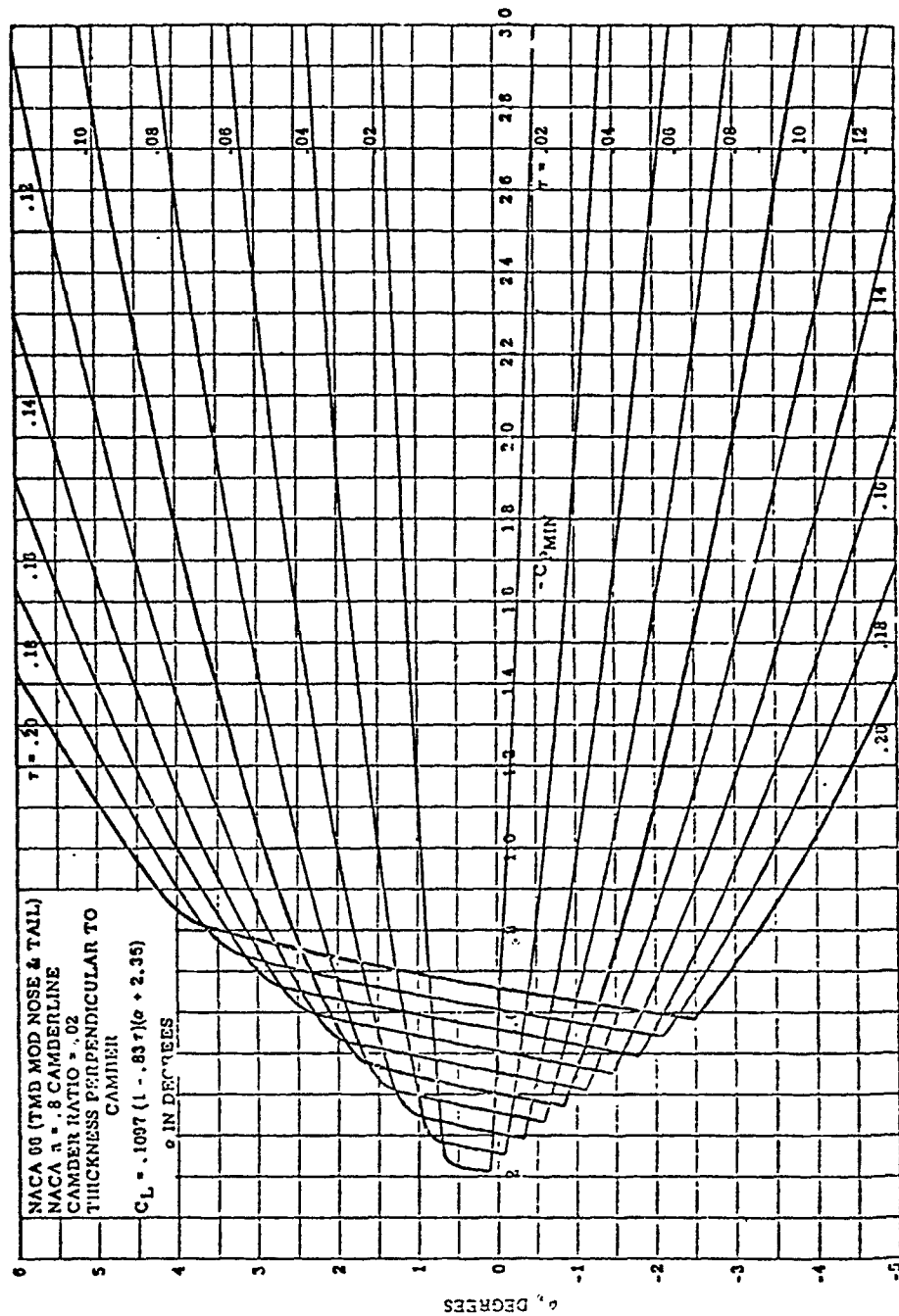


Figure 5.9---Minimum Pressure Envelopes for NACA 66 Sections
 (TMB Modified Nose and Tail) with the NACA $a=0.8$
 Camberline, having a Maximum Camber Ratio of 0.02

It appears certain that the propeller can be designed to be cavitation-free at depths in excess of 50 feet. Also, efficiencies, $\frac{\eta_o \eta_{rr}}{1-w}$, in excess of 0.75 can be expected. The requirement for 19 blades must be reevaluated since design indications point to a number much smaller. Nineteen blades can be retained if the chord ratios are reduced by decreasing the expanded area ratio down from 0.6. This also has the effect of increasing the blade loading and achieving the above results. The tradeoff, of course, is an increased tendency towards cavitation. The weight of the propeller blades also can be drastically reduced upon successful completion of an optimum design. Weights below 6 or 7 tons appear reasonable at this point.

D. Hub Effects

As set forth in this thesis, the MIT-LLL-2 and PBD10 programs do not include the effects of the hub in the propeller analysis. Essentially, this effect is to create a zero normal velocity gradient as a boundary condition at the blade/root interface as well as on the hub itself. In the past, this effect on the flow has been handled in several different ways.⁵⁴ One method used by Lerbs,⁵⁷ among others, is to ignore the hub completely. This approach has been fairly successful in cases where the hub diameter is small compared to the propeller diameter. If the hub is considered to be an infinitely-long cylinder, the boundary condition of zero velocity through the hub surface is approximately satisfied by including images of

the trailing vortex system inside the hub.⁵⁶ This method neglects the effect of the contraction of the flow around the hub and is particularly inappropriate for short hubs. This type of analysis leads to a finite circulation at the blade roots as shown by McCormick⁵⁹ for maximum efficiency.

Andrews⁵⁴ effectively modified the MIT-LLL-2 program to account for the contraction of the flow around the hub. The approach is to calculate the potential flow around an approximation to the hub shape given by a line sink along the hub axis. The propeller blade is considered to be a bound vortex which sheds a helicoidal sheet of trailing vorticity. This vortex sheet is modeled by a number of discrete trailing vortices. In this way, the Cauchy principle value integral for the velocity induced by the sheets is expressed as a summation for central points midway between the discrete vortices. The trailing vortices from the propeller are assumed to follow the streamlines of this potential flow as it contracts behind the hub. As these streamlines approach a constant spacing far downstream, the trailing vortices approach a constant radial spacing. That is, the wake downstream is equivalent to the wake produced by a fictitious zero hub propeller located far downstream. From the streamlines, a correspondence between radial points on the real propeller and radial points on the fictitious propeller is obtained.

Using lifting line theory, the circulation distribution for the fictitious propeller is obtained which produced the

desired thrust and efficiency. This circulation distribution is then transferred to the real propeller using the correspondence between radial points on the two propellers.

Using this circulation distribution, induced velocities are calculated by numerical integration, again assuming that the trailing vortices follow the potential flow. A system of images inside the hub is included to approximately satisfy the boundary condition on the hub surface. This calculation is repeated including the effects of the previously calculated induced velocities, and the process is repeated until the last values of induced velocities agree with the previous values.

The results of Andrews' work, though not confirmed in water tunnel tests, show that the primary effect of the hub is to reduce the circulation in the hub region from the optimum circulation obtained without including the hub effects.

A more elegant approach to the hub effect problem is currently being researched at M.I.T. by Mo-Hwa Wang in the Ocean Engineering Department. Rather than modify MIT-LLL-2, he modifies PBD10. Figure 5.10 illustrates a flow diagram of the PBD10 program with Wang's modifications shown in the block represented with dotted lines. He has, in effect, discretized the hub surface into a lattice network of sources in a manner similar to that done on the blade itself. Thus, the network of vortices and sources on the blade surface does not end at the blade root. Rather, the network continues to include the hub as well. The submersible hull geometry and the

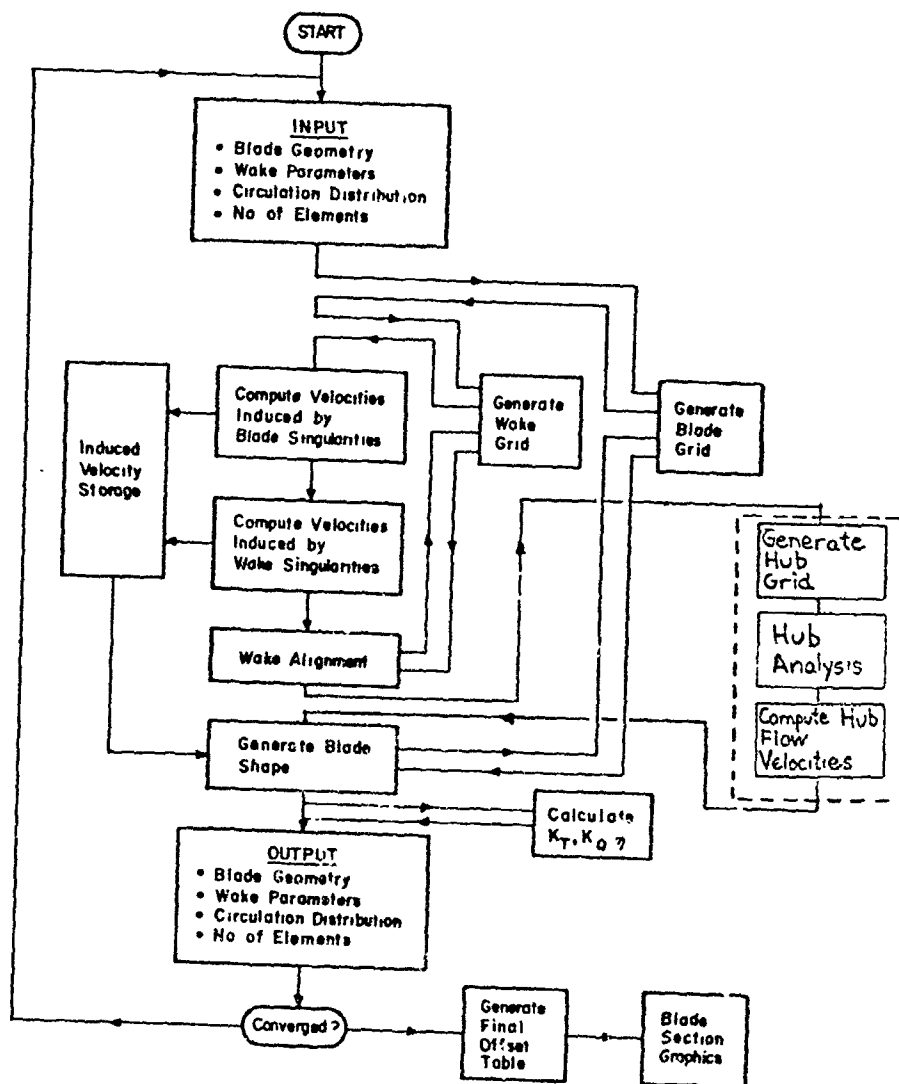


Figure 5.10

boundary condition of zero normal velocity is met in a procedure identical to Andrews by including a line source within the submersible. Though the flexibility to include any hull or hub geometry has not been included in the model yet, future work has this as a goal.

Preliminary hub analysis utilizing this model reveals dramatic changes in blade camber, especially near the blade root, necessary to achieve the required circulation over the blade surface. Final verification via tunnel test data has yet to be accomplished. Certainly any large hub propeller designed for an application similar to the one proposed in this report should analyze the hub effect in great detail. At large hub ratios above approximately 0.5, it can be expected that the camber as illustrated in Figure 5.6 will deviate from the initial NACA $a = 0.8$ meanline at most, if not all, blade sections.

E. Propeller Design Summary

This chapter has attempted to describe the procedures necessary to perform complete propeller design. The tools necessary to develop one complete computer program for the job appear readily accessible but have not been molded together into one unit. The program by Andrews performs the hub analysis adequately but lacks the ability to design around RPM, strength and cavitation requirements.

The model proposed by Wang which modifies the PBD10 program still requires output data from the MIT-LLL-2 program or the program developed by Kroeger and Cummings. Thus, the

logical procedure to follow in the propeller design is to first utilize the Kroeger and Cummings' program to obtain the necessary data for input into the modified PBD10 program. A viable check on this output data could then be obtained by comparing it to the program proposed by Andrews.

An initial preliminary design effort revealed serious limitations in being able to use engineering judgment in the design procedure. Wilson and Bourgeois¹⁷ found 19 blades to provide the best achievable efficiency for a series of blade combinations. In a design where a different hub ratio, different blade section chord ratios and a different expanded area ratio are used, this number of blades is far from being optimum.

Utilizing 19 blades also leads to an overly heavy design weight of 17,700 lbs. This weight can be substantially reduced if the program by Kroeger and Cummings is run once for each number of blades.

Efficiency of the propeller, $\frac{O_{rr}}{1-w}$, can be expected to be comparable or slightly less than existing conventional propellers. The propulsive coefficient, however, cannot at this stage of the research be established analytically since adequate data on the hull thrust deduction coefficient, t , does not exist for a propeller located forward of the control surfaces. It appears reasonable, however, based upon work done at General Dynamics,⁴² that overall propulsive

coefficients would not be substantially different. With their work centering on the NEPPS model, propulsive coefficients at full scale are estimated at 0.90. This value is based on two fixed pitch counter-rotating large hub propellers. A value less than this is to be expected from a single fixed pitch propeller.

Initial cavitation studies indicate that the large hub propeller will cavitate if designed improperly. However, because of the propeller's low RPM, it is possible for the designer to determine the required blade geometry and number of blades that provides cavitation-free performance at virtually all operating depths.

The blade section thickness ratios chosen arbitrarily for this preliminary analysis will have to be increased if cavitation inception is to be avoided at design speed. The larger the thickness, the greater the range of allowable angles of attack are possible. The program by Kroeger and Cummings will provide adequate thickness ratios. The only input needed is the yield stress of the blade material.

Finally, there is some question as to whether a propeller shroud similar to that shown in Figure 5.11 should be incorporated. Obviously, it would serve to protect the blades from damage and improve the flow characteristics around the blades. But, on the other hand, viscous drag would increase substantially. If blades that are removable from the hub are designed, then repair of damaged blades could be achieved easily and the need for a protective shroud would be eliminated.

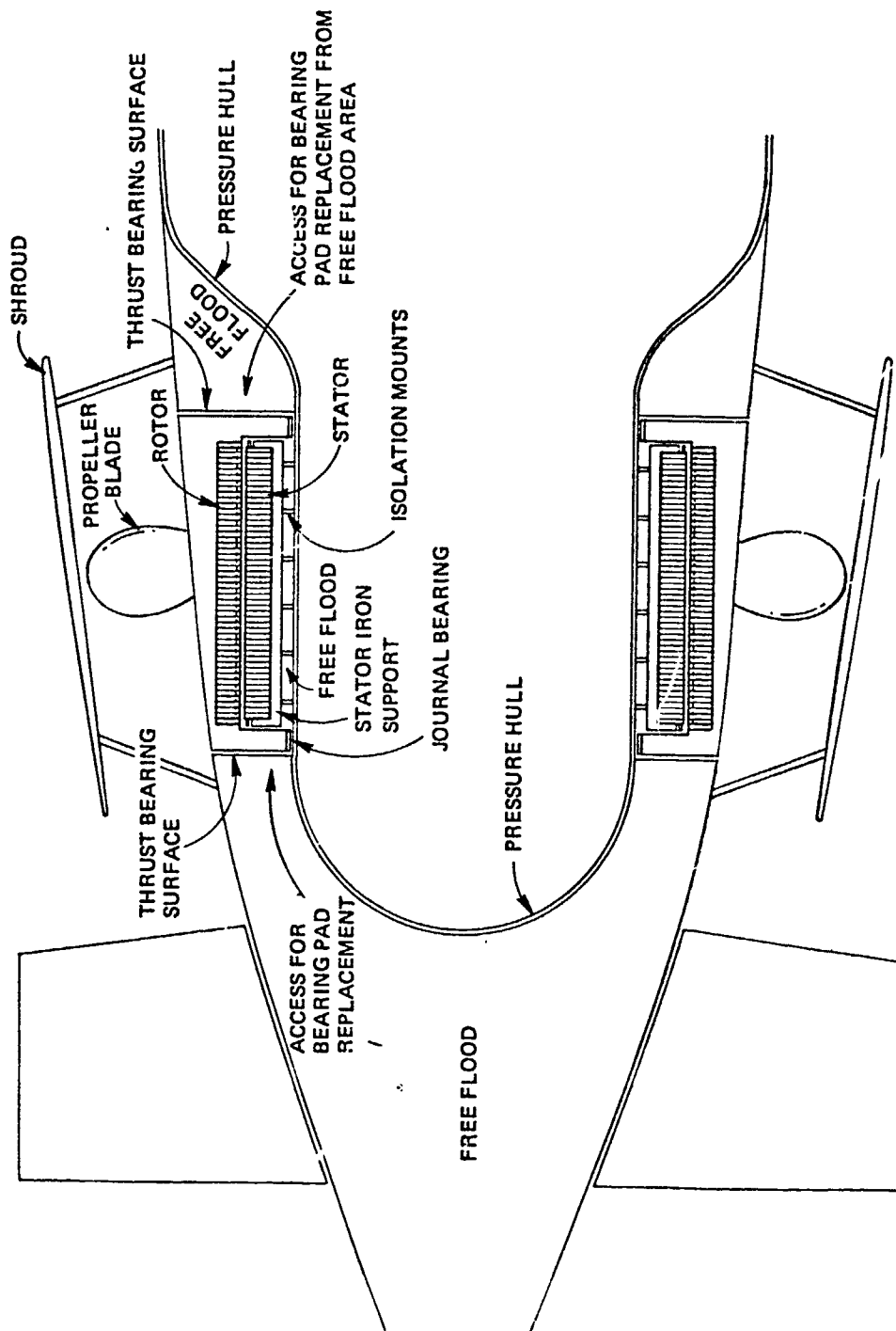


Figure 5.11

Chapter 6

CONCLUSIONS AND SUGGESTIONS FOR FURTHER WORK

A. Summary

This thesis has presented a new approach to powering underwater vehicles that promises several important advantages over conventional designs. Because of limited research in the past, however, there are several fundamental challenges also inherent in this propulsion scheme.

The induction motor design is the focal point of the concept. Its arrangement, size and location affects the rest of the design immensely. Thus, the need for a flexible analysis computer program is important for analyzing impacts of various design decisions. A hypothetical vehicle chosen in this work has proven that the motor is a viable concept that bears further research study.

In comparison to conventional propulsion schemes on large U. S. Navy submarines, the most crucial aspect is weight. Outputs from the motor analysis computer program indicate that the weight of a 21,000 SHP motor is near 56 tons. Results from Chapter 5 are not at this point definitive enough to predict accurately the weight of the large hub propeller. Rough approximations revealed, however, the weight to be between 21 and 28 tons. Therefore, a crude approximation of the weight of the external motor and propeller combination can be established to be 84 tons. Submarines of comparable horsepower with conventional propeller and shafting arrange-

ments have typical weights as follows:

shafting and bearings	-- 14 tons
propeller	-- 15 tons
reduction gears	-- 45 tons
thrust bearing	-- <u>11 tons</u>
TOTAL WEIGHT	<u>85 tons</u>

Hence, by establishing a directly coupled electric motor and propeller combination which eliminates shafting and reduction gears, a competitive system to the conventional system is established. A key area which warrants further investigation is the addition of weights onto the submarine electric propulsion system for journal and thrust bearings and added structural support. Studies are also needed to determine the weights of electric generators and power conditioning equipment for this low-frequency application. How much these weights are offset by reduction in structural foundation needed for main propulsion machinery alignment also needs to be assessed. These structural foundation weights which can run as high as 85 tons can be reduced significantly if the arrangement flexibility of electric machinery is afforded.

B. Suggestions for Further Work

The immediate priority for future work rests in the journal bearing and thrust bearing design. Particularly, as was pointed out in Chapter 4, the clearance between rotor and stator is critical to motor efficiency. The design of

the bearings will also facilitate a cooling water scheme. With this cooling water scheme, convection can be added to the thermal model of Chapter 3 and new thermal resistances computed which ultimately will significantly reduce the upper bound on the temperatures. Preliminary studies on the water-cooled thrust and journal bearings will also facilitate more accurate weight analysis studies.

There are many other areas as yet that require further investigation, particularly in the hydrodynamics area. The above are the most important since they affect any decision to be made to pursue this propulsion system in tradeoff studies against other alternatives.

While the majority of this work has focused on this motor's application to a large submarine, it must be emphasized that potential exists for this system's application to small submersibles as well. Unmanned submersibles are not excluded from this category.

APPENDIX A

Footnotes from Data Input File INDUC.DAT

1. The users' manual for the original program (ref. 11) was set up on the assumption that the input would come in the form of data cards. However, this program uses a datafile INDUC.DAT. Saturation data for core material under consideration is taken from the U.S. Steel data sheets (ref. 9) and input as explained by the users' manual. Care should be exercised when adjusting from data cards to a data file. The units on the flux density are kilolines/square inch and the units on the magnetizing force are ampere turns/inch.
2. It is possible to input data for more than one lamination thickness so that the designer can choose from several options which give best performance. Here the tradeoff arises as to whether one desires a thin lamination with increased manufacturing complexities or a thick lamination and its inherent high core loss. For a large submarine propulsion motor, a thick lamination would provide greater structural strength when subjected to large underwater pressures. It also would reduce fatigue loading considerations for interlamination insulation. Ultimately, the laminations will have to be pressed together and held together under high pressure to insure that there is no movement under cyclic loading. Ref. 12 illustrates one procedure for lamination construction for motors subjected to a corrosive seawater environment and large pressures.
3. Data for the rotor core material must be input whether or not it is different from that of the stator.

4. The governing equation here is:

$$\text{RPM} = \frac{120f}{p}$$

By choosing two of the variables here, say RPM and frequency, the third, the number of poles, is determined. In this thesis, a given number of poles (60) which was consistent with the geometry and size under consideration and a general idea of propeller RPM needed to avoid cavitation led to a frequency of operation. This frequency also has to be consistent with generation machinery that ultimately will have to be designed for the motor being proposed here. The line to neutral voltage, V_l , was chosen so as to minimize the tendency of insulation breakdown and to minimize insulation thickness while simultaneously being consistent with generation requirements. Thus, a high voltage ensures adequate power outputs while keeping currents low since

$$P = 3 VI \cos \theta$$

However, high voltages also tend to break down insulation and require larger insulation thicknesses resulting in less copper in the slots.

5. In the design of an underwater propulsion motor for a large hub propeller there is no known windage loss data available since no design of this nature has ever been attempted. Thus a conservative value of FWL must be assumed or as is done in this thesis a value of FWL equal to zero is assumed. Later, after more detailed thrust bearing and journal bearing design has been carried out, and, if the motor is used in forced cooling water flow, then realistic power dissipations can be obtained.
6. If known values for X_0 , X_1 , X_2 , R_0 , R_1 and R_2 are input under the NAMELIST RATING then all internal calculations

are bypassed except for the equivalent circuit analysis.

7. Since the motor design here is inverted, that is, the rotor is outside the stator, some redefinition of variables from those found in the users' manual was required. In the new program, DIS replaces D and DOS is removed altogether. See Figures 3.2(a) and 3.2(b) for illustration of the change.
8. Stator length, L, is chosen based upon known geometry of the submarine stern. However, one should understand that the motor power density is proportional to D^2L . Thus, since the after end of the submarine tapers, L will have to be chosen so as to maximize D and still meet the taper requirements.
9. Lamination stacking factor, SFS, ideally is not known until construction is complete, however, values from past designs can be assumed.
10. The number of slots, QS, was chosen for this design based upon the circumference being used and the assumption that $\frac{\text{slot width}}{\text{tooth width}} = 1$. Also, QS must be divisible by 3 for three phase motors and it is usual to provide a number of slots which is divisible by the number of poles, but windings can be devised for stators having a fractional number of slots per pole³. See also ref. 1, pp. 306 - 308.
11. The stator slot type, SSTYPE, in the computer program can be chosen from one of the six types. These are described in the users' manual. An open type slot, type 1, was chosen for the stator of this design since this eases manufacturing complexities, reduces stress concentrations in both static and cyclic loading, and most importantly,

eases the repair procedure. Of course, the tradeoff is increased flux leakage.

12. For D2S, D5S, D6S and WS56, use Table XXVI, p. 309 of ref. 1 as a rough guide. Also choose wire size from the Appendix of ref. 1.
13. The stator slot depth, D5S, must not exceed six times the slot width so that excessive slot leakage is not obtained.
14. The slot width is chosen to be equal to the tooth width and thus must be consistent with the stator diameter and the number of slots chosen.
15. The number of conductors per stator slot, CSS, is a very important number as it has large ramifications on equivalent circuit parameters if changed. Specifically, CSS determines the number of coil turns to be used in computing the stator slot leakage and air gap magnetizing reactance. Most importantly though, the coil turns are squared in order to achieve these two quantities. Hence, for higher power outputs, one desires to minimize the number of coil turns. The tradeoff arises in being able to arrange larger coils in the slot and in forming the coil at the end-turn.
16. The armature coil extension is strictly a function of the winding size and the coil pitch. At the outset the value was obtained from ref. 1, p. 309.
17. The stator winding material was chosen to be aluminum. It, of course, has less favorable resistivity characteristics than copper but has the advantage of being much less dense than copper or brass. This can mean nearly six tons of weight savings for the large motor in this

design. Most importantly, according to Walker⁸, it is predicted that at the present rate of consumption of copper existing deposits will be exhausted within a period of about 40 years and with the constantly accelerated rate of consumption, this period may well be as short as 20 years. Furthermore, the eddy current loss varies as the fourth power of the thickness of the strand and inversely as the square root of the resistivity. Thus, the use of aluminum will definitely mean using more coil turns than copper since the coil thickness will have to be smaller. With this comes an increase in leakage reactance and magnetizing reactance. Aluminum in the presence of a seawater environment will also require strict corrosion control.

18. The clearance between armature coils at end turns, S, is initially obtained from ref. 1, p. 309, Table XXVI.
19. The area of the strand is taken from the Appendix of ref. 1. Rectangular wires are used to increase resistance to cyclic loading movement within the slot and to increase the winding space factor.
20. In the ROTOR NAMELIST there again has been a redefinition of variables from that used in the users' manual due to the inverted stator and rotor. In the program the variable D has been substituted for DIR, and DOR has been added as the rotor lamination outside diameter in inches.
21. Since a conventional squirrel cage winding is to be used, a circular slot type 5 was chosen for the rotor. It would also reduce stress concentrations which may be critical at large pressures. Since aluminum has a lower

Young's Modulus of Elasticity than the steel core, the aluminum bar should readily mold and form to the steel slot enclosure. Large pressure cycles then should not create a problem since the aluminum will easily strain to the same proportion as the steel when subjected to large depths in the ocean.

22. For the selection of the number of rotor bars, use the guidance provided by ref. 6:
 - a) To minimize noise and vibration, $S_s - S_r \neq \pm 1, \pm 2, \pm(p \pm 1), \text{ or } \pm(p \pm 2);$
 - b) To avoid dead points or cogging, $S_s - S_r \neq \pm 3p, \text{ or } \pm 3kp, k = 2, 3, \dots;$
 - c) To avoid cusps in the speed-torque curve, $S_s - S_r \neq \pm p, -2p, \text{ or } -5p;$
 - d) S_r must not be divisible by $S_s;$
 - e) For quietness, make S_r differ from S_s by 20% or more.
23. The design of the rotor punching can be derived using ref. 6, p. 392 as a guide.
24. Guidance on the selection of the end-ring dimensions can be obtained from ref. 1, p. 316-322. Also, the method of joining the end-ring to the rotor bar will have to be examined in close detail to avoid stress concentration.
25. The air gap clearance, G , has an extremely large impact on the design since it is inversely proportional to the magnetizing reactance. A small a gap as possible is desired without causing wear on stator and rotor protective coverings. Ultimately the gap will be a function of the tolerances obtained in the journal bearings.

APPENDIX B

Footnotes from Main Program INDUC.FOR

1. The purpose of the DO loop is to allow multiple core loss inputs for different core materials being considered.
2. If SLOPE is omitted from input, the program will assume a value of slope given by

$$\text{SLOPE} = \frac{1. + 164. * \text{LT}}{1. + 82. * \text{LT}} \quad (1)$$

3. For this design, a value of FW1 equal to zero is assumed. By doing so, all scaling is bypassed and hence no entries in the WNDAGE NAMELIST are required. See also footnote 5 for INDUC.DAT.
4. The use of this equation is clearly explained in ref. 11.
5. See Figure 3.2 for illustration of these dimensions.
6. The slot leakage pitch factor, KS, is detailed in reference 2, section 7.3. In section 1.8 of the same reference, the reactance calculations of a C-core reactor with air gap is outlined.

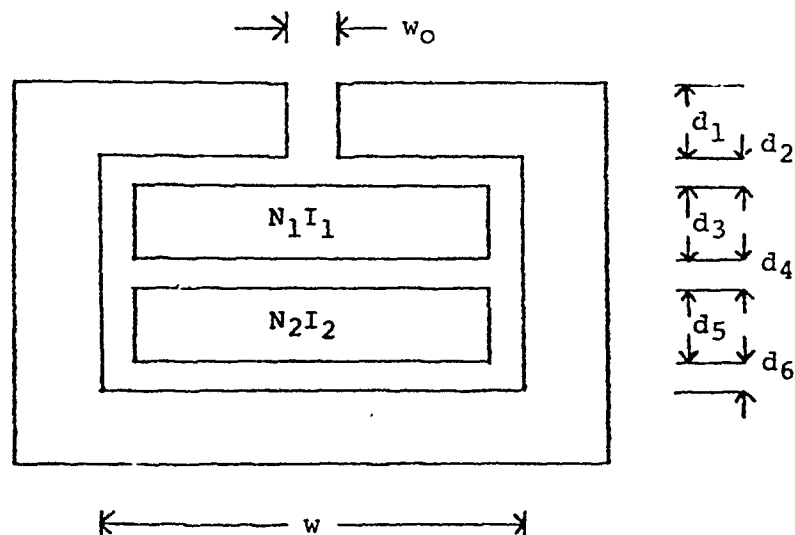


Figure B-1

For winding 1,

$$L_1 = 4\pi N_1^2 10^{-7} \ell \left[\left(\frac{d_1}{w_o} \right) + \left(\frac{d_2}{w} \right) + \left(\frac{d_3}{3w} \right) \right] \text{ henries (2)}$$

For winding 2,

$$L_2 = 4\pi N_2^2 10^{-7} \ell \left[\left(\frac{d_1}{w_o} \right) + \left(\frac{d_2 + d_3 + d_4}{w} \right) + \left(\frac{d_5}{3w} \right) \right] \text{ (3)}$$

The mutual inductance between windings 1 and 2

$$L_m = 4\pi N_1 N_2 10^{-7} \ell \left[\left(\frac{d_1}{w_o} \right) + \left(\frac{d_2}{w} \right) + \left(\frac{d_3}{2w} \right) \right] \text{ (4)}$$

With dimensions in centimeters, the primary slot reactance is equal to the product:

$$\begin{aligned} & 2\pi f \times \text{slots per phase} \\ & \times (\text{series conductors per slot})^2 \times \text{embedded slot length} \\ & \times \text{slot permeance ratio} \times (4\pi \times 10^{-9}) \end{aligned}$$

or

$$X_1 = 2\pi f \left(\frac{s}{m} \right) \left(\frac{2mN_1}{s} \right)^2 (\ell) (P_{S1}) (4\pi \times 10^{-9}) \quad (5)$$

$$= \frac{3.158 f m \ell N_1^2 P_{S1} 10^{-7}}{S_1} \quad \text{ohms per phase}$$

In inches,

$$X_1 = \frac{8.022 f m \ell N_1^2 P_{S1} 10^{-7}}{S_1} \quad (6)$$

Consider a winding now that has the following geometry:

AAA	BBB	CCC	AAA	BBB	CCC
OOO	XXX	●●●	OOO	XXX	●●●
OOO	XXX	●●●	OOO	XXX	●●●
AAA	BBB	CCC	AAA	BBB	CCC

This double layer, two-pole, 18 slot winding has 60° phase belts and a full pitch (pitch = 1.0). Since there are six slots per phase, the primary slot reactance per phase then becomes

$$X_1 = 2\pi f (6) [L_1 + L_2 + 2L_m] \quad (7)$$

or equivalently (in meters)

$$X_1 = 2\pi f \left(\frac{s}{m} \right) \left(\frac{2mN}{s} \right)^2 (\ell) (P_{S1}) (4\pi \times 10^{-7}) \quad (8)$$

where,

$$P_{S1} = \left[\left(\frac{d_1}{w_o} \right) + \left(\frac{d_2}{w} \right) + \left(\frac{d_3}{3w} \right) \right] + \left[\left(\frac{d_1}{w_o} \right) + \left(\frac{d_2+d_3+d_4}{w} \right) + \left(\frac{d_5}{3w} \right) \right]$$

$$+ 2 \left[\left(\frac{d_1}{w_o} \right) + \left(\frac{d_2}{w} \right) + \left(\frac{d_3}{2w} \right) \right]$$

$$= \left[\frac{4d_1}{w_o} + \frac{4d_2}{w} + \frac{7d_3}{3w} + \frac{d_4}{w} + \frac{d_5}{3w} \right] \quad (9)$$

if the slots are modelled as C-cores. For alternate slot geometrics, the permeance ratio, P_{S1} , can be obtained from the literature^{1,2,3,4,6,11}.

Additional complexity arises, however, when the windings are not full-pitched. With a fractional pitch, currents in the top and bottom coils in a slot are out of phase by the amount of the electrical angle between phases, θ . As an example, consider the following geometry:

Slot	123	456	789	10	11	12	13	14	15	16	17	18
	AAA	BBB	CCC	\bar{A}	\bar{A}	\bar{A}	B	B	B	\bar{C}	\bar{C}	\bar{C}
	OOO	XXX	●●●	O	O	O	X	X	X	●	●	●
	OOX	XX●	●●O	O	O	X	X	X	●	●	●	O
	AAB	BBC	CC \bar{A}	\bar{A}	\bar{A}	B	B	B	\bar{C}	\bar{C}	\bar{C}	A

This is identical to the previous example except now there is an 8/9 pitch in the winding instead of 1. Thus, one immediately sees that currents are not identical in all the slots. For phase A, consider slots 1, 2, 3, 10, 11 and 12. Slots 1, 2, 10 and 11 carry identical currents and thus for these four slots:

$$X = 2\pi f(4) \left[L_1 + L_2 + 2L_m \right] \quad (10)$$

For the two remaining slots, 3 and 12, there is only one coil of phase A per slot. For these two slots:

$$X = 2\pi f(2) \left[L_1 + L_2 - 2L_m \cos \theta \right] \quad (11)$$

where θ is the electrical angle between phases (usually 120°). Overall then, the primary slot leakage reactance would be the sum of these two reactances or,

$$X_1 = \left[2\pi f \left(6L_1 + 6L_2 + 10L_m \right) \right], \theta = 120^\circ \quad (12)$$

and an equivalent slot permeance ratio obtained from the term in brackets by dividing by six slots per phase.

Thus, there are in this case two different slot cases to be considered. Alger² obtains a general expression for the slot permeance ratio for an open slot. Consider the following case:

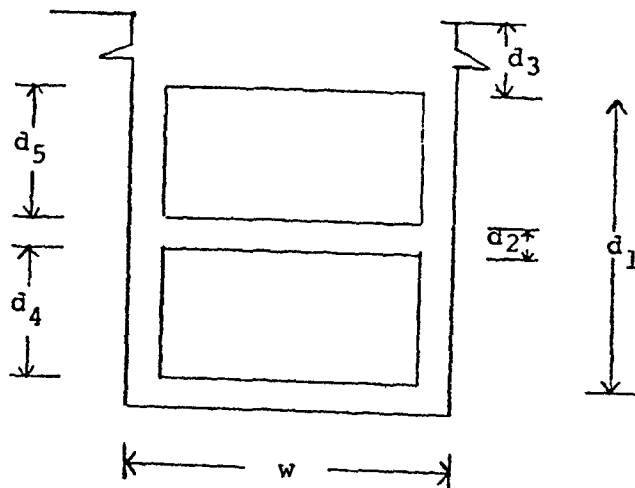


Figure B-2

Here it can be shown that

$$P_{S1} = \frac{K_S}{w} \left(d_3 + \frac{d_1}{3} + \frac{d_1}{12w} \right) \left(1 - K_S \right) - \frac{d_2}{4w} \left(K_S - \frac{2}{3} \right) \quad (13)$$

$$\text{with } K_S = \frac{1 + \cos \theta}{2} \quad (14)$$

and the heights of the two coil bundles, d_4 and d_5 , being equal. Alger explains that if all the slots were alike, as in a full pitch, or a three-phase, $2/3$ pitch, winding a single value of K_S could be used in the above equation. In the general case, however, there are at least two kinds of slots, carrying coil sides of different phases. It is necessary, therefore, to multiply the distinct values of K_S for the different kinds of slots by the proportion of each, and add these, to find an effective value of K_S for the entire winding. Evidently, for a three-phase winding, the effective value of K_S will vary linearly with pitch between the limiting values of one for a full-pitch winding, 0.75 for a $2/3$ -pitch winding, 0.25 for a $1/3$ -pitch winding, and 0 for a zero-pitch winding.

If the dimensions from Figure B-1 are substituted into Figure B-2 and Equation (13), then the permeance ratio for one slot becomes,

$$P_{S1} = \frac{K_S}{w} \left(d_1 + d_2 + \frac{d_3 + d_4 + d_5}{3} \right) + \frac{d_3 + d_4 + d_5}{12w} \left(1 - K_S \right) - \frac{d_4}{4w} \left(K_S - \frac{2}{3} \right) \quad (15)$$

From the previous example of a fractional pitch winding

$$p = 8/9 = .889$$

and from Alger, fig. 7.3, one can obtain the equivalent K_S :

$$K_S = .917$$

so that, substituting,

$$P_{S1} = \frac{1}{w} (.917d_1 + .917d_2 + .313d_3 + .250d_4 + .313d_5) \quad (16)$$

Recall from Eq. (12) that for one phase the primary slot leakage reactance was obtained. If this result is divided by six to obtain the equivalent slot reactance per slot and by four to refer the answer to a single conductor per slot, Eq. (12) becomes

$$X_{1\text{slot}} = 2\pi f \left(\frac{L_1}{4} + \frac{L_2}{4} + \frac{10L_m}{24} \right) \quad (17)$$

and from equations (2), (3) and (4), the equivalent slot permeance ratio can be found to be

$$\begin{aligned} P_{S1} &= \frac{1}{4} \left[\left(\frac{d_1}{w} \right) + \left(\frac{d_2}{w} \right) + \left(\frac{d_3}{3w} \right) \right] + \frac{1}{4} \left[\left(\frac{d_1}{w} \right) + \left(\frac{d_2 + d_3 + d_4}{w} \right) + \left(\frac{d_5}{3w} \right) \right] \\ &\quad + \frac{10}{24} \left[\left(\frac{d_1}{w} \right) + \left(\frac{d_2}{w} \right) + \left(\frac{d_3}{2w} \right) \right] \\ &= \frac{1}{w} \left[.917d_1 + .917d_2 + .542d_3 + .25d_4 + .083d_5 \right] \quad (18) \end{aligned}$$

With $d_3 = d_5$, which will be true in almost all cases, Eq. (18) is identical to Eq. (16) and, thus, Alger's method of using an effective value of K_S is proven.

Alger illustrates this effective value of K_S graphically in Figure 7.3, case 1, for a 3 phase, 60° phase belt winding. In the computer program, the value of K_S is taken from the graph and is broken down into three equations since K_S is linear in three separate regions.

7. See Appendix C.
8. See Figure 3.2 of the main text.
9. See Figure 3.2 of the main text.
10. See Appendix D.

11. See Appendix E. Also note that the phase belt is input here to be 60° .
12. Ref. 2, p. 183 or Ref. 3, p. 93. The equations in the program come from ref. 1, pp. 327 - 328.
13. Ref. 1, p. 331, Equ. 198 and Fig. 135, p. 209.
14. Resistance is a function of resistivity according to the formula

$$R = \frac{rL}{A}$$

where r = resistivity in Ω - inches, L is the length in inches and A is area in square inches. Thus, the resistance of the stator winding per phase is

$$R_s = \frac{L_s N r}{a s_s \times 10^6} \Omega$$

15. The horizontal extension of the armature coil beyond the armature core is equal to the sum of $b + f + g$, Fig. 135, p. 209 of Ref. 1. Here,

$$f = C \sin \alpha$$

where,

$$2C = \frac{\pi (D + d_s)}{p \cos \alpha} \text{ (pitch) in.}$$

16. Dividing by 12 to get the output in feet.
17. Ref. 1, pp. 333 - 334.

18. Ref. 1, pp. 234.
Ref. 2, pp. 201.
19. Ref. 1, pp. 335.
Ref. 2, pp. 201.
Also see footnote 6.
20. Ref. 1, pp. 335.
Ref. 2, pp. 208.
21. Ref. 1, pp. 336, Fig. 199.
22. Ref. 1, pp. 228.
Ref. 2, pp. 337.
23. Ref. 1, pp. 335.
24. Ref. 2, pp. 232.
25. The description of the no-load magnetic calculations is described adequately in the users' manual. The calculations accomplish several things:
 - (1) Computation of flux densities throughout the magnetic circuit of the motor at no-load;
 - (2) Computation of ampere-turn drops across various parts of the magnetic circuit;
 - (3) Computation of magnetizing current and magnetizing reactance X_0 ;
 - (4) Computation of values of core loss W_0 and the value of the resistive element R_0 used in the equivalent circuit to represent the core loss.The calculations are performed by first obtaining initial estimates for X_0 , W_0 and R_0 through the equations shown in the program. Then a double convergence procedure allows one to find R_0 and X_0 for use in the equivalent circuit.

Note that for the equation,

$$W0 = 3. * (WSYOKE + WSTOTH) * WFE$$

only the stator iron weight is used to compute the core loss. Since the relative frequency seen by the rotor is the slip frequency, the hysteresis and eddy current losses seen here will be very small. Hence, they are neglected by the program. The factors 3 in the core loss estimate and 5 in core resistance estimate have no significance except to insure an upper bound on each of these estimations. Also note that in the calculation of the R0 estimate, the line voltage V1 is used. Ideally one would want to use the air gap voltage V2, but at this stage it is not known.

26. The looping process begins here at statement 520.
27. On the initial call to CIRCT, the air gap voltage V2 and the magnetizing current IMAG are computed. See Appendix F for footnotes on CIRCT.
28. If the flux per pole, ϕ , linking an N-turn coil varies sinusoidally in time at a frequency f cycles per second, then at one point in the air gap circumference:

$$\begin{aligned}\phi(t) &= \phi_m \sin 2\pi ft \text{ webers} \\ &= \phi_m \sin 2\pi ft \times 10^5 \text{ kilolines}\end{aligned}$$

then,

$$E = -N \frac{d\phi}{dt} = -2 f N \phi_m \cos 2\pi ft$$

so that the RMS value of E which can also represent the airgap voltage, V_2 , becomes:

$$E_{\text{rms}} = V_2 = \frac{2\pi f N \phi_m}{\sqrt{2}}$$

$$= 4.443 f N \phi_m \text{ volts}$$

Thus, ϕ_m can be found to be

$$\phi_m = \frac{V_2}{4.443 f N}$$

Now, in terms of a spatially varying flux wave in the air gap,

$$\phi(\theta_e) = \phi_m \cos \theta_e$$

In electrical terms, a differential angle, θ , becomes

$$d\theta = d\left(\frac{2\theta_e}{p}\right) = \frac{2}{p} d\theta_e$$

so that upon integrating over the entire pole,

$$\text{total flux} = \int_{-\frac{\pi}{2}}^{\frac{\pi}{2}} \frac{V_2 \cos \theta_e}{4.443 f N} d\theta_e$$

$$= .45 \frac{V_2}{f N}$$

Then, when webers are converted to kilolines and pitch and distribution factors are appropriately added the total flux over p poles becomes,

$$\phi_{\text{total}} = .45 \frac{p V_2 10^5}{f N K_p K_d}$$

or as is used in the program,

$$\phi_{\text{total}} = \frac{.637}{\sqrt{2}} \frac{PV_2 10^5}{fNK_p K_d}$$

The .637 term originates as $\frac{\alpha}{\pi}$, the average value of a sinusoid of magnitude 1. Thus, in terms of the program,

$$FTOTAL = \frac{1}{\sqrt{2}} \frac{PV_2 10^5}{fNK_p K_d}$$

and

$$FPOLE = FTOTAL * \frac{2}{\pi P}$$

29. Ampere turns in the air gap, ATAG, can be found by utilizing Ampere's Law,

$$\int \mathbf{H} \cdot d\mathbf{l} = N \iint \mathbf{J} \cdot \mathbf{n} dA = ATAG$$

the left hand integral is zero everywhere except across the air gap; hence

$$\int \mathbf{H} \cdot d\mathbf{l} = Hg = \frac{B}{N} g$$

The term 313 arises in units conversion of N as follows:

$$\frac{10^5 \frac{\text{lines}}{\text{web}}}{4\pi \times 10^{-7} \text{ H/m}} \frac{1}{.0254 \text{ in/m}} = 313.$$

30. The subroutine MAGNET computes the yoke and tooth flux densities as well as the total magnetomotive force ATTOT. On the first call of MAGNET, values calculated are used to improve the values of W0, R0, and X0. Subsequent calls allow refinement of these values until final convergence is obtained. Consult the users' manual for a more detailed

description of the convergence procedure. Also see Appendix G for footnotes on the MAGNET subroutine.

31. W0 and R0 as calculated here are more accurate values than those previously calculated since the equations use the latest values of stator yoke and flux densities as well as the latest value of the air gap voltage, V2.

32. Ref. 1, pp. 329, Eq. 197.

33. A new value of X0 is computed upon convergence of R0.

34. The current density at no-load is

$$\frac{I_m^2 + \left(\frac{V_2}{R_0}\right)^2}{\text{cross sectional area}}$$

35. Windage calculations for this design are not performed since FW1 is assumed to be zero.

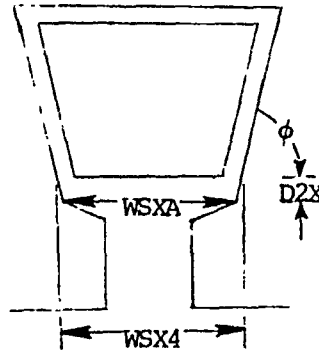
36. TRATED is an input value that is optional. It normally should be put into the data set since it allows calculation of the current densities in the rotor bar, end ring, and armature. TRATED also now must be input in foot-pounds instead of inch-pounds as stipulated in the users' manual.

37. See Appendix F and the users' manual.

APPENDIX C

Footnotes for SLOTS.FOR

1. The function $D(Wa, CAREA)$ is used to compute the dimension $Y1$ in Fig. 14 of the users' manual Ref. 11. It will not be of concern unless using trapezoidal slot types 2, 4 or 6.
2. The function $WB(D, WA)$ is used to compute the dimension $WSX4$ illustrated below:



3. The function A is used to compute the slot area in Fig. 14 of the users' manual, Ref. 11, needed for intermediate calculations for slot type 6 only.
4. $A1$ and $A2$ are used in computing the slot permeance ratio and are explained in the users' manual.

APPENDIX D

Footnotes for WDGFACT.FOR

1. The winding pitch factor is derived in Reference 2. It is equal to,

$$K_{pn} = \sin \frac{n\alpha}{2}$$

for the fundamental flux wave $n = 1$. If one considers a coil pitch of $8/9$, then $\alpha = 8/9 (180) = 160$ and $K_{p1} = .985$. If the coil pitch is $2/3$ then $\alpha = 2/3 (180) = 120$ and $K_{p1} = .866$. In the computer program, an equivalent equation is used for pitch factor. It is

$$K_p = \sin \frac{p\pi}{2}$$

where p is the winding pitch or ratio of coil span to pole pitch.

2. The winding distribution factor is derived in Reference 2. It is equal to,

$$K_{dn} = \frac{\sin \frac{nm\gamma}{2}}{m \sin \frac{n\gamma}{2}}$$

where m = slots per phase belt and γ = angular distance between slots. For the fundamental flux wave, $n = 1$. If one considers a winding which has three slots per phase belt and 18 slots totally on the stator ($\gamma = \frac{360}{18} = 20^\circ$) then $K_{d1} = .960$. In the computer program, an equivalent equation is used for the distribution factor as follows:

$$K_d = \frac{\sin \frac{\pi}{2q}}{n \sin \frac{\pi}{2nq}}$$

where q is the number of phase belts per pole and n is the number of slots per phase belt.

3. For windings that do not have the number of slots per pole per phase being an integer, refer to Ref. 1, p. 195. Kuhlmann reiterates the general equation for the winding distribution factor for the fundamental

$$k = \frac{\sin \frac{180^\circ}{2m}}{q \sin \frac{180^\circ}{2mq}}$$

where for this formula, m = number of phases and q = slots per pole per phase. For windings with mixed number of slots per pole per phase, the equivalent number of slots per pole per phase must be used for q . A fractional-slot armature winding may be represented by

$$f + \frac{g}{h} = \frac{fh + g}{h}$$

This indicates that there are $fh + g$ slots per phase for every h poles. The winding is equivalent to an integral slot winding with $fh + g$ slots per pole per phase. For a $2\frac{1}{4}$ -slot-per-pole-per-phase 3-phase winding, the equivalent integral slot winding would have

$$2 + \frac{1}{4} = \frac{2 \times 4 + 1}{4} = \frac{9}{4}$$

or 9 slots per pole per phase. The winding distribution factor

$$k_d = \frac{\sin \frac{180^\circ}{2 \times 3}}{9 \sin \frac{180^\circ}{2 \times 3 \times 9}} = .955$$

APPENDIX E

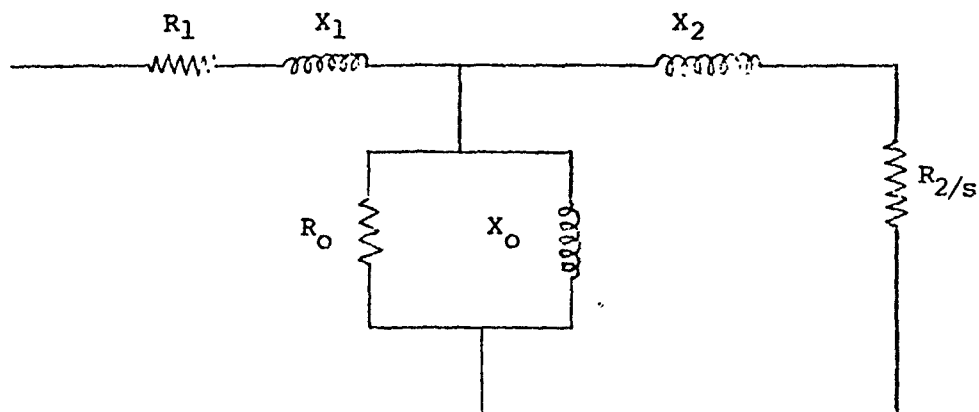
Footnotes for CIRCT.FOR

1. The constant $C = 2.5$ is used in the equation

$$FW = FW1 * \frac{RPM}{NSYNCH} * * C$$

which calculates the windage loss at any other rotor speed besides synchronous speed. Since $FW1$ is zero for the design of the submarine propulsion motor, this equation should not be of any concern. For more detail on this equation, see the users' manual p. 13.

2. From the circuit below

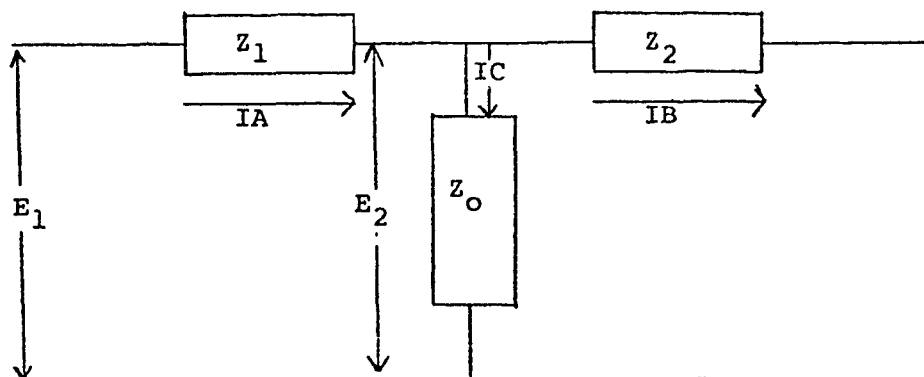


it follows that Z_O is equivalent to R_O in parallel with X_O . Thus,

$$\begin{aligned} Z_O &= R_O // jX_O = \frac{jR_O X_O}{R_O + jX_O} \cdot \frac{R_O - jX_O}{R_O - jX_O} \\ &= \frac{R_O X_O^2}{R_O^2 + X_O^2} + j \frac{R_O^2 X_O}{R_O^2 + X_O^2} \end{aligned}$$

$$3. \quad Z_2 = \frac{R_2}{s} + jX_2$$

4. From the equivalent circuit,



it follows that,

$$\begin{bmatrix} E_1 \\ 0 \end{bmatrix} = \begin{bmatrix} Z_1 + Z_0 & -Z_0 \\ -Z_0 & Z_2 + Z_0 \end{bmatrix} \begin{bmatrix} I_A \\ I_B \end{bmatrix}$$

If $[Z] = \begin{bmatrix} Z_1 + Z_0 & -Z_0 \\ -Z_0 & Z_2 + Z_0 \end{bmatrix}$,

then, $\begin{bmatrix} I_A \\ I_B \end{bmatrix} = [Z]^{-1} \begin{bmatrix} E_1 \\ 0 \end{bmatrix}$

to obtain $[Z]^{-1}$, define $D = \det[Z] = (Z_1 + Z_2) * (Z_2 + Z_0) - Z_0 * Z_0$

5. Stator and rotor currents easily follow from

$$\begin{bmatrix} I_A \\ I_B \end{bmatrix} = \frac{1}{D} \begin{bmatrix} Z_2 + Z_0 & Z_0 \\ Z_0 & Z_1 + Z_0 \end{bmatrix} \begin{bmatrix} E_1 \\ 0 \end{bmatrix}$$

6. For the no-load calculation ($s = 0$), there is no rotor current and all current passes through the magnetizing branch.

7. V_2 and I_{MAG} are vector magnitudes necessary for obtaining R_0 and X_0 .

8. W_1 and W_2 are the stator and rotor copper loss.
9. The windage loss as was stated in footnote 1 is assumed to be zero.
10. The power output is directly a function of the copper loss on the rotor and the term $[(100-S)/100]$. Refining this relationship:

$$P_C = 3I_2^2 R_2 \frac{(100 - S)}{S}$$

$$= 3 \left\{ [\text{Re}(I_B)]^2 + [\text{Im}(I_B)]^2 \right\} R_2 \frac{(100 - S)}{S}$$

where $I_B = \frac{E_1}{D} \left[\frac{R_O X_O^2}{R_O^2 + X_O^2} + j \frac{R_O^2 X_O}{R_O^2 + X_O^2} \right];$

Thus, $D = (Z_1 + Z_0) * (Z_2 + Z_0) - Z_0 * Z_0.$

$$P_O = \frac{3E_1^2}{D} \left[\left(\frac{R_O X_O^2}{R_O^2 + X_O^2} \right)^2 + \left(\frac{R_O^2 X_O}{R_O^2 + X_O^2} \right)^2 \right] R_2 \frac{(100 - S)}{S}$$

$$= \frac{3E_1^2}{D} \left[\frac{R_O^2 X_O^2}{R_O^2 + X_O^2} \right] R_2 \frac{(100 - S)}{S}$$

Thus, to maximize the power output at a particular slip, E_1 , R_O , X_O and R_2 should be made as large as possible while minimizing D (by minimizing Z_1 and Z_2). There are tradeoffs, of course, in all of these assumptions, however. For example, if the line voltage E_1 is raised, a subsequent raise in the stator insulation thickness is required. This means that less copper can be used on the stator,

lowering the maximum stator current obtainable as well as raising Z_1 if smaller conductors are used.

The output power is perhaps most greatly affected by the number of stator turns N since

$$\begin{aligned} P_o &= \eta P_i \\ &= 3 \eta V_1 I_1 \cos \theta \\ &= 3 \eta V_1 \frac{V_1}{Z_{in}} \cos \theta \\ &= 3 \eta V_1^2 \cos \theta \frac{Z_o + Z_2}{Z_o Z_o + Z_o Z_2 + Z_1 Z_2} \end{aligned}$$

Thus, in order to raise the input current to the stator, and assuming the maximum current density of approximately 1700 to 3500 amps per square inch is not exceeded, the quantity $(R_1 + R_o) + j(X_1 + X_o)$ must be lowered. Note that $R_o \gg R_1$, so that $(X_o + X_1)$ is the quantity to focus on. For each of the following quantities, reduction can be achieved by:

- i) XOAG \downarrow $N^2 \downarrow$ D \downarrow L \downarrow P \uparrow G \uparrow
- ii) XSS \downarrow $N^2 \downarrow$ F \downarrow L \downarrow AXS \downarrow QS \uparrow
- iii) XSE \downarrow small-neglect
- iv) XSK \downarrow P \downarrow SKEW \downarrow D \uparrow
- v) XSZ \downarrow QS \uparrow P \uparrow CCS \downarrow KS \uparrow
- vi) XP \downarrow small-neglect

Thus, if D, L, G, P, QS and F are fixed, the N certainly would be the best parameter to work with since it is a squared term. Of course, P, QS and F also could be varied at a later time but their input will not be as large as N 's. It is also assumed that minor changes in AXS, SKEW, CCS and KS will have relatively small impacts on power output.

11. One horsepower equals 33,000 foot-pounds per minute.
One revolution per minute equals 2π rads/min.

$$\Rightarrow \frac{33,000}{2\pi} = 5.25 \times 10^3$$

APPENDIX F

Footnotes for MAGNET.FOR

1. All of the air gap flux density must pass through the stator teeth. Hence, it is a simple matter of dividing the total flux by the area that it passes through to obtain the flux density.
2. Once B has been obtained, the program then obtains the magnetizing force, H, from the B-H curve data obtained as input.
3. The ampere turns across the stator tooth is merely the magnetizing force, AT, in ampere-turns per inch times the tooth depth.
4. The flux per pole in this calculation is divided by 2 since the flux does not enter the stator and rotor yoke at a point; therefore, the yoke density cannot be constant over the length of the flux path. FPOLE is the effective value of the maximum flux per pole, FTOTAL/P. Dividing it by two accounts for variances in the flux density within a pole pitch. To see how this flux density varies through a pole pitch for a four pole machine, refer to Fig. 193 of Ref. 1.
5. The length of the flux path in the stator yoke, LSYOKE, is computed in INDUC.FOR as one-half the pole pitch on the mean diameter of the yoke.
6. Ref. 1, p. 329.

Appendix G
USING THE PROGRAM CURVES

CURVES is a general program that allows computation of submarine curves of form in addition to speed-power requirements for an arbitrary body of revolution. Data is read in via unformatted READ statements. A typical input file is shown below:

```
0.,6.0,8.4,10.0,11.2,12.8,14.0,14.6,15.4,15.8,15.9,16.,  
16.,0.,.6,1.6,2.1,4.8,7.6,11.4,13.6,14.8,15.8,16.  
210.,3.,6.,500.  
1000.,.009,10.,.80
```

The first two input lines are the offsets in feet at stations shown in Figure 4.6. The next line contains the variables LPMB, SFB, SAB and LENGTH. The last line contains the variables AB, CDB, AACDA and PC.

The program contains one intricacy that should later be eliminated. Specifically, the number of waterlines chosen is strictly a function of the hull diameter. For example, if the hull diameter is 32.0 feet, then there will be 32 waterlines calculated at 1-foot intervals. If the hull diameter is 40.00 feet, then there will be 40 waterlines calculated at 1-foot intervals. To account for

different hull diameters, the user must redimension the arrays KB, LCB, DRAFT, DISP, BM, AWP and VOL. The arrays must be dimensioned to be two greater than the number of waterlines being used. Thus, if the user is using 32 waterlines, then the above arrays must be dimensioned as 34 so that the last two storage spaces in each array are available for scaling calculations in the plotting subroutine.

The same logic applies to dimensioning the arrays VK, CF, CTBH, EHP and SHP to account for different speed requirements.

The output data is displayed first assuming a completely submerged submarine. Subsequent calculations display variables as a function of draft. Finally, the output data is passed to the subroutine VERSAPLOT for plotting on a VERSATEL 1200 plotter.

REFERENCES

1. Kuhlmann, John H., Design of Electrical Apparatus, 3rd ed., John Wiley & Sons, Inc., 1950.
2. Alger, Philip L., Induction Machines -- Their Behavior and Uses, 2nd ed., Gordon and Breach Science Publishers, 1970.
3. Still, Alfred, and Siskind, Charles S. Elements of Electrical Machine Design, 3rd ed., McGraw-Hill Book Co., Inc., 1954.
4. Gray, Alexander, Electrical Machine Design, 2nd ed., McGraw-Hill Book Co., Inc., 1926.
5. Nasar, S. A., and Unnewehr, L. E., Electromechanics and Electric Machines, John Wiley & Sons, Inc., 1979.
6. Veinott, Cyril G., Theory and Design of Small Induction Motors, McGraw-Hill Book Co., Inc. 1959.
7. Moore, A. D., Fundamentals of Electrical Design, McGraw-Hill Book Co., Inc., 1927.
8. Walker, J. H., Large A. C. Machines -- Design, Manufacture and Operation, Bharat Heavy Electricals Limited, 1979.
9. Data sheets from U. S. Steel.
10. Jayawaut, B. V., Induction Machines, McGraw-Hill Book Co., Inc., 1968.
11. Bollenbacher, Gary, FORTRAN Program for Induction Motor Analysis, NASA Technical Note TN D-8184, 1976.
12. Flaherty, R. J., "Sea Water Flooded Electric Motor for 13,200 PSI," Digest of Technical Papers of the 1970 IEEE Conference and Engineering in the Ocean Environment, 21-24 Sept., 1970, pp. 186-188.
13. Perez, Ignacio Jose, "Computer-Aided Design of High Speed Synchronous Machines," M.S. Thesis, M.I.T., 1978.
14. Perez, I. J. and Kassakian, J. G., "A Stationary Thermal Model for Smooth Air-Gap Rotating Electric Machines," Electric Machines and Electromechanics: An International Quarterly, 1979.

15. Flaherty, R. J. and Walker, H.P., "Sea Water Flooded Electric Motor for 13,200 PSI," Digest of Technical Papers of the 1970 IEEE Conference and Engineering in the Ocean Environment, 21-24 Sept. 1970, Panama City, Fla., p. 186-8.
16. Rohsenow, Warren M. and Choi, Harry Y., Heat, Mass and Momentum Transfer, Prentice-Hall, Inc., 1961.
17. Wilson, Bryan W., et al, "A Deep Diving Submarine," final project report, course 13 461, M.I.T., 1982.
18. Vickers, V. J., "Recent Trends in Turbogenerators," Proc. IEE, Vol. 121, No. 11R, November, 1974.
19. Neidhoffer, G., "Roebel Bar Windings for Large Synchronous Machines," Brown Boveri Review, Volume 57, January, 1970.
20. Schuler, R., "Insulation Systems for High-Voltage Rotating Machines," Brown Boveri Review, Volume 57, January, 1970.
21. Marti, P. and Schuler R., "Manufacture and Testing of Roebel Bars," Brown Boveri Review, Volume 57, January, 1970.
22. Beveridge, J. L., "Calculation of Optimum Efficiency for a Series of Large-Hub Propellers for a Submerged Body of Revolution," DTNSRDC Report 1826, August, 1964.
23. Smith, A.M.O. and Pierce, J., "Exact Solution of the Neuman Problem, Calculation of Noncirculating Plance and Axially Symmetric Flows About or Within Arbitrary Boundaries," Douglas Aircraft Co., Report No. ES-26988, April, 1958.
24. Granville, P.S., "The Calculation of the Viscous Drag of Bodies of Revolution," DTNSRDC Report 849, July, 1953.
25. Landweher, L. and Gertler, M., "Mathematical Formulation of Bodies of Revolution," DTNSRDC Report 719, September, 1950.
26. Denny, S. B., "Measurement of Forces and Spindle Moments on Individual Blades of a Large-Hubbed Propeller," DTNSRDC Report 3252, December, 1969.
27. Wernli, Robert L., "Experience with an Unmanned Vehicle-Based Recovery System," Marine Technology, Vol. 20, No. 1, Jan., 1983, pp. 71-77.

28. Sejd, James J., "A Submarine Control System Test Vehicle," Naval Engineers Journal, April, 1980.
29. Greeley, David S. and Kerwin, Justin E., "Numerical Methods for Propeller Design and Analysis in Steady Flow," Society of Naval Architects and Marine Engineers, Annual Meeting, New York, N.Y., November 17-20, 1982.
30. Joosen, W.P.A., Van Manen, J. D. and Van Der Walle, F., "Large Hub to Diameter Ratio Propellers with Programmed Blade Control," International Shipbuilding Progress: Shipbuilding and Marine Engineering Monthly, Vol. 10, No. 101, Jan., 1963.
31. "The Tandem Propeller Submarine," Cornell Aeronautical Laboratory, Inc., Cornell University, Buffalo, New York.
32. Kroeger, N. Bernard, and Cummings, Damon, E., "Subcavitating Propeller Design for Maximum Propeller Efficiency or Minimum Fuel Use," Marine Technology, April, 1974.
33. Kuhn, Earl C., "Largest Thrust Bearings are Water Cooled," Power, October, 1971.
34. Boyarko, N. N. and Val'Chuk, V. K., "Rig Tests on Hydro-Mechanical Thrust Bearings for Circulating Pumps in Atomic Power Stations," Russian Engineering Journal, Vol. 56, No. 5, 1975.
35. "New Cage Design Reduces Induction Motor Failure," Electrical Review, Vol. 205, No. 14, October 12, 1979.
36. Merrill, Edgar F., "Temperature Rise Considerations for Large Induction Motors," IEEE Transactions on Industry and General Applications, Vol. IGA-5, No. 4, July/August, 1969.
37. Gerken, T. J., "Feasibility Study, Novel Electric Propulsion System for a Submarine," Electric Machinery Specification U413-61-118, General Dynamics Corporation, Electric Boat Division, May 9, 1961.
38. Aldworth, D. R., "The Effects of Manufacturing Techniques on Motor Efficiency," Insulation/Circuits, July, 1981.
39. Fox, Robert M., "Bibliography--Tandem Propulsion Systems," Machinery Laboratory Technical Note 117/68, DTNSRDC, April, 1968.

40. "Experimental and Theoretical Research on the Hydrodynamic Characteristics of Large Hub to Diameter Ratio Propellers," Contract No. N 62558-3463, Netherlands, Ship Model Basin, Haagstaeg 2, Wageningen, Netherlands, April, 1964.
41. Andrews, James Bruce, "Application of Lifting Line Theory to Large Hub Propellers," M.S. Thesis, M.I.T., 1969.
42. Izzo, A. J., "Feasibility of a Novel Electric Power Propulsion System (NEPPS) for a Submarine, Vol. III, Hydrodynamic Tests," General Dynamics Corp., Groton, Connecticut, Electric Boat Division, Contract NONr 3383(00), Project NR 097-353, July 31, 1963.
43. Riddell, Frederick R. and Dix, Donald M., "Technology Assessment of Advanced Propulsion Systems for Some Classes of Combat Vehicles," Vol. III, Institute for Defense Analysis, IDA Log No. HQ 77-19844, September, 1978.
44. Morrison, T. D., et al, Handbook of Electric Drive Systems for Deep Ocean Applications, DOT Program S4636, Task 14745, David W. Taylor Naval Ship R & D Center, Annapolis, Maryland, July, 1977.
45. Flaherty, R. J., et al, Handbook of Electrical Insulating Materials for Deep Ocean Applications, Report Number PAS-76-8, David W. Taylor Naval Ship R & D Center, Annapolis, Md., June, 1976.
46. Flaherty, R. J., and Codd, R. F., "Design Manual for Submerged Motor Pump," June 1970.
47. IEEE, "Polyphase Induction Motors Having Liquid in the Magnetic Gap," Publication 252, 1963.
48. Fitzgerald, A. E., Kingsley, Charles and Kusko, Alexander, Electric Machinery, Third Ed., McGraw-Hill, Inc., 1971.
49. McPherson, George, An Introduction to Electrical Machines and Transformers, John Wiley and Sons, 1981.
50. "Fluidized Bed Coatings with Plastics; Technology and Potential for Military Applications," Plastics Technical Evaluation Center Report No. 13, January, 1964.
51. Flaherty, Codd, Glod and Walker, "A Wet Winding Induction Motor for 6000 psi Water Environment," IEEE Conference Paper 68CP167-PWR, February, 1968.

52. Bose, Bimal K., ed., Adjustable Speed AC Drive Systems, IEEE Press, New York, 1981.
53. Soderberg, C. Richard, "Steady Flow of Heat in Large Turbine-Generators," AIEE Trans., Vol. 50, June, 1931.
54. Andrews, James Bruce, "Application of Lifting Line Theory to Large Hub Propellers," M.S. Thesis, Department of Ocean Engineering, M.I.T., 1969.
55. Kroeger, N. Bernard, Jr. "Optimization of Propulsion Speeds," M.S. Thesis, Department of Ocean Engineering, M.I.T., 1972.
56. Kerwin, J. E., and Leopold, R. "A Design Theory for Subcavitating Propellers," Transactions of SNAME, Vol. 72, 1964.
57. Lerbs, H. W., "Moderately Loaded Propellers with a Finite Number of Blades and an Arbitrary Distribution of Circulation," SNAME Transactions, 1952.
58. Brockett, T., "Minimum Pressure Envelopes for Modified NACA-66 Sections with NACA $a = 0.8$ Camber and Buships Type I and Type II Sections," Report 1780, David Taylor Model Basin, 1966.
59. McCormick, B. W., "The Effect of a Finite Hub on the Optimum Propeller," Journal of Aeronautical Sciences, Vol. 22, September, 1955.
60. Izzo, A. J., "Feasibility of a Novel Electric Power Propulsion System (NEPPS) for a Submarine, Vol. III, Hydrodynamic Model Tests," General Dynamics Corp., Groton, Conn., Electric Boat Division, AD-342 463/7ST, 31 July 1963.
61. Roberts, T. J., "The Solutions of the Heat Flow Equations in Large Electrical Machines," Heat Transfer and Fluid Flow in Electric Machines Symposium, Institute of Mechanical Engineers, Proceedings 1969-1970, Vol. 184.

Computer Listing

© Michael Scott Hamner, 1983

I hereby assign my copyright of this computer listing to
The Charles Stark Draper Laboratory, Inc.,
Cambridge, Massachusetts.

Michael Scott Hamner
Michael Scott Hamner

Permission is hereby granted by The Charles
Stark Draper Laboratory, Inc. to the
Massachusetts Institute of Technology to
reproduce any or all of this thesis.

```

*****
C THE FOLLOWING PROGRAM WRITTEN BY M. S. HAMNER AND IS USED
C TO OBTAIN SUBMARINE CURVES OF FORM AND VARIOUS OTHER PARAMETERS WHICH ARE
C STRICTLY A FUNCTION OF THE HULL GEOMETRY. THESE INCLUDE:
C
C 1. DISPLACEMENT VS. DRAFT
C 2. LCH VS. DRAFT
C 3. WATERPLANE AREA VS. DRAFT
C 4. UNDERWATER VOLUME VS. DRAFT
C 5. KB VS. DRAFT
C 6. TRANSVERSE METACENTRIC RADIUS (RM) VS. DRAFT
C 9. TONS PER INCH IMMERSION VS. DRAFT
C 10. MOMENT TO TRIM ONE INCH (MT1) VS. DRAFT
C 11. RIGHTING ARM VS. HEEL ANGLE
C 12. WETTED SURFACE AREA
C 13. EHP VS. SPEED IN KNOTS
C 14. SHP VS. SPEED IN KNOTS
C 15. PRISMATIC COEFFICIENT (CP)
C 16. WETTED SURFACE COEFFICIENT (CWS)
C
C THE REQUIRED INPUT IS VERY SPECIFIC AND MUST BE ESTABLISHED IN A DATAFILE.
C AT THIS POINT LITTLE EMPHASIS HAS BEEN PUT ON IMPROVING THE USER INTER-
C FACE OR PRETTYING UP THE OUTPUT. THE MAIN OBJECTIVE WAS TO GET OUT THE
C RAW DATA. NOTE THAT THE SUBMARINE DIAMETER PLAYS A CRITICAL ROLE IN THE
C SIZE OF THE DIMENSIONS FOR ARRAYS KB,LCH,DISP,CF,CTBH,VK,BM,AWP,EHP,AND SHP.
C THUS THE DIMENSION OF THE ARRAY WILL BE EXACTLY THE SAME AS THE SUBMARINE
C DIAMETER PLUS TWO NEEDED FOR PLOTTING ON THE VEKSAILOC. THUS IF THE SUBMARINE
C DIAMETER WAS 32, FOR EXAMPLE, THEN THE ARRAYS WOULD BE DIMENSIONED AS 34.
C ALSO WHEN PLOTTING THE APPROPRIATE SIZE OF THE ARRAYS BEING CONSIDERED
C MUST BE INCORPORATED INTO THE CALL FOR SUBROUTINE VERSAPLOT. REFERENCE IS
C MADE TO "SUBMARINE DESIGN NOTES" BY HARRY J. JACKSON, CAPT, USN(RET).
C ** *****
      REAL LPMB,LENGTH,NU,NUM(24),MOMENT,KB(34),LCH(34),INERT(24)
      REAL KG
C
C DIMENSION OFFSET(24),SIMPNT(24),WL(24),THETA(24),AREA(24),ARM(24),

```

```

1STA(24),FA(24),FM(24),DRAFT(34),CIRCUM(24),CF(34),DISP(34),DM(34),
2VK(34),CIHH(34),FHP(34),SHP(34),AWP(34),VOL(34),CAREA(24),AREASH(24)

DATA STA/0.0,5.1,1.5,2.3,4.5,5.5,6.7,8.9,10.10,9.8,7.7,
16.5,4.3,2.1,0./
DATA SIMPMT/0.5,2.1,2.1,5.4,2.4,2.4,2.4,1.1,4.2,4.1,1.4,2.4,
12.4,2.4,2.4,1./

```

```

C READ THE OFFSETS, REQUIRED LENGTHS, AND OFFSET SPACINGS
C
C
C

```

```

10 READ(5,10) (OFFSET(I),I=1,24)
   FORMAT(8F9.2)
20 READ(5,20) LPMH,SFH,SAB,LENGTH
   FORMAT(4F6.2)
21 WRITE(6,21)
   FORMAT(1H0,'*****THE FOLLOWING DATA ASSUMES A COMPLETELY
   1SUBMERGED SURMARINE*****',/)

```

```

C COMPUTE FOREBODY WETTED SURFACE AREA
C
C
C

```

```

FUFA=0.
DO 30 I=1,13
   CIRCUM(I)=OFFSET(I)*2.*3.1416
   FUFA=FUFA+CIRCUM(I)*SIMPMT(I)
30 CONTINUE
   FAREA=FUFA*SFH/3.
   WRITE(6,35) FAREA
35 FORMAT(1H,'FOREBODY WETTED SURFACE AREA = ',F9.2)

```

```

C COMPUTE AFTERBODY WETTED SURFACE AREA
C
C
C

```

```

FOFA=0.
DO 40 I=1,14,24
  CIRCUM(I)=OFFSET(I)*2.*3.1416
  FOFA=FOFA+CIRCUM(I)*SIMPMT(I)
40 CONTINUE
  AAREA=FOFA*SAH/3.
  WRITE(6,45) AAREA
  FORMAT(1H, 'AFTERBODY WETTED SURFACE AREA = ',F9.2)
45
C
C
C
C
C COMPUTE PARALLEL MID-BODY WETTED SURFACE AREA

  PAREA=2.*3.1416*OFFSET(24)*LPMB
  WRITE(6,46) PAREA
  FORMAT(1H, 'PARALLEL MIDBODY WETTED SURFACE AREA = ',F9.2)
46
C
C
C COMPUTE OVERALL WETTED SURFACE AREA AND PRINT RESULTS
C
C
C
C
  WSAREA=FAAREA+AAREA+PAREA
  WRITE(6,50) WSAREA
  FORMAT(1H, 'TOTAL WETTED SURFACE AREA = ',F9.2)
50
C
C
C COMPUTE THE VOLUME OF THE FOREBODY
C
C
C
C
  FOFA=0.
  DO 52 I=1,13
    AREA(I)=3.1416*(OFFSET(I)**2)
    FOFA=FOFA+AREA(I)*SIMPMT(I)
52 CONTINUE
    FVOL=FOFA*SFH/3.
    WRITE(6,54) FVOL
    FORMAT(1H, 'FOREBODY VOLUME = ',F9.2)
54

```

```

C
C
C COMPUTE THE VOLUME OF THE AFTERBODY
C
C
      FUFA=0.
      DO 56 I=14,24
        AREA(1)=3.1416*(OFFSET(1)**2)
        FUFA=FUFA+AREA(1)*SIMPMT(1)
56      CONTINUE
        AVOL=FUFA*SAH/3.
        WRITE(6,58) AVOL
58      FORMAT(1H , 'AFTERBODY VOLUME = ',F9.2)
C
C
C COMPUTE THE VOLUME OF THE PARALLEL MIDBODY
C
C
      PVOL=3.1416*(OFFSET(24)**2)*LPMH
      WRITE(6,60) PVOL
60      FORMAT(1H , 'PARALLEL MIDBODY VOLUME = ',F9.2)
C
C
C COMPUTE TOTAL UNDERWATER VOLUME (MINUS SAIL AND APPENDAGE VOLUME)
C
C
      TVOL=PVOL+AVOL+PVUL
      WRITE(6,62) TVOL
62      FORMAT(1H , 'TOTAL UNDERWATER VOLUME LESS SAIL AND APPENDAGES = ',
        1F10.2)
C
C
C COMPUTE LCH OF FOREBODY
C
C
      SUM=0.
      DO 64 I=1,13

```

```

FM(1)=3.1416*(OFFSET(1)**2)*SIMPMT(1)*STA(1)
SUM=SUM+FM(1)
CONTINUE
FLCB=0.33333*SFH*SFH*SUM/PVOL
WRITE(6,60) FLCB
FORMAT(1H, 'LCB OF FOREBODY = ',F6.2)

```

64 COMPUTE LCB OF AFTERBODY

```

SUM=0.
DO 67 I=1,24
  FM(1)=3.1416*(OFFSET(1)**2)*SIMPMT(1)*STA(1)
  SUM=SUM+FM(1)
CONTINUE
ALCB=(0.33333*SAB*SAB*SUM/AVOL)+LPMH+(10.*SFB)
WRITE(6,68) ALCB
FORMAT(1H, 'LCB OF AFTERBODY = ',F6.2)

```

67 COMPUTE LCB OF THE PARALLEL MIDBODY

```

PLCH=10.*SFB*LPMH/2.
WRITE(6,70) PLCH
FORMAT(1H, 'LCB OF PARALLEL MIDBODY = ',F6.2)

```

70 COMPUTE OVERALL LCB NOT TAKING SAIL OR APPENDAGES INTO ACCOUNT

```

TUTLCB=(FVOL*FLCB+PVOL*PLCH+AVOL*ALCB)/IVOL
WRITE(6,72) TUTLCB
FORMAT(1H, 'OVERALL LCB MINUS SAIL AND APPENDAGES = ',F6.2)

```

72

```

C COMPUTE PRISMATIC AND WETTED SURFACE COEFFICIENTS
C
C
74 CP=(TVOL*4.)/(3.1416*LENGTH*(2.*OFFSET(24))**2)
  WRITE(6,74) CP
  FORMAT(1H0,'PRISMATIC COEFFICIENT (CP)= ',F5.3)
  CWS=WSAREA/(2.*OFFSET(24))*3.1416*LENGTH
76 WRITE(6,76) CWS
  FORMAT(1H,'WETTED SURFACE COEFFICIENT= ',F5.3)
  WRITE(6,77)
77 FORMAT(1H0,'*****')
  1*****'/'
C
C
C COMPUTE EHP VS. SPEED IN KNOTS
C
C
108 WRITE(6,108)
  FORMAT(1H1,'/')
  WRITE(6,78)
78 FORMAT(1H0,'*****THE FOLLOWING DATA IS USED IN OBTAINING THE
  1SPEED-POWER CURVE*****')
  WRITE(6,79)
79 FORMAT(1H,'9X','SPEED','9X','CF','11X','CTBH','11X','EHP','11X','SHP',/)
  DELCF=.0008
  NU=1.25E-5
  READ(5,80) AB,CDB,AACDA,PC
  FORMAT(4F9.2)
  DO 90 I=1,32
    VK(I)=FLOAT(IFIX(1+0.01))
    RW=VK(I)*1.689*LENGTH/NU
    CF(I)=0.075/((LOG10(RW)-2.))**2)
    CR=.07477*CF(I)
    CTBH(I)=CF(I)+DELCF+CR
    EHP(I)=.00872*((WSAREA*CTBH(I))+(AB*CDB+AACDA))*(VK(I)**3)
    SHP(I)=EHP(I)/PC
    WRITE(6,100) VK(I),CF(I),CTBH(I),EHP(I),SHP(I)
  
```

```

100      FORMAT(1H ,F14.3,F14.6,F14.3,F14.3)
90      CONTINUE
C
C
C COMPUTE WATERPLANE AREA VS. DRAFT, UNDERWATER VOLUME VS. DRAFT, AND DISPLACE-
C MENT VS. DRAFT
C
C
95      WRITE(6,95)
      FORMAT(1H1,6X,'DRAFT',8X,'AWP',9X,'VOLUME',5X,'DISPLACEMENT',5X,
1'KB',9X,'ICH',8X,'RM',/)
      DO 110 I=1,32
          DRAFT(I)=FLOAT(1F1X(I+0.01))
          SUM=0.
          SUM1=0.
          SUM2=0.
          SUM3=0.
          SUM4=0.
          DO 120 J=1,13
              X=OFFSET(J)**2-(DRAFT(I)-OFFSET(24))**2
              Y=OFFSET(24)-OFFSET(J)
              IF (X .LE. 0. .AND. DRAFT(I) .GT. Y) GO TO 130
              IF (DRAFT(I) .LE. Y) GO TO 135
              WL(J)=SORT(X)
              IF (DRAFT(I) .LT. OFFSET(24)) GO TO 125
              THETA(J)=2.*3.1416-(2.*ASIN(WL(J)/OFFSET(J)))
              GO TO 126
          THETA(J)=2.*ASIN(WL(J)/OFFSET(J))
          CAREA(J)=((2.*OFFSET(J))**2)*(1.ETA(J)-SIN(THETA(J)))/8.
          ARM(J)=OFFSET(24)-((1.333*OFFSET(J))*(SIN(THETA(J)/2.))**3))/
1(THETA(J)-SIN(THETA(J)))
          GO TO 140
          WL(J)=0.
          THETA(J)=0.
          CAREA(J)=3.1416*OFFSET(J)**2
          ARM(J)=OFFSET(24)
          GO TO 140
125
126
130

```



```

135      WL(J)=0.
        THETA(J)=0.
        CAREA(J)=0.
        ARM(J)=0.
        SUM=SUM+WL(J)*SIMPMT(J)
        AREASH(J)=CAREA(J)*SIMPMT(J)
        MOMENT(J)=AREASH(J)*ARM(J)
        FM(J)=AREASH(J)*STA(J)
        INERT(J)=SIMPMT(J)*WL(J)**3
        SUM1=SUM1+AREASH(J)
        SUM2=SUM2+MOMENT(J)
        SUM3=SUM3+FM(J)
        SUM4=SUM4+INERT(J)
        CUNTINUE
        FAMP=2.*SFB*SUM/3.
        FVUL1=SUM1*SFB/3.
        FDISP1=FVUL1/35.
        FKB=SFB*SUM2/3.
        FLCB=0.33333*SFB*SUM3/FVUL1
        FINERT=2.*SUM4*SFB/9.
        SUM=0.
        SUM1=0.
        SUM2=0.
        SUM3=0.
        SUM4=0.
        DO 150 J=14,24
            X=OFFSET(J)**2-(DRAFT(I)*OFFSET(24))**2
            Y=OFFSET(24)-OFFSET(J)
            IF (X.LE. 0.)AND. DRAFT(I).GT. Y) GO TO 160
            IF (DRAFT(I).LE. Y) GO TO 165
            WL(J)=SQRT(X)
            IF (DRAFT(I).LT. OFFSET(24)) GO TO 155
            THETA(J)=2.*3.1416-(2.*ASIN(WL(J)/OFFSET(J)))
            GO TO 156
            THETA(J)=2.*ASIN(WL(J)/OFFSET(J))
            CAREA(J)=((2.*OFFSET(J))**2)*(THETA(J)-SIN(THETA(J)))/8
            ARM(J)=OFFSET(24)-(1.3333*OFFSET(J)*(SIN(THETA(J)/2.))

```

```

160      1**3)))/(THEIA(J)-SIN(THETA(J)))
      GU TO 170
      WL(J)=0.
      THETA(J)=0.
      CAREA(J)=3.1416*OFFSET(J)**2
      AKM(J)=OFFSET(24)
      GU TO 170
      WL(J)=0.
      THETA(J)=0.
      CAREA(J)=0.
      AKM(J)=0.
      SUM=SUM+WL(J)*SIMPMT(J)
      AREASM(J)=CAREA(J)*SIMPMT(J)
      MUMENT(J)=AREASM(J)*AKM(J)
      FM(J)=AREASM(J)*STA(J)
      INERT(J)=SIMPMT(J)*WL(J)**3
      SUM1=SUM1+AREASM(J)
      SUM2=SUM2+MUMENT(J)
      SUM3=SUM3+FM(J)
      SUM4=SUM4+INERT(J)
      CONTINUE
150      AAWP=2.*SAB*SUM/3.
      AVOL1=SUM1*SAB/3.
      ADISP1=AVOL1/35.
      AKB=SAB*SUM2/3.
      ALCB=(0.33333*SAB*SAB*SUM3/AVOL1)+LPMB+(10.*SFB)
      AINER1=2.*SUM4*SAB/9.
      PAWP=2.*WL(24)*LPMB
      PVOL1=CAREA(24)*LPMB
      POISP1=PVOL1/35.
      PKB=AREASM(24)*ARM(24)*LPMB
      PLCB=10.*SFB+LPMB/2.
      PINER1=LPMB*((2.*WL(24))**3)/12.
      AWP(I)=FAWP+PAWP+AAWP
      VOL(I)=AVOL1+PVOL1
      DISP(I)=FUIISP1+ADISP1+POISP1
      KB(I)=(FKB+PKB+AKB)/VOL(I)

```

```

LCB(I)=(FVOLI*FLCB+PVOLI*PLCB+AVOLI*ALCB)/VOL(I)
BM(I)=(FIMPRT+AINERT+PINERT)/VOL(I)
WRITE(6,180) DRAFT(I),AWP(I),VOL(I),DISP(I),KB(I),LCB(I),BM(I)
FORMAT(1H ,5X,F6.2,5X,F8.2,5X,F9.2,5X,F8.2,5X,F6.2,5X,F7.2,
16X,F5.2)
IF (DRAFT(1) .EQ. 31.) GO TO 182
GO TO 110
WRITE(6,200) (WL(K),THETA(K),CAREA(K),AREASM(K),ARM(K),
1MOMENT(K),K=1,24)
FORMAT(1H ,6F12.2)
CONTINUE

```

180

C

C

C 182

C

C 200

110

C

C

C

C

C

C PLOT THE CURVES OF FORM ON A VERSATEC 1200 PLOTTER

```

CALL VERSAPLOT(0,0,0,
11.,1.,-3,
21.0,
31.8,7.,2,22HDISPLACEMENT VS. DRAFT,0.,22,
4DRAFT,7.,32,1,
5DISP,9.,32,1,
6DRAFT,DISP,32,1,0,0,
70.,0.,12HDRAFT (FEET),-12,7.,0.,DRAFT(33),DRAFT(34),
80.,0.,19HDISPLACEMENT (TONS),+19,9.,90.,DISP(33),DISP(34),
90.,0.,35,0.2,45,0.2,-30584)

```

C

```

CALL VERSAPLOT(0,0,0,
11.,1.,-3,
21.0,
33.,3.,2,16HVOLUME VS. DRAFT,0.,16,
4DRAFT,7.,32,1,
5VOL,9.,32,1,
6DRAFT,VOL,32,1,0,0,
70.,0.,12HDRAFT (FEET),-12,7.,0.,DRAFT(33),DRAFT(34),
80.,0.,19HVOLUME (CUBIC FEET),+19,9.,90.,VOL(33),VOL(34),
90.,0.,35,0.2,45,0.2,-30584)

```

C

```

CALL VERSAPLOT(0,0,0,
11.,1.,-3,
21.0,
31.5,7.,.2,25HWATERPLANE AREA VS. DRAFT,0.,25,
4DRAFT,7.,32,1,
5AWP,9.,32,1,
6DRAFT,AWP,32,1,0,0,
70.,0.,12HDRAFT (FEET),-12,7.,0.,DRAFT(33),DRAFT(34),
80.,0.,25HWATERPLANE AREA (SQ. FT.),+25,9.,90.,AWP(33),AWP(34),
90.,0.,35,0.2,45,0.2,-30584)

```

C C

```

CALL VERSAPLOT(0,0,0,
11.,1.,-3,
21.0,
32.5,7.,.2,12HKB VS. DRAFT,0.,12,
4DRAFT,7.,32,1,
5KB,9.,32,1,
6DRAFT,KB,32,1,0,0,
70.,0.,12HDRAFT (FEET),-12,7.,0.,DRAFT(33),DRAFT(34),
80.,0.,9HKB (FEET),+9,9.,90.,KB(33),KB(34),
90.,0.,35,0.2,45,0.2,-30584)

```

C C

```

CALL VERSAPLOT(0,0,0,
11.,1.,-3,
21.0,
33.,4.,.2,13HLCH VS. DRAFT,0.,13,
4DRAFT,7.,32,1,
5LCH,9.,32,1,
6DRAFT,LCH,32,1,0,0,
70.,0.,12HDRAFT (FEET),-12,7.,0.,DRAFT(33),DRAFT(34),
80.,0.,10HLCH (FEET),+10,9.,90.,LCH(33),LCH(34),
90.,0.,35,0.2,45,0.2,-30584)

```

C C

```

CALL VERSAPLOT(0,0,0,
11.,1.,-3,
21.0,
32.5,7.,.2,12HBM VS. DRAFT,0.,12,
4DRAFT,7.,32,1,
5BM,9.,32,1,
6DRAFT,BM,32,1,0,0,
70.,0.,12HDRAFT (FEET),-12,7.,0.,DRAFT(33),DRAFT(34),
80.,0.,9HBM (FEET),+9,9.,90.,BM(33),BM(34),
90.,0.,35,0.2,45,0.2,-30584)

```

```

C
C
C PLOT THE SPEED POWER CURVE
CALL VERSAPLOT(0,0,0,
11.,1.,-3,
21.0,
33.5,7.0,.2,13HEHP VS. SPEED,0.,13,
4VK,7.,32,1,
5EHP,9.,32,1,
6VK,EHP,32,1,0,0,
70.,0.,13HSPEED (KNOTS),-13,7.,0.,VK(33),VK(34),
80.,0.,16HEHP (HORSEPOWER),+16,9.,90.,EHP(33),EHP(34),
90.,0.,35,0.2,45,0.2,-30584)

```

```

C
C
CALL VERSAPLOT(0,0,0,
11.,1.,-3,
21.0,
33.5,7.0,.2,13HSHP VS. SPEED,0.,13,
4VK,7.,32,1,
5SHP,9.,32,1,
6VK,SHP,32,1,0,0,
70.,0.,13HSPEED (KNOTS),-13,7.,0.,VK(33),VK(34),
80.,0.,16HSHP (HORSEPOWER),+16,9.,90.,SHP(33),SHP(34),
90.,0.,35,0.2,45,0.2,-30584)

```

```

C
C TERMINATE PLOTTING

```

CALL PLOT(0.,0.,+999)
STOP
END

C

```

SFOM/LIS INDUC
SFOR VERSA
SFUR MATRIX
SFOR SLOTS
SFOR MAGNET
SFOR CIRCT
SFUR WDGFCF
SFOR CMBNIN
SFOR FRIC
SFOR RESIST
SFOR DEIGEN
$LINK INDUC,SLOTS,CIRCT,MAGNET,WDGFCF,CMBNIN,FRIC,RESIST,DEIGEN,-
VERSA,MATRIX,[DEF.EISPAC]EISPAC/LIB,SYS$LIBRARY:PHASE1/LIH,-
SYS$LIBRARY:STAKLET/INCLUDE=LIBSESTEMU
SPURGE INDUC.FOR
SPURGE INDUC.URJ
SPURGE INDUC.DAT
SPURGE MATRIX.FOR
SPURGE MATRIX.URJ
SPURGE VERSA.FOR
SPURGE VERSA.URJ
SPURGE *.LIS
SPURGE SLOTS.FOR
SPURGE SLOTS.URJ
SPURGE MAGNET.FOR
SPURGE MAGNET.URJ
SPURGE CIRCT.FOR
SPURGE CIRCT.URJ
SPURGE WDGFCF.FOR
SPURGE WDGFCF.URJ
SPURGE CMBNIN.FOR
SPURGE CMBNIN.URJ
SPURGE RESIST.FOR
SPURGE RESIST.URJ
SPURGE FRIC.FOR
SPURGE FRIC.URJ
SPURGE DEIGEN.FOR

```

SPURGE DEIGEN.OBJ
 SDEL *.PLV;*
 SASSIGN/USER INDUC.DAT FOR005
 SASSIGN/USER INDUC.UUF FOR006
 SASSIGN/USER LOSSES.UUT FOR007
 SASSIGN/USER SLIPDAT.UU1 FOR013
 SASSIGN/USER EIGEN.UU1 FOR014
 SASSIGN/USER RESIST.UUT FOR015
 SASSIGN/USER MATRIX.UUT FOR017
 SASSIGN/USER TEMP.UUT FOR019
 SASSIGN/USER SLOPES.UUT FOR020
 SKUN INDUC
 SDEL INDUC.EXE;*
 SDEL INDUC.OBJ;*
 SDEL VERSA.OBJ;*
 SDEL MATRIX.OBJ;*
 SDEL SLOTS.OBJ;*
 SDEL MAGNET.OBJ;*
 SDEL CIRCI.OBJ;*
 SDEL WDGFACT.OBJ;*
 SDEL CMNTN.OBJ;*
 SDEL FRIC.OBJ;*
 SDEL RESIST.OBJ;*
 SDEL DEIGEN.OBJ;*
 SPURGE INDUC.UUT
 SPURGE RESIST.UUT
 SPURGE EIGEN.UUT
 SPURGE LOSSES.OUT
 SPURGE SLIPDAT.UUT
 SPURGE MATRIX.OUT
 SPURGE TEMP.OUT
 SPURGE FOR018.DAT
 SPURGE SLOPES.OUT


```

C *****
C MAIN PROGRAM INJUC.FOR RUN ON DIGITAL VAX 11/780 HANDLES ALL INPUT
C AND OUTPUT FUNCTIONS (WITH THE EXCEPTION OF SOME ERROR MESSAGES)
C AND MOST OF THE CALCULATIONS. FIGURE 2 OF THE USERS' MANUAL SHOWS A
C SIMPLIFIED FLOWCHART OF THE MAIN PROGRAM AND ITS SUBROUTINE USAGE.
C *****
C
C      IMPLICIT REAL*16 (A-H,O-Z)
C
C      REAL*16 I1,IJAR,JBAR,JRING,LARM,I,I,ITS,LTR,LSYKE,LYNKE,LTOTAL,
C      IIMAG,IMAG2,NSYNCH,KPS,KDS,N,LB,NB,KRING,L,LS,KS,KSS,LREF,
C      2KLY,KLX,LEFS,LPRUP,KIN,KEND,KE,KEI,KI
C
C      REAL*4 TORQUE(103),SLIP(103),T1(102),ZZ(102),T4(102),T5(102),
C      IT8(102)
C
C      CHARACTER*70 SNAME,RNAME,TITLE
C      CHARACTER*1 BLANK,PHASE
C
C      INTEGER*4 IDUMMMYABCDEFGHI
C      INTEGER SSTYPE,RSTYPE,AWG,RWMAT,SWMAT
C
C      LOGICAL LAST
C
C      REAL*8 AMAT(8,8),VVMAT(8,8),WWR(8),WWI(8)
C      REAL*16 KC(3)
C      DIMENSION AI(60),AMAT(8,8),BMAT(8,5),
C      IWAREA(40),RSTVY(5),TNPCF(5),DNSTY(5),UMAT(5),SMAT(8),PP(8),
C      2CLOSS(5,10),RSEF1(38),RESET2(7),X(8),VMAT(8,8),WI(8),WR(8),
C      3C(H),AINV(8,8),ADUM(8,8),DMAT(8,8),BINV(8,8),ALPHA(8),DALPHA(8),
C      4DELGVEC(8,8),DELGINV(8,8),EXPON(8,8),SUBVEC(8),HOMUG(8),
C      5GAMMA(8),ALPHAS(H),PPP(8)
C
C      COMMON/PHAS/PHASE
C      COMMON/CTR/R0,R1,R2,X0,X1,X2,FW1,NSYNCH,V1,S,I1,RPM,PF,T,HP,EFF,
C      1PIN,W1,W2,W0,FW,IMAG,V2,POUT
C      COMMON/IMAG/RST,HSY,HRT,ARY,ATST,ATSY,ATHT,ATRY,ASYKE,ASTUTH,ARY

```

```

1 UKE,ARTUM,LSYUKE,LRUYKE,DSS,DSR,FIOTAL,FPULE,KSAT,ATAG,ATTOT
COMMON/INITL/ASIRWD,CSRATU,DER1,DER2,D1K,D1S,D2K,D2S,D3K,D3S
1 D4R,D4S,D5S,JOKK,LH,LS,PFLUID,RTWIDH,SB,SCAREA,SFR,SFS,SKEW,
2 SSAREA,STWIDH,TRATED,VSCFLD,WSR1,WSR2,WSK3,WSR4,WSR5,WSS,WSS1,
3 WSS2,WSS3,WSS4
COMMON/GEUM/WX,WY,U,OS,WSS6,TEN,L,DIS,G,D,DS,LEFS,TEFS,LPROP,
1 FTR,DOR,D6K,NA,TFR,TENGAP,BK
COMMON/RESIST/KE1,RE2,R412,R430,R810,R411,R812,RE3,KEU1,REQ2,REQ3,
1 KEQ4,R611,K86
COMMON/DUMMY/ANG

```

C

```

EQUIVALENCE (RESET1(1),ASTKND),(RESET2(1),KU)

```

C

```

DATA RSTVY/1.08,2.95,0.678,0.,0.,TMPCT/.00415,.002,.00393,0.
1 0./,DWSLY/0.0975,0.308,0.321,0.,0./
DATA (WAREA(1),I=1,40)/0.06573,.05213,.04134,.03278,.02600,
1 0.2062,.01635,.01297,.01028,0.008155,0.006467,0.005129,
2 0.004067,0.003225,0.002558,0.002028,0.001609,0.001276,0.001012,
3 0.0008023,0.0006363,0.0005046,0.0004002,0.0003173,0.0002517,
4 0.0001996,0.0001583,0.0001255,9.9530-5,7.8940-5,6.2600-5,
5 4.9640-5,3.9370-5,3.1220-5,2.4760-5,1.9640-5,1.5570-5,1.235
6 0-5,9.7930-6,7.7660-6/
DATA KC/2.881,1.563,5.426/,KLY/.077/,KLX/.710/,KS/.610/,KE/.003/,
1 KEI/.002/,KIN/.066/,KIN/.003/

```

C

```

NAMELIST/RAJING/NSYNCH,F,X0,X1,X2,RO,K1,R2,FW1,V1,TRATED/STATOR/
1 DIS,L,LTS,SFS,LEFS,TEFS,SSLUTS/DOS,WSS6,OS,DSS,WSS,SSTYPE,D2S,D1S,D4S,
2 D3S,WSS1,WSS2,PHIS,DSS,STWIDH,SCAREA,CSRATO/STWIDG/CSS,PC,B,WX,WY,U,
3 SWMAT,SPITCH,LS,ASTRND,TSW,S,AWG,STRNDS/MOTOR/SKEW,LTR,SFR,D,DOR,LPROP
4 ,TER,FTR/SSLUTS/SH,DOR,WSK6,KSTYPE,D4R,D3R,WSR1,WSK,D2R,D1R,WSR2,PHIR,
5 DSK,RTWIDH/KIRWDG/LR,NA,DER1,DER2,TER,RWNAT,TRW,BR/AIRGAP/G,
6 PFLUID,VSCFLD,PFLUID/ENCAP/TEN,TENGAP

```

C

```

NAMELIST/FELOSS/WCUKE,FCORE,SLOPE,BK,LT,LT,LT/WNDAGE/WL,DIAREF,
1 LREF,RPMPEI,VSCREF,CO,C1,C2,C3,C4,GAPREF,TRF,PREF

```

C

C THE FOLLOWING ARITHMETIC FUNCTION GIVES THE VISCOSITY OF THE FLUID IN

C THE MOTOR CAVITY AS A FUNCTION OF TEMPERATURE -- VSCSTY IS IN LBM/FT-SEC
 C AND T IN DEGREES CENTIGRADE. IF THE COEFFICIENTS ARE NOT PART OF THE
 C INPUT THEN THIS FUNCTION OUTPUT WILL ALWAYS BE ZERO AND A CASE WHERE
 C EITHER FW1 IS AN INPUT OR FW1 EQUALS ZERO MUST BE ASSUMED. FOR A NEW
 C MOTOR DESIGN, PAST WINDAGE DATA WILL NOT BE KNOWN AND THUS COMPUTATION
 C OF VISCOSITY WILL NOT BE NECESSARY (THOUGH IT CAN STILL BE DONE IF ONE
 C INPUTS THE COEFFICIENTS).

C VSCSTY(T)=C0+T*(C1+T*(C2+T*(C3+C4*T)))

C 10 READ(5,20) SNAME
 C 20 FORMAT(A)

C C INITIALIZATION AT THE START OF NEW DATA SET

LAST=.FALSE.
 TREF=25.00
 VSCREF=0.
 PREF=0.
 RPMREF=0.
 LREF=0.
 CIAREF=0.
 GAPREF=0.
 C0=0.
 C1=0.
 C2=0.
 C3=0.
 C4=0.
 WL=0.

C C READ AND WRITE STATOR MATERIAL MAGNETIZATION DATA OBTAINED FROM B-H CURVE

C READ(5,60) (A1(I),I=1,29)

```

60      FORMAT(8F9.2)
      WRITE(6,70) SNAME
70      FORMAT(1H1,/,4X,18HSTATOR MATERIAL---,2X,A)
      WRITE(6,80) (AI(1),I=2,29)
80      FORMAT(1H1,12X,1H3,20X,1HH//5X,17H(KILOLINE.S/SQ-IN),7X,11H(A-TURN
      1/IW)/(F16.2,F21.2))
C
C
C READ AND WRITE COPE LOSS DATA FOR STATOR MATERIAL
C
C
90      WRITE(6,90)
      FORMAT(' ',6X,14HCORE-LOSS DATA/10X,9HCURE-LOSS,5X,7HLAM THK,5X,
      14HREQ,5X,10HFLUX DNSTY,5X,5HSLOPE)
      DO 100 I=1,11
      SLOPE=0.
      READ (UNIT=5,NML=FELOSS)
      IF (LAST) GO TO 120
      CLOSS(1,I)=WCORE
      CLOSS(2,I)=FCURE
      IF (SLOPE.LT. 1.00-15) SLOPE=(1.0+164.*LT)/(1.0+82.*LT)
      CLOSS(3,I)=SLOPE
      CLOSS(4,I)=RK
      CLOSS(5,I)=LT
      WRITE(6,110) WCORE,LT,FCORE,BK,SLOPE
100      CONTINUE
110      FORMAT(1H ,F15.1,F14.3,F11.1,F11.1,F11.1,F12.2)
120      NCARDS=I-1
C
C
C READ AND WRITE ROTOR MATERIAL MAGNETIZATION DATA OBTAINED FROM B-H CURVE
C
C
130      READ(5,20) RNAME
      READ(5,60) (AI(1),I=31,59)
      WRITE(6,130) RNAME
      FORMAT(1H0,4X,17HROTOR MATERIAL---,1X,A)

```

```
WRITE(6,80) (AI(I),I=32,59)
```

```
C
C
C
```

```
C READ WINDAGE DATA FROM NAMELIST
```

1.3

```

READ(UNIT=5,NML=WINDAGE)
14 VSCREF,LI,1.0(1-15) VSCREF=VSCSTY(1:15)
READ(5,20) TITLE
140 WRITE(6,150) TITLE
150 FORMAT(1H1,//////,2X,A,/)

```

```
C
C
C
```

```
C INITIALIZATION AT THE BEGINNING OF A NEW MOTOR DESIGN DATAFILE
```

```

DO 160 I=1,37
  RESET1(I)=0.
160 CONTINUE
DO 170 I=1,7
  RESET2(I)=0.
170 CONTINUE

```

```

DSR=0.
USS=0.
PHIR=0.
PHIS=0.
RWMAT=3
SWMAT=3
STPND=1.0
TFLUID=TRPF
TRW=25.
TSW=25.

```

```
C
C
C
C
```

```
C READ DATA FROM 'MOTOR DESIGN' SECTION OF DATAFILE
```

```

READ(UNIT=5,NML=RATING)
IF (X0*X1*X2*RO*R1*R2 .GT. 1.00-15) GO TO 720
READ(UNIT=5,NML=STATUR)
READ(UNIT=5,NML=SSLOTS)
READ(UNIT=5,NML=STRWDG)
READ(UNIT=5,NML=PLUR)
READ(UNIT=5,NML=RSLOTS)
READ(UNIT=5,NML=RTKWDG)
READ(UNIT=5,NML=AIRGAP)
READ(UNIT=5,NML=ENCAP)

C
C
C RETRIEVE CORE LOSS DATA FROM ARRAY CLOSS FOR DESIGN LAMINATION THICKNESS
C
C
DIFF=10.
DO 190 I=1,NCARDS
  DIFF1=OARS(LTS-CLOSS(5,1))
  IF (DIFF1 .GT. DIFF) GO TO 190
  IA=1
  DIFF=DIFF1
190 CONTINUE
IF (DIFF .GT. 0.0005) WRITE(6,200) CLOSS(5,IA)
200 FORMAT(1H,68HCURR-LOSS DATA IS NOT GIVEN AT SPECIFIED STATOR LAM
      1INATION THICKNESS/1H ,3X,12HUSE DATA FOR,F6.3,12H LAMINATIONS)
C
C
C CALCULATE CORE LOSS AT DESIGN FREQUENCY
C
C
WFE=CLOSS(1,IA)*((F/CLOSS(2,IA))**CLOSS(3,IA))
BK=CLOSS(4,IA)
C
C
C CALCULATE VARIOUS DIMENSIONS FROM INPUT DATA
C
C

```

```

DS=D-2.*G
TIR=(3.1416*D)/NB
TIS=(3.1416*DS)/OS
IF (SKEW .LT. 1.00-15) SKEW=QMAX1(TIR,TIS)
IF (LH .LT. 1.00-15) LB=QSORT(L*L+SKEW*SKEW)+2.*(HR+TER)
IF (ASTRID .LT. 1.00-15) ASIRND=WAREA(AWG)
SS=ASTRID*ASIRND
IF (SFR .LT. 1.00-15) SFR=LIR/(LIR+0.0005)
IF (SFS .LT. 1.00-15) SFS=LTS/(LTS+0.0005)
IF (USS .GT. 1.00-15 .OR. DIS .GT. 1.00-15) GO TO 230
IF (SCAREA .GT. 1.00-15) GO TO 240
IF (CSRATO .GT. 1.00-15) GO TO 220
WRITE(6,210)
FORMAT(1HK,59HINSUFFICIENT STATOR SLOT DATA, SPACE FACTOR OF 0.70
1 ASSUMED)
CSRATO=0.70
SCAREA=(SS*SS/CSRATO
GO TO 250
SCAREA=0.
CSRATO=0.
IF (SPITCH .LE. 0.3333) KSS=0.75*SPITCH
IF (SPITCH .GT. 0.3333 .AND. SPITCH .LT. 0.6667) KSS=1.5*SPITCH-
10.25
IF (SPITCH .GE. 0.6667) KSS=0.75*SPITCH+0.25

C
C
C COMPUTE SLOT AREAS AND SLOT PERMEANCE RATIOS FOR STATOR AND ROTOR
C
C
CALL SLOTS (1.000,WSS,WSS1,WSS2,WSS3,WSS4,WSS5,WSS6,DS,D1S,D2S,
1D3S,D4S,D5S,STWDTH,SCAREA,SSAREA,OS,D6S,WSS6,DS,KSS,AXS,STWMAG,
2PHIS,STYPE)
C
CALL SLOTS (-1.000,WSR,WSH1,WSH2,WSH3,WSH4,WSH5,WSR4,D1H,D2R
1,D3R,D4R,0.000,RTWDTH,SH,HSAREA,NB,DBH,WSH6,D,1.000,AXR,RTWMAG,
2PHIR,STYPE)
C

```

! 6

! 7

```

C
C COMPUTE STATOR AND ROTOR IRON WEIGHTS
C
C
      WSTUTH=(3.1416*(DS-DSS)*DSS-(SSAREA*DS))*L*SFS*0.27648
      WSYOKE=(0.7854*((DS-2*DSS)**2-DIS*DIS))*L*SFS*0.27648
      WSTAT=WSTUTH+WSYOKE
      WKRI=(0.7854*(DOR*DOR-D*D)-(NB*RSAREA)*L*SFR*0.27648
! 8

C
C COMPUTE FEMMING DIMENSIONS
C
C
      IF (DER1 .LT. 1.00-15) DER1=D+2.*(1.1*DSR)
      IF (DER2 .LT. 1.00-15) DER2=D+2.*D4K
      SER=0.5*(DER1-DER2)*TER
      IF (CSKATU .LT. 1.00-15) CSRATO=CSS*SS/SSAREA
      P=QFLUAT(FIX(SNGLO((120.*F)/NSYNCH)+0.1))
      N=(QS*CSS)/(PC*J.)
      DHS=(DS-DIS)*0.5-DSS
      D*DS=(DOR-D)*0.5-DSR
! 9

C
C CHECK IF STATOR-ROTOR SLOT COMBINATION IS ACCEPTABLE
C
C
      CALL CMHMIN(QS,NB,P)
! 10

C
C CALCULATE DISTRIBUTION AND PITCH FACTORS
C
C
      CALL WDGFACT(60.,P,QS,ADS,PC,KPS,SPITCH)
! 11

C
C CALCULATE CARTER COEFFICIENTS AND EFFECTIVE AIRGAP
C
C

```



```

C
IF (KSTYPE .GT. 2) GO TO 260
CCR=(TIR*(5.*G+WSR))/(TIR*(5.*G+WSR)-WSR*WSR)
GO TO 270
260 CCR=(TIR*(4.4*G+0.75*WSR1))/(TIR*(4.4*G+0.75*WSR1)-WSR1*WSR1)
270 IF (SSTYPE .GT. 2) GO TO 280
CCS=(TIS*(5.*G+WSR))/(TIS*(5.*G+WSR)-WSR*WSR)
GO TO 290
280 CCS=(TIS*(4.4*G+0.75*WSR1))/(TIS*(4.4*G+0.75*WSR1)-WSR1*WSR1)
290 GE=G*CCR*CCS
! 12
C
C STATOR RESISTANCE CALCULATION (R1)
C
C
IF (SSTYPE .EQ. 2 .OR. SSTYPE .EQ. 4 .OR. SSTYPE .EQ. 6) SALPHA=
1(0.5*(WSS4+WSS5)+S-2.*WSS6)/(3.1416*(D+DSS)/OS)
IF (SSTYPE .EQ. 1 .OR. SSTYPE .EQ. 3) SALPHA=(WSS+S-2.*WSS6)/TIS
IF (SSTYPE .EQ. 5) SALPHA=(WSS3+S-2.*WSS6)/(3.1416*(D+2.*D4S+
1WSS3)/OS)
CALPHA=USORT(1.-SALPHA**2)
AY=(3.1416*(DS-DSS)*SPITCH)/(P*CALPHA)
IF (IN .LT. 1.00-15) LS=AY+2.*D+DSS+L
IF (R1 .GT. 1.00-15) GO TO 300
R1=(LS*PI*RS*VY(SWMT)*1.(U-6))/(PC*SS)
R1=R1*(1.+T*PCF(SWMT))*(TSW-20.)
! 13
! 14
C
C CALCULATION OF AXIAL EXTENSION OF END TURN AND OVERALL ARMATURE LENGTH
C
300 ENDTURN=AY+0.5*SALPHA+B+DSS
! 15
LTOTAL=L+2.*ENDTURN
C
C CALCULATION OF ARMATURE WEIGHT AND TOTAL WIRE LENGTH
C

```

```
C
C      LARM=(LS*CSS+US*STRNDS)/12.
C      WARM=DNSTY(SWMT)*LARM*ASTRND*12.
C
C      CALCULATION OF ROTOR RESISTANCE
C
C      KRSTVY=1.00-6*KRSTVTY(RWMAT)*(1.0+TMPCT(RWMAT)*(TRW-20.))
C      IF (RZ.GT. 1.00-15) GO TO 310
C      KATIO=DER2/DEK1
C      KRING=0.50*P*(1.-KATIO)*(1.+RATIO**P)/(1.-RATIO**P)
C      AY=((W*KPS*KDS)**2)**3.*KRSTVY
C      R2PAK=AY*((LB-TER)/(S3*NB))
C      R2RING=AY*((O.64*DEK1*KPING)/(P*P*SER))
C      RZ=R2BAR+R2RING
C
C      ! 17
C
C      CALCULATION OF ROTOR WINDING WEIGHT AND TOTAL ELECTROMAGNETIC MOTOR WEIGHT
C
C      310   WRWWDG=DNSTY(RWMAT)*(NB*SH*(LB-2.*TER)+SER*J.1416*(DER1+DER2))
C           WPICHI=WARM+WRWWDG+WROT+WSTAT
C
C      CALCULATION OF MAGNETIZING REACTANCE (AIR GAP ONLY)
C
C      XUG=7.660-7*F*(N/2.**KPS*KDS)**2*DSD*L/(P*P*GE.)
C
C      ! 18
C
C      CALCULATION OF PRIMARY SLOT LEAKAGE REACTANCE (XSS)
C
C      AY=6.0-7*F*H*F*L
C      XSS=AY*AXS/US
C
C      ! 19
```

```

C C CALCULATION OF SECONDARY SLOT LEAKAGE REACTANCE (XRS)
C C
C C XRS=AY*(KPS*KDS)**2*AXR/NB
C C
C C
C C
C C
C C CALCULATION OF ROTOR AND STATOR END-CONNECTION LEAKAGE REACTANCE
C C
C C
C C DC=(0.50*(DER1+DER2)-DS+2.*(D4S+DJS+D2S)+D1S)*0.50
C C AY=((W**P*(KPS*KDS)**2)/P)*2.40-7
C C F1=1.5708*(DS-DSS)*SPITCH*OSQRT(1.0-CALPHA*CALPHA)/(P*CALPHA)
C C XSE=AY*(H+0.5*(F1+DSS/2.))
C C XRE=(0.725*AY/P)*(2.*P*BR+(3.1416*DS*DC)/(1.7*IEK+0.5*(DER1-DER2)
C C 1+1.4*DC))
C C
C C
C C
C C XSK=0.5*(XOAG/12.)*(P*SKEW/D)**2
C C
C C
C C
C C CALCULATION OF STATOR AND ROTOR ZIGZAG LEAKAGE REACTANCE
C C
C C
C C XZ=0.833*XOAG*(KSS/(KPS*KDS)**2)
C C XKZ=XZ*(6./CCW-1.)/(5.*(NH/P)**2))
C C XSZ=XZ*((6./CCS-1.)/(5.*(US/P)**2))
C C
C C
C C CALCULATION OF PERIPHERAL AIR-GAP LEAKAGE REACTANCE
C C
C C
C C XP=0.525*XOAG*(P*G/US)**2
C C
C C

```

```

C
C CALCULATION OF TOTAL ARMATURE AND ROTOR LEAKAGE REACTANCES (X1 AND X2)
C
C
      IF (QABS(X1) .LT. 1.00-15) X1=XSS+XSE+XSK+XSZ+XP
      IF (X2 .LT. 1.00-15) X2=XKS+XKE+XSK+XKZ
C
C
C WRITE OUTPUT
C
C
      WRITE(6,319)
      FORMAT(1H0,5X,6H-----)
      WRITE(6,320) NSYNCH,F,P,V1
      FORMAT(1H+,5X,6HHRATING/10X,17HSYNCHRONOUS SPEED,F26.0,4H RPM/10X,
      19HFREQUENCY,F34.0,3H HZ/10X,5HPOLES,F38.0/10X,11HL-N VOLTAGE,
      2F33.1,5H VOLT)
      IF (THATPS .GT. 1.00-15) WRITE(6,330) PRATED
      FORMAT(1H,9X,12HPRATED TORQUE,F32.1,7H FT-LBS)
      WRITE(6,335)
      FORMAT(1H0,5X,6H-----)
      WRITE(6,340) DIS,DS,DBS,L,LTS,SFS,WSTAT
      FORMAT(1H+,5X,6HSTATOR/10X,15HINSIDE DIAMETER,F31.3/10X,16HOUTSIDE
      1 DIAMETER,F30.3/10X,16HDEPTH BELOW SLUT,F30.3/10X,6HLENGTH,F40.3
      2/10X,20HLAMINATION THICKNESS,F26.4/10X,15HSTACKING FACTOR,F31.4
      3/10X,16HSTATOR IRON WEIGHT,F28.3)
      WRITE(6,345)
      FORMAT(1H0,5X,12H-----)
      WRITE(6,350) SSTYPE,OS
      FORMAT(1H+,5X,12HSTATOR SLUTS/10X,9HSLUT TYPE,18,9X,12HNO. OF S
      1LUTS,F5.0)
      IF (SSTYPE .EQ. 1 .OR. SSTYPE .EQ. 3) WRITE(6,360) WSS,DSS
      IF ((SSTYPE/2)*2 .EQ. SSTYPE) WRITE(6,370) STWOTH,DSS
      IF (SSTYPE .EQ. 5) WRITE(6,380) WSS3,DSS
      16HSTAT(10X,10HSLUT WIDTH,F10.3,6X,10HSLUT DEPTH,F10.3)
      16HSTAT(10X,11HTOOTH WIDTH,F9.3,6X,10HSLUT DEPTH,F10.3)
      16HSTAT(10X,13HSLUT DIAMETER,F7.3,6X,10HSLUT DEPTH,F10.3)

```

```

390 WRITE(6,390) WSS1,D1S,WSS2,D2S,WSS3,D3S,WSS4,D4S,WSS5,D5S,WSS6,
106S,SCAPEA,SSAPPA,CSHAU
FORMAT(10A,4HWS1,F16.3,6X,3HD1S,F17.3/10X,4HWS2,F16.3,6X,3HD2S
1,F17.3/10X,4HWS3,F16.3,6X,3HD3S,F17.3/10X,4HWS4,F16.3,6X,
23HD4S,F17.3/10X,4HWS5,F16.3,6X,3HD5S,F17.3/10X,4HWS6,F16.3
3,6X,3HD6S,F17.3/10X,11HUSABLE AREA,F9.3,6X,10HTOTAL AREA,F10.3
4/10X,12HSPACE FACTOR,F8.3)
WRITE(6,395)
FORMAT(1H1,//////,6X,14H-----)
WRITE(6,400) SWMAI,CSS,PC,SPITCH,H,SS,ASTRND,LS,S,TSW,ENDTRN,LTOT
1AL,KPS,KUS,WARM,LARM,STRNDS
FORMAT(1H+,5X,14HSTATOR WINDING/10X,8H MATERIAL,135/10X,19HCUNDUC
1TURNS PER SLOT,F24.0/10X,17H PARALLEL CIRCUITS,F26.0/10X,5HPITCH
2,F41.3/10X,2H AXIAL EXTENSION BEYOND CORE,F19.3/10X,23H CONDUCT
3OR CROSS-SECTION,E27.3/10X,20H STRAND CROSS-SECTION,E30.3/10X
4,16H CONDUCTOR LENGTH,F30.3/10X,21H CLRNC BTWN END-TURNS,F25.3
5/10X,15H TEMPERATURE (C),F28.0/10X,21H AXIAL END-TURN LENGTH,F25.3
6/10X,23H OVERALL ARMATURE LENGTH,F23.3/10X,12HPITCH FACTOR,F34.3
7/10X,19H DISTRIBUTION FACTOR,F27.3/10X,25H ARMATURE CONDUCTOR WEIGHT,
8F21.3/10X,26HTOTAL ARMATURE WIRE LENGTH,F20.3,5H FEET/10X,17H
9STRANDS/CONDUCTOR,F26.0)
IF (AWG .GT. 0) WRITE(6,410) AWG
FORMAT(1H+,9X,11H STRAND SIZE,132)
WRITE(6,415)
FORMAT(1H1,//////,6X,5H-----)
WRITE(6,420) DNR,D,LTR,SFR,SKW,DBKS,WRUT
FORMAT(1H+,5X,5H ROTOR/10X,16H OUTSIDE DIAMETER,F30.3/10X,15H INSIDE
1 DIAMETER,F31.3/10X,20H LAMINATION THICKNESS,F26.4/10X,15H STACK
2ING FACTOR,F31.4/10X,9H SLOT SKW,F37.3/10X,16H DEPTH BELOW SLOT,
3F30.3/10X,17H ROTOR IRON WEIGHT,F29.3)
WRITE(6,425)
FORMAT(1H0,5X,11H-----)
WRITE(6,430) RSTYPE,NB
FORMAT(1H+,5X,11H ROTOR SLOTS/10X,9H SLOT TYPE,I8,9X,12H NO. OF SLO
1TS,F5.0)
IF (RSTYPE .EQ. 1 .OR. RSTYPE .EQ. 3) WRITE(6,440) WSR,DSR
IF ((RSTYPE/2)*2 .EQ. PSTYPE) WRITE(6,450) RTWIDTH,DSK

```

```

440 IF (RSTYPE .EQ. 5) WRITE(6,460) WSR3,USR
450 FURMAT(10X,10HSLUT WIDTH,F10.3,6X,10HSLUT DEPTH,F10.3)
460 FURMAT(10X,11HTUOTH WIDTH,F9.3,6X,10HSLUT DEPTH,F10.3)
    FURMAT(10X,13HSLUT DIAMETER,F7.3,6X,10HSLUT DEPTH,F10.3)
    WRITE(6,470) WSR1,D1R,WSR2,D2R,WSR3,D3R,WSR4,D4R,WSR5,D5R,WSR6
    1,SB,RSAREA
470 FURMAT(10X,4HWSK1,F16.3,6X,3HD1R,F17.3/10X,4HWSR2,F16.3,6X,3HD2R,
    1F17.3/10X,4HWSR3,F16.3,6X,3HD3R,F17.3/10X,4HWSR4,F16.3,6X,3HD4R,
    2F17.3/10X,4HWSR5,F16.3,6X,3HD6R,F17.3/10X,4HWSR6,F16.3/10X,11H
    3USABLE AREA,F9.3,6X,10HTOTAL AREA,F10.3)
    WRITE(6,475)
475 FURMAT(10X,5X,13H-----)
    WRITE(6,480) KMMAT,LB,SB,DER2,TRW,WRWWDG,R2BAK,R2RING
480 FURMAT(1H+,5X,13HROTOR WINDING/10X,8HMAKEMIAL,135/10X,10HBAR LENG
    1TH.F36.3/10X,17HFAK CROSS-SECTION,F29.3/10X,20HEND-RING OUTSIDE
    2 DIA,F26.3/10X,19HEND-RING INSIDE DIA,F27.3/10X,18HEND-RING
    3THICKNESS,F28.3/10X,24HSTACK-TO-END-RING CLRNCE,F22.3/10X,23HWIN
    4DING TEMPERATURE (C),F20.0/10X,6HWEIGHT,F40.3/10X,27HCOMPONENT
    5 OF R2 DUE TO BARS,F20.4/10X,32HCOMPONENT OF R2 DUE TO END-RING
    6S,F15.4)
    WRITE(6,485)
485 FURMAT(1H1,//////////,6X,6H-----)
    WRITE(6,490) G,GE,XOAG
490 FURMAT(1H+,5X,6HATRGAP/10X,13HACTUAL AIRGAP,F34.4/10X,16HEFFECTIV
    1E AIRGAP,F31.4/10X,36HMAGNETIZING REACTIANCE (AIR GAP ONLY),
    2F10.3)
    WRITE(6,495)
495 FURMAT(1H0,5X,24H-----)
    WRITE(6,500) ASS,XRS,XSE,XRE,XSK,XSK,ASZ,XKZ,XP
500 FURMAT(1H+,5X,24HLEAKAGE REACTANCES (UHM)/33X,6HSTATOR,11X,5HRO
    1TOR/10X,4HSLUT,F26.3,F16.3/10X,14HEND-CONNECTION,F16.3,F16.3
    2/10X,4HSEW,F26.3,F16.3/10X,7HZIG-2AG,F23.3,F16.3/10X,10HPERI
    3PHERAL,F20.3)
    WRITE(6,505)
505 FURMAT(1H0,5X,6H-----)
    WRITE(6,510) WEIGHT
510 FURMAT(1H+,5X,6HWEIGHT/10X,23HTOTAL (ELECTROMAGNETIC),F23.3/1H1)

```

C C CROSS SECTIONAL AREAS AND LENGTHS OF FLUX PATHS NEEDED FOR MAGNETIC
C C CALCULATIONS

ASYUKE=D65*L*SFS
LSYUKE=J.1416*(DS+DLS-2.*DS)/(4.0*P)
ARYUKE=D8RS*L*SFK
IKYUKE=J.1416*(DOR+D+2.*DSK)/(4.0*P)
ARTUTH=RTWMAG*L*SFK*NP
ASTUTH=STWMAG*L*SFS*OS

C C NO-LOAD MAGNETIC CALCULATIONS

XX=1.0
XY=1.0
IF (X0 .GT. 1.00-15) XX=0.0
IF (R0 .GT. 1.00-15) XY=0.0
XU=X0+(0.5*AOAG)*XX
WU=(WSYUKE+WSTUTH)*WFF*3.0
WU=(5.*V1+V1/WU)*XY+R0
S=0.

! 25

520 ICN12=0
ICN12=ICN12+1
IF (ICN12 .GE. 11) GO TO 550

! 26

530 ICN11=0
ICN11=ICN11+1
IF (ICN11 .GE. 11) GO TO 540
CALL CIRC1

! 27

PODD=RO
FTOTAL=V2*P+1.0E+05/(1.414*N*F*KPS*KDS)

! 28

FPDUE=FTOTAL*0.637/P

RG=FTOTAL/(J.1416*DS*L)

ALAG=RG*GE*313.

! 29

```

1 30
C CALL MAGNET
C WRITE(6,531) STWAG,WSYUKE,WSUTUH,WFE,BK,SFS
C WRITE(6,531) ASYUKE,LSYUKE,ARYUKE,IWYUKE,ARTUHF,ASTOTH
C 531
C FORMAT(1H,6F13.5)
C WRITE(6,531) ATAG,ATST,ATSY,ATRT,ATRY,ATTOT
C WRITE(6,532) BST,BSY,BRT,BRY
C 532
C FORMAT(1H,4F13.5)
C WU=(WSYUKE*(HSY/BK)**2+WSUTUH*(BST/HK)**2)*WFE*3.0
C R0=((3.*V2*V2/WU)-R0)*XY+R0
C WRITE(6,531) X0,W0,R0,FTOTAL,FPOLE,BG
C IF (QARS(K0-R001,0)/R0 .GE. 0.001) GO TO 530
C 540
C IMAG-2=2.22*P*ATOT/(3.*N*KPS*KDS)
C X0=X0+((V2/(0.5*(IMAG+IMAG2)))-X0)*XX
C 550
C IF (QABS((IMAG-IMAG2)/IMAG) .GT. 0.005) GO TO 520
C CURDEN=(QSORT(IPAG**2+(V2/R0)**2))/(PC*SS)
C IF (ICNT1 .GE. 11) WRITE(6,560)
C IF (ICNT2 .GE. 16) WRITE(6,570)
C IF (FSAT .EQ. 0) WRITE(6,580)
C 560
C FORMAT(1H,/,/,/,/ SHUNT RESISTANCE R0 FAILED TO CONVERGE'//)
C 570
C FORMAT(1H,/,/,/,/ MAGNETIZING CURRENT FAILED TO CONVERGE'//)
C 580
C FORMAT(1H,/,/,/,/ MACHINE SATURATED, TOOTH AMPERE-TURNS N(
C 1CALCULATED'//)
C
C WRITE RESULTS OF NO-LOAD MAGNETIC CALCULATIONS
C
C
C WRITE(6,590) SNAME,AI(1),BK,WFE
C 590
C FORMAT(1H,/,/,/,/,/SX,17HSTATOR MATERIAL --,1H,A/24X,7HB MAX =,F5.0
C 1/24X,12HCOKE LUSS AT,F6.1,10H KL/SQ-IN=,F5.1,5H W/LB)
C WRITE(6,600) RNAME,AI(31)
C 600
C FORMAT(1HK,5X,17HROTOR MATERIAL --,1H,A/24X,7HB MAX =,F5.0)
C
C
C WRITE NO-LOAD MAGNETIZATION CHARACTERISTICS

```



```

605      WRITE(6,605)
        FORMAT(1H0,5X,29H-----)
        WRITE(6,610) FTOTAL,FPOLE,BG,BSF,BSY,BRT,BRY,ATAG,AFST,ATSY,ATRI,
        1ATHY,ATUT,IMAG,V2,CURDEN,W0
        FORMAT(1H4+,5X,29HMAGNETIZATION CHARACTERISTICS/7X25H (WU-LOAD, RA
        1TED VOLTAGE))/9X,1EH TOTAL USEFUL FLUX,F26.2,10H KILOLINES/9X17H
        2 USEFUL FLUX/POLE,F29.2//9X15H FLUX DENSITIES/13X7H AIRGAP,
        3F35.2,9H KL/SU-1N/13X13H STATOR TOOTH,F29.2/13X12H STATOR YOKE,
        4F30.2/13X12H ROTOR TOOTH,F30.2/13X11H ROTOR YOKE,F31.2//9X22H A
        5MPERE-TURNS PER POLE/13X7H AIRGAP,F35.2//13X13H STATOR TOOTH,
        6F29.2/13X12H STATOR YOKE,F30.2/13X12H ROTOR TOOTH,F30.2/13X11H
        7 ROTOR YOKE,F31.2//13X6H TOTAL,F36.2//9X20H MAGNETIZING CURRENT
        8,F26.2,8H AMPERES/10X,14HAIRGAP VOLTAGE,F31.2/10X,20HN.L. CURRE
        9NT DENSITY,F25.2/10X,9HCORE LOSS,F34.0,5H WAIT)

```

C
C SCALE WINDAGE LOSS FROM REFERENCE CONDITIONS TO DESIGN CONDITIONS I 35
C
C

```

614      WRITE(6,614)
        FORMAT(1H1,////)
        WRITE(6,615)
        FORMAT(1H0,6X,7H-----)
        WRITE(6,620)
        FORMAT(1H+,6X,7HWINDAGE)
        IF (FW1 .GT. 1.00-15) GO TO 700
        IF (WL .LE. 1.00-15) GO TO 630
        IF (DIAREF*LRPF*RPMREF*GAPREF .GT. 1.00-15) GO TO 650
        WRITE (6,640)
        FORMAT(1H6,6X,39HINSUFFICIENT DATA TO SCALE WINDAGE LOSS//)
        GO TO 700
        FW1=WL*((DR/DIAREF)**3.25)*(L/LREF)*((NSYNCH/RPMREF)**2.5)*((GAP
        1REF/G)**0.25)
        IF (VSCREF .LT. 1.00-15) GO TO 670
        IF (VSCFLD .GT. 1.00-15) GO TO 660
        VSCFLD=VSCSY(FLDUT)
        IF (VSCFLD .LT. 1.00-15) GO TO 670

```

```

660 F 1=FW1*((VSCFLD/VSCREF)**0.50)
670 IF (PREF.LT. 1.00-15) GO TO 680
    IF (PFLUID.LT. 1.00-15) GO TO 680
    FW1=FW1*(PFLUID/PREF)
C
C
C WRITE WINDAGE DATA
C
C
680 WRITE(6,690) FW1,wL,DR,DIAREF,L,LREF,NSYNCH,RPMREF,G,GAPREF,TFLU
110,TREF,VSCFLD,VSCREF,PFLUID,PREF
690 FORMAT(1H,31X,6DESIGN,9X,9HREFERENCE/26X,2(6X,9HCONDITION)//
110X,15HWINDAGE LOSS, W,F13.0,F15.0/10X,8HDIAMETER,F23.3,F15.3/
210X,6HLENGTH,F25.3,F15.3/10X,3HRPM,F25.0,F15.0/10X,3HGAP,F28.3,
3F15.3/10X,11HTEMP, DEG C,F17.0,F15.0/10X,18HVSCSTY, LBM/FT-SEC,
4E13.3,E15.3/10X,19HPRESSURE,LBS/SQ-IN,F11.3,F15.3//)
    GO TO 720
700 WRITE(6,690) FW1
710 FORMAT(1H,9X,33HWINDAGE LOSS AT SYNCHRONOUS SPEED,F10.0,5H WATT/
11H1)
C
C
C WRITE VALUES OF EQUIVALENT CIRCUIT ELEMENTS
C
C
C
715 WRITE(6,715)
720 FORMAT(1H0,////,6X,29H-----)
730 WRITE(6,730) R1,X1,R2,X2,R0,X0
    FORMAT(1H+,5X,29HEQUIVALENT CIRCUIT PARAMETERS/10X,
14H R1 =,F10.3,15X,5HX1 =,F10.3/10X,4HR2 =,F10.3,15X,5HX2 =,
2F10.3/10X,4HR0 =,F10.3,15X,4HX0 =,F11.3)
C
C
C EQUIVALENT CIRCUIT ANALYSIS
C
C
    KT=1

```

```

IF (TMAFED .LT. 1.00-15) NT=3
DELTAS=1.0
SMAX=100.
S=0.
I=0
TOLD=0.
WRITE(6,741)
FORMAT(1H1,/)
WRITE(6,740) V1,F
FORMAT(1H0,5X,20H MOTOR PERFORMANCE AT, F9.2,7H VOLTS,, F7.1,3H HZ,/,/,
16X,6HTORQUE,4X,4HSLIP,6X,3H RPN,12X,5HP-OUT,11X,1H1,8X,3H I/A,7X,
23HEFF,7X,2H PF,6X,4HP-IN/5X,8H (FT-LBS),1X,9H (PERCENT),
312X,4H (HP),5X,7H (KWATT),4X,5H (AMP),1X,12H (AMPS/SQ IN)
4,9H (PERCENT),11H (*LEADING),7H (KWATT))
WRITE(7,745)
FORMAT(1H0,23X,6HTORQUE,7X,3HPRI,7X,3HSEC,8X,4HIRON,6X,2HFW/23X,
18H (FT-LBS),6X,4HLOSS,6X,4HLOSS,7X,4HLOSS,4X,7H (KWATT)/35X,7H
2(KWATT),3X,7H (KWATT),5X,7H (KWATT)/)
S=S+DELTAS
I=I+1
IF (S .GT. SMAX) THEN
I=I-1
GO TO 870
ENDIF
CALL CIRC1
IF (T .GT. 1.00-15) GO TO 780
WRITE(6,770) S
FORMAT(1H ,5X,44HF+W TORQUE EXCEEDS AVAILABLE SHAFT TORQUE AT,
1F8.3,13H PERCENT SLIP)
IF (S .GT. 15.) GO TO 870
T=0.
GO TO 820
GO TO (740,840,800),KI
IF (T .GE. IRATED) GO TO 830
TOLD=T
SOLD=S
CURDEN=11/(PC+SS)

```

741

740

745

750

760

770

780

790

800

```

810 WRITE(6,810) T,S,RPM,HP,POUT/1000.,I1,CURDEN,EFF,PF,PHASE,PIN/1000.
   FORMAT(1H,2X,F11.2,F7.2,F10.2,F8.2,A,F10.2)
815 WRITE(7,815) T,W1/1000.,W2/1000.,W0/1000.,FW/1000.
   FORMAT(1H,20X,F11.2,4F10.2)
   TORQUE(1)=0.
820 SLIP(1)=0.
   SLIP(1+1)=SWGLQ(S)
   TORQUE(1+1)=SWGLQ(T)
822 WRITE(13,822) I,S,1,T
   FORMAT(1H,10X,BHSLIP(,I3,3H) =,F6.1,3X,7HTORQUE(,I3,3H) =,F12.2)
   GO TO 750

C
C
C CALCULATE VALUE OF S AT TORQUE TRATED
C
830 S=((TRATED-TOLD)/(T-TOLD))*(S-SOLD)+SOLD
   KT=2
   GO TO 760

C
C
C WRITE MOTOR CHARACTERISTICS AT RATED TORQUE
C
840 IF ((NARS(I-TRATED)) .GT. 0.005) GO TO 830
850 WRITE(6,850)
   FORMAT(1H)
   WRITE(7,850)
   WRITE(6,810) T,S,RPM,HP,POUT/1000.,I1,CURDEN,EFF,PF,PHASE,PIN/1000.
   WRITE(7,815) T,W1/1000.,W2/1000.,W0/1000.,FW/1000.
   WRITE(6,850)
   WRITE(7,850)

C
C
C COMPUTE [A] MATRIX AT RATED TORQUE. SEE EQUATION (3.123).
C
C
C

```

```

TRAVER=100.
T12=60.
T11=60.

CALL RESISTANCES(TRAVER,T12)

ACORES=(3.1416*(DIS+DS)/2.*DBS)+(DSS*STWAG*DS)
ACURER=(3.1416*(D+DUR)/2.*(DRKS+DSR))-(KSAREA*NB)
DO 852 IF=1,8
  DO 853 JJ=1,8
    AMAT(11,JJ)=0.
  CONTINUE
CONTINUE
AMAT(1,2)=1./(KC(SWMAT)*SCAREA*2.*US*RE1)
AMAT(1,4)=-AMAT(1,2)
AMAT(2,1)=1.
AMAT(3,2)=-1./(ALY*ACORES*REQ2*L)
AMAT(3,4)=1./(KLY*ACORES*REQ1*L)
AMAT(3,6)=-.5/(KLY*ACORES*R410*L)
AMAT(4,3)=1.
AMAT(5,6)=1./(KC(RWMAT)*SB*2.*NB*RE3)
AMAT(5,8)=-AMAT(5,6)
AMAT(6,5)=1.
AMAT(7,2)=-.5/(KLY*ACURER*R810*L)
AMAT(7,6)=-1./(KLY*ACURER*REQ4*L)
AMAT(7,8)=1./(KLY*ACURER*REQ3*L)
AMAT(8,7)=1.
WRITE(18,52) ACORES,ACURER,KC(SWMAT),KC(RWMAT),ALY
  FORMAT(1H1,'STATOR CORE AREA = ',F10.4,/,', MOTOR CORE AREA = ',
  F10.4,/,', STATOR WINDING THERMAL CONDUCTIVITY = ',F10.4,/,',
  2' ROTOR WINDING THERMAL CONDUCTIVITY = ',F10.6,/,', IRON LAMINATION
  3 AXIAL THERMAL CONDUCTIVITY = ',F10.6)
WRITE(17,33)
  FORMAT(1H1,'THE [A] MATRIX FOLLOWS: ',/,/)
CALL RITEMAT(AMAT,8,8,17)

```

C

C

853
852

52

33

C
C,

C INPUT VALUES INTO THE [H] MATRIX. SEE EQ. (3.124).

C

```

C
      DO 856 JI=1,8
      DU 856 JU=1,5
        BMAT(JI,JU)=0.
      CONTINUE

```

858 *
856

```

      CONTINUE
      BMAT(1,1)=-1./(KC(SWMAT)*SCAREA*OS)
      BMAT(3,2)=-1./(KLY*ACURES)
      BMAT(3,5)=-1./(KLY*ACURES*H412)
      BMAT(5,3)=-1./(KC(HWMAT)*SH*WB)
      BMAT(7,4)=-1./(KLY*ACURER)
      BMAT(7,5)=-1./(KLY*ACURER*H812)
      WRITE(17,34)
      FORMAT(1H1,'THE [H] MATRIX FOLLOWS: ',//)
      CALL RITEMAT(BMAT,8,5,17)

```

34

C

C INPUT VALUES INTO THE [U] MATRIX. NOTE THAT ROTOR CORE LOSS IS ASSUMED
C TO BE ZERO DUE TO LOW RELATIVE FREQUENCY SEEN ON ROTOR (EQUAL TO SLIP FREQ.).
C SEE EQ. (3.122), (3.45), AND (3.46).

C

```

      H1=L/2.
      H2=(LS-L)/2.
      UMAT(1)=W1/(H1+H2)
      UMAT(2)=W0/(H1+H2)
      UMAT(3)=W2/(H1+H2)
      UMAT(4)=0.
      UMAT(5)=T12
      UMAT(1)=0.
      UMAT(2)=0.
      UMAT(3)=0.
      UMAT(4)=0.
      UMAT(5)=T12
      WRITE(17,35)
      FORMAT(1H1,'THE [U] VECTOR FOLLOWS: ',//)

```

35

```

C
C      CALL RITEVEC(UMAT,5,17)
C
C      COMPUTE THE EIGENVALUES AND EIGENVECTORS OF THE [A] MATRIX AND PRINT THE
C      RESULTS INTO LOGICAL UNIT 014. FIRST GO BACK TO READ*8 SINCE EISPAC
C      SOFTWARE REQUIRES THIS.
C
C
C      DO 483 J8=1,8
C      DO 484 J8=1,8
C      AAMAT(I8,J8)=DBLEU(AMAT(I8,J8))
C      CONTINUE
C      CONTINUE
C
C      CALL DEIGEN(AAMAT,8,8,WMR,WWI,VVMAT,14)
C
C      NOW CONVERT EIGENVALUES AND EIGENVECTORS BACK TO REAL*16.
C
C
C      DO 481 J9=1,8
C      WR(19)=DEXTD(WMR(19))
C      WI(19)=DEXTD(WWI(19))
C      DO 482 J9=1,8
C      VMAT(19,J9)=DEXTD(VVMAT(19,J9))
C      CONTINUE
C      CONTINUE
C      WRITE(17,36)
C      FORMAT(1H1,'THE [V] MATRIX OF EIGENVECTORS FOLLOWS: ',//)
C      CALL RITEMAT(VMAT,8,8,17)
C      WRITE(17,37)
C      FORMAT(1H1,'THE REAL EIGENVALUES FOLLOWS: ',//)
C      CALL RITEVEC(WR,8,17)
C      WRITE(17,38)
C      FORMAT(1H1,'THE IMAGINARY EIGENVALUES FOLLOWS: ',//)
C      CALL RITEVEC(WI,8,17)
C
C
C      COMPUTE THE RIGHT HAND VECTOR, GAMMA, IN EQUATION (3.143).

```

```

C
C
58      CALL DMATVMUL(BMAT,UMAT,SNAT,n,5)
        WRITE(17,5H)
        FORMAT(1H1,'THE SECONDARY VECTOR, SMAT, FOLLOWS. ',//)
        CALL KIEVEC(SMAT,8,17)
        CALL MATINV(VMAT,AINV,ADUM,8,IER)
        CALL DMATVMUL(AINV,SMAT,GAMMA,8,8)
        WRITE(17,42)
42      FORMAT(1H1,'THE EIGENVECTOR MATRIX INVERSE, AINV, FOLLOWS: ',//)
        CALL KIEMAT(AINV,8,8,17)
        WRITE(17,43)
43      FORMAT(1H1,'THE RIGHT HAND VECTOR, GAMMA, FOLLOWS: ',//)
        CALL KIEVEC(GAMMA,8,17)

C
C COMPUTE THE MODIFIED ALPHA VECTOR TO BE USED IN EQUATION (3.145). NOTE THAT
C Z HAS BEEN SET TO L/2 SINCE THIS VECTOR WILL ULTIMATELY BE USED WITH
C THE BOUNDARY CONDITIONS AT Z=L/2 TO OBTAIN THE C VECTOR
C
      DO 872 JK=1,8
        ALPHAS(JK)=(OEXP(WR(JK)*L/2.)-1.)*GAMMA(JK)/WR(JK)
872      CONTINUE
        WRITE(17,45)
45      FORMAT(1H1,'THE SECONDARY ALPHA VECTOR FOLLOWS: ',//)
        CALL KIEVEC(ALPHAS,8,17)
        CALL DMATVMUL(VMAT,ALPHAS,ALPHA,8,8)
        WRITE(17,46)
46      FORMAT(1H1,'THE ALPHA VECTOR FOLLOWS: ',//)
        CALL KIEVEC(ALPHA,8,17)

C
C COMPUTE CONSTANTS TO BE USED WITH THE BOUNDARY CONDITIONS IN EQ. (3.125) TO
C (3.128).
C
      KEND=((TEFS+TEN)*KE*KS)/(IEFS*KE+TEN*KS)
      AE=2.*3.1416*PI*IS*UFS
      AN=2.*3.1416*PI*(0.5*(DER1-DEK2))+TEFS)
      AII=AN-2.*NN*SH

```



```

C
C COMPUTE THE VECTOR TO BE USED WITH CHAMBERS' RULE FOR EQ. (3.166).
C
DALPHA(1)=0.
DALPHA(2)=0.
DALPHA(3)=0.
DALPHA(4)=0.
DALPHA(5)=- (ALPHA(2)+R2*TIM*KEI*ALPHA(1)-T11)
DALPHA(6)=- (ALPHA(4)+R41*AE*KE*ALPHA(3)-T11)
DALPHA(7)=- (ALPHA(6)+R611*AR*KE*ALPHA(5)-T11)
DALPHA(8)=- (ALPHA(8)+R86*KIN*AI*ALPHA(7)+R611*KE*AR*ALPHA(5)-T11)
WRITE(17,47)
47 FORMAT(1H1,'THE MODIFIED ALPHA VECTOR FOLLOWS: ',//)
CALL R1EVEC(DALPHA,8,17)
C
C
C COMPUTE THE MODIFIED EIGENVECTOR MATRIX TO BE USED IN EQUATION (3.166).
C
C
C
DO 871 JK=1,8
  DEIGVEC(1,JK)=VMAT(1,JK)
  DEIGVEC(2,JK)=VMAT(3,JK)
  DEIGVEC(3,JK)=VMAT(5,JK)
  DEIGVEC(4,JK)=VMAT(7,JK)
  DEIGVEC(5,JK)=(VMAT(2,JK)+VMAT(1,JK)*PE2*TIM*KEI)*
  IDEXP(WR(JK)*L/2.)
  DEIGVEC(6,JK)=(VMAT(4,JK)+VMAT(3,JK)*R411*AE*KE*END)*
  IDEXP(WR(JK)*L/2.)
  DEIGVEC(7,JK)=(VMAT(6,JK)+VMAT(5,JK)*R611*AR*KE)*
  IDEXP(WR(JK)*L/2.)
  DEIGVEC(8,JK)=(VMAT(8,JK)+VMAT(7,JK)*R86*KIN*AI+VMAT(5,JK)*
  IR611*KE*AR)*IDEXP(WR(JK)*L/2.)
CONTINUE
871 WRITE(17,44)
44 FORMAT(1H1,'THE MODIFIED EIGENVECTOR MATRIX, DEIGVEC, FOLLOWS:
1 ',//)
CALL R1EVENAT(DEIGVEC,8,8,17)

```

```

C
C
C COMPUTE THE VECTOR OF CONSTANTS, C, TO BE FOUND IN EQUATION (3.166).
C
C
      CALL MATINV(DLIGVFC,DEIGINV,ADUM,8,IKR)
      WRITE(17,98/)
987   FORMAT(1H1,'THE INVERSE OF DEIGVEC FOLLOWS: ',//)
      CALL K11FBI(DEIGINV,8,8,17)
      CALL DMATVMUL(DEIGINV,DALPHA,C,8,8)
      WRITE(17,48)
48    FORMAT(1H1,'THE VECTOR OF CONSTANTS, C, FOLLOWS: ',//)
      CALL K11FVEC(C,8,17)
C
C
C SOLVE EQUATION (3.145) BY BREAKING THE AXIAL DIMENSION INTO 100
C EQUAL SEGMENTS AND ITERATIVELY LOOPING THROUGH EACH VALUE OF Z.
C
C
      WRITE(19,1030)
1030  FORMAT(1H1,7X,'Z',11X,'T1(Z)',10X,'T4(Z)',10X,'T5(Z)',10X,'T8(Z)')
      WRITE(20,1021)
1021  FORMAT(1H1,7X,'Z',11X,'X1(Z)',10X,'X3(Z)',10X,'X5(Z)',10X,'X7(Z)')
      DO 1005 JN=1,8
         DO 1006 JNM=1,6
            EXPON(JN,JNM)=0.
            CONTINUE
1006  CONTINUE
1005  DO 1000 JL=1,100
         Z=(DFLOAT(JL-1))*L/200.
         DO 1010 Jm=1,8
            PP(JM)=(DEXP(WR(JM)*Z)-1.)*GAMMA(JM)/WR(JM)
            EXPON(JM,JM)=DEXP(WR(JM)*Z)
            CONTINUE
1010  CALL DMATVMUL(VMAT,PP,PPP,8,8)
      CALL DMATVMUL(EXPON,C,SUBVEC,8,8)
      CALL DMATVMUL(VMAT,SUBVEC,HUMUG,8,8)

```

```

CALL WVECADU(HOMUG,PPP,X,8,1)
ZZ(JL)=SNGLO(Z)
T1(JL)=SNGLO(X(2))
T4(JL)=SNGLO(X(4))
T5(JL)=SNGLO(X(6))
T8(JL)=SNGLO(X(8))
WRITE(19,1040) Z,X(2),X(4),X(6),X(8)
WRITE(20,1040) Z,X(1),X(3),X(5),X(7)
FORMAT(1H ,2X,E10.4,5X,E10.4,5X,E10.4,5X,E10.4)
IF (JL.EQ. 100) THEN
  WRITE(17,1044)
  FORMAT(1H1,'THE PAYNTER VECTOR (PIX[GAMMA]=[PF] FOR
1 Z=L/2 FOLLOWS: ',//)
  CALL R1FVEC(PP,8,17)
  WRITE(17,1043)
  FORMAT(1H1,'THE PPP VECTOR FOLLOWS: ',//)
  CALL R1FVEC(PPP,8,17)
  WRITE(17,1045)
  FORMAT(1H1,'THE EXPONENTIATION MATRIX, EXPON, FOR Z=L/2
1 FOLLOWS: ',//)
  CALL R1EMAI(EXPON,8,8,17)
  WRITE(17,1046)
  FORMAT(1H1,'THE SUBVECTOR, SUBVEC, FOLLOWS: ',//)
  CALL R1FVEC(SUBVEC,8,17)
  WRITE(17,1047)
  FORMAT(1H1,'THE HOMOGENEOUS VECTOR, HOMUG, FOLLOWS: ',//)
  CALL R1FVEC(HOMUG,8,17)
  ENDIF
1000 CONTINUE
C
C
C PLOT THE TEMPERATURES ON A VERSAFEC 1200 PLOTTER.
C
C
CALL VERSAPLOT(0,0,0,
12.,1.,-3,
21.0,

```

```

34.0,8.2,.2,8HT16 VS. 4.0.,8,
42Z,6.,100,1,
518,9.,100,1,
62Z,T8,100,1,0,0,
70.,0.,19HAXIAL DISTANCE (IN),-19,6.,0.,ZZ(101),ZZ(102),
80.,0.,24HSTATOR CORE TEMP (DEG F),+23,9.,90.,T8(101),T8(102),
90.,0.,30.,2,45.,2,-30584)

CALL VERSAPLOT(0,0,0,
12.,1.,-3,
21.0,
34.0,8.2,.2,8HT1 VS. 2.0.,8,
42Z,6.,100,1,
518,9.,100,1,
62Z,T1,100,1,0,0,
70.,0.,19HAXIAL DISTANCE (IN),-19,6.,0.,ZZ(101),ZZ(102),
80.,0.,27HSTATOR WINDING TEMP (DEG F),+27,9.,90.,T1(101),T1(102),
90.,0.,30.,2,45.,2,-30584)

```

C

```

CALL VERSAPLOT(0,0,0,
12.,1.,-3,
21.0,
34.0,8.2,.2,8HT4 VS. 2.0.,8,
42Z,6.,100,1,
514,9.,100,1,
62Z,T4,100,1,0,0,
70.,0.,19HAXIAL DISTANCE (IN),-19,6.,0.,ZZ(101),ZZ(102),
80.,0.,24HSTATOR CORE TEMP (DEG F),+24,9.,90.,T4(101),T4(102),
90.,0.,30.,2,45.,2,-30584)

```

C

```

CALL VERSAPLOT(0,0,0,
12.,1.,-3,
21.0,
34.0,8.2,.2,8HT5 VS. 2.0.,8,
42Z,6.,100,1,
515,9.,100,1,
62Z,T5,100,1,0,0,

```

C

```

70.,0.,19MAXIAL DISTANCE (IN),-19,6.,0.,22(101),22(102),
80.,0.,22HROTOK BAR TEMP (DEG F),+22,9.,90.,15(101),15(102),
90.,0.,30.,2,45.,2,-30584)

```

C
C
C
C
C

C CURRENT DENSITY'S AT RATED TORQUE

```

IF (NB .LT. 1.00-15) GO TO 860
WBAR=(W2/WR)*(W2BAR/WR2)
IBAR=USUR((WBAR*SB)/(RRSTVY*LB))
JBAR=IBAR/SR
WING=(W2-WBAR)*0.5
JRING=QSORT(WRING/(RRSTVY*SER*1.5708*(DER1+DER2)))
CDEN=CURDEN

```

860

KT=3

S=SQLO+DELTA5

GO TO 760

870

880

```

IF (JBAR .GT. 1.00-15) WRITE(6,880) JBAR,JRING,CDEN
FORMAT(1H0,10X,46HCURRENT DENSITY AT RATED TORQUE IN ROTOR BAR =
1,F9.2/44X,13HIN END RING =,F9.2/44X,13HIN ARMATURE =,F9.2)

```

C
C
C
C
C
C

C PLOT TORQUE-SPEED CURVE ON VERSATEC 1200 PLOTTER UTILIZING ARRAYS TORQUE
C AND SLIP

```

INITIALIZE FOR PLOTTING
CALL PLOTS(0,0,0)
CALL FACTOR(1.0)
CALL PLOT(2.,1.,-3)

```

C...

```

DETERMINE SCALING FACTORS
CALL SCALE(SLIP,5.,1+1,-1)
CALL SCALE(TORQUE,9.,1+1,1)
WRITE(13,883)SLIP(102),SLIP(103),TORQUE(.02),TORQUE(103)

```

C...

```

883  FORMAT(1H ,4F10.2)

C...  PLOT THE DATA
      CALL NEWPEN(5)
      CALL LINE(SLIP,TORQUE,I+1,1,0,0)

C...  DRAW AXES
      CALL NEWPEN(5)
      CALL AXIS(0.,0.,14HSLIP (PERCENT),-14,5.,0.,SLIP(I+2),SLIP(I+3))
      CALL AXIS(0.,0.,15HTORQUE (FT-LBS),+15,9.,90.,TORQUE(I+2),TORQUE
      1(I+3))

C...  DRAW GRID
      CALL NEWPEN(3)
      CALL GRID(0.,0.,30,0.2,45,0.2,-30584)

C...  END OF PLOTTING
      CALL PLOT(0.,0.,+999)

      STOP
      END

```

```

*****
C THE FOLLOWING SUBROUTINE IS CALLED TWICE BY THE MAIN PROGRAM: ONCE FOR
C THE STATOR SLOTS AND ONCE FOR THE ROTOR SLOTS. ITS FUNCTION IS TO COM-
C PUTE ALL SLOT DIMENSIONS THAT ARE NOT INPUT TO THE PROGRAM BUT THAT ARE
C NEEDED IN SUBSEQUENT CALCULATIONS. SLOTS ALSO COMPUTES SLOT AREAS AND
C THE SLOT PERMANENCE RATIO. THE USERS' MANUAL REFERENCE 11 CONTAINS A GOOD
C EXPLANATION OF THE DETERMINATION OF THE SLOT PERMANENCE RATIO, AX, FOR
C EACH SLOT. THIS INFORMATION IS ALSO SUPPLEMENTED BY THE DERIVATIVE IN
C APPENDIX B, FIGURE 6 WHICH EXPLAINS THE USE OF THE EFFECTIVE VALUE OF
C KX IN OBTAINING AX. IN ANY CALCULATIONS OF CAREA, SAREA, OR XTWMAG REFER
C TO THE USERS' MANUAL FIG. 14 FOR ILLUSTRATIONS.
*****

```

```

C
      SUBROUTINE SLOTS(SLLOC,WSX,WSX1,WSX2,WSX3,WSX4,WSX5,DSX,
      1DIX,D2X,D3X,D4X,DSX,XTWDTH,CAREA,SAREA,N,D6X,WSX6,DIA,KX,AXX,X
      21WMAG,PHIX,XSTYPE)

```

```

C
      FOR STATOR SLOTS SLLOC=1.0 * FOR ROTOR SLOTS SLLOC=-1.0

```

```

C
      IMPLICIT REAL*16 (A-H,O-Z)
      REAL*16 N,KX

```

```

C
      INTEGER XSTYPE

```

```

C
      U(WA,CAREA)=((-WA+QSQR1(WA*WA+4.*CAREA*TANPHI)))/(2.*TANPHI)
      WB(U,WA)=WA+2.*U*TANPHI
      A(W)=0.25*W*W*((1.5708+PHIX)/(COSPNI*CUSPHI))+TANPHI

```

```

C
      IF (CAREA+DSX+DIX .LT. 1.0E-15) GO TO J10
      A1=0.25*KX+(1.0/12.0)
      A2=0.25*(KX-0.666667)

```

```

C
      GO TO (10,20,30,90,210,90),XSTYPE

C
      WSX1=0.
      DX=0.
      D4X=0.

```

```

      10

```

```

C
20
  AXX=0.
  GO TO 40

  WSXA=WSX
  WSX1=0.
  WSX2=0.
  D3X=0.
  D4X=0.
  AXX=0.
  GO TO 100

C
30
40
  AXX=KX*(D4X/WSX1+(D3X/(WSX-WSX1)))+(DLUG(WSX/WSX1)))
  WSX2=0.
  WSX3=0.
  WSX4=WSX
  WSX5=WSX
  XTWPH=0.
  IF (DSX .GT. 1.00-15) GO TO 50
  IF (D1X .LT. 1.00-15) GO TO 60
  DSX=D1X+D4X+D3X+D2X+D6X
  GO TO 80
  IF (D1X .LT. 1.00-15) GO TO 70
  GO TO 80
  DSX=CAREA/(WSX-2.*WSX6)+D5X+D6X+D2X+D3X+D4X
  D1X=DSX-(D4X+D3X+D2X+D6X)
  SAREA=WSX*(D1X-D4X-D3X)+0.5*(WSX1+WSX)*D3X+WSX1*D4X
  IF (CAREA .LT. 1.00-15) CAREA=(WSX-2.*WSX6)*(D1X-D5X)
  AXX=AXX+(D1X*A1-D5X*A2+KX*D2X)/WSX
  XTWPHAG=((D1A-0.6667*SLTLUC*DSX)*(3.1416/N))-WSX
  GO TO 300

C
90
  WSXA=WSX2
  WSX=0.
  IF (WSXA .GT. 1.00-15) GO TO 130
  IF (XTWPH .LT. 1.00-15) GO TO 110
  WSXA=((3.1416*(D1A+2.*SLTLUC*(D4X+D3X)))/N)-XTWPH
  PHIX=(3.1415927/N)*SLTLUC
  GO TO 110

```



```

C 210
GU TU 300
WSX=0.
WSX2=0.
WSX4=0.
XTWOTH=0.
D2X=0.
D3X=0.
D5X=0.
WSX5=0.
WSX6=0.
IF (DSX .GT. 1.00-15) GU TU 240
IF (DIX .LT. 1.00-15) GU TU 220
DSX=DIX+2.*D0X+D4X
GO TU 250
DSX=(USQR(4.*CAREA/3.1416))+D4X+2.*D6X
DIX=DSX-2.*D0X-D4X
GO TU 250
IF (DIX .LT. 1.00-15) GU TU 230
IF (DABS(DIX+D4X+2.*D0X-DSX) .GT. 0.001) GO TU 310
IF (WSX2 .LT. 1.00-15) WSX2=DSX-D4X
SARXA=0.7854*WSX2+WSX2+WSX1*D4X
IF (CAREA .LT. 1.00-15) CAREA=0.7854*(WSX2-2.*D6X)**2
AXX=(0.025+D4X/WSX1)*KX
XIMMAG=(DIA-(2.*D4X+1.333*WSX2)*SLILUC)*(3.1416/N)-0.94*WSX2
GO TU 340

C 260
W1=W-2.*D0X
AS=A(W1)
IF (2.*AS/CAREA .GT. 1.00) GO TU 310
AR=0.5*CAREA-AS
Y2=D(W1,AR)
W2=AR(Y2,W1)
AS=A(W2)
IF (DABS(2.*(AR+AS)/CAREA-1.0) .GE. 0.001) GO TU 270
DSX=D4X+D3X+D2X+D6X+Y1+Y2+D5X+(W2/2.)*(1./CUSPHI+TANPHI)
DIX=DSX-D4X-D3X-D2X-D6X

```

```

280      WSX3=(2.*(DSX-D4X-D3X)*SINPHI+WSX2*CUSPHI)/(SINPHI+1.0)
      WSX5=WSX3
      SAREA=A(WSX3*CUSPHI)+0.5*(WSX3*CUSPHI+WSX2)*(DSX-0.5*WSX3*(1.0+
1      SINPHI)-D4X-D3X)+0.5*D3X*(WSX2+WSX1)+WSX1*D4X
      AXS=AXX+((2.*FX*D2X)/(WSXA+WSA4))+(D1X/WSX4)*A1-((2.00*DSX)/(WSX4
1+WSX5))*A2
      XTWAG=((D1A+2.*SLUDUC*(D4X+D3X))*(3.1416/N))-WSX2
      IF (CAREA .GT. 1.00-15) GO TO 300
      Y1=0.5*DSX
      W=0.5*(WSX4+WSX5)
      CAREA2=1000.
      CAREA=A(WSX3*CUSPHI-2.*D6X)+0.5*(WSX3*CUSPHI+W-4.*D6X)*(DSX-0.5*
1      WSX3*(1.0+SINPHI)-D4X-D3X-D2X-Y1-D5X)+(0.5*(Y1+D5X)*(W+WSX4-4.*
2      WSX6))-(W-2.*WSX6)*D5X
      IF (OABS(CAREA2/CAREA-1.0) .LT. 0.001) GO TO 300
      Y1=D(WSX4-2.*WSX6,CAREA/2.)
      W=Wb(Y1+D5X+D2X,WSX2)
      CAREA2=CAREA
      GO TO 290

C      300      IF (OABS(D1X+D2X+D3X+D4X+D6X-DSX) .LT. 0.001) GO TO 340
C
310      IF (SLUDUC .LT. 0.) WRITE(6,320)
      IF (SLUDUC .GT. 0.) WRITE(6,330)
320      FORMAT(1HK,41HINSUFFICIENT OR INCORRECT ROTOR SLOT DATA)
330      FORMAT(1HK,42HINSUFFICIENT OR INCORRECT STATOR SLOT DATA)
      RETURN
      END

```

```

C *****
C THE FOLLOWING SUBROUTINE CHECKS IF THE NUMBER OF ROTOR SLOTS, THE NUMBER
C OF STATOR SLOTS, AND THE NUMBER OF POLES ARE MUTUALLY COMPATIBLE. AN
C INCOMPATIBLE COMBINATION IS ONE THAT MAY RESULT IN NOISE OR VIBRATION
C PROBLEMS OR ONE THAT MAY CAUSE UNDESIRABLE TORQUE-SPEED CHARACTERISTICS.
C IF COMPATIBILITY EXISTS, CONTROL IS RETURNED TO THE MAIN PROGRAM; IF NOT,
C THE SUBROUTINE PRINTS OUT AN ERROR MESSAGE AND LISTS THE NUMBER OF
C ROTOR SLOTS THAT MAY BE USED INSTEAD. REFERENCE 6 IS USED AS GUIDANCE IN
C DETERMINING VIABLE ALTERNATIVES.
C *****

```

```

SUBROUTINE CM6NIN (US,NH,P)

```

```

IMPLICIT REAL*16 (A-H,O-Z)
REAL*16 NH
DIMENSION L(100)

```

```

X=1.00-15
K=0
F=NH
D=QABS(US-F)
M=1
DO 20 I=1,1000

```

```

A=3.*QFLUAT(I)*P
IF (QABS(D-A) .LT. X) GO TO 40
IF (A .GT. D) GO TO 30

```

```

CONTINUE

```

```

IF (QABS(D-P) .LT. X) GO TO 40
IF (QABS(P-QFLUAT(1+FIX(SNGLQ(F/P+0.0001)))) .LT. X) GO TO 40
M=2
IF (F .GT. US+P/2.) GO TO 40
M=3

```

```

IF (QABS(D-P/2.) .LT. X) GO TO 40
IF (QABS(US-F) .LT. X) GO TO 40
IF (QABS(D-1.) .LT. X) GO TO 40

```

```

IF (QABS(P-2.) .LT. X) GO TO 40
IF (QABS(P-1.) .LT. X) GO TO 40
IF (QABS(P-1.) .LT. X) GO TO 40
IF (QABS(P-2.) .LT. X) GO TO 40
IF (QABS(P-2.) .LT. X) GO TO 40
IF (K .EQ. 0) GO TO 150
I1=I1+1
L(11)=FIX(SNGLQ(F+0.01))
GO TO 110
IF (K .GT. 0) GO TO 110
K=1
F=0FLVAL(FIX(SNGLQ(0.60*QS)))
I1=0
GO TO (50,70,90),M
C
C
50
60
WRITE(6,60)
FORMAT(1HK,62HRUTUM-STATOR SLOT COMBINATION MAY PRODUCE UNDESIRAB
1LE TORQUE-SPEED CHARACTERISTICS)
GO TO 110
C
70
WRITE(6,60)
FF=(P/2.)/(P/2.+QS)
WRITE(6,80) FF
FORMAT(1H ,19HMINIMIZE BY SKEWING,F6.3,30H TIMES ROTOR CIRCUMFER
LENCE, 0H)
GO TO 110
C
90
100
WRITE(6,100)
FORMAT(1HK,61HRUTUM-STATOR SLOT COMBINATION MAY PRODUCE NOISE AND
1 VIBRATION)
C
110
F=F+1.0
IF (F .LE. 1.4*QS) GO TO 10
IF (I1 .LT. 1) GO TO 130
WRITE(6,120) (L(1),I=1,I1)
C

```

```

120  FORMAT(1H ,2HCHANGE NUMBER OF ROTOR SLOTS TO ONE OF THE FOLLOWING
      1/((1016))
      GO TO 150
C
130  WRITE(6,140)
140  FORMAT(1H ,2HCHANGE NUMBER OF STATOR SLOTS)
C
150  RETURN
      END

```

```

C *****
C THE FOLLOWING SUBROUTINE COMPUTES THE DISTRIBUTION FACTOR AND PITCH
C FACTOR FOR THE STATOR WINDING. IT ALSO CHECKS THAT THE WINDING SPECI-
C FIED IS PHYSICALLY REALIZABLE; IF IT IS NOT, AN ERROR MESSAGE IS
C PRINTED.
C *****
C
C SUBROUTINE WDGFACT (PBA,P,QS,DP,PC,PF,WDGPCH)
C
C IMPLICIT REAL*16 (A-H,U-Z)
C
C PITCH FACTOR CALCULATION
C
C      YY=QFLOAT(1+IX(SNGLO((QS/P)*WDGPCH)+0.01))
C      IF (DABS(YY-QS/P*WDGPCH) .GT. 1.00-2) WRITE(6,10) WDGPCH
C      FORMAT(1H,F5.3,22H PITCH IS NOT POSSIBLE)
C      PF=Q/SIN(YY*1.571/(QS/P))
C
C 10
C
C DISTRIBUTION FACTOR CALCULATIONS
C
C      IPX=1+IX(SNGLO(P+0.1))
C      IQQ=1+IX(SNGLO(QS+0.1))
C      IC=1+IX(SNGLO(PC+0.1))
C      IPN=3
C      PNI=3
C      QN=QS/(3.*P)
C
C CHECK IF WINDING HAS INTEGRAL NO. OF SLOTS PER POLE PER PHASE

```

```

IF (P2A .GT. 61.0) D=2.0
IZY=IPX*IPN
IDM=0
IDM=IDM+IZY
IF (IOO-IDM) 40,30,20

```

20

C

C CALCULATE DISTRIBUTION FACTOR FOR INTEGRAL SLOT WINDING

C

```

30 DF=QSIN(1.571*D/PN)/(GN*D*QSIN(1.571/(PN*GN)))
GO TO 90

```

30

C

C REDUCE THE FRACTION IOO/IZY TO LOWEST TERMS

C

```

40 IIOQ=IOO
I=2

```

40

```

50 IF ((IZY/I)*I .EQ. IZY .AND. (IIOQ/I)*I .EQ. IIOQ) GO TO 60

```

50

```

IF (I .GT. IZY) GO TO 70

```

```

I=I+1

```

```

GO TO 50

```

```

IZY=IZY/I

```

60

```

IIOQ=IIOQ/I

```

```

GO TO 50

```

C

C CALCULATE DISTRIBUTION FACTOR FOR FRACTIONAL SLOT WINDING

C

```

70 FNO=IIOQ

```

70

```

DF=QSIN(1.571*D/PN)/((FNO*D*QSIN(1.571/(FNO*PN))))
IF ((IZY/3)*3 .EQ. IZY) WRITE(6,80)

```

```

IF ((IPX/IZY)*IZY .NE. IPX) WRITE(6,80)

```

```

FORMAT(1HN,40HINTEGRAL FRACTIONAL-SLOT WINDING IS USED)

```

80

C

! 2

! 3

```

C CHECK IF SPECIFIED NUMBER OF PARALLEL CIRCUITS ARE POSSIBLE
C
C
C
    IPX=IPX/12Y
    IF ((IPX/1C)*1C .EQ. IPX) ( TO 110
    WRITE(6,100) 1C
100  FORMAT(1H*,12,35H PARALLEL CIRCUITS ARE NOT POSSIBLE)
110  RETURN
    END

```



```

C *****
C THE FOLLOWING SUBROUTINE TREATS THE INDUCTION MOTOR AS A TWO-TERMINAL
C ELECTRICAL CIRCUIT CONSISTING OF RESISTORS AND INDUCTORS WHILE CONDUCT-
C ING THE NECESSARY CIRCUIT ANALYSIS. ON THE FIRST CALL TO CIRCT THE AIR
C GAP VOLTAGE V2 AND THE MAGNETIZING CURRENT IMAG ARE COMPUTED FOR USE
C IN OBTAINING IMPROVED ESTIMATES OF R0 AND X0. SUBSEQUENT CALLS TO CIRCT
C IN THE NO-LOAD CALCULATIONS FURTHER REFINES V2 AND IMAG UNTIL FINALLY R0
C AND X0 HAVE CONVERGED. FOR DESCRIPTION OF THE DOUBLE CONVERGENCE PRO-
C CEDURE REFER TO THE USERS' MANUAL. SUBROUTINE CIRCT IS ALSO USED IN
C THE EQUIVALENT CIRCUIT ANALYSIS ONCE R0 AND X0 HAVE BEEN FOUND. DATA
C IS PASSED TO AND FROM THE MAIN PROGRAM VIA THE COMMON BLOCK CIR AND PHAS.
C *****

```

SUBROUTINE CIRCT

```

IMPLICIT REAL*16 (A-H,O-Z)
CHARACTER*1 PHASE,STAR,BLANK
REAL*16 NSYNCH,I1,IMAG,I2
INTEGER*4 IARCDERGHJKLMN
COMPLEX*16 Z,Z0,Z1,Z2,E1,E2,IA,IB,IC
COMMON/PHAS/PHASE
COMMON/CIR/R0,R1,R2,X0,X1,X2,FW1,NSYNCH,V1,S,I1,RPM,PF,T,HP,EFF,
1PIN,W1,W2,W0,FW,IMAG,V2,POUT

```

```

STAR='*'
BLANK=' '
C=2.5
PHASE=BLANK
POUT=0.
EFF=0.
HP=0.
T=0.

```

```

E1=DCMPLX(V1)
Z1=DCMPLX(R1,X1)
Z0=DCMPLX(R0*X0*(R0*R0+X0*X0)/(R0*R0+X0*X0))
IF (S.LT. 1.00-10) GO TO 10
Z2=DCMPLX(R2*100./S,X2)
D=(Z1+Z0)*(Z2+Z0)-Z0*Z0

```

! 1

! 2

! 3

! 4

10	IA=(E1*(20+22))/D	! 5
	IB=(E1*20)/D	
	IC=IA-IB	
	GO TO 20	
20	IA=E1/(Z1+Z0)	! 6
	IB=(0.,0.)	
	IC=IA	
	E2=(IA-IB)*Z0	
	A=QEXTD(DREAL(E2))	
	B=QEXTD(QIMAG(E2))	
	V2=QSQR1(A*A+B*B)	
	IMAG=V2/X0	
	W0=V2*V2/R0*3.	! 7
	A=QEXTD(DREAL(IA))	
	B=QEXTD(QIMAG(IA))	
	IF (B.GT. 0.) PHASE=SIAR	
	I1=QSQR1(A*A+B*B)	
	PF=A/I1	
	A=QEXTD(DREAL(IB))	
	B=QEXTD(QIMAG(IB))	
	I2=QSQR1(A*A+B*B)	
	W1=I1*I1*R1*3.	! 8
	W2=I2*I2*R2*3.	! 9
	RPW=NSYNCH*(1.-S/100.)	
	PW=FW1*(RPW/NSYNCH)**C	
	PIN=V1*I1*PF*3.	
	IF (S.GT. 0.) GO TO 30	
	P011=-PW	
	GO TO 40	! 10
30	P001=W2*((100.-S)/S)-PW	
40	EFF=100.*P001/PIN	
	HP=P001/745.7	
	IF (S.LT. 99.9) GO TO 50	
	T=((-.84704/S)*W2)/(NSYNCH*12.)	
	GO TO 60	
50	T=(HP/HPW)*5.25d3	! 11
60	RETURN	
	END	

```

C *****
C THE FOLLOWING SUBROUTINE COMPUTES THE FLUX DENSITIES IN THE STATOR AND
C ROTOR BACK IRON AND IN THE STATOR AND ROTOR TEETH. IT ALSO COMPUTES
C THE AMPERE TURN DROPS THROUGHOUT THE MAGNETIC CIRCUIT. IF ANY PORTION
C OF THE MOTOR SATURATES AN INDICATOR IS SET TO ALERT THE MAIN PROGRAM.
C DATA IS PASSED TO AND FROM THE MAIN PROGRAM VIA THE COMMON BLOCK MAG.
C *****
C

```

```

      SUBROUTINE MAGNET
      IMPLICIT REAL 16 (A-H,O-Z)
      COMMON /MAG/HST,BSY,RKT,HRY,ATST,ATSY,ATNT,AIRY,ASYKE,ASTOTH,ARY
      YUKE,ARTOTM,I,SYUKE,LRYUKE,DSS,DSR,FTOTAL,FPULE,KSAT,AI,ATAG,ATTOT
      DIMENSION AI(60)
      REAL*16 I,SYUKE,LRYUKE
      BSY=0.
      HRY=0.
      RKT=0.
      HRY=0.
      AISI=0.
      ATSY=0.
      AIRT=0.
      ATRY=0.
      ATTOT=0.
      KSAT=10

```

```

C
C STATOR TOOTH
C

```

```

      BST=FTOTAL/ASTOTH
      NA=1
      K=1

```

```

      X=HST
      GO TO 90
      ATSI=AT*DSS

```

```

10

```

```

C
C STATOR YUKE
C

```

```

      BSY=FPULE/(2.*ASYKE)

```

```

20

```

```

      NA=1
      K=2
      X=BSY
      GO TO 90
      AISY=AT*LSYUKE
      ! 5
      C ROTUR TUOTH
      C
      40 BKT=FTOTAL/ARTOTH
      NA=31
      K=3
      X=BKT
      GO TO 90
      50 ATK1=AT*DSR
      C
      C ROTUR YUKE
      C
      60 BRY=FPOLE/(2.*ARYUKE)
      NA=31
      K=4
      X=BRY
      GO TO 90
      70 ATRY=AT*LRUYUKE
      C
      80 ATUT=ATAG+ATST+AISY+ATHT+ATRY
      RETURN
      C
      C INTERPOLATION PRUCEDURE FOR MATERIAL CURVES
      C
      90 IF (AI(NA) .LT. X) GO TO 130
      NA=NA+3
      100 IF (AI(NA)-X) 110,120,120
      110 NA=NA+2
      GO TO 100
      120 XX=(AI(NA)-AI(NA-2))/(LOG(AI(NA+1)/(AI(NA-1)+0.0001)))
      Y=AI(NA)-XX*LOG(AI(NA+1))
      AI=QEXP((X-Y)/XX)
      ! 6

```

GU IQ (10,30,50,70),K
KSAT=0
GU TU (20,40,60,80),K
END

130


```

*****
C THE FOLLOWING SUBROUTINE COMPUTES THE THERMAL RESISTANCES SEEN IN THE MODEL
C OF THE SUBMARINE PROPELLSION MOTOR. THESE ARE STRICTLY A FUNCTION OF THE
C GEOMETRY, MATERIAL STRUCTURE, AND TYPE OF COOLING.
*****
C
C SUBROUTINE RESISTANCES(I8AVE,T12)
C
C   IMPLICIT REAL*10 (A-H,O-Z)
C   REAL*16 K1,KX,KY,KEI,KE,KS,K9,L,NNU,NTA,NPR,MU,NSYNCH,LEFS,LPROP,NB,
C   I10,I1,IMAG,JHAR,LS,KIN
C   INTEGER*4 IDUMKUKDKDKKDKF
C
C   !TWO COLUMNS ON P/PINTER
C
C   COMMON/CIR/K0,R1,R2,X0,X1,X2,FW1,NSYNCH,V1,S,I1,RPM,PF,T,HP,EFF,
C   1PIN,W1,W2,W0,FW,IMAG,V2,PUUT
C   COMMON/INIFL/ASTRND,CSRAT0,DER1,DER2,D1R,D1S,D2R,D2S,D3R,D3S
C   1,D4R,D4S,D5S,JHAR,LB LS,PFLUID,R"WDTH,SB,SCAKEA,SFR,SFS,SKEW,
C   2SSAPEA,SIWDTH,TRATED,VSCFLD,WSR1,WSR2,WSR3,WSR4,WSR5,WSS,WSS1,
C   3WSS2,WSS3,WSS4
C   COMMON/GEOM/WX,WY,U,OS,WSS6,IEN,L,D1S,G,D,DS,LEFS,TEFS,LPROP,
C   1PTR,DOR,D6R,NH,TFR,IENGAP,PR
C   COMMON/RESIST/RE1,RE2,R412,R410,R810,R411,R812,RE3,REQ1,REQ2,REQ3,
C   1REQ4,R611,R86
C   COMMON/DUMNY/AWG
C
C   DATA KIN,KI,KEI,KE,H4,RHU,MU,KS,K9,H6,NPR/.003,.002,.003,.1546,
C   1.03605,3.4720-5,.610,.610,.1546,7./
C
C COMPUTE RESISTANCE OF THE STATOR WINDING TO THE STATOR CORE, RE1. SEE
C EQUATIONS (3.49) TO (3.56) AND (3.61).
C
C   KX=KI*(1.+WX/(2.*U))
C   KY=KI*(1.+WY/(2.*U))
C   RXC1=(WSS-2.*WSS6)/(24.*OS*D1S*KX)
C   RYC1=D1S/(6.*OS*KY*(WSS-2.*WSS6))

```

```

RX11=WSS6/(2.*QS*DIS*KE1)
RY11=UBS/(2.*QS*KE1*(WSS-2.*WSS6))
RX1=RXC1+RX11
RY1=RYC1+RY11
RE1=((RX1*RY1)/(RX1+RY1))*(1.-(RXC1*RYC1)/(5.*RX1*RY1))

C COMPUTE RESISTANCE OF THE STATOR ENDWINDING TO THE OVERHANG REGION, RE2.
C SEE EQUATIONS (3.62) TO (3.66).
C
RXC2=RXC1
RYC2=RYC1/4.
RX2=RX1
RY2=RY1-0.75*RYC1
RE2=((RX2*RY2)/(RX2+RY2))*(1.-(RXC2*RYC2)/(5.*RX2*RY2))

C COMPUTE RESISTANCE OF THE STATOR CORE TO THE BACKIRON COOLING WATER, R412.
C SEE EQUATION (3.71).
C
R412=(TEN/KE+1./H4)/(3.1416*DIS)

C COMPUTE RESISTANCE OF THE STATOR CORE TO THE WATER GAP, R410. SEE EQUATIONS
C (3.72) TO (3.78).
C
R=DS/2.
OMEGA=2.*3.1416*NSYNCH/60.
CALL FHC(R,MU,RHU,UMF,GA,CF)
NTA=(RHU*OMEGA*R*(G-2.*TENGAP)/MU)*((G-2.*TENGAP)/R)**0.5
NNU=0.44*CF*((R/(G-2.*TENGAP))**.5)*NTA*(NPR**.3333)
RUV=KE*NNU/(G-2.*TENGAP)
R410=1./((4.*3.1416*KUV*R)+TENGAP/(4.*3.1416*KS*R))

C COMPUTE RESISTANCE OF THE ROTOR CORE TO THE WATER GAP, R810. SEE EQUATION
C (3.73)
C
R=D/2.
R810=1./((4.*3.1416*FOV*R)+TENGAP/(4.*3.1416*KS*R))
C

```



```

C COMPUTE RESISTANCE OF THE STATOR IRON IN THE AXIAL DIRECTION THROUGH THE
C ENDFRAME. SEE EQUATION (3.88)
C
      H12=H6
      R411=1./((2.*3.1416*DS*LEFS)*(TER/KS+TEN/KE+1./H12))
C
C COMPUTE RESISTANCE OF THE IRON CORE IN THE RADIAL DIRECTION TO THE
C ENVIRONMENT, R412. SEE EQUATIONS (3.89) AND (3.90).
C
      H9=0.29*((TRAVE-T12)/LPROP)**0.25
      R412=1./((3.1416)*(FIR/((DOR+PTR)*K9))+1./((DOR+PTR)*H9))
C
C COMPUTE RESISTANCE OF THE ROTOR SQUARKEL CAGE TO THE ROTOR CORE, RE3.
C SEE EQUATIONS (3.92) TO (3.103).
C
      U=0.806227*D6K
      W=0.806227*(WSP2-2*D6K)
      KA=K1*(1.+W/(2.*U))
      KY=KX
      RXC3=1./((24.*NB*KX)
      RYC3=1./((6.*NB*KY)
      RX13=U/(4.*NB*KX*KE1)
      RY13=KYJ3
      QX3=RXC3+RX13
      QY3=RYC3+RY13
      WRTIE(15,23) U,W,KX,KY,RXC3,RYC3,RX13,RY13,RX3,RY3
      FURNAF(110,////,16X,'U = ',F10.5,/,15X,' W = ',F10.5,/,15X,
1' KX = ',F9.5,/,15X,
2' KY = ',F9.5,/,15X,' RXC3 = ',F7.5,/,15X,
3' RYC3 = ',F7.5,/,15X,
4' RX13 = ',F7.5,/,15X,' RY13 = ',F7.5,/,15X,
5' RX3 = ',F8.5,/,15X,
6' RY3 = ',F8.5,/)
      RE3=((RX3*RY3)/(RX3+RY3))*(1.-((RXC3+RYC3)/(5.*RX3*RY3))
23
C
C COMPUTE RESISTANCE OF THE ROTOR END RING TO THE OVERHANG REGION, R611.
C SEE EQUATION (3.105).

```

```

C
      R611=1./(.1416*U)*(TEN/((DER1-DEK2)*KE)+U.5*TEN/(TER*KE))+
      11./((DER1-DEK2)+TER)*H6))
C
C   COMPUTE RESISTANCE BETWEEN LAST ROTOR LAMINATION AND ENDRING, R86.
C
      R86=BR/(2.*J.1416*(DER1-DEK2)*D*KJN)
C
C   COMPUTE EQUIVALENT RESISTANCES FOR USE IN EQUATIONS (3.113) TO (3.116).
C
      REQ1=1./((1./RE1)+(1./R410)+(1./R412))
      REQ2=1./((1./RE1)+(.5/R410))
      REQ3=1./((1./RE3)+(1./R810)+(1./R812))
      REQ4=1./((1./RE3)+(.5/R810))
C
C
C   WRITE OUT THE RESISTANCE VALUES INTO LOGICAL UNIT 15.
C
C
      WRITE(15,10)RE1,RE2,RE3,R412,R410,R810,R411,R86,R611,R812,REQ1,REQ2,
      1REQ3,REQ4
      FORMAT(1H1,////,16X,'RE1 = ',F10.5,/,15X,
      1' RE2 = ',F10.5,/,15X,
      1' RE3 = ',F10.5,/,15X,
      2' R412 = ',F10.5,/,15X,
      3' R410 = ',F10.5,/,15X,
      4' R810 = ',F10.5,/,15X,
      5' R411 = ',F10.5,/,15X,
      5' R86 = ',F10.5,/,15X,
      5' R611 = ',F10.5,/,15X,
      6' R812 = ',F10.5,/,15X,
      7' REQ1 = ',F10.5,/,15X,
      8' REQ2 = ',F10.5,/,15X,
      9' REQ3 = ',F10.5,/,15X,
      9' REQ4 = ',F10.5,/)
      10
C
C   WRITE OUT WATER GAP DATA INTO LOGICAL UNIT 15.
C

```

C

11

```
WRITE(15,11) NNU,MIA,OMEGA,ROV,CF
FORMAT(1H0,15X,'NUSSELT NUMBER = ',F10.5, '//,15X,
1' TAYLOR NUMBER = ',F10.5, '//,15X,
2' OMEGA = ',F10.5, '//,15X,
3' OVERALL RESISTANCE COEF = ',F10.5, '//,15X,
4' COEFFICIENT OF FRICTION = ',F10.5)
RETURN
END
```

C

11

```
WRITE('5,11) NNU,MIA,OMEGA,RUV,CF  
FORMA,(1H0,15X,'NUSSELT NUMBER = ',F10.5, '//,15X,  
1' TAYLOR NUMBER = ',F10.5, '//,15X,  
2' OMEGA = ',F10.5, '//,15X,  
3' OVERALL RESISTANCE COEF = ',F10.5, '//,15X,  
4' COEFFICIENT OF FRICTION = ',F10.5)  
RETURN  
END
```

```

C*****
C THE FOLLOWING SUBROUTINE ITERATIVELY COMPUTES THE FRICTIONAL DRAG
C COEFFICIENT, CF, IN THE STATOR-HOIOR GAP OF THE SUBMARINE PROPUSSION
C MOTOR. SEE EQ. (69) OF THE TEXT. THIS SUBROUTINE WAS REMOVED FROM I.J.
C PEREZ' MIT MASTERS THESIS.
C*****
C
C SUBROUTINE FRIC(R,MU,RHO,OMEGA,CF)
C
C IMPLICIT REAL*16 (A-H,O-Z)
C REAL*16 MU,L,LEFS,LPROP,NB
C
C COMMON/GEOM/WX,WY,U,QS,W,SB,TEN,L,DIS,G,D,DS,LEFS,TEFS,LPROP,
C 1FTR,DOR,D6K,NB,TER,TENCAP
C
C CF1=.476*(MU/(RHO*UMF...))**.5/((G-2.*TENGAP)**.25*R**.75)
C ESTCF2=CF1
C CF2=ESTCF2
C N=1
C C1=1.18*(R+G-2.*TENGAP)/(R+(G-2.*TENGAP)/2.)
C C2=-2.*ULUG(2.83*MU*(R+G-2.*TENGAP)/(RHO*OMEGA*(G-2.*TENGAP)
C 1*R**2))+17.16
C
C 10 CONTINUE
C
C FUNC=ULUG(CF2)-C1/CF2**.5+C2
C DRUNC=1./CF2+.5*C1/CF2**1.5
C CF2NEW=CF2-FUNC/DFUNC
C
C CORRECTING THE EVENTUAL NEGATIVE ROOT
C
C IF (CF2NEW .LT. 0.) CF2NEW=CF2/2.
C IF (N-20) 1,2,2
C IF (NABS(CF2NEW-CF2)-1.0-6) 3,4,4
C 1 CF2=CF2NEW
C 4 N=N+1
C 2 GU TO 10
C 100 WRITE(6,100)
C 100 FORMAT(1H0,'WARNING IN FRIC')

```

IF (CF1-CF2) 5,5,6
CF=CF2
GO TO 7
CF=CF1
RETURN
END

3
5
20
6
7

```

C *****
C THE FOLLOWING SUBROUTINE TAKES DATA IN ARRAY FORM AND PLOTS IT ON A
C VERSATEC 1200 PLOTTER AVAILABLE AT THE CHARLES STARK DRAPER LABORATORY
C FLIGHT SIMULATION LAB.
C *****
C *****
C SUBROUTINE VERSAPLOT(IHUF,NLOC,LDEV,
1XX1,YY1,IPEN,
2FACT,
3XX2,YY2,HEIGHT,ITEXT,ANGLE,NC,
4ARRAYX,AXLENX,NPTSX,INCX,
5ARRAYY,AXLENY,NPTSY,INCY,
6XARRAY,YARRAY,NPTS,INC,LINTYP,INTEQ,
7XX1,YY1,LABELX,NCHARX,AXLEN,XANGLE,FVALX,DVX,
8XX2,YY2,LABELY,NCHARY,YAXLEN,YANGLE,FVALY,DVY,
9XXX1,YYY1,NXX,AD,NY,YD,LMASK)
C
C IMPLICIT REAL*4(A-H,U-Z)
C DIMENSION ARRAYX(102),ARRAYY(102),XARRAY(102),YARRAY(102)
C
C...
C INITIALIZE FOR PLOTTING
CALL PLOTS(IHUF,NLOC,LDEV)
CALL FACTOR(FACT)
CALL PLOT(XX1,YY1,IPEN)
C
C...
C DETERMINE SCALING FACTORS
CALL SCALE(ARRAYX,AXLENX,NPTSX,INCX)
CALL SCALE(ARRAYY,AXLENY,NPTSY,INCY)
C
C...
C PLOT THE DATA
CALL NEWPEN(5)
CALL LINE(XARRAY,YARRAY,NPTS,INC,LINTYP,INTEQ)
C
C...
C DRAW AXES
CALL NEWPEN(5)

```

```

CALL AXIS(XXX1,YYY1,LABELX,NCHARX,XAXLEN,XANGLE,FVALX,DVX)
CALL AXIS(XXX2,YYY2,LABELY,NCHARY,YAXLEN,YANGLE,FVALY,DVY)

C      C...
C      DRAW GRID
C      CALL NEWPEN(3)
C      CALL GRID(XXXX1,YYYY1,NXX,XD,NY,YD,LMASK)

C      C...
C      DRAW ALPHANUMERIC ANNOTATION
C      CALL NEWPEN(5)
C      CALL SYMBOL(XX2,YY2,HEIGHT,ITEXT,ANGLE,NC)

C      C...
C      END PLOT BUT DO NOT TERMINATE PLOTTING ROUTINE.
C      ALL PLOTTING IS INTRODUCED IN THE MAIN PROGRAM.
C      CALL PLOT(0.,0.,-999)
C      RETURN
C      END
C      TERMINATE

```



```

C*****
C      SUBROUTINE WLEMAT(A,N,N,IUNIT)
C*****
C      THIS SUBROUTINE WRITES OUT A MATRIX TO UNIT IUNIT
C*****
C*****
C      REAL*16 A(N,M)
C      IF (N.LE. 0 .OR. M .LE. 0) GO TO 1000
C      WRITE(IUNIT,50)
C      FORMAT(/)
C      DO 100 I=1,N
C          WRITE(IUNIT,90)(A(I,J),J=1,M)
C          FORMAT(8X,8(1X,1PG9.2),/)
C          CONTINUE
C          WRITE(IUNIT,50)
C          RETURN
C      1000 STOP
C      END
C*****

```

```

C *****
C SUBROUTINE R1FVEC(VEC,N,IUNIT)
C *****
C      THIS SUBROUTINE WRITES OUT A VECTOR TO UNIT IUNIT
C *****
C      REAL*16 VEC(N)
C      IF (N .LE. 0) GO TO 1000
C      WRITE(IUNIT,50)
C      FORMAT(/)
C      DO 100 I=1,N
C          WRITE(IUNIT,90) VEC(I)
C          FORMAT(1H0,5X,E24.18)
C      CONTINUE
C      WRITE(IUNIT,50)
C      RETURN
C      1000 STOP
C      END
C *****
C SUBROUTINE CMPRINT(A,IA,JA,LOUT)
C *****
C      THIS PROGRAM PRINTS THE MATRIX [A] ON DEVICE LOUT
C *****
C      COMPLEX*16 A(IA,JA)
C      REAL*8 TEMP1(20),TEMP2(20)
C
C      WRITE(LOUT,1001)
C
C      DO 10 I = 1,IA
C      DO 5 J=1,JA
C          TEMP1(J)=DREAL(A(I,J))

```

```

5  TEMP2(J)=UIMAG(A(1,J))
   WRITE(LOUT,1000)(TEMP1(J),J=1,JA)
   WRITE(LOUT,1000)(TEMP2(J),J=1,JA)
10  WRITE(LOUT,1001)
    WRITE(LOUT,1001)
C
1000 FORMAT(b(1X,1PG13.6,1X))
1001 FORMAT(/)
      RETURN
      END

```

```

C*****
C      THIS SUBROUTINE MULTIPLIES A (COLUMN) VECTOR BY A MATRIX
C*****
C      SUBROUTINE DMATVMUL(A,B,C,N,M)
C*****
C      C = A*B
C
C      N: ROW DIMENSION OF A (AND C)
C      M: COLUMN DIMENSION OF A (AND ROW DIMENSION OF B)
C*****
C      REAL*16 A(N,M),B(M),C(N)
C      DO 10 I = 1,N
C          C(I) = 0.0
C          DO 10 J = 1,M
C              C(I) = C(I) + A(I,J)*B(J)
C          RETURN
C      END
10

```

```

C*****
C  THIS ROUTINE COMPUTES THE SUM OR DIFFERENCE OF
C  TWO VECTORS
C*****
C  SUBROUTINE DVECCADD(A,B,C,N,ISUM)
C*****
C      C = A - B      ISUM .EQ. -1
C      C = A + B      ELSE
C
C      N: LENGTH OF VECTOR
C*****
C      REAL*16 A(N),B(N),C(N)
C      REAL*16 X
C      X = 1.00
C      IF (ISUM .EQ. -1) X = -1.00
C      DO 100 I=1,N
C          C(I) = A(I) + X*B(I)
C      RETURN
C      END
100

```



```

RETURN
2 AINV(1,1) = 1.0/A(1,1)
RETURN
END IF
C*****
C*****
C*****
C*****
C*****
C*****
COPY [A] INTO [ADUM] BECAUSE [A] IS CHANGED DURING COMPUTATION.
C
DO 6 I = 1,N
DO 6 J = 1,N
6 ADUM(I,J) = A(I,J)
C
INITIALIZE [AINV] TO [I].
C
DO 20 I = 1,N
DO 20 J = 1,N
AINV(I,J) = 0.000
IF(1.EQ.J) AINV(I,J) = 1.000
20 CONTINUE
C
FIND THE LARGEST ELEMENT IN COL-1.
C
30 IC = 0
II = 0
T = QABS(ADUM(1,1))
DO 40 I = 2,N
IF(T-QABS(ADUM(I,1))) .GE. 0.000)GO TO 40
II = I
T = QABS(ADUM(I,1))
40 CONTINUE
C
IF(1J.EQ.0) GO TO 80

```

```

C      IC = IC + 1
      DO 50 J = 1,N
      S = AINV(1,J)
      AINV(1,J) = AINV(11,J)
      AINV(11,J) = S
50      CONTINUE
C      DO 70 J = 1,N
      S = ADUM(1,J)
      ADUM(1,J) = ADUM(11,J)
      ADUM(11,J) = S
70      CONTINUE
C      DO 80 P = ADUM(1,1)
      IF(0ABS(P)-EPS) 90,90,100
C
C      DETERMINANT IS ZERO.
C      90      CONTINUE
      D = 0.0
      IER = 1
      RETURN
C
C      DETERMINANT IS NON-ZERO, CONTINUE
C      100      DO 110 J = 2,N
      ADUM(1,J) = ADUM(1,J)/P
      110      CONTINUE
C      DO 120 J = 1,N
      AINV(1,J) = AINV(1,J)/P
      120      CONTINUE
C
C      DO 130 K = 2,N
      KM = K - 1
      T = -1.0

```



```

C      AINV(II,J) = DP
C
C      280 CONTINUE
C      290 CONTINUE
C      300 CONTINUE
C
C      RETURN
C      END

```

11 PUG - A1 A1 A1
 34 P1

```

C
DP = ADUM(K,J)
DO 200 I = 1,KM
DP = DP - ADUM(K,I)*ADUM(I,J)
200 CONTINUE
C
ADUM(K,J) = DP/DT
210 CONTINUE
220 CONTINUE
C
DO 240 J = 1,N
DP = AINV(K,J)
C
DO 230 I = 1,KM
DP = DP - ADUM(K,I)*AINV(I,J)
230 CONTINUE
C
AINV(K,J) = DP/DT
240 CONTINUE
250 CONTINUE
C
IF(MOD(IC,2).EQ.0)GO TO 260
P = -P
C
D = P
260 II = N
C
DO 290 K = 2,N
KP = II
II = II - 1
C
DO 280 J = 1,N
DP = AINV(II,J)
C
DO 270 I = 1,KP,N
DP = DP - ADUM(II,I)*AINV(I,J)
270 CONTINUE

```